University of Bath

PHD

A study of liquid crystals by inverse gas chromatography

Shillcock, Ian Michael

Award date:
1995

Awarding institution:
University of Bath

Link to publication

Alternative formats

If you require this document in an alternative format, please contact:
openaccess@bath.ac.uk

A STUDY OF LIQUID CRYSTALS BY
INVERSE GAS CHROMATOGRAPHY

submitted by Ian Michael Shillcock
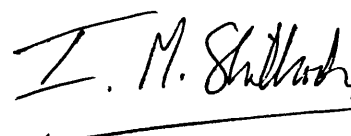
for the degree of PhD

of the University of Bath

1995

UMI Number: U074897

UMI®

Dissertation Publishing

UMI U074897

ProQuest®

ACKNOWLEDGEMENTS

CONTENTS

SUMMARY

Inverse gas chromatography has been used to study the solution and phase behaviour of a number of liquid crystalline materials. This thesis extends previous work and illustrates that the technique can be useful for studying the solution behaviour of isotropic and mesophases of liquid crystals, particularly for studying the mesophase behaviour without disrupting the long range order.

The phase behaviour of two commercially important cyanobiphenyls, a prototype chiral liquid crystal, and a side chain liquid crystal polymer with a cyanobiphenyl mesogen has been studied by IGC. Although IGC required longer time to accumulate the data to determine phase transition temperatures, it was shown to exhibit greater sensitivity than DSC, particularly when studying the supercooled mesophases. The results also indicate that a phase transition occurs on entering the supercooled region of the liquid crystals. For one of the liquid crystals, 4,4'(n-hexyloxy)cyanobiphenyl, the kinetics of solidification could be measured.

The thermodynamics of solution at infinite probe dilution was then considered for these materials. The results were interpreted with the aid of a qualitative partition function model and the solution behaviour of the polymeric liquid crystal was found to be largely governed by the properties of the mesogen. The Flory-Huggins model of polymer solutions was applied to the cyanobiphenyl systems studied and the results indicated that the enthalpic interactions were the major factor determining the observed thermodynamics. Results were also used to determine liquid crystal solubility parameters and more refined solution models showed the same trends as predicted by the Flory-Huggins model. A more contemporary model allowing for anisotropy in molecules showed that the systems studied were insufficiently anisotropic to affect the calculated parameters.

Binary mixtures of 4,4'(n-hexyloxy)cyanobiphenyl with PDMS were also considered. The two compounds were found to be generally incompatible although there was some indication that the two components interact in some of the compositions

CHAPTER 1

INTRODUCTION

Today liquid crystal technology forms an everyday part of our lives. Perhaps the best known applications are in small digital displays found in watches and calculators and, in recent years, colour screens in laptop computers and hand held T.V.s. However, they are also present in detergent formulations, and strong oriented fibres, (such as Kevlar found in bullet proof vests)[1]. The novel behaviour of these materials appears to have captured the imagination of many researchers and a scan of modern publications reveals the use of liquid crystals in a wide area of applications; including analytical separations, polymer chemistry, and non-linear optics. Few areas of chemistry appear to exist where liquid crystals have not been employed and yet only a few decades ago few people even knew of their existence and it was felt necessary to stir enthusiasm into further research on these materials[2].

Liquid crystals were first discovered in 1888 by an Austrian botanist called Reinitzer[3] who noticed an intermediate phase between liquid and solid in cholesterol benzoate. In the years following much research was done into isolating, synthesising and characterising liquid crystal phases; greatly aided by the invention of the hot stage microscope[4]. However, by 1933 interest in liquid crystals had peaked and during the next three decades interest waned. This was probably because, at that stage in their development, they were viewed as well understood curios with no technological application. Although the renewed interest born out of the 1958 Faraday Society meeting on liquid crystals[5] saw increased research applications, the discovery of the electro-optic behaviour of liquid crystals and realisation of the potential for digital displays was the turning point in the popularity of these materials[1]. Many new materials were synthesised and when Gray[6] reported a series of liquid crystals with improved stability and the ability to operate at room temperature, liquid crystal displays (LCDs) became commercially viable. By 1980 LCD's had become commonplace. It was during the 1970s that similar liquid crystal behaviour was first

recognised in polymers[7] and a few years later Finkelmann *et al.*[8] synthesised a polymer with liquid crystal moieties as side groups from a methacrylate precursor. In the last decade coupling polymer and liquid crystal properties has gained much interest[9] but recent reports[10,11] point out that, at present, these materials are not commercially viable. However, in the last couple of years a growing number of these liquid crystal polymers have become commercially available in research quantities[12].

As research has progressed in liquid crystals, interest has also grown in their behaviour in solutions with both non-liquid crystalline and liquid crystalline components[13]. Whilst there have been many studies on phase behaviour and performance there have been fewer attempts to model the solution behaviour of liquid crystals in terms of their molecular components. The structure of the liquid phase still remains relatively unknown compared to the structure of solids and gases and models of molecular behaviour approach the problem by extrapolating gas phase models or constructing a pseudo-crystal lattice. The anisotropic nature of liquid crystals further complicates such models. However, knowledge of the absolute structure of a pure liquid or solution is not usually necessary and it is adequate to know how a solution differs from a liquid phase of the pure component.

This report describes the use of gas chromatography to study a set of thermotropic liquid crystals, including a liquid crystal copolymer. Gas chromatography allows the study of concentrated solutions where the liquid stationary phase is only slightly perturbed from that of the pure material. Chapter 4 illustrates how this technique can be used to study phase transitions within the liquid crystal whilst chapter 5 describes solution behaviour in terms of changes in the observed thermodynamic quantities. The description of the solution is advanced to the molecular level in chapter 6 where "simple" solution theories are discussed and more advanced theories considered and chapter 7 looks at the effect of mixing a liquid crystal with a polymer.

1.1 LIQUID CRYSTALS

Liquid crystals are formed by anisotropic, dichotomous molecules composed of rigid and flexible portions. The term "liquid crystal" was first introduced by Lehmann[4] to describe the fluid phase between solid and melt that exhibited crystal like optical properties. Although it was pointed out that this nomenclature is strictly incorrect[14], as the phase is neither crystalline or liquid in the usual sense, it is commonly used today synonymously with "mesophase" and variants of this. For consistency in this thesis, "liquid crystal" will denote the material and "mesophase" and "mesogen" will describe, respectively, the intermediate phase and the part of the molecule that is responsible for its formation.

Mesophases may arise from variation in liquid crystal concentration within a solution, termed a "lyotropic" liquid crystal, but this thesis will be concerned with mesophases which arise from temperature changes, the so called "thermotropic" liquid crystals. By far the most common type of liquid crystal is one composed of "rod-like", or calamitic, molecules. However, discotic, ("disc-like"), and phasm, ("pyramid-like") liquid crystals have been discovered in the last decade or so[11]. These exhibit alternative mesophases but a description of them falls outside the scope of this report.

When a calamitic material is heated from the crystal phase it may form the random melt, or "isotropic" phase, directly or it may retain a degree of order and form a mesophase. The schematic diagram in *figure 1.1* illustrates the possible phase transitions. If the mesophase retains orientational order a "nematic" phase is formed. The material may form a more ordered phase where some positional order is also present. This is called the "smectic" phase and a number of different phases have been identified and classified according to the arrangement within layers and the tilt of the molecule within a layer[15]. Some of the smectic phases commonly encountered are shown schematically in *figure 1.2*.

CRYSTALLINE 3-D ORDER

SMECTIC:
2-D ORDER;
Positional and
Orientational

NEMATIC: 1-D ORDER;
Orientational

CHOLESTERIC: HELICAL
NEMATIC LAYERS

ISOTROPIC RANDOM MELT
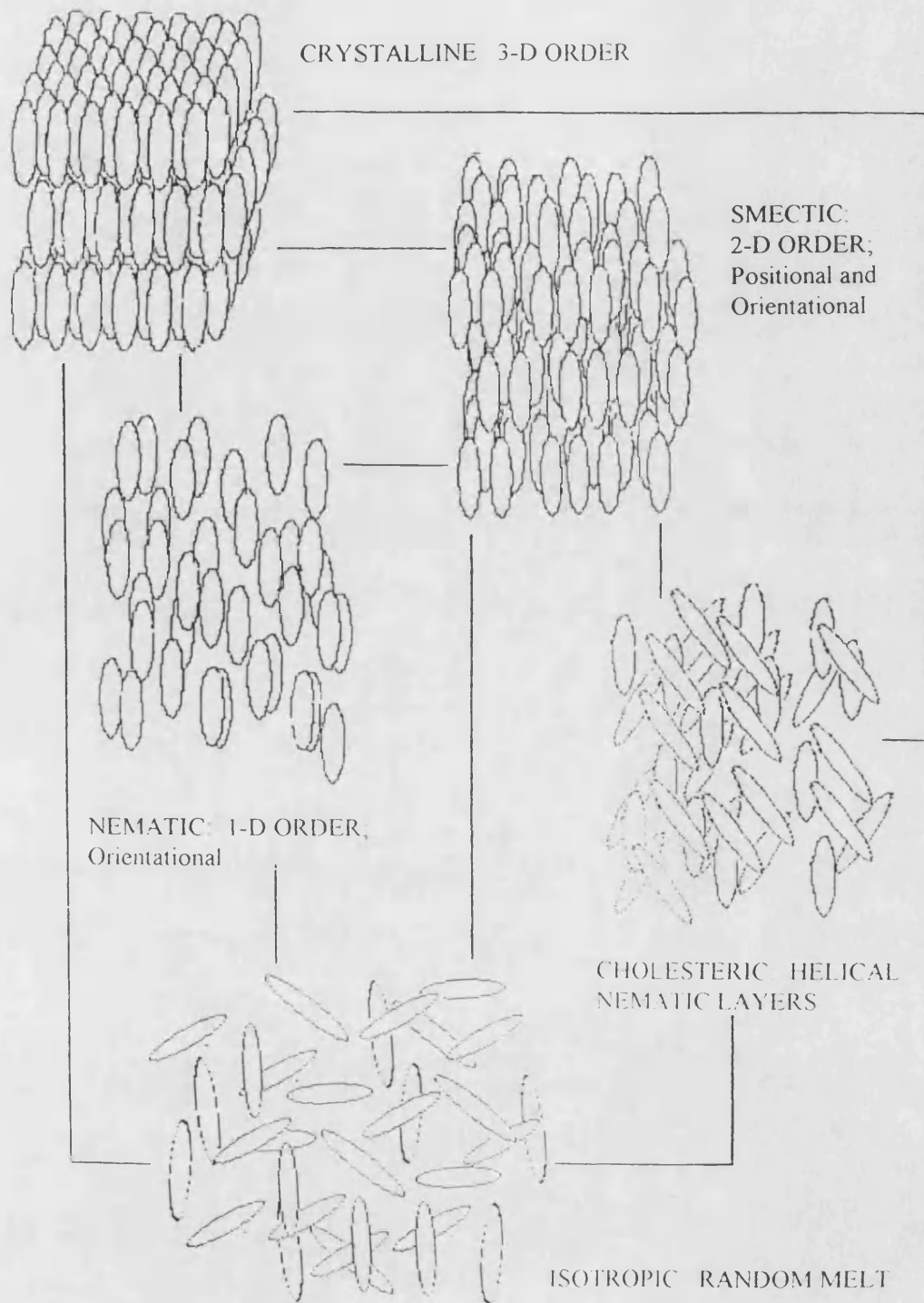
Figure 1.1: A schematic diagram of the possible phase transitions in calamitic materials on heating from the crystalline phase.

S_A

S_B

S_C

S_F
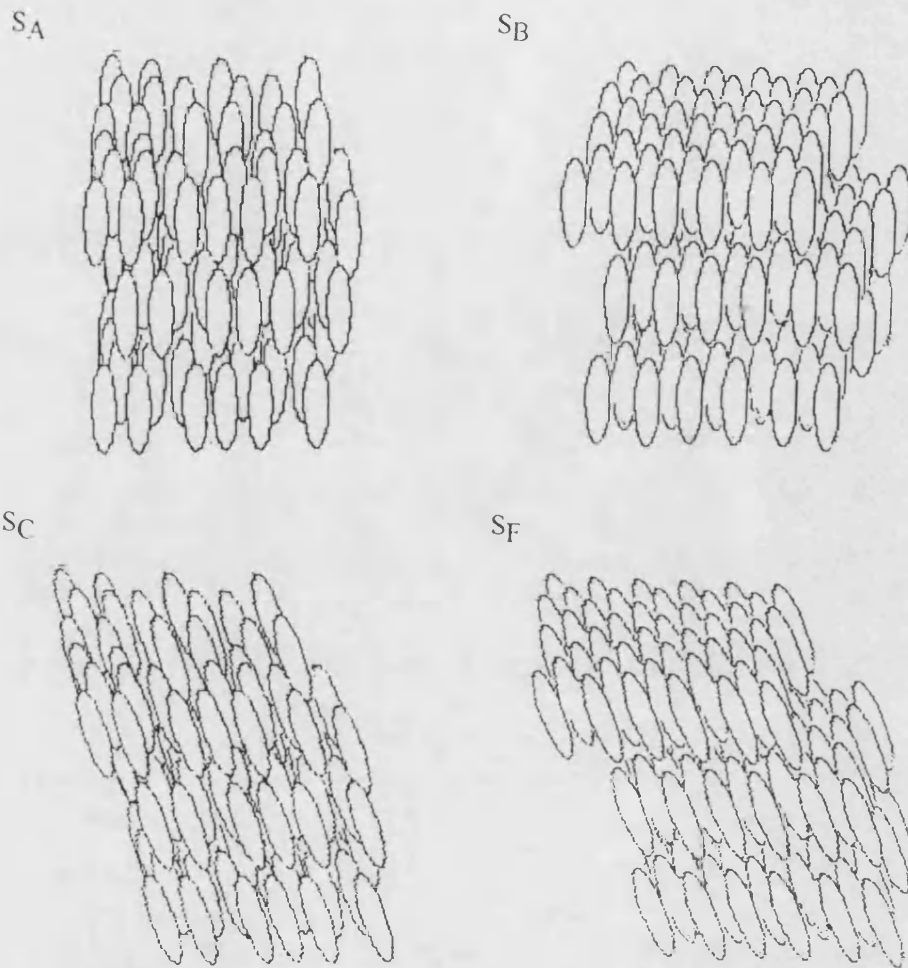
Figure 1.2: Schematic diagram of some common smectic phases showing disorder within each layer (S_A), hexagonal packing within each layer (S_B), and the respective tilted forms (S_C) and (S_F)

Where chiral liquid crystals are present a "cholesteric" or "twisted nematic" phase may be formed which can be described by nematic layers twisted with respect to adjacent layers. A given liquid crystal may exhibit one or more such mesophases, including several smectic phases, as it melts from the crystal but nematic and cholesteric phases are not found in the same material. Mesophase formation cannot be predicted *a priori*

but an idea of behaviour can be obtained from trends in homogenous series of liquid crystals[1,16].

The above schematics are idealised pictures and in reality the individual molecules will be able to move quite freely with respect to the crystal phase. However, as it moves freely the long axis of the molecule will have a preference for a given direction, the "director", which is quantified by the order parameter, S;

$$S = <(3\cos^2\theta-1)/2>$$ [1.1]

where θ is the angle between the director and the long axis of the molecule and < > denotes an averaged value. This can be the time averaged value of an individual molecule or the mean from a "snapshot" of a domain of molecules, about 10^5 molecules[17]. The liquid crystal behaviour can be modelled as a collection of domains or as a continuum, the former probably being the easier to visualise.

The generalised structure of a liquid crystal molecule is illustrated in *figure 1.3*. The rectangles represent rigid portions of the molecule, usually aromatic, linked by a moiety L with end groups X and Y.
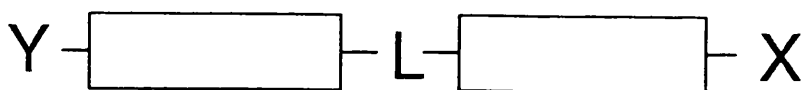
Figure 1.3: Schematic structure of a typical liquid crystal

This is a generalised representation and not all liquid crystals conform to this structure but they all exhibit common features. Mesophase formation is a consequence of the retention of anisotropy by molecules in the fluid against the thermal disruption they experience. Hence, the molecules must be sufficiently linear to retain their anisotropy as they start to rotate within the fluid. To form a mesophase it is not necessary to have strong interactions between molecules but any interactions promoting parallel alignment of the molecules may assist mesophase formation and liquid crystals often

contain a dipole, either in the linking moiety or in the end group. A loss of linearity greatly reduces the attractions between parallel molecules and they are less likely to form an anisotropic fluid. The link, L, is usually a linear moiety such as $-CH_2=CH_2-$, or $-N=N-$. This couples the two linear portions of the molecule. At least one end group will be a flexible moiety. If the molecule is too rigid with too strong an interaction with neighbouring molecules the crystal phase will persist up to temperatures where the thermal motion of the molecule in the fluid cannot support a mesophase.

The anisotropy of the liquid crystal gives it birefringent properties, exhibiting different refractive indices dependent upon whether light travels parallel or normal to the long axis of the molecule. The presence of a dipole allows the molecule to be switched between the two optical behaviours which forms the basis of LCD behaviour. The fluidity of the mesophases and sharpness in the switching voltage needed to effect a change makes LCDs compact, low power devices compared to more traditional displays, such as cathode ray tubes. Also, the tendency for alignment in the mesophase can be induced during flow under pressure in the manufacture of fibres and plastics. The alignment is then "frozen" into the finished product adding strength to the material. The exploitation of the electro-optic properties of liquid crystals for LCDs accounts for the major portion of the commercial liquid crystal market. However, both technologies are developing rapidly and require the study of pure liquid crystals and their mixtures to underpin these developing areas.

The liquid crystals studied here are two alkoxycyanobiphenyl compounds, well established as commercial materials for liquid crystal displays, and a prototype chiral compound. A cyanobiphenyl copolymer, recently available commercially in research quantities, was also studied. These present a variety of mesophases which will be discussed further in chapter 4.

1.2 POLYMERS

In the last fifty years polymers have become a major part of our everyday life with a wide variety of commercial materials now available. Most of these are carbon based materials. They can be manufactured easily, in large quantity from readily available starting materials and their properties can be tailored to individual requirements by selecting the appropriate feed stocks or altering the structure of preformed materials. Today polymers can be made which have strength and durability comparable with traditional metallic and inorganic materials whilst being easier to process and giving lighter, more portable products. Thus polymers find use in structural materials, machine components, housings, facings, and surface coatings, as well as many other uses. The development and study of polymers not only allows for their wider application but improves the quality of existing materials as well as making their production and use more economical and environmentally friendly.

Strictly, a "polymer" is a substance composed of "macromolecules". A macromolecule is one composed of a large number of identical sequences, "monomers", linked by covalent bonds. The terms polymer and macromolecule tend to be used interchangeably[18]. Polymers exist in the three basic forms shown schematically in *figure 1.4*.
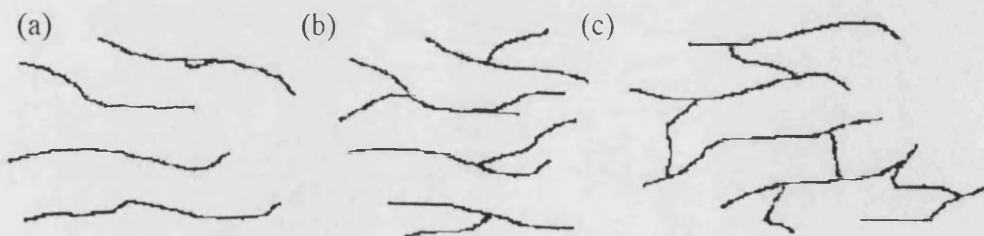
Figure 1.4: Schematic representation of a *linear* (a), *branched* (b), and *cross-linked* (c) polymer.

The different forms can be synthesised by using the appropriate monomer molecule or "branching"/"cross-linking" can be induced after polymerisation. The degree of cross-linking affects the thermal and mechanical properties of the polymer and as this increases polymers are classified as "thermoplastics", "elastomers", and "thermosets", successively.

Some macromolecules are partially crystalline when cooled. The long times required to allow the long, random coils of a typical macromolecule to access the thermodynamically most stable conformation to align in the crystal form usually preclude the formation of a totally crystalline polymer. If the degree of cross-linking between macromolecules is increased the melting point of the polymer generally increases. More accurately this is a softening temperature as the molecules are long enough to remain significantly intertwined and do not possess the mobility and freedom associated with a low molar mass melt. On cooling the melt, if the polymer chains do not have sufficient time to reach internal equilibrium at each temperature a glass may form. At such a sufficiently low temperature the low thermal energy available precludes chain movement resulting in the formation of this amorphous solid. This temperature is called the glass transition temperature, Tg. This transition may occur over a temperature range and so the value quoted is the temperature where a change in the increase in free volume occurs.

In real polymers the macromolecule may be a "homopolymer", composed of one monomer, or "copolymer", where more than one monomer is present. The latter leads to a number of classifications shown schematically in *figure 1.5*.

Unlike small molecule compounds, synthetic polymers contain a distribution of macromolecule sizes. The number of monomers in a macromolecule is called the "degree of polymerisation". For most work the exact distribution of macromolecule sizes is not needed and it is adequate to characterise the distribution in terms of the

```
A-A-A-A-A-A-A-A-A-A-A-A          HOMOPOLYMER

A-B-A-B-A-B-A-B-A-B-A-B          ALTERNATING COPOLYMER

A-A-A-A-A-B-B-B-B-B-B            BLOCK COPOLYMER

A-A-B-A-B-B-A-A-B-B-B-A          RANDOM COPOLYMER

A-A-A-A-A-A-A-A-A-A-A            GRAFT COPOLYMER
    |             |
  B-B-B         B-B-B-B
```
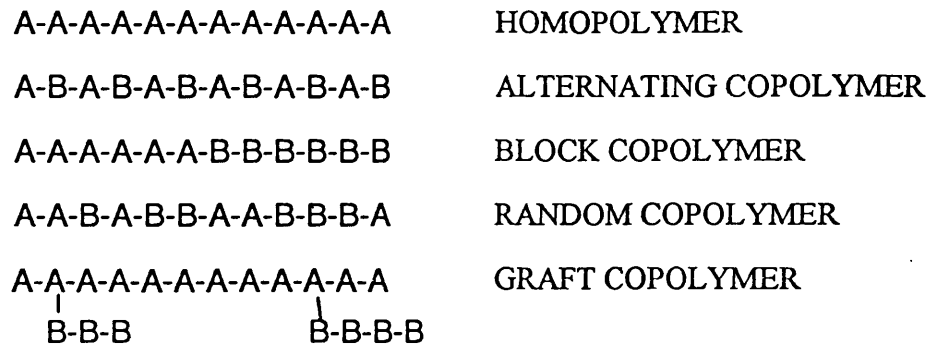
Figure 1.5: Schematic diagram of the five types of polymer molecules

average molecular mass of the polymer. The average is usually obtained from the

summation of number fraction or weight fraction of individual molecule masses,

although in some cases higher statistical averages are employed[18].

$$\overline{M}_n = \frac{\sum_i n_i M_i}{\sum_i n_i} \qquad\qquad \overline{M}_w = \frac{\sum_i w_i \cdot M_i}{\sum_i w_i} \qquad\qquad [1.2]$$

where n and M are the number of molecules and molar mass of the i component and w

is the weight of the i component. The weight average molecular mass is always higher

than the number average molecular mass unless all the macromolecules are of identical

size. The ratio of the former over the latter can be used as a measure of the

distribution of macromolecule size and is termed the "polydispersity", γ.

1.2a Liquid Crystal Polymers

Liquid crystal polymers, (LCPs), can be divided into two groups dependent upon the

position of the mesogen within the macromolecule. If the mesogen forms part of the

backbone it is called a "main chain LCP", (MCLCP), and if it is grafted onto the

macromolecule it is called a "side chain LCP", (SCLCP). The latter exhibit reasonable

chromatographic separation of analytes and electro-optical properties comparable with

low mass liquid crystals but MCLCPs do not possess the required flexibility for these

applications and are mainly considered as strengtheners in materials science[10], as discussed in section 1.1.

In this work a SCLCP copolymer with a cyanobiphenyl mesogen grafted onto a polysiloxane backbone was studied. This was chosen to enable comparison with the low molar mass equivalents studied. These SCLCPs are synthesised by hydrosilylation of a double bond on the mesogen[19]. Thus the polymer is preformed and the mesogen added to form a random copolymer. The structure and formation of such a copolymer is outlined in *figure 1.6*.
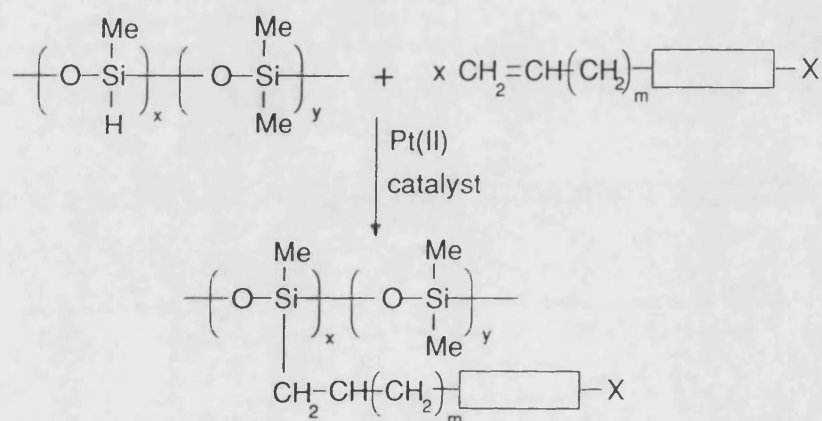
Figure 1.6: General synthetic strategy for a polysiloxane based SCLCP where the catalyst would be a Pt(II) salt

A lot of work has concentrated on siloxane backbone SCLCPs because of the relative flexibility of the "O-Si-O" bond compared to a carbon backbone but several copolymers and homopolymers have also been synthesised based on acrylates and methacrylates[20]. The phase behaviour of SCLCPs does not vary greatly once the molecule contains more than a few tens of monomers[21]. Hence most materials studied, including the copolymer here, are strictly "oligomers" where the size of the molecule is intermediate between that of monomer and polymer.

1.3 SOLUTIONS

A solution is composed of two or more miscible components where the "solvent" and "solute" refer, conventionally, to the major and minor components respectively. In inverse gas chromatography organic compounds, commonly used as solvents, are the minor components but most reports on polymers retain the label "solvent" when referring to the more volatile phase. The term "probe" molecule is also used, especially when the volatile component approaches infinite dilution. These two terms will be used synonymously in this thesis to avoid confusion. The thermodynamic parameters describing a solution as a whole, such as the free energy of solution, are extensive properties which can be difficult to measure accurately and which will tend to zero as one component approaches the composition of a pure liquid. A more meaningful quantity in the gas chromatography composition range is the partial molar quantity, given in general terms by; $(\delta X_i/\delta n_i)_{P,T,n_{1...j}}$.

X and n are the parameter of interest and the number of moles of component i, respectively, (the mole fraction, x, replaces n when X is given per mole). P and T denote pressure and temperature and the subscript 1...j refers to all other components apart from i. When X is a free energy this is called the chemical potential, μ. This enables an intrinsic parameter with a finite value to be obtained for the volatile component which can be linked to other components of the solution by the Gibbs-Duhem equation[22];

$$\Sigma x_i \, d\mu_i = 0 \qquad\qquad\qquad [1.3]$$

As we do not know the structure of a pure liquid or solution it is useful to define a standard solution with which others can be compared. This has been done by comparing the solution behaviour with that of the pure solvent. The reference state is therefore the pure liquid and the standard solution is defined in terms of it. The solution has to be one which has properties readily predictable from those of the pure

liquid components without the need for adjustable scalars. Note that this does not imply any structural knowledge of either fluid.

1.4 THE IDEAL SOLUTION

An ideal solution can be described in a number of ways but the most general definition is a solution that obeys Raoult's law[23];

$$p_i = P^o_i x_i \qquad [1.4]$$

where p_i and P^o_i are the partial pressure of i over the solution and pure liquid i and x is the mole fraction. From this it follows directly that the chemical potential varies linearly with the logarithm of the mole fraction, although [1.4] is a consequence of [1.5];

$$\mu_i^{ID} = \mu^o_i + R\,T\,\ln x_i \qquad [1.5]$$

R is the gas constant and the superscripts ID and o denote the ideal solution and the pure liquid, respectively.

For a solution to be ideal the observed behaviour must be a consequence of the changes in entropy alone. The components must be randomly mixed and miscible in all proportions and the interactions within the solution must equal those of the pure liquid components, such that; $\qquad \varepsilon_{ij} = (\varepsilon_{ii} + \varepsilon_{jj})/2$

where ε is the pair potential energy between molecules. Hence there is no compression or expansion of the liquids on mixing[24] and the respective enthalpy and volume change is given by the expressions below;

$$\Delta H^m = 0$$

$$\Delta V^m = 0 \qquad [1.6]$$

The free energy change of mixing is governed by the entropy change alone. The entropy change of mixing for an ideal solution was first derived by Stern[25,] using a lattice model for a binary solid solution comprised of equal sized molecules, and is given below;

$$\Delta S^m = -R \left(x_1 \ln x_1 + x_2 \ln x_2 \right)$$

$$\Delta G^m = R\,T \left(x_1 \ln x_1 + x_2 \ln x_2 \right) \tag{1.7}$$

This is a theoretical model. No real solutions exhibit this behaviour exactly but some binary mixtures approximate very closely to this model and follow Raoult's law, within experimental uncertainty, across the whole composition range. Benzene and toluene is an example. Here the molecular size and interactions are very similar. For any binary solution a component will obey Raoult's law as its mole fraction approaches unity.

1.5 REAL SOLUTIONS

1.5a The Ideal-Dilute Solution

Real solutions can exhibit positive or negative deviations from Raoult's law as illustrated schematically for binary systems in *figure 1.7*.
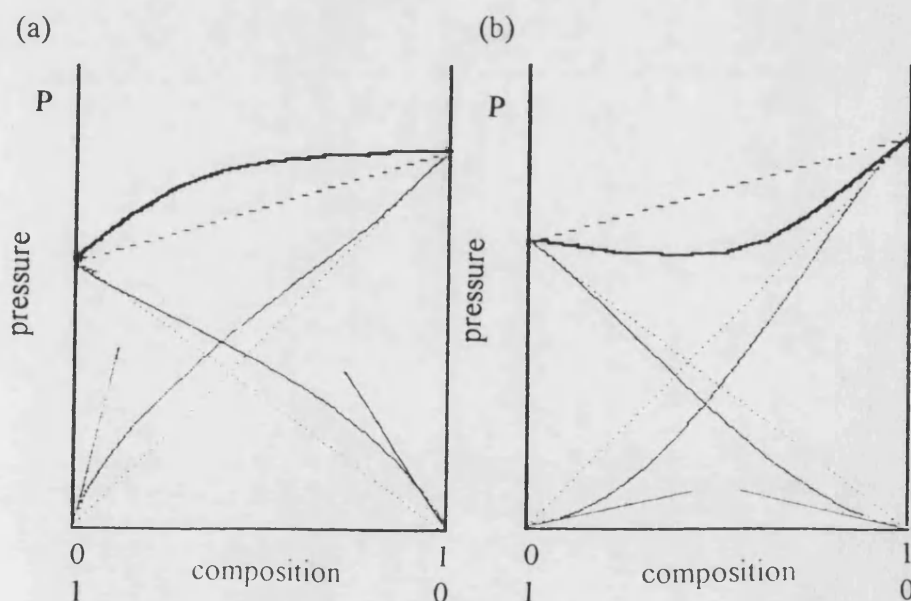
Figure 1.7: Schematic graph of partial pressure versus composition for systems exhibiting (a) positive deviation and (b) negative deviation. The bold line shows the total pressure of the system and the dotted lines illustrate Raoult's law behaviour. The Henry's law regions are also illustrated for both components.

Where two components have dissimilar interactions and do not associate in solution, for example water and dioxane, an excluded volume effect exists. Energy is required to form the solution, the volume is greater than the sum of the parts, and the molecules have a lower tendency to remain in solution compared to the pure liquids. Hence, the partial pressure is greater than Raoult's law predicts and the system exhibits positive deviation. If the components of the solution associate, for example acetone and chloroform, energy is released, the volume contracts, and the molecules are less likely to escape into the gas phase compared to the pure liquids. The system is said to exhibit negative deviation.

The diagrams show that as one component becomes concentrated enough to obey Raoult's law the second component also exhibits a linear dependence between partial pressure and composition. The coefficient is no longer the partial pressure of the pure liquid and is termed the Henry's law[26] constant, H;

$$p_i = H_i \, x_i \tag{1.8}$$

In a binary solution, if one component obeys Raoult's law the other must obey Henry's law[27]. The dilute component is said to form an ideal-dilute solution.

1.5b General Solutions

In the composition region between that of ideal behaviour and ideal-dilute behaviour of a component the departure from an ideal solution can be expressed in a number of ways[28]. One of the most convenient is to define an excess quantity describing the degree of departure from the ideal case. We can express this in terms of chemical potential as; $\mu^E = \mu - \mu^{ID}$

where E denotes the excess quantity. By defining the excess chemical potential by;

$$\mu^E = R \, T \ln \gamma \tag{1.9}$$

we can introduce it more easily into existing relationships.

$$\mu - \mu^o = R \, T \ln (x \, \gamma) = \ln a \tag{1.10}$$

Where a is the activity, or effective composition, and γ is the activity coefficient[29]. We can readily apply this idea to Raoult's law and use the activity coefficient as a measure of the deviation from an ideal solution. As the chemical potential is a partial molar free energy we can define a corresponding excess partial molar enthalpy and entropy of mixing from [1.9];

$$\ln \gamma = (H^E/R\ T) - (S^E/R) \qquad [1.11]$$

where the enthalpy and entropy are given by H^E and S^E respectively.

In a real case the ratio of partial pressures in [1.4] gives the effective composition of the solution, or activity. From equation [1.10] it follows that;

$$a_i = p_i/P^o_i = x\ \gamma \qquad [1.12]$$

Thus by measuring the pressures and actual mole fraction of the solution, by weighing for instance, the activity coefficient may be obtained and it is a direct indicator of the deviation from Raoult's law behaviour.

Thus we have a model of an ideal solution, based on the requirements outlined in section 1.3 and developed in section 1.4, which enables prediction of the behaviour of an ideal solution. By introducing the activity coefficient as an empirical adjustment of the model to account for the observed behaviour we are able to discuss deviations in terms of interactions and orientation within the solution compared to the pure liquid. These are quite general equations where the parameters are defined empirically and are thus not restricted in their application.

In the following sections some of the approaches towards *ab initio* descriptions of solutions based on the component molecules will be outlined. These have approached the problem of a real solution from two extremes. The regular solution approach considers cases where only the excess partial molar enthalpy contributes to the activity coefficient and the athermal solution approach considers only the entropy contribution.

First the process of forming a solution will be considered and the factors affecting phase separation discussed.

1.6 THERMODYNAMICS OF MIXING

In the gas chromatography experiment we initially have the solvent as a vapour and the liquid phase coated on an inert support. We can envisage the formation of a solution as a series of individual steps. The vapour condenses upon the liquid, the two components form an ideal solution, the ideal solution is perturbed to form the real solution. This is shown in *figure 1.8* along with the respective molar free energy changes.
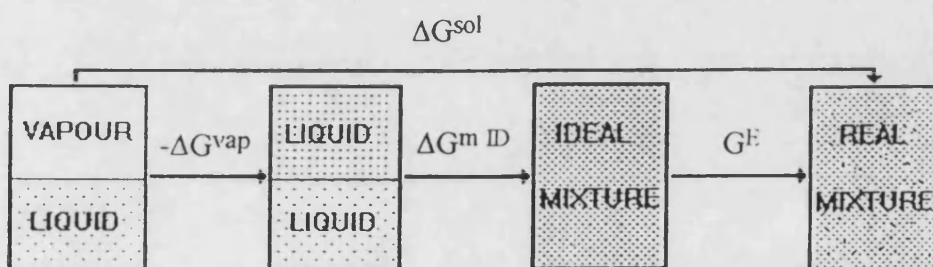
Figure 1.8: Schematic diagram of solution formation between a liquid and vapour

The overall process is described by the partial molar free energy change of solution, $\Delta \overline{G}^s$. $\Delta \overline{G}^{m\ ID}$ is the ideal partial molar free energy change of mixing and G^E is the excess partial molar free energy change, where the partial molar free energy change of mixing is given by;

$$\Delta \overline{G}^m = \Delta \overline{G}^{m\ ID} + G^E \qquad [1.13]$$

These and the corresponding enthalpies and entropies are the parameters commonly used in the literature[30]. Note that in the gas chromatography experiment the component of interest approaches infinite dilution. From section 1.5a it is seen that such a mixture would form an ideal-dilute solution. As the free energies are given as partial molar quantities, G^E describes the change in going from an ideal to an ideal-dilute solution. Now let us consider the mixing process as a whole.

Consider a given composition of two components in a mixture. For this composition to separate into two phases of differing compositions the free energy of the new phases must be lower than that of the mixture. Also there must be no chemical potential gradient between the two phases if they are at equilibrium otherwise a given component will transfer until it has minimised the free energy. This can be expressed generally as;

$$\mu_i{}^a = \mu_i{}^b = \mu_i{}^c \ldots\ldots \qquad\qquad [1.14]$$

Where the superscripts denote different phases. Thus mixing occurs to remove potential gradients and minimise the free energy. Two types of mixing can occur and these are illustrated in *figure 1.9*.

(a)   (b)
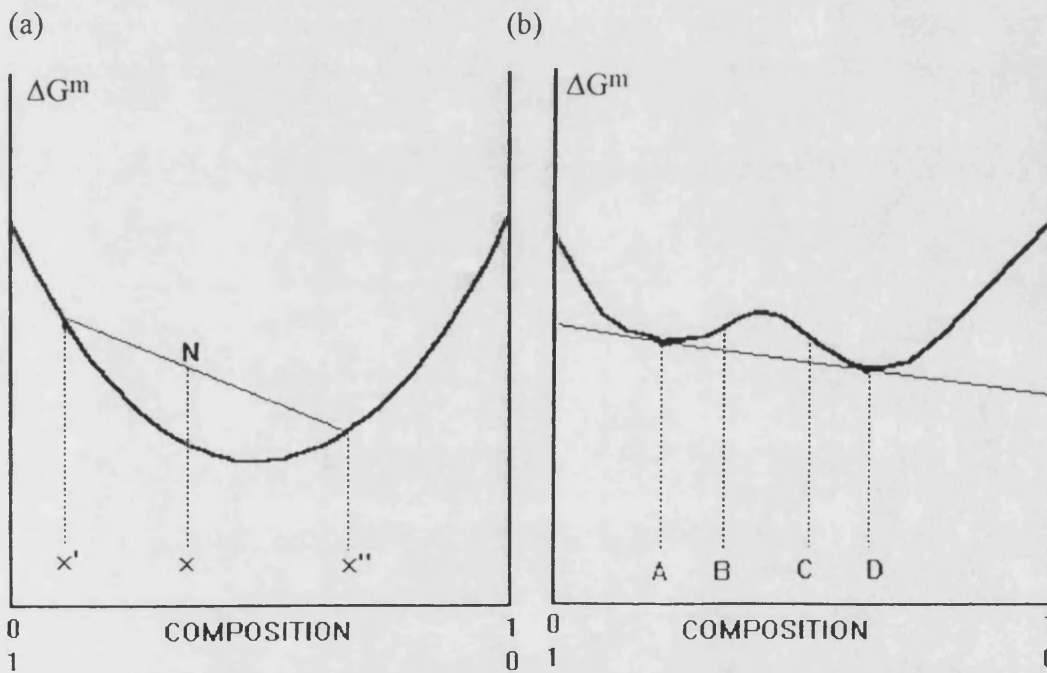
Figure 1.9: Schematic graphs illustrating the free energy of mixing profile for (a) a single phase binary system and (b) a binary system exhibiting biphasic behaviour

Figure 1.9a describes a binary system that mixes at all compositions. If we take a composition x and attempt to form two new phases x' and x" we can see the new free energy of the system occurs at N. Also, the gradients of the curve differ at x' and x". Section 1.3 shows the gradient to be equal to the chemical potential. We have two phases with a potential gradient between them and a higher free energy. Hence, the

composition of the two phases would alter until equilibrium was reached, which can only occur at x, where there is a uniform composition. Some binary systems do separate into two phases and such a free energy profile is shown in *figure 1.9b*. If the composition, x, is such that x≤A or x≥D the system behaves as in *figure 1.9a* and the two components mix. However, at compositions between A and D the mixture is thermodynamically unstable with respect to a biphasic system of composition A and D. If x is between the minima and the respective points of inflexion, B and C, the free energy loss by one phase is insufficient for the other phase to surmount the free energy maximum and the mixture is said to be metastable.

1.6a Phase Transitions

The free energy of mixing can be split into an enthalpy and entropy term in the usual way;

$$\Delta G^m = \Delta H^m - T \Delta S^m \qquad [1.15]$$

The free energy is negative if ΔH^m is negative and ΔS^m is positive. If the two quantities have the same sign mixing will depend upon the relative magnitudes and will be governed by temperature. When the enthalpy of mixing is zero mixing occurs when the entropy is positive and the free energy-composition curve will follow the form of *figure 1.9a*. Non zero enthalpies can result in local maxima and minima in the free energy-composition curve.

When both enthalpy and entropy of mixing are positive the free energy increases as the mixture cools and a temperature may be reached where further cooling results in a biphasic region. This is called the upper critical solution temperature, UCST. Alternatively the enthalpy may be negative and the entropy negative leading to a biphasic region on heating. The onset of the two phase region being the lower critical solution temperature, LCST. Solutions with an UCST are more commonly encountered. For example, acetonitrile-pentane and methanol-pentane have UCSTs at 341K and 287K, respectively. As enthalpy and entropy are functions of temperature

some systems may exhibit both types of behaviour. One such system is

tetrahydrofuran-water[31] which has an LCST at 345 K and UCST at 410 K. Where

solutions exhibit an LCST there is a tendency to show an UCST as well, though this

may not always be achieved if the gas phase is reached first[18]. The minimum or

maximum in a phase boundary plot of temperature versus composition is termed the

Plait point[32].

The above arguments for a binary system can be extended to systems containing more

components. This report will only be concerned with binary and ternary systems and

these will form the basis of the following molecular model arguments.

1.7 THEORETICAL SOLUTION MODELS

1.7a Regular Solutions

The term "regular" solution was introduced by Hildebrand[33] who defined it as "one

involving no entropy change when a small amount of one of its components is

transferred to it from an ideal solution of the same composition, the total volume

remaining unchanged"[34]. That is, the entropy change of mixing is given by the ideal

expression, equation [1.7]. This model is reasonable for mixtures of small molecules

where any ordering of the molecules is weak compared to the thermal motion of the

system[35].

Hildebrand suggested internal pressure (internal energy) as an empirical measure of

the inequivalence of interactions between components of a mixture. He defined a

cohesive energy density, c, for a pure component;

$$c = \Delta U^{vap}/V^o \qquad\qquad [1.15]$$

where ΔU^{vap} is internal energy of vaporisation and V^o is the molar volume of the

component. Scatchard[36] combined this approach with a model developed by

van Laar[37] to define the enthalpy of mixing. The resultant Hildebrand-Scatchard equations are given below;

$$\Delta H^m = (x_1 V_1 + x_2 V_2) A_{12} \phi_1 \phi_2 \qquad [1.16]$$

$$A_{12} = (c_{11}^{1/2} - c_{22}^{1/2})^2 = (\delta_1 - \delta_2)^2 \qquad [1.17]$$

where the numbered subscripts refer to different components and A_{12} is a measure of the difference in interaction between the two solution components. The square root of the cohesive energy density is a quantity that is used so extensively in this approach that it has been termed the "solubility parameter", δ.

An alternative approach to those outlined above was given by Guggenheim[38]. He defined a "strictly regular solution" based upon a lattice model and arrived at an expression for the enthalpy of mixing given below;

$$\Delta H^m = z \, \varepsilon \, x_1 \, x_2 \, N \qquad [1.18]$$

N is the total number of molecules, z is the co-ordination number of the lattice and ε is the interchange energy, given as $\varepsilon = 2\varepsilon_{12} - \varepsilon_{11} - \varepsilon_{22}$, where subscripts denote the pair potentials for type 1 and type 2 components in the binary solution.

Guggenheim's approach, and others reviewed in the above reference, is potentially less empirical than the Hildebrand-Scatchard theory. However, only solutions conforming to the lattice model restrictions can be described by it and a suitable determination of the interchange energy is necessary. Guggenheim assigned ε an arbitrary value to give the best fit to experimental data obtained by Scatchard, benzene and cyclohexane for example, when testing his solution models. The Hildebrand-Scatchard theory is a more general approach which does not necessarily preclude pure liquids where the molecules are not randomly mixed. However, equations [1.15] to [1.17] show that the enthalpy of mixing can only take positive values. Mixing is favoured when the enthalpy of mixing is small or approaches zero, that is when the two components have similar interactions. This is a consequence of the limitation to descriptions of non-polar molecules exhibiting only London forces[39]. Where polar

molecules and hydrogen bonding are present each system must be judged separately to determine whether the enthalpy of mixing is likely to be negative.

1.7b Athermal Solutions

An athermal solution is one that does not exchange heat with its surroundings when formed from its components, that is the enthalpy change of mixing is zero. However, if the two components contain different size molecules the solution may deviate from Raoult's law and "athermal" is usually used to describe such a non-ideal solution. For low molar mass components this discrepancy is small[40]. Fowler and Rushbrooke[41] first considered size effects by studying monomer-dimer solutions and found these showed a slight deviation from the ideal model. However, for solutions containing macromolecules Raoult's law is far from obeyed[42]. To model athermal solutions a lattice model is usually invoked and the placing of each component within the lattice is considered.

The problem of mixing small molecules and long chain molecules was first tackled independently by Flory and Huggins[43,44]. The approach was to divide the long chain molecule into segments, equal in size to the small molecule component. By considering the placement of these segments on the lattice, such that adjacent segments within a chain occupied adjacent lattice sites, they arrived at the expression for the molar entropy of mixing and partial molar entropy of mixing given below;

$$\Delta S^m = - R \left(x_1 \ln \phi_1 + x_2 \ln \phi_2 \right)$$

$$\Delta \overline{S}^m{}_1 = - R \left[\ln \phi_1 + (1 - V^o{}_1/V^o{}_2) \phi_2 \right] \qquad [1.19]$$

where the subscripts 1 and 2 refer to the solvent and polymer components, respectively. The logarithm of the volume fraction now replaces the logarithm of the mole fraction of equation [1.7] and V^o is the molar volume. When the molar volumes of each component are equal the ideal equation is retrieved and is a special case of this general model.

Models have subsequently been derived for other systems where the macromolecule forms dilute solutions, and the mixing of other geometrically identical shapes where size differs greatly[45]. Guggenheim has also refined the approach[46] to consider the effect of the co-ordination number, z, where the Flory-Huggins model is retrieved if z is allowed to approach infinity. Polydisperse chains can also be described by the Flory-Huggins model[45] and the approach has been expanded to cover ternary systems[47]. The theory gives a reasonable description of athermal systems where the true behaviour lies between the limits of the Flory-Huggins approach and the ideal solution[48]. In their theories Flory and Huggins included an enthalpy term to account for non-zero heat changes of mixing. This is discussed in the next section where the full Flory-Huggins theory is given.

1.8 THE GENERAL SOLUTION MODEL

A general solution is one where both the size difference and interaction energies contribute to deviations from the ideal solution model, that is a real solution. In such a system the excess partial molar enthalpy and entropy, defined in section 1.5b, are assumed to act independently and the athermal and regular solution approaches are combined. Flory applied the regular solution approach to a lattice, in a similar manner to that of Guggenheim given in section 1.7a, and defined a "reduced residual enthalpy of mixing", and heat of mixing[49];

$$\chi = z \, \varepsilon \, / \, R \, T \qquad [1.20]$$

$$\Delta H^m = R \, T \, \chi \, \phi_1 \, \phi_2 \, (x_1 + (V^o{}_2/V^o{}_1) \, x_2) \qquad [1.21]$$

The reduced residual enthalpy of mixing is the interaction energy per mole of interactions divided by the thermal energy whereas the heat of mixing is the energy per mole of solution. The parameter χ is known as the Flory-Huggins interaction parameter and can be found from Hildebrand-Scatchard solubility parameters;

$$\chi = V^o{}_1 \, (\delta_1 - \delta_2)^2 \, / \, R \, T \qquad [1.22]$$

Combining this with the partial molar entropy of mixing from equation [1.19] gives the Flory-Huggins equation;

$$(\mu_1 - \mu_1^o) / R.T = \ln a_1 = \ln \phi_1 + [1 - (V_1^o/V_2^o)] \phi_2 + \chi \phi_2^2 \qquad [1.23]$$

In section 1.6 it was shown that, at constant temperature and pressure, the free energy change of solution must be less than zero to be thermodynamically favourable. From equation [1.23] it follows that there is a corresponding critical interaction parameter, χ^{crit}, below which solution formation is favourable, given by[47];

$$\chi^{crit} = 1/2 [(1/V_1)^{1/2} + (1/V_2)^{1/2})]^2 \qquad [1.24]$$

Thus, the solution behaviour is described in terms of the combination of molecules of mismatched size and an enthalpic interaction parameter that is a dimensionless constant that varies with temperature. This theory is able to approximate the free energy changes in many instances and predict trends in solution behaviour. However, a closer inspection reveals that the entropy and enthalpy terms are a poorer fit to data[50].

1.8a Limitations of the Flory-Huggins Theory

Many solutions exhibit an entropy of mixing similar to that predicted by the theory but the interaction parameter, χ, is often in poor agreement. The temperature dependence of χ may be at variance with that predicted and it may be concentration dependent[49]. Also, the theory is only capable of predicting an UCST and cannot account for the existence of both an UCST and LCST, as found by Freeman and Rowlinson[51] in the polyisobutylene-benzene system.

The major flaw in the theory may be seen as the basis of a pseudo crystal lattice employed. There is no evidence to suggest any fluid conforms to such a crystalline arrangement but evidence exists to the contrary[52]. However, a number of researchers have derived the same expression without invoking the use of a lattice[53]. The variation of the interaction parameter has been tackled, with some success, by

describing it as a power series in terms of composition[49] but it is most usefully dealt with as an empirical parameter describing the free energy of interaction as outlined below.

Instead of splitting the chemical potential into an ideal and an excess contribution we can split it into an athermal and a "residual" part. The first describes the combinatorial entropy contribution, resulting from placement of segments upon the lattice. The second describing the configurational contribution, accounting for the interaction between segments. Thus we can write;

$$\mu_1^R = \mu_1 - \mu_1^{ath} = R \ T \ \phi_2^2 \ \chi \qquad [1.25]$$

where the superscripts R and ath refer to the residual and athermal chemical potential contributions, respectively. Thus, the reduced residual enthalpy of mixing of equation [1.20] is redefined as a "reduced residual chemical potential". We can define corresponding residual enthalpy and entropy terms and their respective contributions to the interaction parameter;

$$\mu_1^R = H^R - T \ S^R = R \ T \ \phi_2^2 \ (\chi^H + \chi^S) \qquad [1.26]$$

Superscripts H and S refer to the enthalpic contribution and configurational entropy contribution to the interaction parameter, respectively. The term "configurational" is employed to distinguish between the combinatorial entropy, arising from placement of segments on the lattice, and entropy arising from the conformational restrictions imposed upon a segment through interactions with adjacent segments. If the system under study is composed of non-polar or slightly polar components the Hildebrand-Scatchard method can be used to find χ^H. Flory[49] reviews such a treatment for polyisobutylene, polystyrene, polydimethylsiloxane, and poly(methyl methacrylate) at 25 °C with various hydrocarbon and chlorinated alkane probes. Guillet and co-workers[54,55] have discussed this approach for gas chromatography results at 30 °C and 75 °C with a variety of stationary phase-probe systems, such as polypropylene-n-octane and poly(ethylene vinylacetate)-chloroform.

Despite the drawbacks outlined above and the existence of several more involved

theories, the Flory-Huggins theory is still widely used in modern analysis of

experimental data due to its comparative simplicity, lack of adjustable parameters and

ability to account for the large deviations from Raoult's law found in polymer

solutions. Also, the advanced, classical theories generally do not offer significantly

improved fits to data in general[49]. The imposition of a lattice was seen not to be

detrimental to the model in itself. However, the approach places restrictions on

molecular and segment size and does not allow for differences arising due to expansion

and contraction with temperature change or volume changes on mixing. Later theories

consider the state of the components and solution.

1.9 EQUATION OF STATE THEORIES

The problem with classical lattice theories is that the volume of a segment is fixed and

it is assumed there is no change in this volume as the temperature changes. However,

this is not the case and, worse, the segments of different components usually exhibit

different expansion coefficients. This problem was approached by Prigogine and co-

workers[56] who introduced the concept of a "cell" model combined with a

corresponding states approach. A segment is allowed to move freely about the centre

of a lattice site and interact identically with adjacent molecules that form a rigid "cage",

or cell. Prigogine employed a Lennard-Jones-Devonshire potential[57] to describe pair

interactions and reasoned that the distance and energy between pairs at a given

temperature was a characteristic, or "hard core", value multiplied by a positional and

energy scalar. Thus the liquid can be described by a characteristic equation of state;

$$P^*.V^* = R.T^*.C \qquad\qquad [1.27]$$

where * denotes hard-core values and C is a constant describing the effective degrees

of freedom which the segments experience within a cell. The actual pressure,

temperature and volume of the system are expressed as a ratio of their respective hard-

core properties. The model invokes a number of assumptions;

i) different components of the solution can be described by the same pair potential,

ii) different components have identical hard-core parameters

iii) the effective degree of freedom in solution is additive for components

iv) a constant number of pair interactions is maintained on changing the temperature.

Hence a solution is modelled in terms of a constant interaction term, a combining of hard-core segments and an expansion term, or "free volume", where the residual chemical potential, equivalent to the expression in equation [1.25], is given below;

$$\mu^R_1 = V^*_1 X_{12} \theta_2^2 [-\tilde{G}(\tilde{T}) + \tilde{T}(\delta\tilde{G}/\delta\tilde{T})\tilde{p}]$$
$$+ P^*_1 . V^*_1 [\tilde{G}(\tilde{T}) - \tilde{G}(\tilde{T}_1) + (\tilde{T}_1 - \tilde{T})(\delta\tilde{G}/\delta\tilde{T})\tilde{p}] \qquad [1.28]$$

where G is the free energy of the system and subscript 1 refers to the pure component. The ~ denotes a reduced parameter given as the measured parameter divided by the hard-core value. The second term describes the free-volume contribution and the first term describes the interaction where X_{12} is the "exchange interaction parameter" and θ_2 is the surface fraction of polymer, given by;

$$\theta_2 = (s_2/s_1)\phi_2/[\phi_1 + (s_2/s_1)\phi_2] \qquad [1.29]$$

where s is the surface to volume ratio of a component.

The equations the theory produces are quite involved but they have been applied to a number of polymer solutions, notably by Patterson and co-workers[58], and the cell model has formed the basis of more advanced approaches. Recently, Dee and Walsh[59] have proposed a modified cell model based on a hexagonal lattice. They show the extra parameters introduced can be approximated by constants found empirically and they claim comparable accuracy to the best lattice models available. However, the cell method is not employed in this report and will not be discussed further.

A similar approach was used by Flory and co-workers[60] a few years later. He rejected the cell model because of the high degree of order it imposed upon the liquid and the difficulty in acquiring the necessary parameters accurately. They argued that

allowing free motion of a segment within a cell was also paradoxical when you then considered the cell and motion for an adjacent segment. By invoking a van der Waals attraction and a hard sphere repulsion for the pair potential he reasoned that their model allowed for the more realistic gas-like properties of a solution as well as being applicable to more general segment shapes. The equation of state derived is given in the reduced form below;

$$\tilde{P}\ \tilde{v}\ /\ \tilde{T} = \tilde{v}^{1/3}/(\tilde{v}^{1/3} - 1) - 1/(\tilde{v}\ \tilde{T}) \qquad [1.30]$$

where $\tilde{v}$-is the reduced segment volume, given by;

$$\tilde{v} = \{1 + [\alpha\ T\ /\ 3(1 + \alpha\ T)]\}^3 \qquad [1.31]$$

where α is the coefficient of thermal expansion. The characteristic pressure is defined by;

$$P^* = \tilde{v}^2\ T\ \gamma \qquad [1.32]$$

where γ is the coefficient of compressibility. Thus, by measuring the compressibility and expansion coefficients and the molar volume at the temperature of interest, the model can be used to obtain the characteristic parameters of the liquid. From equations [1.31] and the molar volume the characteristic volume is obtained and equation [1.32] yields the characteristic pressure. The characteristic temperature is found by substituting $\tilde{P} = 0$ into equation [1.30]. This approach, credited to Flory-Orwoll-Vrij (FOV), offers a reasonably tractable description of solution behaviour. This has led to its use, in original and modified forms, in several works including those involving inverse gas chromatography. The corresponding equation for the residual chemical potential is similar in form to equation [1.28];

$$\mu^R = \chi^*\ R\ T\ \varphi_2^2 = (V^*_1\ X_{12}/\tilde{v})\theta_2^2$$

$$+ P^*_1\ V^*_1\{3\ \tilde{T}_1\ln\ [(\tilde{v}_1^{1/3} - 1)/(\tilde{v}^{1/3} - 1)] + (1/\tilde{v}_1) - (1/\tilde{v})\} \qquad [1.33]$$

where χ^* is the hard-core interaction parameter which may be found in gas chromatography work from the expressions given in section 1.11a by substituting the molar volumes by characteristic volumes.

These early theories suffer from a major drawback. The characteristic parameters should be constant, by definition, but from their inception they were found to vary with temperature[60]. This has led to several advanced lattice and off-lattice theories being developed over the last three decades. These include alternative equations of state, introduction of vacant lattice sites to account for expansion, and consideration of "random walks" of macromolecules in solutions. These approaches are not considered in this present work and the reader is directed to the reviews given in the references[61,62] for further discussion.

Past work concentrated on studying systems that closely matched the assumptions a model employed to allow systematic evaluation of that model. Today, computer generated results using molecular dynamics or Monte Carlo simulations enable individual assumptions in a model to be assessed, and more reports are emerging comparing theory and computer generated data[63].

In recent years a number of comparisons between models have been presented[64] and the general criteria employed is that a theory which is capable of describing P-V-T relationships best over a wide range will contain the assumptions closest to the real system. This is not necessarily the case as employing different models at high and low fluid density may offer the most realistic and closest description to data. Also, in solutions the different components may show the best fit for different models. In this report the FOV theory will be used because it offers a reasonable description of the solution at the pressures studied whilst requiring a minimum number of measured parameters.

1.10 COMPLEX SOLUTIONS

The theories above are based upon non polar components which are randomly mixed in the solution. Many solutions, whilst consisting of non-electrolytes, do not adhere to

the assumptions of the models. This can lead to a number of effects such as clustering or the non-random ordering encountered with solutions involving liquid crystal solutions. These effects have been tackled by considering the enthalpy parameter, the entropy of orientation or by comparing directly with model non-polar systems. Hildebrand[65] pointed out that components exhibiting specific interactions would have a non-polar, random mixing contribution to their overall behaviour with the orienting behaviour superimposed. Hence, in the first two approaches listed we introduce additional parameters to the existing theories.

Hansen[66] first suggested a development of the solubility parameter approach by considering the effect of polar interactions. He proposed the cohesive energy densities could be considered as additive contributions from dispersion and more polar energies;

$$\delta^2 = \delta_d^2 + \delta_p^2 + \delta_h^2 \qquad [1.34]$$

Where the subscripts d, p, h denote contributions from dispersion, polar, and hydrogen bonding energies, respectively. This approach has been employed more recently to analyse solubility parameters of non volatile components using the inverse gas chromatography technique[67].

An alternative approach is to describe the effects of specific interactions in terms of the entropy of configuration. This thesis has already alluded to a number of approaches using this idea. The χ^S, in section 1.8a, and some of the more advanced equations of state, discussed in section 1.9, give an indication of the degree of ordering in solution. Flory and Eichingher[68] also introduced a modification to the FOV exchange interaction parameter;

$$X_{12}^A = X_{12} - Q_{12} \, \bar{v} \, T \qquad [1.35]$$

Where X_{12} is the exchange interaction parameter and superscript A denotes the measured value. The introduction of the second adjustable term Q_{12} means only concentration dependence of a system can be predicted. The thermodynamic

significance of this extra term is unclear but it may be used as an empirical measure of the degree of ordering within a solution.

1.10a Liquid Crystal Theories

One of the earliest models for liquid crystal fluids was that proposed by Maier and Saupe[69] using a mean field approximation applied to rigid rod nematic phases. Equation [1.1] was used to describe the alignment of a nematic phase. They reasoned that the orientational energy for any given molecule of the mesophase, relative to the isotropic phase, was proportional to the molecular alignment multiplied by the average alignment of the neighbours. In their original theory the potential between a pair of molecules was modelled as dipole-dipole interactions. The resulting expression for the Helmholtz free energy of orientation was minimised with respect to the order parameter to obtain equilibrium conditions. The approach has been used, with reasonable success, to determine order parameters as a function of temperature and predict nematic to isotropic transitions. However, the work in this thesis is primarily concerned with the effect the anisotropy of a liquid crystal has upon the measured solution behaviour between a solvent and liquid crystal. Hence, a model that can be compared and contrasted more directly with non-mesomorphic models employed in this work will be used instead. The interested reader is referred to reference 70 for descriptions of the application, modification, and extended models for binary nematic phases of the Maier-Saupe theory.

In the 1970s Chow and Martire[71] developed a self consistent theory for solution behaviour specifically to describe experimental observations for the gas chromatography experiment. They based their theory on the partition function of the probe between the mobile and stationary phase. The infinite dilution activity coefficient was related to the partition functions through the change in free energy of solution and expressions for the activity coefficient and partial molar enthalpy change of solution are given below;

$$\gamma^{\infty} = \left(\frac{1}{Z_s}\right)_{trans} \cdot \left(\frac{Q_g}{Q_s}\right)_{rot} \cdot \left(\frac{Q_g}{Q_s}\right)_{vib} \cdot e^{-1} \qquad [1.36]$$

$$\Delta \overline{H}^{sol} = \Delta E_{pot} + \Delta E_{rot.vib} - R.T \qquad [1.37]$$

where Z and Q are partition functions for configuration and internal energy, respectively. Subscript s refers to the stationary phase and g refers to the gas phase and the partition functions have been split into translational, rotational, and vibrational contributions. E is the internal energy. The first term on the right in equation [1.37] is due to interactions with neighbouring molecules and the rotational and vibrational contributions have been combined. Both energy terms are negative. The model predicts the effect that the three energy contributions have on the observed parameters;

i) Stronger interactions between the probe and stationary phase lower both the translational partition function and the potential energy term.

ii) A greater loss of rotation in the stationary phase increases the second factor in equation [1.36] and lowers the energy term.

iii) A loss of accessible conformations in the stationary phase increases the final factor in equation [1.36] and lowers the energy term.

Thus, effects i) to iii) increase the magnitude of the molar enthalpy of solution but only i) lowers the activity coefficient and results in a more favoured solution.

Chow and Martire used the model qualitatively to describe the observed trends in homologous series of common solvents with p-azoxyanisole (PAA) and 4,4'-dihexoxyazoxybenzene (DHAB). Since then a number of groups have employed the model to describe observations in other systems[72] but it has not been widely used in the literature, possibly because the cruder formalism that "like dissolves like" is often adequate to qualitatively explain many of the systems studied. In chapter 5 the model will be employed to discuss the activity coefficient and enthalpy and entropy data for the cyanobiphenyl systems studied in this thesis. However, for a more quantitative description a more detailed model of the mesophase is required.

Recently, Martire and Yan[73] have presented a theory for the nematic and isotropic

phase of a liquid crystal based upon an earlier lattice treatment[74]. A general liquid

crystal molecule is considered to be composed of a rigid cuboid with a length c and

minor axes a and b. From one or both of the a.b faces a flexible chain may propagate

from one of the corners, and is comprised of cube segments. Martire allows the rigid,

mesogen portions to align with the lattice in any of the three orthogonal directions and

assumes that a "+z" and "-z" alignment are equivalent. Using this approach Martire

presented expressions for the chemical potentials of a probe in both the nematic and

isotropic phase and, thus, could relate them to the activity coefficients. The equations

generated by this model are quite general and Martire[75] considered a range of model

probes with varying linear dimensions in both rigid rod and rigid core-flexible end

stationary phases. The model requires a detailed assignment of molecular dimensions

of both the rigid core of the liquid crystal and the flexible chains as well as an estimate

of the energy required to deform the flexible chain. A number of secondary parameters

defining the order within the solution must be calculated and the final equations are

quite involved. As they will not be used in the present work, the relevant relationships

will not be reproduced here and the interested reader is directed to the references cited.

An alternative liquid crystal model has been proposed by Flory and co-workers who

approached the problem from a consideration of rigid polymer components. In 1956

Flory[76] first presented a modification to his lattice model of polymer solutions to

account for semi-flexible and rigid rod polymer systems. The approach has been

reviewed and refined more recently by Flory and Ronca[77,78]. Although the theory is

not as general as that of Martire in application to solutions of widely different

geometries, it does not suffer the restraints of orthogonal filling of the lattice that Flory

criticised as conceptually unrealistic and of "no apparent advantage" in describing

those systems which could be modelled as rigid cylinders. Flory and co-workers

considered a number of systems including rigid rod solutions[77], identical systems with

orientation-dependent interactions[78], and polydisperse rods in a solvent[79]. The theory

provided semiquantitative agreement with the observed phase behaviour in a number of

systems including poly(p-benzamide) in N,N-dimethylacetamide and

poly(hexyl isocyanate) in tetrachloroethane. The theory has also been applied to

poly(p-phenylene) polymers[80] and recently Brostow and co-workers[81] have

considered polymer liquid crystals in solutions. However, close agreement between

theory and experiment was not achieved and this was attributed to the fact that the

rigid portions of the molecules are only partially rigid. Flory and Irvine[80] considered

the semi-rigid behaviour poly(p-phenylene) exhibits but an alternative semi-rigid

behaviour, more realistic for the materials considered in this thesis, was considered by

Flory and Matheson[82]. The behaviour of a general polymer-solvent system where the

polymer was composed of a fixed number of rigid portions of varying length, governed

by the molecular composition, joined by flexible chains was modelled. This model was

applied by Brotow[83] to a ternary system; poly(ethylene terephthalate)-

p-hydroxybenzoic acid co-polymer, poly(bisphenol-A carbonate) and chloroform.

Although no firm conclusions were drawn about the usefulness of the model it

provided a reasonable description of the phase behaviour.

. Generally, Flory[77] reports that the anisotropic nature of the mesophase is governed

predominantly by molecular shape and size with the interactions between molecules

contributing a perturbation to the liquid. A general polymer molecule is divided into

segments and assigned lattice sites in the manner outlined for athermal solutions in

section 1.7b. This is illustrated in *figures 1.10a* and *1.10b*. However, one of the

lattice axes now coincides with the director of the mesophase and Flory introduces two

extra parameters, η and y. The first denotes the number of segments in a given rigid

sequence, obtainable from the molecular structure, and y is the "disorientation

parameter" describing the number of adjacent rows of a lattice required to

accommodate a rigid portion at an angle ψ to the director. Using this model Flory
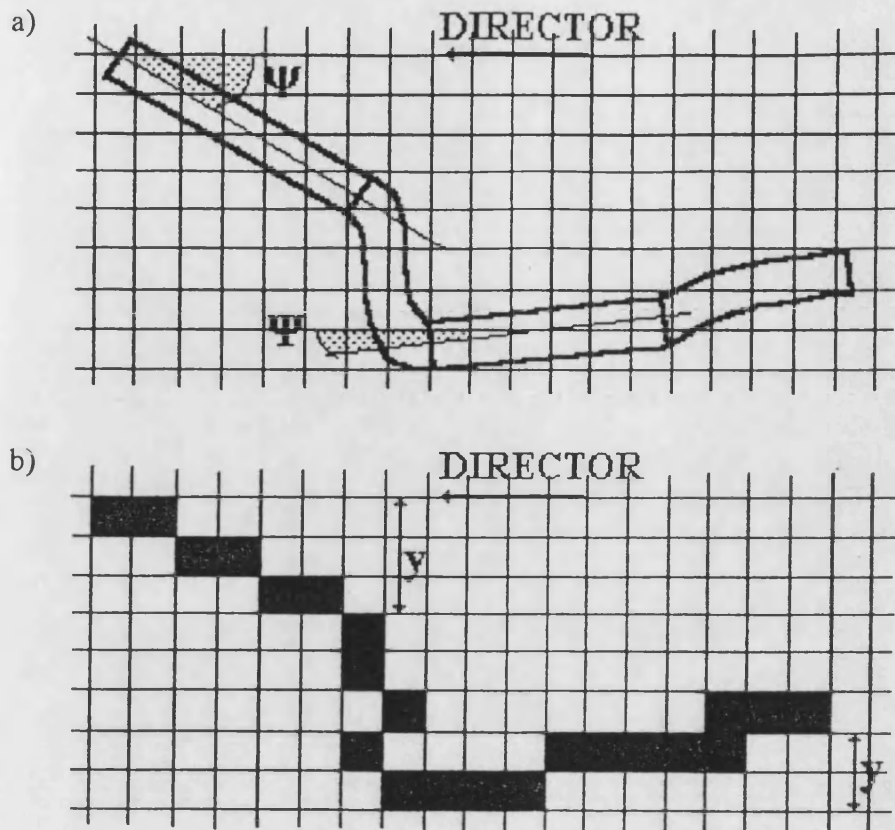
Figure 1.10: Schematic representation of the placement of a semi-rigid molecule on a two dimensional lattice showing a) the true molecular structure and b) the model approximation to that structure.

derived expressions for the activity of the solvent in both the isotropic and anisotropic phases of the polymer;

$$\ln a^i_1 = \ln \phi_1 + [1 - (V^o_1/V^o_2)] \phi_2 + \chi \phi_2^2 \qquad [1.23]$$

$$\ln a^a_1 = \ln \phi_1 + [1 - (V^o_1/V^o_2)] \phi_2 + (2/y) - [1 - \exp(-2/y)] + \chi \phi_2^2 \quad [1.38]$$

where i and a denote the isotropic and anisotropic phases, respectively. Flory was able to show that the disorientation parameter is independent of η and only depends on the proportion of the rigid sequences of the polymer that are aligned, taken as $y \leq \eta$, and at equilibrium y is given as the lower of the solutions of;

$$\exp(-2/y) = 1 - \phi_o^a[1 - (y/\overline{\eta}^a)] \qquad [1.39]$$

where $\phi_0{}^a$ is the volume fraction of aligned, rigid sequences in the polymer and $\bar{\eta}{}^a$ is the average number of segments in the aligned portions of the polymer chain. The theory does not specify a particular type of anisotropic ordering, although a nematic mesophase is often implicitly assumed.

1.11 MEASUREMENT OF ACTIVITY

In the above sections a number of models describing liquid solutions have been outlined but in order to obtain the parameters contained within each model the activity of the components of a solution must be measured, as illustrated in section 1.5b for instance. Techniques employed measure the solvent activity in a solution, obtained from comparison of solvent partial pressure above a solution compared to that above pure solvent, and the parameters for other components can be found from this as outlined in section 1.3, if required.

Solvent activity has been measured using a number of methods and comprehensive reviews are provided by Orwoll[84] and Bonner[85]. The three main approaches used have been osmotic pressure measurement, vapour sorption, and gas liquid chromatography.

Osmotic pressure measurements are usually limited to dilute solutions, particularly in polymer studies where poor solubility and increased viscosity limit the usefulness of this technique. Nehage and Meys[86] managed to obtain values for polystyrene in toluene and cyclohexane up to a higher limit of about 30% polymer composition but the method is usually limited to much lower dilution.

A number of vapour sorption techniques have been employed[84,85]. Ashworth and Price[87,88], for instance, have used three types of vacuum microbalance to study absorption in squalane and polydimethylsiloxane (PDMS) systems. The non-volatile

component is coated as a thin film on an inert particulate support forming part of a balance arm and exposed to solvent vapour atmospheres at various partial pressures. Absorption is monitored as an increase in mass of the coated solid. The technique can be time consuming but a wide range of compositions can be studied with an accuracy typically better than 1% uncertainty. However, the method is usually limited to near ambient temperature studies and values become inaccurate as solvent partial pressure becomes low.

The gas liquid chromatography technique can be used as a pseudo-equilibrium method which relates the retention time of a given solvent to the partial pressure above the stationary phase solution and compares the value to calculated partial pressures above pure solvent under identical conditions. The technique is comparatively more rapid than the above techniques and a wide range of temperatures can be studied. The method is complementary to those above in that the more accurate values are obtained when the solvent composition is small and the majority of work measures activities as the solvent tends to infinite dilution. Condor and Purnell[89] developed the theory to measure finite solvent compositions and Brockmeier *et al.*[90] managed to obtain values for hexane in polyethylene down to 50% composition that they reported were in agreement with static measurements. However, it is the infinite dilution region that generally supplies the most accurate activity values, due to the straightforward model the method employs, and in this region the solubility of the non-volatile component is not a problem which makes it particularly useful for polymer solution studies.

1.12 GAS CHROMATOGRAPHY

Chromatography is an important separation method for mixtures that was first used by Tswett[91] nearly a hundred years ago and the use of gas chromatography has grown rapidly since it was introduced nearly fifty years ago[92,93]. In gas chromatography a non-volatile material is coated onto an inert support contained within a column housed

in a thermostatted oven, "packed column", or coated directly onto the column wall, "capillary column". This thesis employs the former method. The coated support constitutes the "stationary phase". A steady stream of inert gas, such as helium or nitrogen, passes through the column and is termed the "mobile phase". A small amount of volatile solvent is injected at the column head and the mobile phase acts as a "carrier gas" transporting the solvent to a detector at the end of the column. The elution time of a substance from a chromatography column depends upon the degree of partitioning between the mobile and stationary phases and two substances with differing affinity for the stationary phase may be separated. Gas liquid chromatography is a particularly powerful method capable of separating complex mixtures of volatile components.

Since it was first introduced by Martin and James[93], the technique has become one of the most widely used tools in analytical chemistry. Today there are hundreds of commercial stationary phases around and choosing a particular system for a particular separation process may require years of accumulated knowledge on the part of the chromatographer. In the last two decades inverse gas chromatography, (IGC), has also become a widely used method for studying non-volatile materials[94,95] and is estimated to account for a third of the current gas chromatography literature[96]. The term "inverse" has been associated with this work because, unlike analytical gas chromatography, the stationary phase is the unknown and the retention of solvents with known properties are used to characterise the stationary phase.

IGC studies fall broadly into two areas. The technique is used as a characterisation tool for measuring physical properties and solution behaviour of the liquid or the stationary phase is characterised as a potential separation medium. As outlined in section 1.11, the method is rapid and a wide range of temperatures can be accessed. These qualities along with the ready availability and durability of the apparatus makes the method attractive. In solution studies the stationary phase liquid is the major

component of the solution and the mobile, solvent phase is used to probe the stationary phase structure. This is an extremely useful technique in polymer chemistry where it allows quantitative measurement of interactions in a concentration range of considerable industrial importance, which may not be possible by other techniques due to the intractable nature of the polymer. Perhaps this area, more than any other, has been responsible for the large interest in IGC, and the technique is now well established as a characterisation technique for polymers[95]. However, application is not limited to polymers and over the last two decades an increasing number of low molar mass and liquid crystal stationary phases have been studied[17,30].

The major portion of research concentrates on the "infinite" dilution region of the solvent. Here, the probe is injected onto the column in sub-microgram quantities where the retention behaviour is identical to that at vanishingly small concentrations of solvent. More involved descriptions of retention developed for finite solvent compositions are outlined in the previous section but this report concentrates on the former method.

Most of the early work on IGC was involved with the development of the methodology and accounting for vapour non ideal behaviour and pressure dependence of the partition coefficient[97]. Early activity coefficient measurements were compared to the more traditional static measurements of Ashworth and Everett[98] and McGlashan and Williamson[99]. Comparison of techniques suffered from the error in extrapolating static data to infinite dilution of the solvent, and the standard of gas chromatograph equipment available. However, improved static measurements were found to agree closely with those obtained from IGC[100]. There was renewed concern about the accuracy of such parameters when polymer stationary phases were studied. During the 1970s work on polymer stationary phases resulted in conflicting conclusions. For instance, IGC studies of PDMS and polyisobutylene (PIB) by Summers et al.[101] and Hammers and deLigny[102], respectively, were reported to be in good agreement with

static, bulk measurements while Lichtenthaler *et al.*[103] reported values for PDMS that were consistently lower than static measurements. Cheng and Bonner[104] only found agreement within 10% for a poly(ethylene oxide) system. However, more recent studies[88,105] have shown IGC and static data do agree for polymer solutions and meaningful thermodynamic data can be obtained from the former method provided a few simple procedures are followed[95]. Today the method is used in a diverse range of studies.

1.12a Solution Thermodynamics

The primary parameter governing solvent retention is the partition coefficient, K.

$$K = C_{sp} / C_g \qquad [1.40]$$

where C_{sp} and C_g are the concentration of solvent in the stationary phase and gas phase, respectively. The partition coefficient may also be expressed in terms of the measured net retention volume, V_N;

$$K = V_N / V_L \qquad [1.41]$$

where V_L is the volume of liquid coating in the column. Littlewood and *et al.*[106] introduced the parameter "specific retention volume", V_g, as a more fundamental property of the solvent-stationary phase interaction. When this is corrected to standard temperature and pressure it is given the superscript o;

$$V^o_g = (273.2/T) \, (P/760) \, V_N/W \qquad [1.42]$$

P is atmospheric pressure and W is the mass of liquid stationary phase. The pressure is usually close to 760 mmHg and in most reports the pressure quotient is neglected. Hence, the specific retention volume is proportional to the partition coefficient and in many works partition coefficients are not calculated directly. At solvent infinite dilution the activity coefficient, γ^∞, is related to the specific retention volume by[107];

$$\ln \gamma^\infty = \ln \frac{R273.2}{(V^o_g P^o M_L)} - \frac{P^o \left[B_{11} - V^o_1 + J_3^4 \left(2B_{12} - V^\infty_1 \right) \right]}{(RT)} \qquad [1.43]$$

where M_L is the molecular mass of the stationary phase and P^o is the saturated vapour pressure of the probe. B_{11} and B_{12} are the probe and mixed virial coefficients and V^o_1

and $V^{\infty}{}_1$ are the molar volume of the probe and partial molar volume at infinite dilution, respectively. J_3^4 is a correction term for gas compressibility. The mixed virial coefficients are difficult to obtain, although a growing number of measurements are being made using gas chromatography[97]. Close to ambient pressures the correction term for the mixed vapour is the minor correction term. The correction for the molar volume of the probe is also small and may not be additive with the mixed vapour correction term. Thus, for most work it is adequate to use;

$$\ln \gamma^{\infty} = \ln R\ 273.2/(V_g{}^o\ P^o\ M_L) - P^o\ B_{11}/(R\ T) \qquad [1.44]$$

The Flory-Huggins interaction parameter follows directly from equation [1.23] in section 1.8;

$$\chi^{\infty} = \ln \gamma^{\infty} + \ln (V^o{}_2/V^o{}_1) - [1 - (V^o{}_1/V^o{}_2)] \qquad [1.45]$$

As outlined in section 1.5b, we can use the activity coefficient to obtain excess partial molar quantities at infinite dilution;

$$\ln \gamma^{\infty} = (H^E/R\ T) - (S^E/R) = G^E/R\ T \qquad [1.46]$$

We can also obtain the partial molar solution parameters directly from the specific retention volume by considering the relationship between the partial molar free energy and the partition coefficient;

$$\Delta \overline{G}^{\,sol} = -\ R\ T\ \ln K = -\ R\ T\ \ln V_g{}^o - C \qquad [1.47]$$

where C is a constant and follows directly from equations [1.41] and [1.42]. By invoking the Clausius-Clapeyron expression for the saturated vapour pressure[108] and substituting equation [1.46] into [1.44] we can arrive at the expression given below for the van't Hoff isochore;

$$d\ \ln V_g{}^o\ /d(1/T) = (H^E/R) - (\Delta H^{vap}/R) = \Delta \overline{H}^{\,sol}/R \qquad [1.48]$$

where ΔH^{vap} is the enthalpy change of vaporisation and the excess enthalpy is given as the sum of the enthalpy change of vaporisation and partial molar enthalpy change of solution of the probe. Hence, a "van't Hoff" plot of the logarithm of specific retention volume versus reciprocal temperature enables the enthalpy to be determined assuming it is constant over the temperature range studied. The associated entropy change may be found from the intercept of such a plot;

$$\Delta \overline{S}^{sol} = -\Delta S^{vap} + S^E + C' \qquad\qquad [1.49]$$

C' is a constant accounting for the proportionality factor between the partition

coefficient and specific retention volumes and will be discussed further in chapter 3.

Gray[109] and Moegel *et al*[110] have introduced corrections for the curvature in the

plots. The second group considered a liquid crystal nematic phase and proposed the

method for studying the heat capacity changes at infinite dilution. They reported an

improved fit to data by employing a first order approximation but found higher

quadratic temperature terms did not improve the fit and a relatively wide temperature

range was studied. The mesophases in this thesis generally have much narrower

temperature ranges.

A given material may exhibit different phases as the temperature changes. For any

given solvent the partition coefficient is likely to change as the phase changes and the

above arguments illustrate that this would lead to different slopes on a van't Hoff plot.

Smidsrod and Guillet[111] were the first to exploit this method in polymer

characterisation to measure glass transition temperatures and melting points. A typical

polymer van't Hoff plot is shown schematically in *figure 1.11*. The different phases

exhibit linear portions and at the transitions there are gradient reversals. Between A
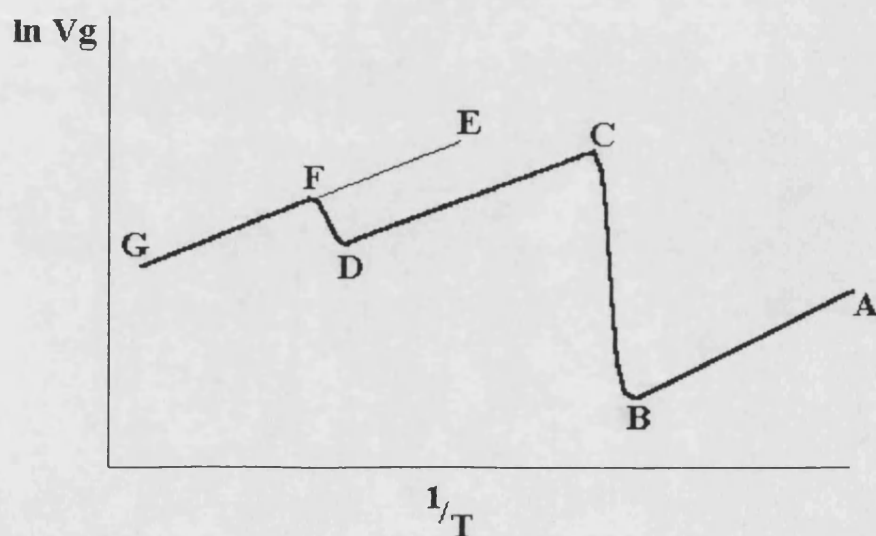
Figure 1.11: Schematic van't Hoff plot for a semicrystalline polymer

and B the polymer is glassy and the partial molar enthalpy change is actually due to adsorption onto the polymer surface. As the temperature is raised, at B the glass transition occurs and Guillet[94] has shown that B to C is a non-equilibrium region where the probe penetration is dependent upon the relative rates of probe diffusion through the polymer and carrier gas flow. By the time the temperature is at C probe diffusion through the stationary phase is sufficiently fast for probe partitioning to reach equilibrium and the linear plot is restored. If the polymer is semicrystalline a further transition occurs at D when the crystallite regions melt and allow the probe to penetrate through all the stationary phase. Between F and G only the isotropic liquid is present. Guillet and co-workers[112,113] compared the hypothetical retention of the isotropic liquid below the melting point, given by F to E, against the retention between F to D to C as a means of estimating the degree of crystallinity in the polymer;

$$\% \text{ Crystallinity} = 100[1 - (V^o_g/V^o_g{}')] \qquad [1.50]$$

$V^o_g{}'$ is the hypothetical specific retention volume given by line FE. Guillet pointed out that IGC does not suffer from inaccuracy arising from surface energy effects of different sized crystal regions[114]. Stein *et al*[115] used this estimation to study the crystallisation kinetics in quenched polyethylene samples and recently Al Saigh[116] used the technique to obtain interaction parameters between poly(ethyl methacrylate) and a semicrystalline poly(vinylidene fluoride).

1.12b Polymer Solutions

IGC quickly found uses characterising glass transitions, crystallisation and evaluating probe polymer interactions at infinite dilution. However, calculation of the activity coefficients presented problems in polymer solutions. Equation [1.44] requires an accurate mass for the determination of the molar activity coefficient. Often this is not known for polymer solutions and all synthetic polymers pose the added problem of polydispersity. Also, early work on long chain alkane stationary phases[117] gave activity coefficients which became increasingly dependent on molecular mass as the chain length increased, which was at variance with the asymptotic behaviour of the

observed physical parameters. Patterson *et al.*[117] circumvented this problem by introducing a weight activity coefficient, Ω, which better describes the observed behaviour of the solutions;

$$a = \gamma x = \Omega w \qquad [1.51]$$

where w is the weight fraction of a component. The weight activity coefficient has become the most widely used parameter in IGC but any coefficient that is not coupled to the number of moles of the stationary phase component can be used, such as the volume activity coefficient[118]. Where the probe tends to infinite dilution the relationship between the weight and molar activity coefficients is given by;

$$\Omega = \gamma (M_L/M_1) \qquad [1.52]$$

Thus, the weight activity is obtained from equation [1.44] by substituting the molar mass of the stationary phase for the molar mass of the probe, M_1. From equation [1.45] it follows that the Flory-Huggins interaction parameter at infinite dilution is given by;

$$\chi^\infty = \ln \Omega^\infty - 1 + (V^o_1/V^o_2) + \ln(M_1 V^o_2/M_L V^o_1) \qquad [1.53]$$

Over the last two decades there has been a vast increase in the number of studies of polymer solutions by IGC. This ranges from the early studies on PDMS based stationary phases, widely used in analytical columns[119], to a host of polymers such as polycarbonates, polyesters, and synthetic rubbers with applications outside chromatography[95]. Early studies concentrated on reconciling solution parameters with other methods of measurement, as discussed in section 1.11, and investigations of reproducibility. In particular, Lichtenthaler *et al.*[120] compared the behaviour of packed and capillary columns with PIB stationary phases. The packed column method results in larger liquid surface areas. Discrepancies between columns were attributed to slow diffusion of the probes arising from the thickness of PIB films. The problem is resolved by measuring retention at a series of flowrates and extrapolating to zero. Concern over the method of extrapolation has been voiced[30] but the approach works where the retention dependence approximates linearly to the flowrate. This has now become a standard procedure where such behaviour occurs. Later studies have

employed IGC as an established characterisation technique for comparison with solution theories. Recent work, outlined in the next section, has concentrated on binary stationary phases and reconciling the dependence of interaction parameters between stationary phase components on the probe molecule used.

The gas chromatography technique is not limited to studies on bulk adsorption. De Vries and co-workers[121] were among the first to apply the technique to determine adsorption isotherms of polymers using cellulose acetate as the stationary phase. The amount adsorbed and the partial pressure above the surface can be extracted from the area under the chromatogram and the run conditions. The method has recently been used by Manuel Sa and Sereno[122] and Kontominas and co-workers[123] to study polyamide and polystyrene systems, respectively. Gas chromatography is also frequently used to characterise polymer surface interactions directly. Recently, for instance, Schreiber and co-workers[124] have characterised surfaces of polycarbonate and polystyrene-polybutadiene co-polymer in terms of their specific and dispersion interactions with a series of hydrocarbon and polar probes.

As a last example of IGC application to polymers, Guillet and co-workers[125] have developed the method to measure polymer solubility parameters. Despite the fact that these only offer a rough guide to miscibility, solubility parameters are still widely used commercially. However, the low volatility of polymers precludes direct measurement. Guillet used the description of the Flory-Huggins interaction parameter as a residual free energy, section 1.8a (equation [1.26]), and described the enthalpy contribution according to Hildebrand-Scatchard theory, section 1.8 (equation [1.22]). By measuring the interaction parameter, χ^{∞}, for various probes with differing solubility parameters he used the expanded equation below to extract the polymer solubility parameter;

$$(\delta_1^2/R\ T) - (\chi/V^o_1) = (2\ \delta_2/R\ T)\ \delta_1 - [(\delta_2^2/R\ T) + (\chi^S/V^o_1)] \qquad [1.54]$$

where χ^S is the residual entropy contribution and 1 and 2 refer to probe and polymer, respectively. A plot of the left hand side against the probe solubility parameter yields the polymer solubility parameter from the gradient and the entropic contribution to the interaction parameter from the intercept, where the gradient and intercept are equal to the expressions given in bold. This approach was recently reviewed by Price[126] and has been extended to other non volatile stationary phases[127].

1.12c Binary Polymer Stationary Phases

Since Deshpande *et al*[128] first suggested IGC as a means of studying polymer-polymer interactions there has been a large number of studies of stationary phases where a polymer forms one or both components of a binary mixture as well as co-polymers[129]. The majority of the research on interactions in blends has concentrated on probe dependence whilst other work has concentrated on retention volume prediction for separation applications.

Prediction of retention volumes where mixed stationary phases are used is an important field of research. The aim is to reduce the number of stationary phases necessary to a set of standards which can be mixed to meet individual separation requirements. This area was reviewed in the late 1980s by Price[130]. If a system is set up with care, a mixture of stationary phases coated onto separate supports will behave identically to a system with two columns in series containing the equivalent amount of pure stationary phases. Their retention can be described in an additive manner from the retention behaviour of the pure components, for example;

$$V_g = V_{g2}\, w_2 + V_{g3}\, w_3$$

$$K = K_2\, \phi_2 + K_3\, \phi_3 \qquad\qquad [1.55]$$

where w and ϕ are, respectively, the weight fraction and volume fraction of the stationary phase components 2 and 3. A number of modifications, accounting for interactions, have been derived when the stationary phase is prepared by coating support from a solution of both components. Generally. these offer a better

description of retention unless the components are very similar or they do not blend at all. Purnell and Laub[131] found that the partition coefficient expression in [1.55] gave a reasonable approximation to the data in all cases. They developed this approach into the "windows diagram" determination of optimum column performance for a given separation and have demonstrated the power of their approach in a number of binary systems.

A number of methods can be employed to determine interaction parameters between binary solutions[132]. IGC offers a potentially rapid method but values have been found to be probe dependent. First, the interaction parameter is defined per mole of probe so that when we have two stationary phase components of differing size the interaction parameter defined with respect to each component will be different, that is $\chi_{23} \neq \chi_{32}$. However, we can write[132];

$$\chi_{23}/V^o_2 = \chi_{32}/V^o_3 = B_{23}/R\,T \qquad [1.56]$$

where B_{23} is the energy density parameter. The interaction parameter of the probe with the binary stationary phase, $\chi_{1(23)}$, can be calculated in a similar manner to a one component system outlined in section 1.11a[129];

$$\chi_{1(23)}{}^\infty = \ln\,[273.2\,R(w_2\,v_2 + w_3\,v_3)/(V_g{}^o\,P^o\,V^o_1)] - P^o\,B_{11}/(R\,T)$$

$$-[1-(V^o_1/V^o_2)]\,\phi_2 - [1-(V^o_1/V^o_3)]\,\phi_3 \qquad [1.57]$$

where v_2 and v_3 are the respective segment volumes, from the molar volume divided by the number of lattice segments a molecule occupies. From this and the interaction parameters for the pure components we can find the interaction parameter between stationary phase components[129], χ_{23};

$$\chi_{1(23)}{}^\infty = \phi_2\,\chi_{12}{}^\infty + \phi_3\,\chi_{13}{}^\infty - \phi_2\,\phi_3\,\chi_{23}(V^o_1/V^o_2) \qquad [1.58]$$

The corresponding "hard core" values can be obtained in a similar fashion by replacing volumes with their respective "hard core" volumes and volume fractions with site fractions, where a site is the volume occupied by one "hard core" segment.

The probe dependence of the stationary phase component interaction parameter has been tackled in a variety of ways. One method is to quote an average of values obtained but this is not very satisfactory. Su and Patterson[133] suggested the differences arise due to differences in the pure component interaction parameters and suggested using probes that exhibit similar values in the pure components. Shi and Schreiber[134] have found less probe dependence in immiscible blends by considering the role of adsorption. Horta and co-workers[135] and Sanchez and co-workers[136] have adapted equation of state approaches to account for the non-additivity of the residual free energy whilst Chee[137] has used the solubility parameter method of Guillet to decouple the interaction parameter from residual entropy effects. These approaches were recently reviewed by Farooque and Deshpande[138] who also introduced their own simplified approach. They rearranged equation [1.58] and plotted the left hand side of the expression below against the difference between the pure component interaction parameters reduced by probe volume;

$$(\chi_{1(23)} - \chi_{13})/V^o{}_1 = \phi_2 \cdot (\chi_{12} - \chi_{13})/V^o{}_1 - \phi_2 \, \phi_3 \, \chi_{23}/V^o{}_1 \qquad [1.59]$$

where ∞ has been omitted for clarity. The expressions in bold may be extracted from the slope and intercept. Thus by knowing the probe molar volume and stationary phase composition the stationary phase interaction parameter can be evaluated. The gradient gives a measure of the effective volume fraction the probe experiences. The methods of Farooque and Deshpande and of Chee were found to give better interpretation of the polystyrene-polybutadiene system studied than the more rigorous molecular arguments. Etxeberria *et al.*[139] have compared this simplified method and that of Horta and co-workers to other polymer systems and find the two methods are in good agreement. However, they caution that the uncertainties in the parameters obtained are relatively large in both cases. The values found by IGC are comparable with those found by other methods[132], such as vapour sorption and scattering techniques.

Although the above examples constitute the bulk of IGC work on polymer blends and mixtures other applications exist. Another, for example, is highlighted by Galin and co-workers[140] who used the technique to estimate the size of glassy domains in rubbery polymers. They considered the contributions from adsorption on the glass and absorption in the rubber were additive and that the respective partition coefficients remained constant. The adsorption retention was defined as;

$$V_g^{gl} = K^{gl}/A^{gl} \tag{1.60}$$

where K is the partition coefficient and A is the total surface. If K is known A can be found allowing domain size to be estimated. Although the technique suffers from inaccuracy where partial miscibility occurs, it is an important method for studying micro structure in composites.

1.13 LIQUID CRYSTAL STUDIES BY IGC

The majority of IGC studies on liquid crystals have evaluated thermodynamic characteristics for analytical stationary phase use. The importance of liquid crystals as stationary phases stems from their mode of separation of analytes. Most conventional stationary phases rely on the analyte exhibiting differing degrees of solubility in the supported liquid, or differing extents of adsorption on solid stationary phases. In non-polar systems this is governed by the relative partial pressures and thus analytes with close boiling points become difficult to separate. Where the analytes are enantiomers stationary phases which separate via complexation or inclusion mechanisms are employed[141]. Liquid crystals offer a fourth alternative of separation by shape selectivity.

To be useful as a stationary phase a liquid crystal must exhibit good separation of analytes, have reasonable column efficiency, and have a wide mesophase range to allow temperature programming. Generally these requirements are best met by the nematic phase[142], although a number of smectic and cholesteric phases have been

used[143]. Martire and co-workers[144] were the first to characterise liquid crystal

mesophases according to thermodynamic parameters in a series of papers which

included the study of the effects of column loading on separation behaviour. Since

then Witkiewicz and co-workers[145] have carried out a more detailed study of the

effects of coating onto diatomaceous supports. Kelker[146] first recognised mesophases

were good stationary phases for geometric isomer separation and managed to resolve

all three xylene isomers. Since then mesophases have been widely applied to

environmentally important separations of poly(chlorinated biphenyl)s, (PCBs), and

poly(aromatic hydrocarbons), (PAHs), where resolution of non-carcinogenic

compounds and carcinogenic compounds with similar boiling points is possible. In

recent years the N,N'-bis(p-alkoxybenzylidene)-α,α'-bi-p-toluidene homologues

developed by Jannini and co-workers[147] have become the most widely used nematic

phases in separation work by virtue of their large mesophase range and stability to

high temperatures. Since mesophases were first used in gas chromatography the

existence of supercooled regions, on cooling between the nematic and crystalline

phases, have been observed in many systems. These can exhibit stability for up to

several months[148] and this supercooled region can be used to extend the useful

operating range of the mesophase[149].

Martire and Chow[71] developed a model for the activity coefficient of a probe in a

mesophase molecule, based upon internal energy changes upon forming a solution, and

this has been discussed in section 1.10a. The approach has been employed by a few

groups to discuss solutions in terms of solvent restriction within a mesophase[72] but has

not been widely used. In recent years Martire and co-workers[73,75] developed the

theory into a more rigorous statistical mechanical model based on a perturbation

theory as described in section 1.10a. Bocquet and Pommier[150] extended the technique

to finite concentration and proposed a retention model based on a mesophase

composed of both nematic and isotropic portions. Recently Coca and

co-workers[151] applied the classical Flory-Huggins theory to mesophases with non-mesomorphic probes to account for the difference in sizes of the respective molecules. In recent years attention has shifted from the characterisation of cholesteric and nematic mesophases important in separations to more general characterisations. Martire and co-workers[152] have studied a series of alkylcyanobiphenyl molecules, important in LCDs, characterising them in terms of activity coefficients and the associated enthalpies and entropies associated with the solution process. Work has now begun on the alkoxycyanobiphenyl molecules[153,154], often blended with the alkylcyanobiphenyl molecules in LCDs[155] to improve the display characteristics.

Mixing liquid crystals to obtain eutectic compositions, where the mesophase range is increased, has been exploited almost since the emergence of the first LCDs[155]. This method can also be used to extend the mesophase range to separations at lower temperatures, where it is generally possible to get improved performance[149]. An alternative way of extending the mesophase range and developing stationary phases with potentially higher thermal stability is to use polymeric liquid crystals. Side chain liquid crystal polymers (SCLCPs) are used in preference to polymers with the mesogen within the backbone (MCLCPs) to preserve as much of the ordered separating phase as possible. Over the last decade a growing number of these materials have been studied, particularly by the groups of Jannini and Laub[156]. The majority of work employs a siloxane backbone with mesogen side groups (MEPSILs) due to the flexibility of the main chain. However, acrylate polymer backbones have also been studied[157] (MEPCRYLs) and comparable separating performances noted but they have not yet gained the same popularity as MEPSILs. To date characterisation has concentrated on chromatography behaviour within the mesophases, although the IGC technique also allows the phase transitions to be measured with comparable accuracy to more conventional methods[154]. Most recently Guillet and co-workers[158] have applied IGC to the characterisation of main chain polyesters but few polymeric liquid crystals (LCPs) have been studied. Despite a large number of studies on blends and

mixtures of liquid crystals and LCPs with each other and low and high molecular mass additives[159], very few blends have been studied by IGC. However, work by Jannini *et al.*[160] on MEPSIL and poly(dimethylsiloxane) blends for fatty acid methyl ester (FAME) and PAH separation illustrates the potential synergistic separating power of such blends.

1.14 COMPLICATIONS WITH IGC

Previous sections have already eluded to some of the considerations necessary to obtain true equilibrium values for retention at infinite dilution in the bulk solution. Where diffusion through the stationary phase is slow compared to carrier gas flowrate a series of readings at different flowrate are extrapolated to zero flowrate. To ensure work is at injected volumes approximating to infinite dilution the independence of retention on injected volume can be tested. This is a simplified picture of the retention process. In section 1.12c the estimation of glassy domain surface area within a glassy polymer-rubbery polymer blend was shown to be determinable from consideration of adsorption from the glass and absorption from the rubber. However, the supported stationary phase also presents the possibility of adsorption at the support-stationary phase and gas-stationary phase interface. A further assumption is that the carrier gas does not absorb in the stationary phase. Dissolution in a stationary phase-carrier gas mixture may differ from dissolution in the pure stationary phase. The last assumption is considered reasonable as carrier gas solubility is generally negligible[97]. The adsorption effects cannot be so easily dismissed.

Adsorption at the gas-stationary phase interface was first suggested and observed by Martin[161] for hydrocarbon probes on a polar stationary phase. His findings were supported by static measurements of Martire *et al.*[162] who also encountered support-stationary phase adsorption effects. Similar effects were noted for polar probes on hydrocarbon stationary phase. Martin proposed a model where adsorption and absorption act independently and are additive;

$$V_N = K_B V_L + K_G A_G \qquad\qquad [1.61]$$

K_B and K_G are the bulk and liquid-gas interface partition coefficients, respectively, and A_G is the surface area of the interface. The surface partition coefficient is defined with the unit of area. Where adsorption occurs at the solid-liquid interface a similar approach is used and a general retention equation is given by[163];

$$V_N/V_L = K_B + [(K_S A_S) + (K_G A_G)]/V_L \qquad\qquad [1.62]$$

Where the extra K and A terms refer to the support-stationary phase interface. Hence the true partition coefficient for the bulk, stationary phase liquid can be obtained from the intercept of a V_N/V_L, or V_g, versus $1/V_L$ plot. Where both types of adsorption are present and the gas-liquid interface varies significantly, and can be accurately determined, the individual contributions to retention may be determined from plots of *SLOPE*/A_G versus $1/A_G$. Thus, it is seen that constant, infinite dilution specific retention values, are indicative of negligible adsorption effects. Support-liquid adsorption can be particularly significant in packed columns, where the ratio of bulk volume to surface area is high.

Adsorption can effect retention in two ways. The specific retention volume can vary with the amount of stationary phase coated onto the support. Also, where adsorption occurs at specific sites, the probe can be retained longer leading to peak tailing and a decrease in retention as the injected volume increases. To circumvent these problems retention may be measured on several columns with different amounts of stationary phase and extrapolated to infinite loading, as above. An alternative is to use an amount of stationary phase which is large enough to reduce the adsorption contributions to insignificant levels. Several studies on polymer and liquid crystal stationary phases in packed columns report this is possible where the coating is above 5% to 7% of the total packing mass[164]. However, Munk *et al.*[165] propose that much higher coatings are necessary.

When the support surface is non-polar the high concentration of stationary phase competes for adsorption with a negligible concentration of a hydrocarbon probe resulting in the support surface being masked from the probe. When the support surface contains polar adsorption sites, as found with the diatomaceous supports commonly used in chromatography, the same may occur when the stationary phase is polar. However, as probes get increasingly polar they may be preferentially adsorbed at the support interface and retention will be affected. Such supports are usually reacted with dimethyldichlorosilane to eliminate polar silanol groups on the support surface[166]. This reduces the surface tension of the support and hence probe retention. On such a support the stationary phase may not wet the surface as readily. Witkiewicz[167] has illustrated this with scanning electron micrographs (SEMs) of a cholesteric liquid crystal. As probe molecules are not in competition for adsorption sites on the uncoated support the partition coefficient may be different from that of the covered support and the resultant contribution to retention may be higher. The extent of support coverage by the stationary phase and the contribution of the support to retention has been the subject of debate over the last two decades. Munk and co-workers[165] suggest the support effect should be taken as additive at any loading and must be subtracted from the measured retention to obtain the bulk liquid value. Gas-liquid interface adsorption is assumed negligible. Conversely, Conder et al[168] have studied polar probe retention on squalane and report a temperature independent transition to complete wetting of the surface close to 7% stationary phase loading. Studies by Witkiewicz and co-workers[145] on liquid crystal stationary phases support complete surface wetting above a limiting column loading. Generally, the gas chromatograph method is considered to provide true equilibrium retention for the bulk phase if the chromatogram peaks are symmetrical, obtained on columns with reasonably high loading, and at injected volumes of probe sufficiently high to minimise adsorption effects whilst remaining in the infinite dilution region.

Liquid crystal stationary phases present a further complication. The retention may be an equilibrium value at infinite dilution, for the bulk liquid only, but the bulk liquid in the thin surface coated films may be different due to the surface inducing long range ordering effects within the liquid. Chow and Martire[169] compared IGC and differential scanning calorimetry (DSC) studies on two azoxy liquid crystals and reported no measurable adsorption effects from either interface above a film thickness of 100 nanometers. Witkiewicz[170] reported surface orientation up to a depth of 2 nanometers and in later work reported constant specific retention volumes above a stationary phase loading of above 5%[145]. Haky and Muschik[171] report surface effects which lower transitions in a binary liquid crystal blend. The loading used is below the reported limits given above and at present there are no studies to confirm or refute the extent of support effects in liquid crystal blends. Generally it is accepted that coated liquid crystal phases behave identically to bulk liquid crystal above a minimum loading, in a similar manner to other stationary phases already discussed.

1.15 CRYSTALLISATION KINETICS

Gas chromatography has been used very little to study the kinetics of crystallisation of the stationary phase liquid. Stein et al.[115] used the technique to follow crystallisation in quenched polyethylene samples but they did not attempt to fit data to a model. It is more usual to observe crystallisation directly using optical methods[172] or to employ DSC[173,174] or dilatometry[175].

The common method used to interpret crystallisation is that developed by Avrami[176] which relates the fraction of crystalline material, F^c, to time, t, by;

$$(1 - F^c) = \exp{-(K\,t^n)} \qquad\qquad [1.63]$$

where K is effectively a rate constant and n is the Avrami exponent representing[177] the sum of growth dimensions (1 for rods, 2 for discs, 3 for spherulites) and the order of time dependence of nucleation (0 for instantaneous and 1 for sporadic growth). The

value of n should theoretically be an integer but the presence of concurrent mechanisms can lead to fractional exponents. The model assumes crystallisation is isothermal, nucleation occurs at random sites throughout the sample, and growth rate is linear with time. The method can also be used to describe other ordering processes.

A number of studies have considered ordering kinetics in low molar mass liquid crystals. Price and co-workers[175], for instance, have studied the kinetics of ordering on forming the crystalline phase and mesophases of a number of cholesteric materials. More recently the Avrami method has been employed to interpret ordering in main chain liquid crystal polymers (MCLCPs)[178] of polyethers, polyesters and polyphosphazene materials. Generally, Avrami exponents between 2 and 4 have been reported. However, Cheng and Wunderlich[179] have observed values between 0.2-0.8 for n in some thermotropic copolyesters which has lead to them introducing a modified Avrami type expression to describe the ordering process.

Cheng suggested that two particular effects could lead to very low exponent values. Crystallisation from a viscous medium, so called "cold crystallisation", could restrict crystal growth due to poor mobility of the higher temperature phase. Also, where nucleation commences rapidly but the growth sites become inhibited as time progresses the effective Avrami exponent may be very low. Cheng introduced parameters m and a to account for the above effects, respectively, and recast equation [1.61] as;

$$\ln(-\ln(1 - F^c)) = \ln K^* + (n(m + 1) + a)\ln t \qquad [1.64]$$

where K^* is the effective rate constant but is different from K in equation [1.63]. The value m is less than 0 and the value a less than 1. When the ordering process is diffusion controlled the value of the apparent Avrami exponent is predicted to be 0.5, 1, or 1.5 for one dimensional, two dimensional, and three dimensional growth respectively.

1.16 THIS WORK

In this work the use of IGC to characterise the behaviour of liquid crystal systems is extended to consider cyanobiphenyl low molar mass and oligomeric systems and a prototype chiral material. Initially the technique has been used to study phase behaviour and the results compared to DSC measurements. IGC has also been used to study crystallisation kinetics for one of the low molar mass cyanobiphenyls and the results interpreted using the Avrami method. The observed thermodynamics of solution formation at probe infinite dilution are discussed qualitatively using the model of Chow and Martire. The various solution models discussed above have been applied to these results to enable a discussion of the role of probe-liquid crystal interactions in the solution forming process and the implications about the mesophase structure discussed. The thesis concludes by considering how introduction of a second, polymer component to the stationary phase affects the liquid crystal behaviour. The results are discussed both in the context of the binary stationary phase effect on the chromatography and in terms of the liquid crystal-polymer miscibility, by employing the method of Deshpande and Farooque to quantify the interaction.

CHAPTER 2

EXPERIMENTAL

2.1 MATERIALS

All liquid crystals were supplied or donated by MerckUK (Poole). The liquid crystals 4-(n-hexyloxy)-4'-cyanobiphenyl (HCB) and 4-(n-octyloxy)-4'-cyanobiphenyl (OCB) were reported as 99.5% pure. The polysiloxane based, random co-polymer, (LCP), was polydimethylsiloxane with a quarter of the methyl groups substituted by a p-(cyanobiphenyloxy)-p-butylene mesogen. The quoted purity was >99.85% with <3% of the "Si-H" bonds unreacted and the average number of repeat units was given as 40. The chiral liquid crystal 4-(n-octyloxy)biphenyl 4'-(sec-octyloxy)-benzoate (OBIB), was a prototype donated by MerckUK. *Figure 2.1* shows the structures of these liquid crystals along with transition temperatures quoted by the suppliers.

HCB

$C_6H_{13}O$ — CN

4, 4' (n - hexyloxy) cyanobiphenyl

$$K \xrightarrow{57} N \xrightarrow{75.5} I$$

LCP

$(CH_3)_3Si$ — Si — O — Si — O — $Si(CH_3)_3$, with CH_3, CH_3, $(CH_2)_4$, CH_3, O — CN

poly[dimethyl - co - methyl 4,4' (butyloxy-cyanobiphenyl) siloxane]

$$Glass \xrightarrow{-3.9} S_A \xrightarrow{79.1} I$$

OCB $C_8H_{17}O$ — CN

4, 4' (n - octyloxy) cyanobiphenyl

$$K \xrightarrow{54.5} S_A \xrightarrow{67} N \xrightarrow{80} I$$

OBIB $C_8H_{17}O$ — O — O — C_6H_{13}, with CH_3

4,4' - octyloxy biphenyl (4 - isooctyloxy) benzoate

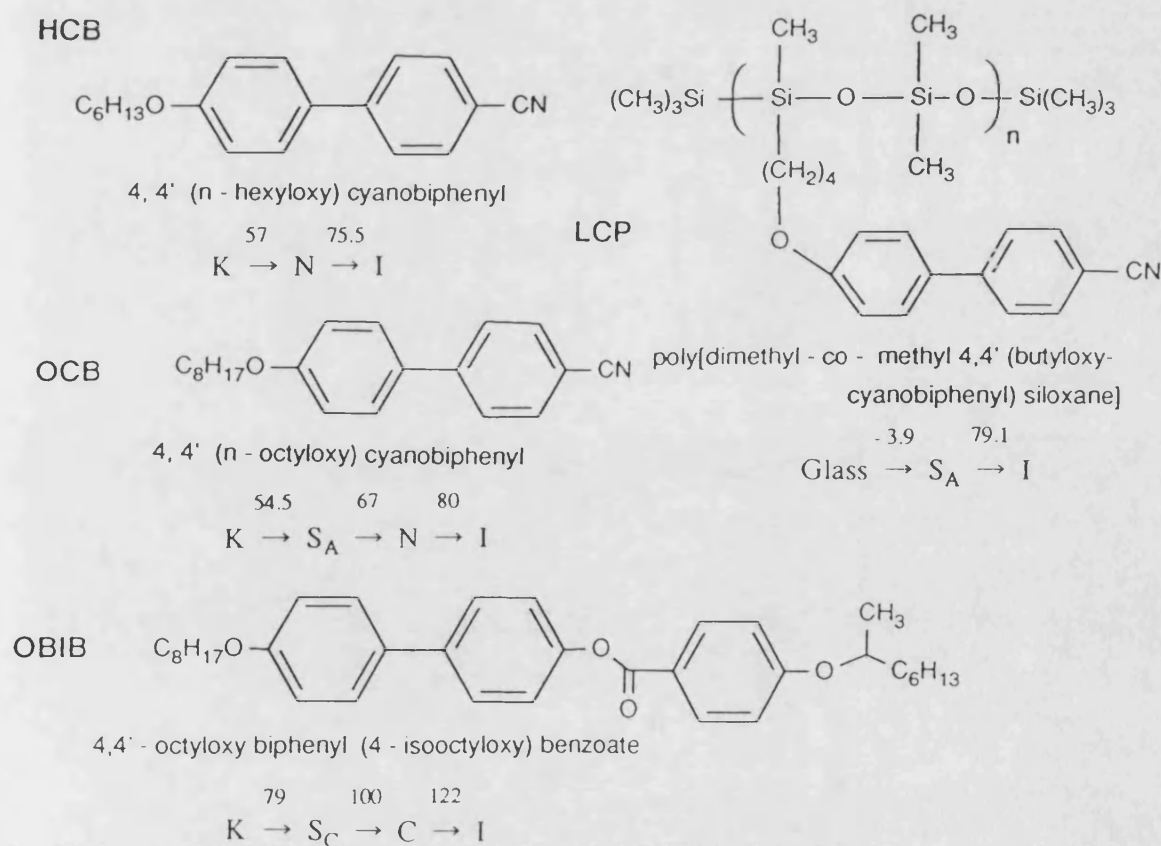$$K \xrightarrow{79} S_C \xrightarrow{100} C \xrightarrow{122} I$$

Figure 2.1: Liquid crystal structures and expected phase transitions (°C)

DSC thermograms are given in *figure 2.2* and NMR spectra shown in *figures 2.3* to *2.6*. These corroborate the quoted purities from the suppliers and show OBIB was of a comparable purity to the other materials. All liquid crystals were used as received.

The polydimethylsiloxane (PDMS) was a high fractionation sample of a broad polydispersity polymer from Dow Corning. The NMR spectrum is shown in *figure 2.7*. LCP and PDMS were characterised by gel permeation chromatography using a Bruker LC41 system with a 60cm Polymer Laboratories PLGel column, polystyrene standards, and toluene as the solvent at 25 °C. The results are given in *table 2.1*.

Table 2.1: Data from GPC characterisation

	PDMS	LCP
M_n	24120	3800
M_w	92670	6260
γ	3.84	1.65

The Mark-Houwink relationship[180] can be used to relate the effective polystyrene molar mass of PDMS, M_{PS}, to the true molar mass, M_{PDMS};

$$K_{PS}M_{PS}{}^{a_{PS}} = K_{PDMS}M_{PDMS}{}^{a_{PDMS}} \hspace{3cm} [2.1]$$

where K and a are constants and the subscripts denote values pertaining to different polymers. The molar mass of PDMS was calculated to be 37930 from literature values[181] of K and a (Polystyrene: K=7540 cm^3/g, a=0.783 PDMS: K=21500cm^3/g, a=0.65). Strictly the approach is an approximation as individual mass fractions within the mass distribution should be converted and the results averaged. However, the approximation yields a molar mass closer to the true value than the polystyrene equivalent.
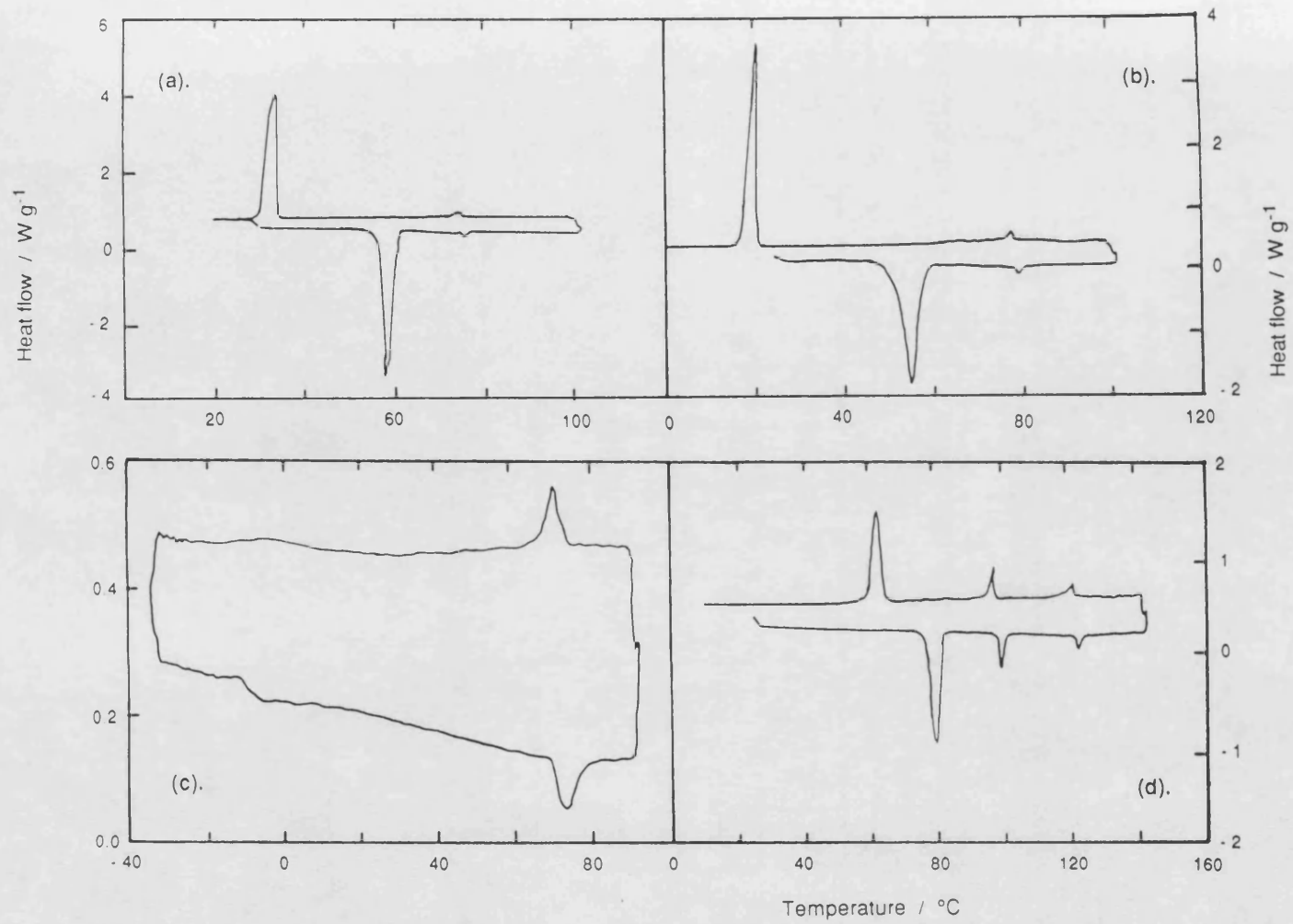
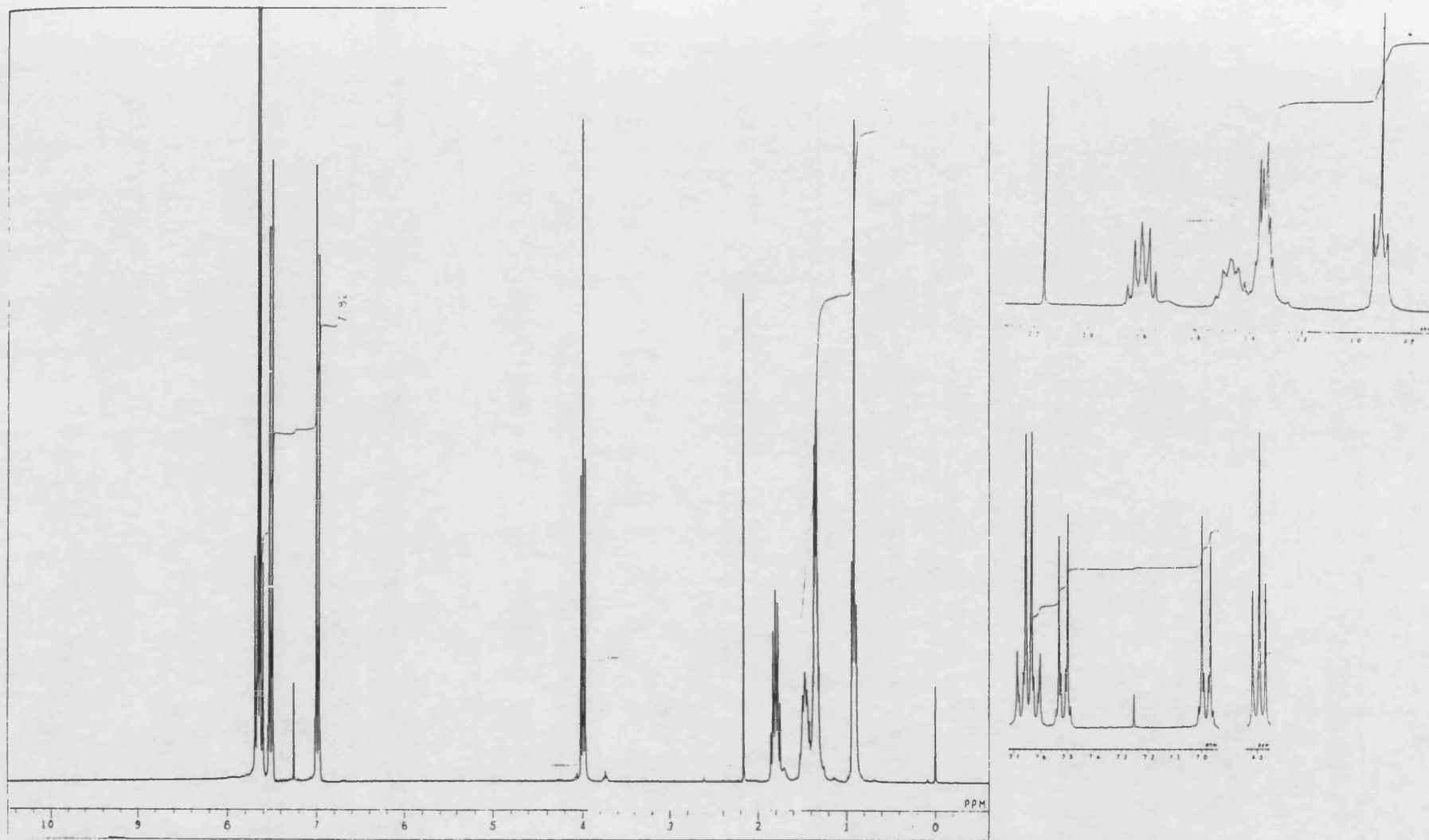**Figure 2.2:** DSC thermograms for a) HCB, b) OCB, c) LCP and d) OBIB.
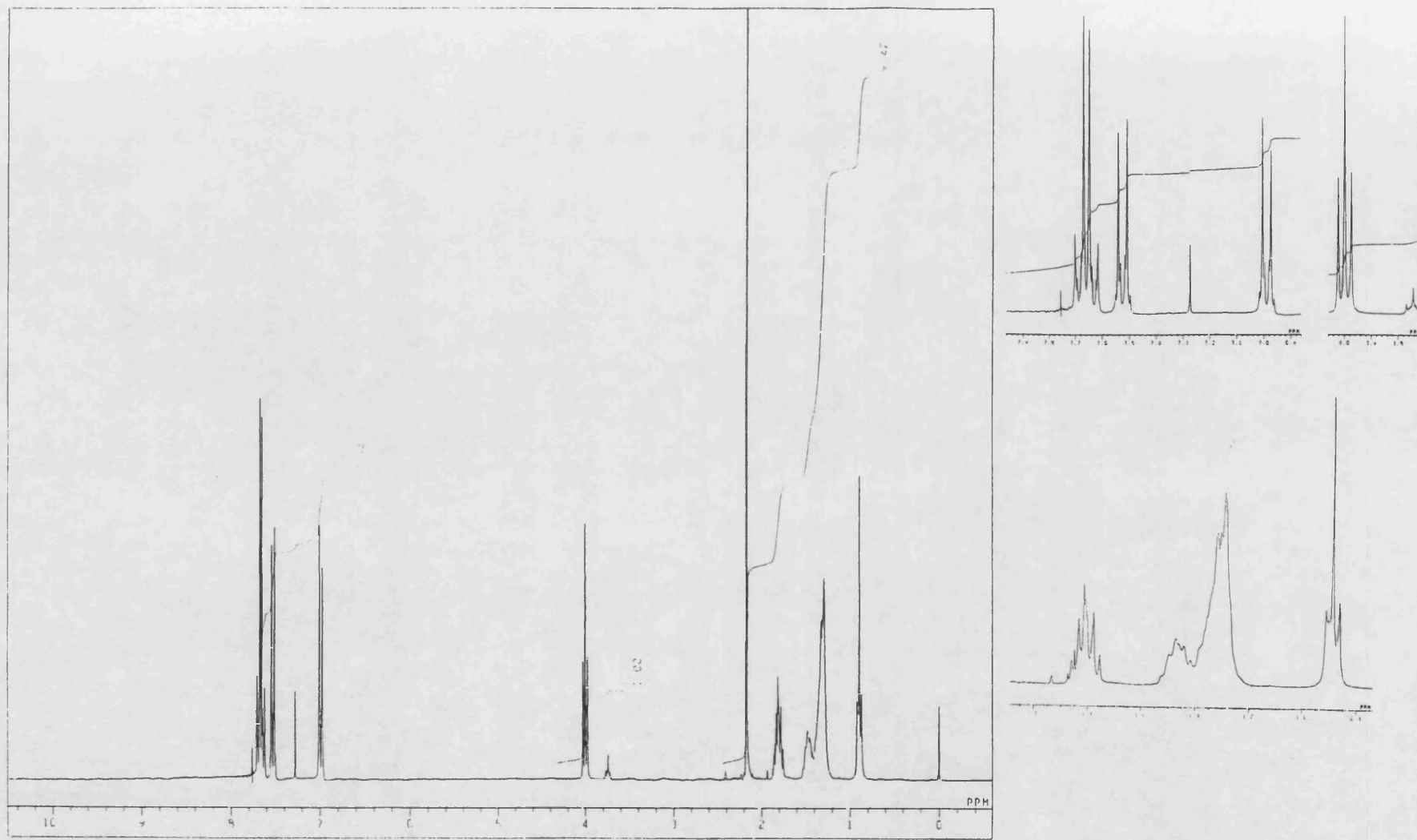
Figure 2.3: NMR spectrum for HCB

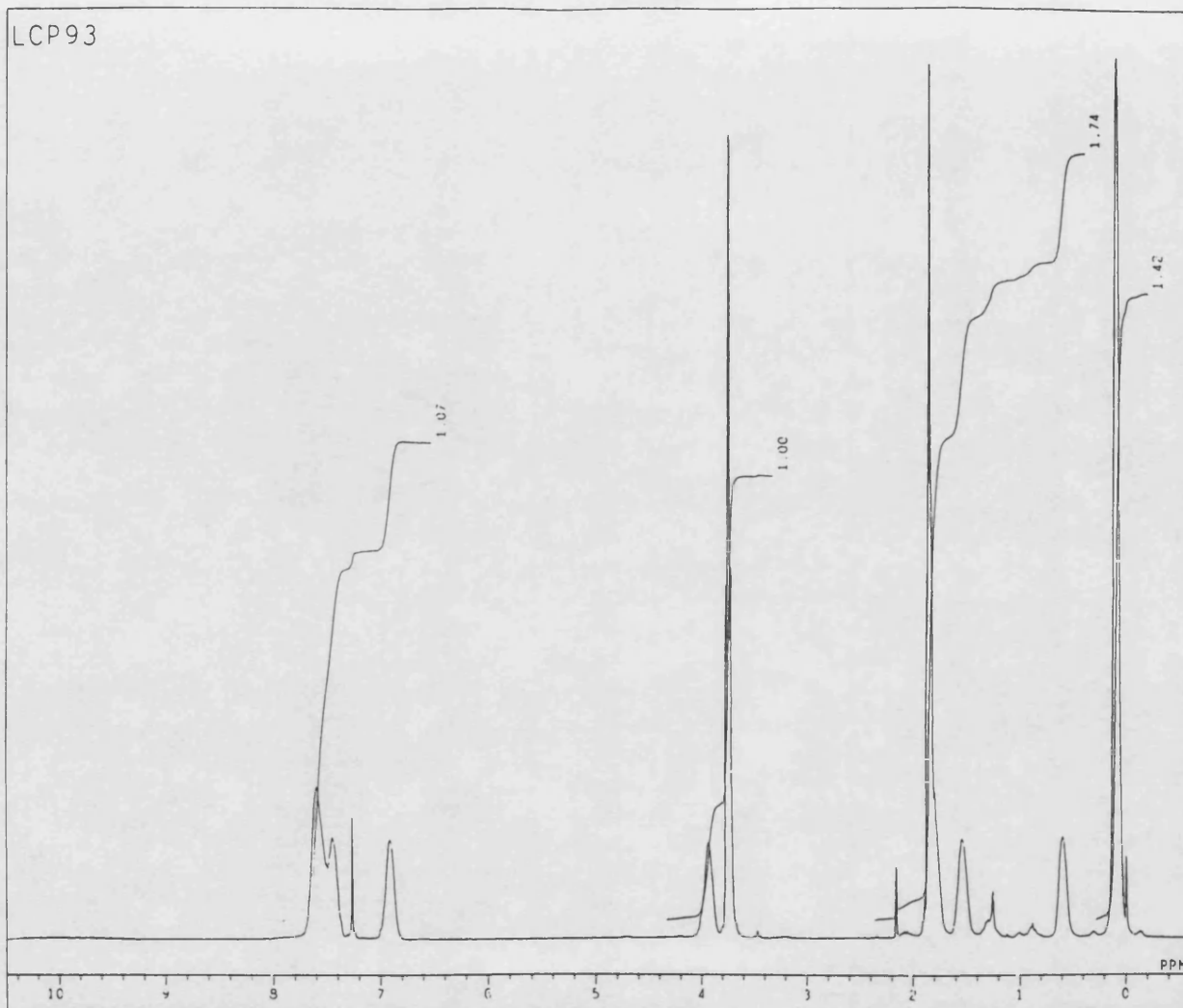**Figure 2.4:** NMR spectrum for OCB.
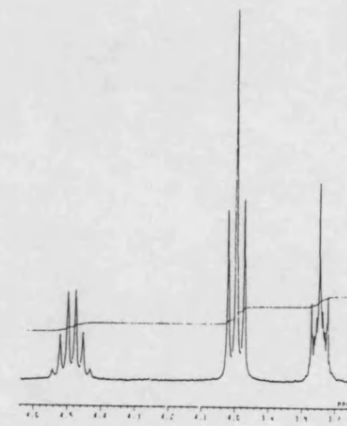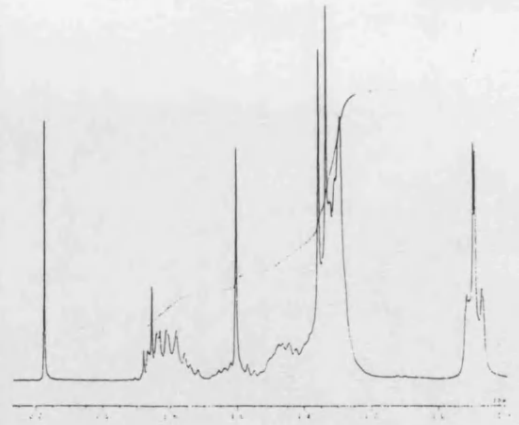
Figure 2.5: NMR spectrum for LCP.
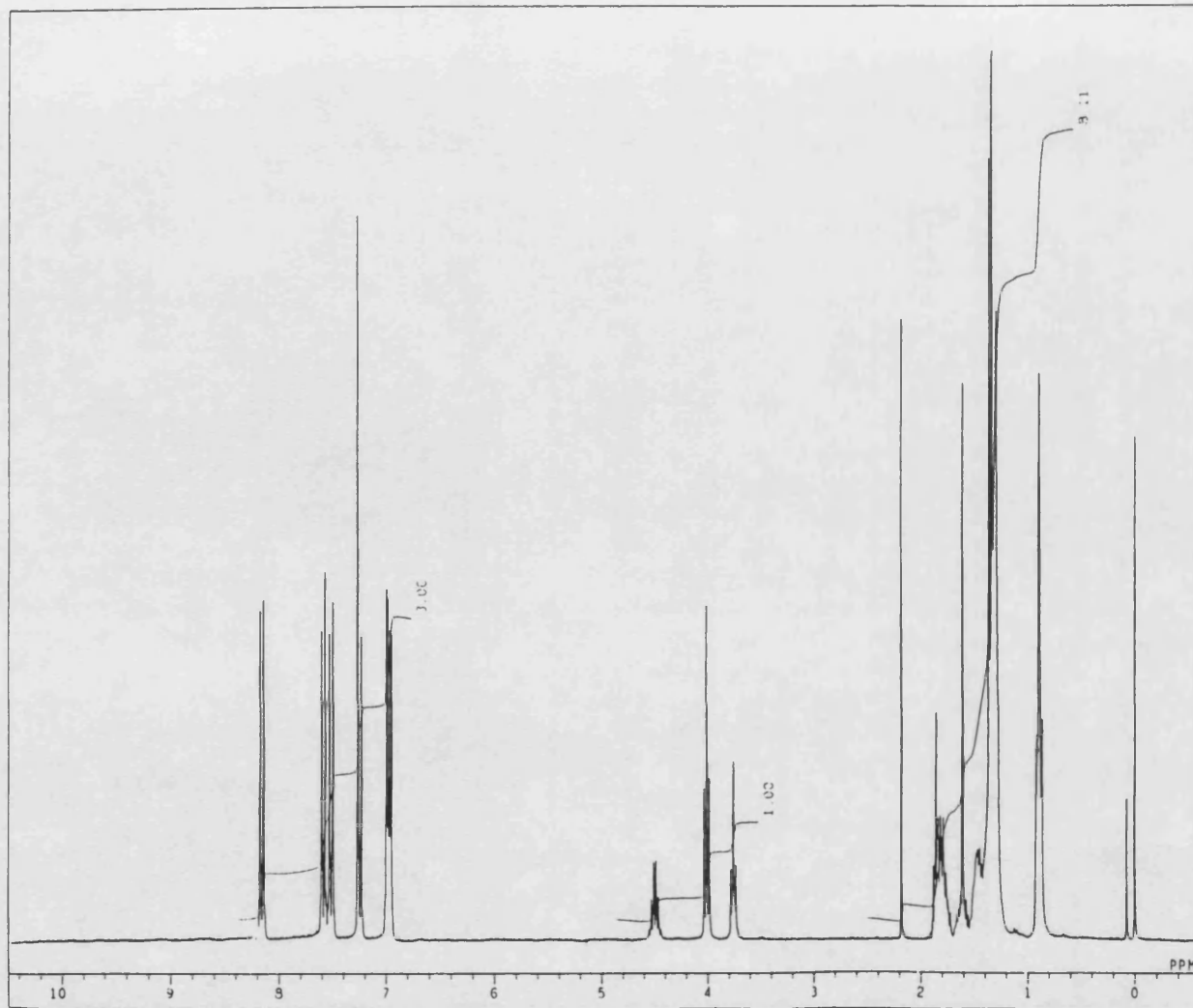
Figure 2.6: NMR spectrum for OBIB.

64
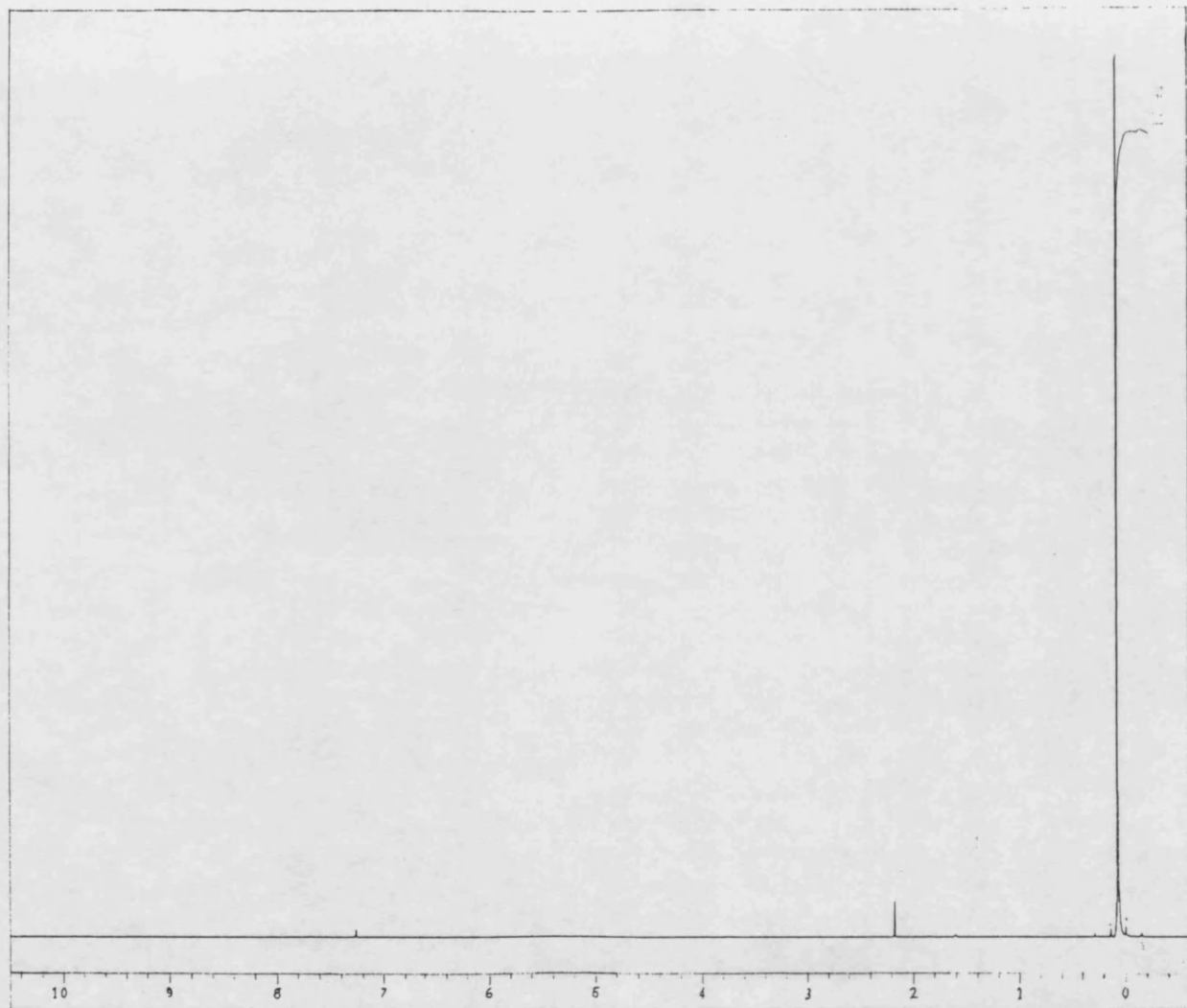
Figure 2.7: NMR spectrum for PDMS.

65

All solvents were supplied by Aldrich Chemicals or BDH Chemicals and were 99% pure or better. No further purification was undertaken.

The stationary phase support was acid washed, silanized Chromosorb P, of 100-120 mesh size, ($\approx$130-155μm diameter), supplied by Phase Sep or Jones Chromatography. The columns were prepared from 1/8" ID copper tubing obtained from Wednesbury Tube and the column ends plugged with silanised glass wool from Phase Sep.

2.2 THE GAS CHROMATOGRAPH

Two analytical gas chromatographs were modified by adding a mercury manometer, accurate to $\pm$1 mmHg, at the column head to enable inverse gas chromatography measurements. A Pye Unicam 204 chromatograph was used together with a Spectra-Physics SP4270 integrator and a Carlo Erba 400 chromatograph was used with a Hewlett Packard 3390A integrator. Gas flowrates were controlled using the cylinder head valves and the needle valves within the chromatograph and both machines were fitted with a flame ionisation detector, (FID). The columns were mounted with the entire length residing within the air oven. A schematic diagram of the apparatus is shown in *figure 2.8*.

The temperature was constantly monitored to $\pm$ 0.1 K using Digitron thermocouples calibrated against a Tinsley Type 5840 Pt resistance thermometer between 293 K and 353 K in an isothermal water bath. The thermocouple calibration data is given in *figure 2.9*. The true temperature, T, was obtained from the linear regressions of the data;

PYE 204:   T = 1.0898 Th - 3.0281

CARLO-ERBA: T = 1.0113 Th - 1.4566

where Th is the thermocouple reading and temperatures are in °C. Spatial variation

Figure 2.8: Schematic diagram of the chromatograph

Figure 2.9: Calibration curves for the two Digitron thermocouples measured against a

Platinum resistance thermometer.

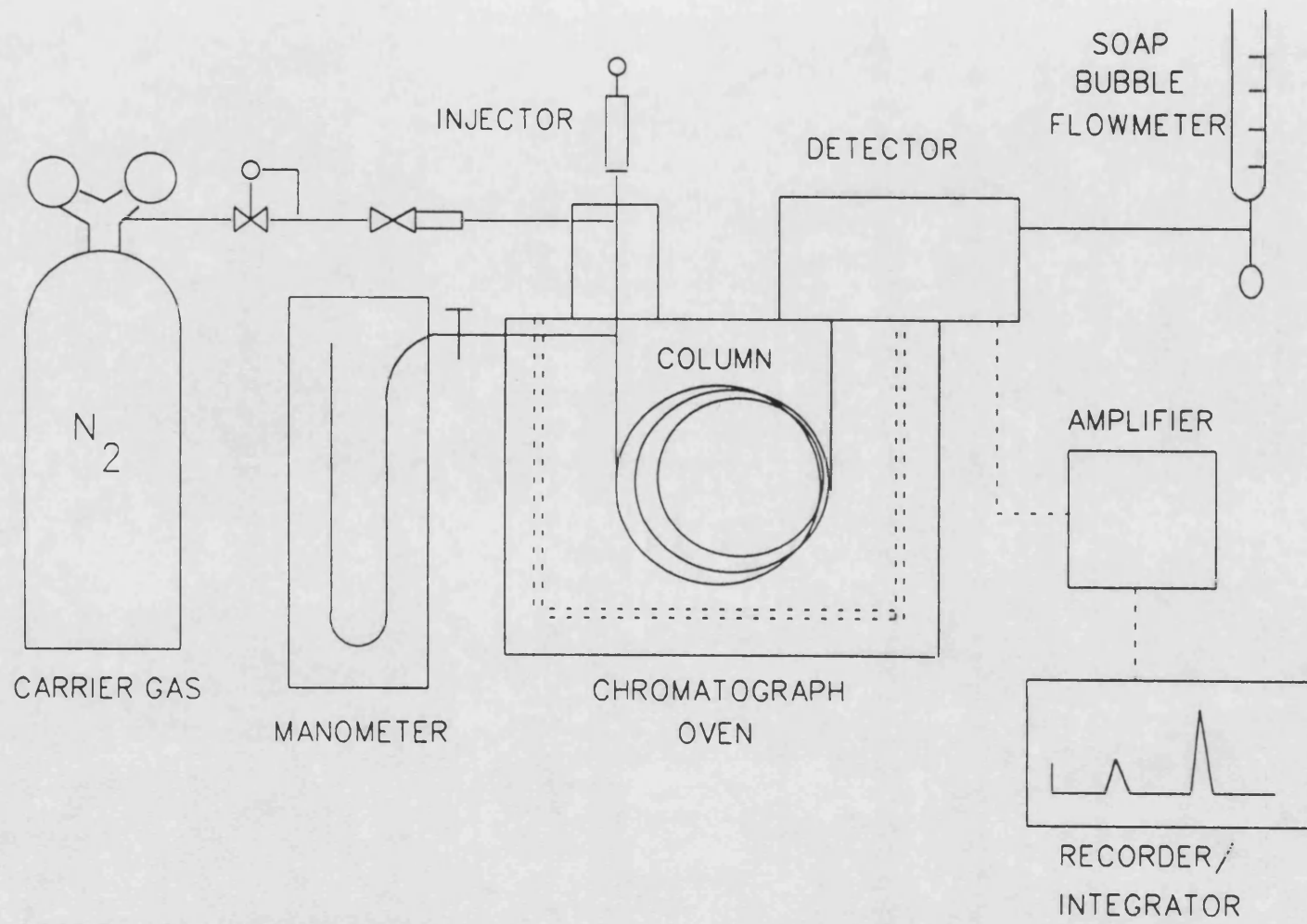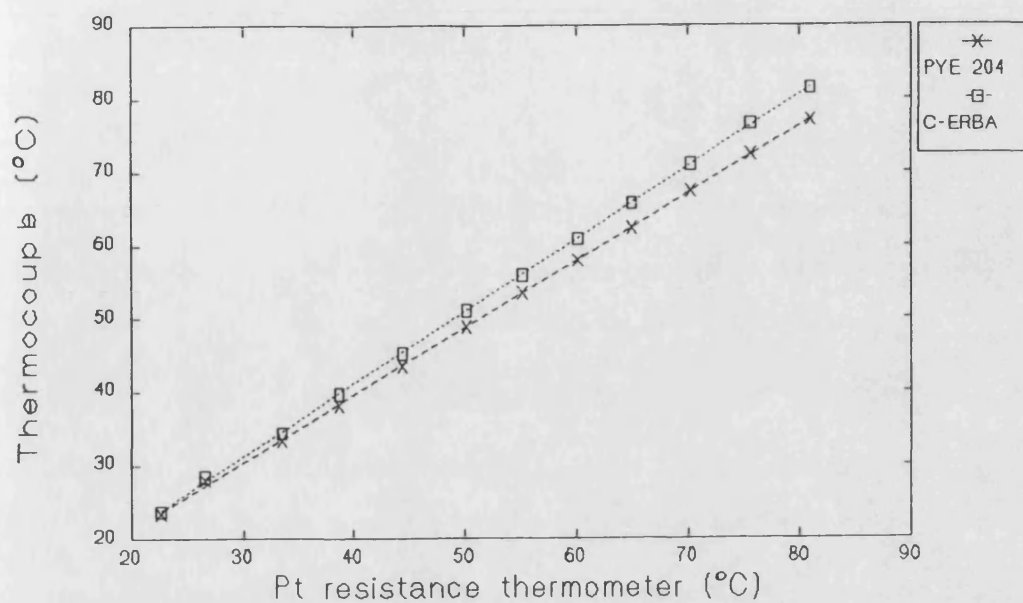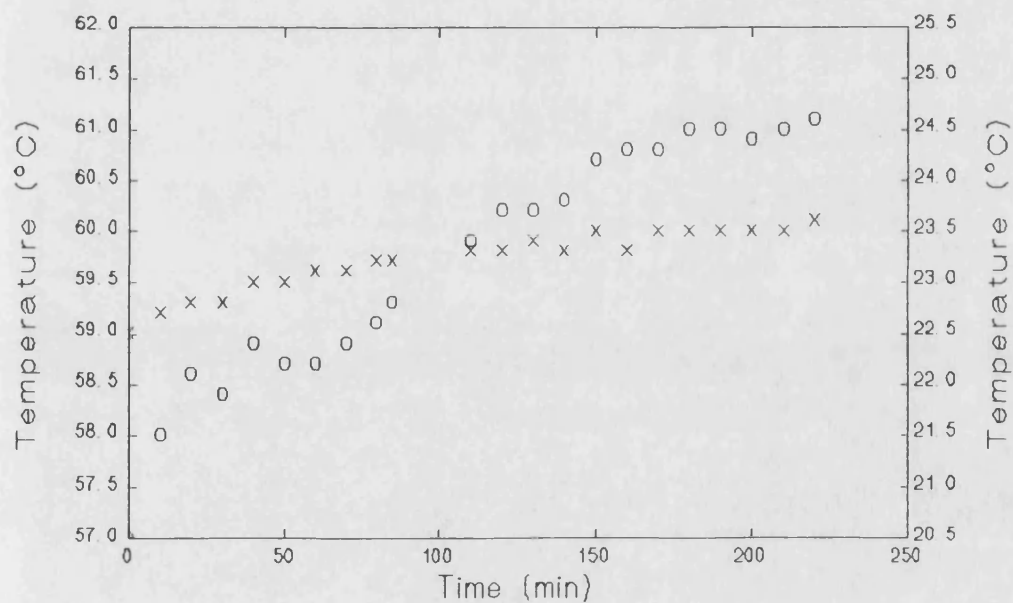**Figure 2.10:** Thermal drift within the chromatograph (x), left hand scale, with time compared

to the variation in laboratory temperature (o), right hand scale.

of the oven temperature was found to be of the same order as the uncertainty in the thermocouples but the temperature drifted during the course of the day. A typical drift profile is shown in *figure 2.10*. For most retention times the change was within the bounds of uncertainty but the average temperature was taken for long retention times.

The hydrogen and air were fed directly to the FID detector while the nitrogen carrier gas was passed through a Puritube prior to entering the chromatograph. The probe was injected ≈ 3 cm away from the head of the column and the injector block contained a 4-5 cm length of empty column. The manometer on the Carlo Erba machine was connected directly to the head of the column with a minimum length of 1/16" ID stainless steel tubing. For the Pye 204 the manometer was connected prior to the injector port but the pressure drop across it was negligible. The column outlet was connected, via a three way tap, to the FID and soap bubble flowmeter. The pressure drop between column outlet and flowmeter was negligible but a significant pressure drop across the detector was noted. The hydrogen and air were adjusted to obtain the best signal response, which was found at 1.4 bar and 1 bar above atmospheric pressure, respectively. The injector and detector ports were maintained at least 50 K above the column temperature to ensure quick passage of the probe through the dead volume. No attempt was made to fill the dead volume before or after the column as this may have contributed significantly to the probe retention. The integrator recorded retention times to ± 0.01 min and the atmospheric pressure was read from a precision barometer, to ± 0.05 mmHg, mounted at a comparable level to the manometer.

2.2a Retention Measurements

The packed column was placed within the chromatograph and conditioned by leaving it overnight at 80 °C and carrier gas flowrate of ≈ 20 cm^3 min^{-1}. The temperature was reduced to the lowest temperature of interest and retention measurements taken. A 1 µL or 0.5 µL Hamilton syringe was used to inject ≈ 0.01 µL probe made up to

0.4 μL with methane marker. Where baseline separation was possible several different probes were injected together. A minimum of three measurements at a given temperature were made to ensure a precision to within ± 1 % of the net retention time. Retention volumes were found to be independent of the carrier gas flowrate and the amount of probe injected for each system studied in this thesis. Further measurements were made on increasing the temperature, with at least four readings in each phase or mesophase and more around the transition temperatures. Values about the transition temperature were also measured on decreasing temperature. Where supercooling occurred the column was kept at room temperature for a few days and then purged with carrier gas before measuring retention on increasing temperature.
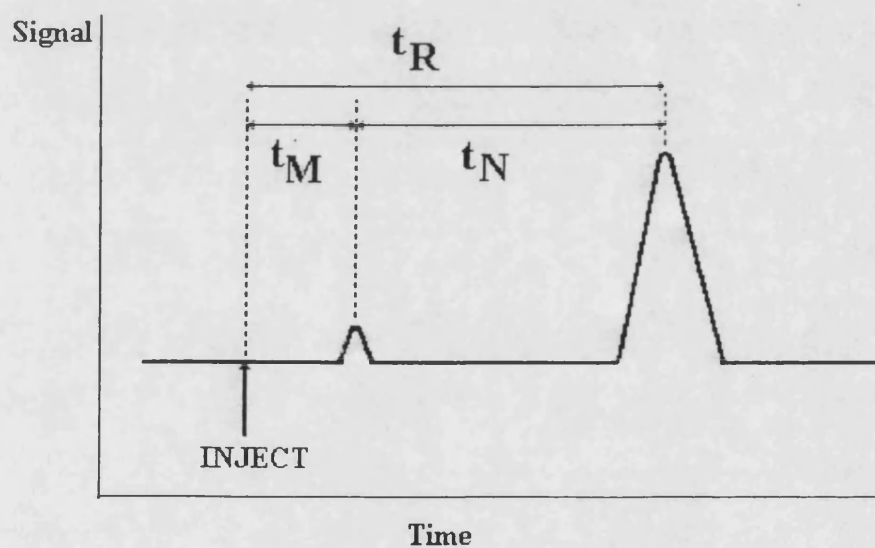
Figure 2.11: Schematic diagram of a chromatogram for probe and marker showing retention times for marker, t_M, probe, t_R, and that part of probe retention due to interaction with stationary phase, t_N.

A typical chromatogram is shown schematically above, in *figure 2.11*. The net retention due to partitioning between the stationary phase, t_N, is found from the probe retention time, t_R, relative to a non-interacting marker, t_M. The marker measures the contribution from the dead volume within the column. Methane is commonly used for

this purpose and was employed in this thesis. The method of Peterson and Hirsch[182] was used to calculate the retention time due to dead space from retention measurements of three consecutive n-alkanes. Values were in close agreement with values for methane retention. Some tailing of the chromatogram peak did occur, even at concentrations comparable to methane. Conditions were adjusted to minimise this effect and peaks were obtained where the centre of mass and retention times for the peak maximum agreed within experimental uncertainty.

To circumvent variation in flowrate, due to temperature and pressure drift during the day flowrates were measured at each new temperature. At least three recordings were made to give precision to within ± 0.2 % of the measured value.

2.2b Crystallisation Kinetics

Prior to a kinetic run the column was maintained at 60 °C, in the nematic mesophase of HCB. The column was then cooled as rapidly as possible to the temperature of interest and retention measurements recorded, for a given set of probes, as a function of time. The cooling process typically took 3-4 minutes and the start of the kinetic transformation was taken from the moment the temperature of interest was reached. It should be noted that transformation from the higher temperature phase can occur during the cooling process and that the column may take a further time to equilibrate at the lower temperature before conditions are truly isothermal. However, the time for total transformation at a given temperature was of the order of several hours and this initial process was taken to have an insignificant contribution to the overall process.

The carrier gas flowrate was set close to 20 cm^3 min^{-1} which preliminary investigation had shown would yield retention times between 1 and 15 min for the probes used. Three n-alkane probes and two aromatic probes were used and these were injected periodically until constant retention volumes were recorded for each probe.

2.2c Column Preparation

Packed columns were prepared from 1 m to 1.5 m lengths of 1/8" I.D. copper tubing which had been shaped then washed with methanol, acetone, and toluene in succession. The column was thoroughly dried and weighed. Coated support was then packed into the column with the aid of a water suction pump and mechanical vibrator. The ends of the column were blocked with small amounts of silanised, glass wool and the column reweighed prior to conditioning in the chromatograph oven.

The stationary phase was prepared by the slurry method[183]. An accurate mass of stationary phase was dissolved in chloroform and an accurate mass of support added to effect the desired loading. The resultant slurry was swirled to effect total wetting of the support and the chloroform then removed slowly by rotary evaporation. The packing was then placed under vacuum at 25 °C for several hours to remove traces of chloroform prior to packing the column.

The amount of stationary phase on the support was determined directly by calcination or soxhlet extraction. Where the stationary phase was composed of only organic elements, duplicate ashings on about 1 g of material were made. For silicon containing samples duplicate soxhlet extractions were done on a similar amount of packing, using chloroform, and the solvent removed in a vacuum oven. Duplicate determinations of the uncoated support were also made to account for the dimethylchlorosilane pre-treatment. The determined column loadings are listed in *table 2.2*.

2.2d The Support

Throughout this work Chromosorb P was used as the support. This is a pink, diatomaceous earth. The Chromosorb was supplied acid-washed and coated with dimethylchlorosilane which reduces the polar nature of the support surface. The grade was 100-120 mesh which corresponds to a particle diameter of roughly 100 μm,

Table 2.2: Composition of column stationary phases.

Components	Coating (g)	Support (g)	% Loading
HCB	1.478	8.812	14.36
OCB	1.584	9.356	14.48
OBIB	0.729	8.311	8.06
LCP	0.355	3.205	9.98
PDMS:HCB [8:2]	0.668	7.202	8.49
PDMS:HCB [6:4]	0.794	10.066	7.31
PDMS:HCB [4:6]	0.768	9.822	7.25
PDMS:HCB [2:8]	0.654	8.516	7.13

as shown in micrograph in *figure 2.12a*. The particles have a narrow size distribution and are composed of rough surfaces and large areas of porous plates, shown in *figure 2.12b*. Micrographs of liquid crystal coated support, see chapter 7, show the stationary phase tends to avoid the porous regions although it is distributed reasonably homogeneously across the rest of the Chromosorb.

The Brunauer-Emett-Teller[184] (BET) method was used to measure the surface area of the Chromosorb P by measuring the adsorption of nitrogen onto the surface at 77 K. A vacuum frame apparatus was used where known aliquots of gas were admitted to the apparatus and a differential mercury manometer measured the gas pressure above the solid support. The cross-section-area of a nitrogen molecule was taken as 1.62×10^{-19} m^2 [185]. The isotherm of a sample of silica gel with known surface area was measured and found to agree with the suppliers data. *Figure 2.13* shows the isotherm for the Chromosorb P support composed from results from three different experiments. The specific surface area was found to be 260 ± 30 m^2g^{-1}. This is considerably higher than the value of 25 m^2 g^{-1} obtained by extrapolating values for

a)
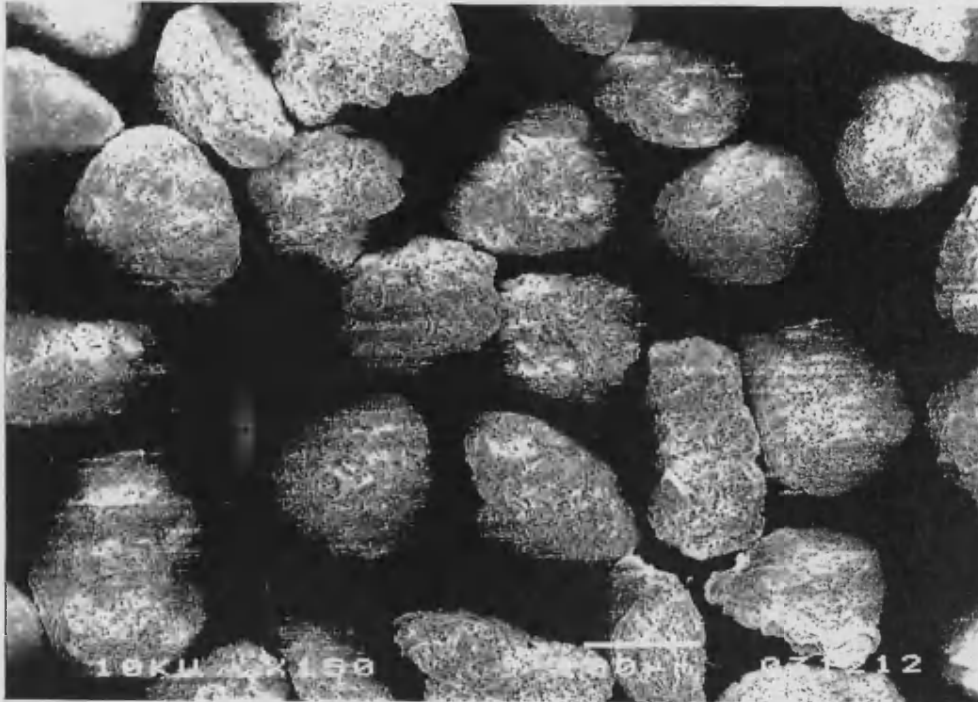
b)
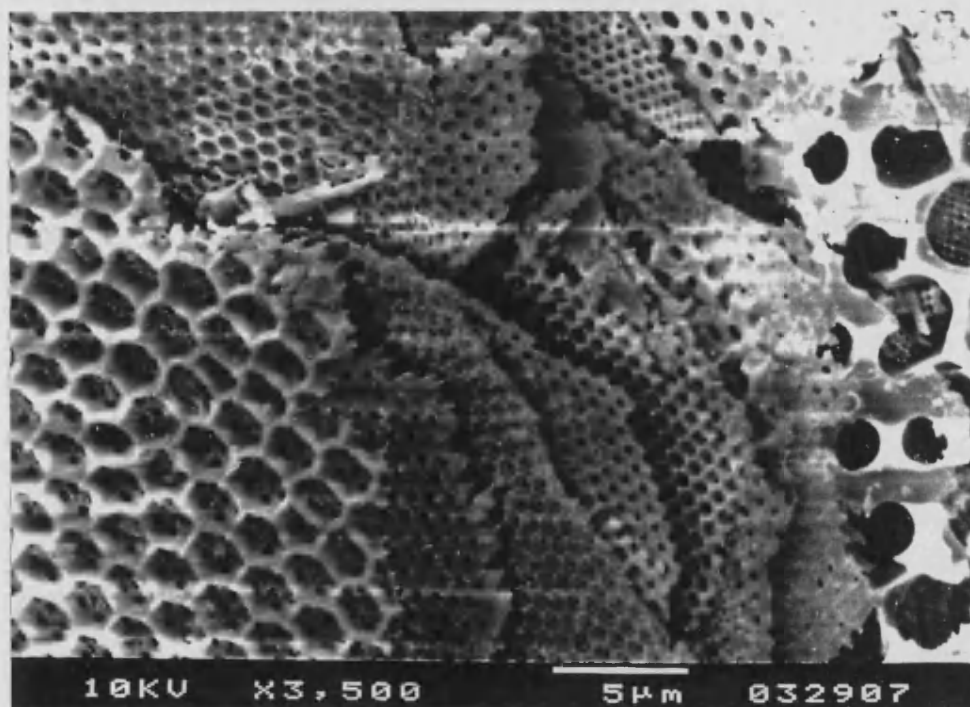
Figure 2.12: SEMs of uncoated Chromosorb P support showing a) particle size distribution

and b) the large areas of porous support surface.

Chromosorb P supports of various sizes given in a report by Witkiewicz[186]. The literature values were obtained from gas chromatography measurements by comparing values for Chromosorb P and a series of well defined glass beads. The discrepancy implies the porous plates seen in the micrographs have negligible retention in the gas chromatography experiment.
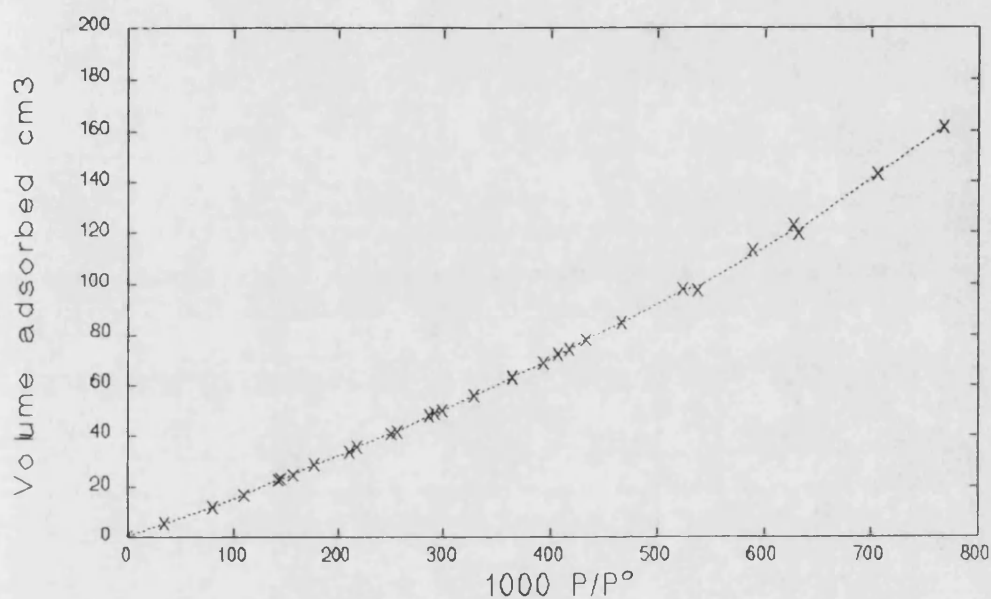
Figure 2.13: Adsorption isotherm of nitrogen on Chromosorb P AW DMCS (100-120 mesh)

2.3 DENSITY MEASUREMENTS

In order to calculate certain solution parameters from the models introduced in chapter 1 it was necessary to have densities for both the probe and stationary phase. Literature values for the liquid crystals were not available and only a small quantity of material was available. Thus it was necessary to employ a method that would yield values with a reasonable precision, over a wide temperature range, covering several different phases and mesophases, and which allowed easy recovery of the material at the end of the experiment. To meet these requirements a method involving the displacement of water was employed.

A number of cells were made, as illustrated in *figure 2.14*, of about 5 cm³ capacity. The actual volumes were obtained from measurements with freshly distilled water across the temperature range of the study. The cell volume was found to be constant at all temperatures, inferring negligible effects from glass expansion on heating, and degassing only became significant above 70 °C. The small degree of degassing was
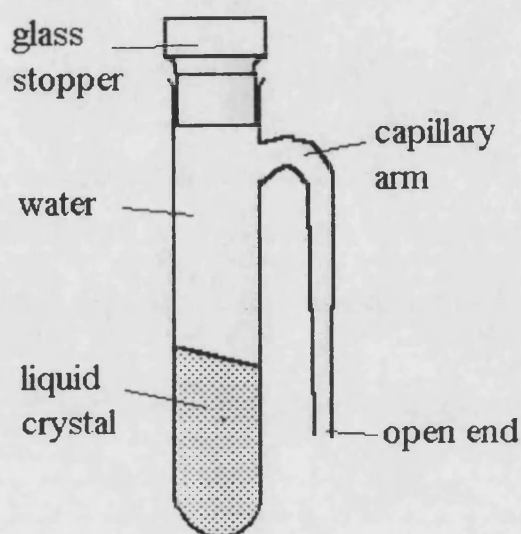
Figure 2.14: Schematic diagram of a density cell prepared for measurement of liquid crystal density.

accounted for by assuming the effect was proportional to the amount of water present.

With the volume of the cells accurately known, between 1 g and 1.5 g of liquid crystal was placed into the cell and weighed. The sample was heated to the isotropic phase and maintained at this high temperature until no air was trapped in the sample. This was then cooled and reweighed. A layer of water was placed over the sample and the procedure repeated to ensure good wetting between the water and the sample. On cooling the cell was completely filled with freshly distilled water, as shown in *figure 2.14*, and placed in a clean water bath that also contained distilled water. The sample was allowed to equilibrate for 30 min and removed, quickly dried, and reweighed. The procedure was repeated at a higher temperature. Masses were accurate to ± 0.0005 g,

the water bath was isothermal to within ± 0.1 °C, and readings were taken every 3 °C

between 20 °C and 95 °C. Results were obtained from at least two separate sets of

measurements. Densities were obtained by using the expression;

$$\rho_{LC} = \frac{M_{LC}}{\left(V - \left(M_{H_2O} / \rho_{H_2O}\right)\right)}$$
[2.2]

where V is the volume of the cell and ρ and M are the density and masses, respectively,

of the two components, water (H_2O) and liquid crystal (LC).

Results for the cyanobiphenyl materials are shown in chapter 4 but there was

insufficient OBIB to obtain densities. Results were calculated to a precision of within

± 1 % of the measured value and *table 2.3* gives the equations of linear fit to the

measurements. These were obtained using the computer package "SIGMA PLOT".

Quadratic and cubic fits to the data were obtained but these did not give improved

description of the data. The water was sufficiently incompatible with the liquid crystals

to enable accurate density measurements across the whole temperature range. Density

measurements were also made on the PDMS sample, used in this thesis, as a function

Table 2.3: Linear equations describing density (g cm^{-3}) as a function of temperature where temperature is in °C and σ is the standard deviation of the line.

	Phase	Equation	σ
HCB	K	$1.140 - 5.53 \times 10^{-4}$ T	0.005
	N	$1.107 - 1.267 \times 10^{-3}$ T	0.003
	I	$1.080 - 9.30 \times 10^{-4}$ T	0.004
OCB	K	$1.103 - 4.76 \times 10^{-4}$ T	0.005
	S_A	$1.079 - 1.270 \times 10^{-3}$ T	0.002
	N	$1.075 - 1.145 \times 10^{-3}$ T	0.002
	I	$1.064 - 1.029 \times 10^{-3}$ T	0.003
LCP	S_A	$1.149 - 7.82 \times 10^{-4}$ T	0.004
	I	$1.186 - 1.412 \times 10^{-3}$ T	0.004

Table 2.4: Comparison of density method with literature values.

Temperature (°C)	PDMS measured	g cm⁻³ literature[a]	PS measured	g cm⁻³ literature[b]
25.0	0.9713	0.9697	1.084	1.04-1.08
34.9	0.9627	0.9607		
46.5	0.9508	0.9514		
58.5	0.9394	0.9402		
71.5	0.9191	0.9290		

a: calculated from the expression in reference 187. b: from reference 181.

of temperature and a polystyrene (PS) sample at 25 °C. Table 2.4 shows the measurement are in good agreement with the literature.

2.4 DIFFERENTIAL SCANNING CALORIMETRY (DSC)

Differential Scanning Calorimetry, (DSC), was used to obtain the transition temperatures of the stationary phases studied by IGC and the results are reported in chapter 4. The apparatus used was a DuPont 3000 machine calibrated with Indium and water. Most chromatograms were obtained at a heating rate of 5 °C min⁻¹ but where other heating rates were used they will be referred to in the text. Where both heating and cooling cycles were studied the machine was fitted with a DuPont 3000A head attachment for controlled cooling. Sample sizes varied between 4 mg and 12 mg for pure materials to 15 mg to 25 mg for materials coated on Chromosorb P. The transition temperatures were recorded as the endotherm or exotherm peak or the point of inflexion for glass transitions.

M18-PDMS samples, not coated on Chromosorb, were prepared by dripping stock

solutions, of a prepared composition of the two components in chloroform, into a DSC

pan over a period of time and allowing solvent evaporation between additions.

2.5 NUCLEAR MAGNETIC RESONANCE (NMR)

In chapter 7 the transition temperatures of HCB for a series of different PDMS-HCB

compositions are reported as measured by DSC. The compositions of each sample

were predicted from the amounts of each component in the stock solutions used to

prepare the DSC samples. Nuclear Magnetic Resonance, NMR, spectra were obtained

to determine the actual composition of these samples. The spectra of the pure

materials were also recorded to confirm their purity. All NMR spectra were obtained

from a Jeol GX270MHz machine. Samples were taken from the stock solutions

prepared for DSC and the solvent allowed to evaporate in a glass sample jar. The

samples were then placed in a vacuum oven at 25 °C for a few hours. The residue was

redissolved in deuterated chloroform with trace tetramethylsilane (TMS) reference and

the spectrum recorded. The signal for the PDMS protons occurred downfield of TMS

and so the PDMS peak integral was unaffected by the latter. The integral of the

characteristic doublet at 6.9 ppm was used to quantify the amount of HCB present.

For every 279.4 g of HCB (1 mole) there are two identical protons contributing to

the doublet at 6.9 ppm in the NMR spectrum. The polymer was assumed to be

comprised of chain segments only and the end groups were ignored. Thus every

74.2 g of polymer contains six identical protons contributing to the integral in the

spectrum. If the relative integrals for HCB and PDMS are taken as I_1 and I_2,

respectively the ratio of weights, HCB:PDMS, for a given composition is given as;

$$279.4 \, I_1/2 : 74.2 \, I_2/6 \qquad\qquad [2.3]$$

Hence, the weight fraction of the liquid crystal, w_1, was calculated from;

$$w_1 = \frac{1}{\left(\dfrac{74.2 I_2 2}{279.4 I_1 6}\right) + 1}$$

[2.4]

The predicted and measured compositions are listed in *table 2.5*.

Table 2.5: Composition of HCB-PDMS samples prepared for DSC measurements on bulk samples.

Predicted w_1	Measured w_1
0.800	0.799
0.700	0.731
0.600	0.640
0.500	0.502
0.450	0.435
0.400	0.389
0.300	0.331
0.200	0.178
0.100	0.111

CHAPTER 3

DATA REDUCTION

3.1 SPECIFIC RETENTION VOLUME

The primary datum in physicochemical studies is the specific retention volume, V_g. This is the volume of carrier gas required to elute the chromatogram peak maximum from a column containing 1 g of stationary phase. Specific retention volumes are usually calculated at S.T.P. whereupon the superscript o is used;

$$V^o_g = F(t_R - t_M)/W \qquad [3.1]$$

where t_R and t_M are the probe and marker retention times taken from the chromatogram, as shown in *figure 2.11*, W is the mass of stationary phase and F is the corrected flowrate of carrier gas.

Carrier gas flowrates must be corrected to account for three factors;

    i) The partial pressure in the flowmeter due to the soap solution

    ii) The compressibility of the carrier gas

    iii) The difference between measuring conditions and S.T.P.

i) The soap bubble meter: The flowrate is measured at a pressure of carrier gas less than that of the surrounding atmosphere due to the contribution of the soap solution in the flowmeter. This is approximated by the partial pressure of water at the same temperature[188] and the measured flowrate was multiplied by $(P_a - P_w/P_a)$. P_a is the atmospheric pressure and P_w is the partial pressure of water vapour, found using the Antoine equation[189] with literature constants[190].

ii) Carrier gas compressibility: The pressure at the column head is greater than at the column outlet resulting in a variation in carrier gas flowrate along the column. Martin and James[93] introduced a factor J_3^2 allowing an average flowrate to be determined;

$$J_3^2 = \frac{3}{2}\left[\frac{(P_i/P_o)^2 - 1}{(P_i/P_o)^3 - 1}\right] \qquad [3.2]$$

where i and o refer to the conditions at the column inlet and outlet, respectively.

iii) Correction to S.T.P.: Measurements of flowrate are made at laboratory pressures and temperatures and so must be corrected to S.T.P.. The factor $(273.2/T_f).(P_a/760)$ is introduced where T_f is the temperature of the flowmeter.

The difference between atmospheric pressure and the column outlet pressure was small and the overall equation used to calculate V^o_g is given by;

$$V^o_g = F_0(t_R - t_M)[1 - (P_w/P_0)](273.2\, P_0/T_f\, 760)J_3^2/W \qquad [3.3]$$

where F_0 is the flowrate measured at the column outlet.

3.2 CRYSTALLISATION KINETICS

In chapter 4 the crystallinity of the solid liquid crystal phase, as measured by IGC, is reported for the low molar mass materials and in chapter 7 the crystallinity of HCB when mixed with PDMS is reported. The degree of crystallinity in the crystalline phase of a liquid crystal was estimated by using the method introduced by Guillet[112], as discussed in section 1.12a;

$$\% \text{ Crystallinity} = 100.[1 - (V^o_g/V^o_g')] \qquad [1.48]$$

where V_g' is the hypothetical specific retention volume of the isotropic phase at the temperature of interest. The method was also used to obtain the "effective degree of crystallisation" in the mesophases of the liquid crystals by considering the mesophase to be comprised of totally crystalline and totally isotropic portions, similar to the approach of Bocquet and Pommier[150] discussed in section 1.13. These values were used as a guide to the fraction of ordered mesogens necessary to discuss the advanced theory of liquid crystal solutions proposed by Flory.

For the measurements on HCB, following the transformation from nematic to crystalline phase, the fraction of crystalline phase, F^c, was calculated from;

$$F^c = \frac{V^o{}_s(t) - V^o{}_s(0)}{V^o{}_s(\infty) - V^o{}_s(0)} \qquad [3.4]$$

where 0, t, and ∞ denote values at the start, at time t, and at the end of the transformation, respectively. This expression is essentially the same as equation [1.50] but the values have been normalised, assuming total crystallinity in the crystalline phase. Formally, the Avrami treatment of crystallisation refers to the volume fraction of crystallinity whereas IGC results yield mass fraction values. However, the density difference between the mesophase and the crystalline phase was sufficiently small to result in only a minor correction and the two are assumed to be equivalent in this thesis. The K and n parameters from the Avrami treatment, given in section 1.15, where calculated from linear regressions of the rearranged form of equation [1.63];

$$\ln[-\ln(1 - F^c)] = \ln K + n \ln t \qquad [3.5]$$

The regression program was part of the "ASEASYAS" spreadsheet employed in this thesis.

3:3 THERMODYNAMIC PARAMETERS

In section 1.12a the specific retention volume was shown to be proportional to the partition coefficient. As the partition coefficient is also the equilibrium ratio of probe concentrations between the stationary phase and mobile phase, the activity coefficient of the probe in the stationary phase can also be related to the specific retention volume. When probe concentration tends to infinite dilution the activity coefficient is obtained from;

$$\ln \gamma^\infty = \ln[R\ 273.2/(V^o{}_g\ P^o\ M_L) - P^o\ B_{11}/R\ T \qquad [1.42]$$

$$\ln \Omega^\infty = \ln[R\ 273.2/(V^o{}_g\ P^o\ M_1) - P^o\ B_{11}/R\ T \qquad [3.6]$$

where γ^∞ and Ω^∞ are the infinite dilution molar and weight activity coefficients, as defined in sections 1.5b and 1.12b respectively. M_L and M_1 are the molar masses of the stationary phase and probe, respectively. P^o is the saturated vapour pressure of the probe and B_{11} is the second virial coefficient of the probe. Pressure was measured in

torr and the specific retention volume was measured in cm^3 g^{-1} so the gas constant, R, takes the value of 62400 torr cm^3 K^{-1} mol^{-1}. Equation [3.6] was used for stationary phases with no discrete molar mass, for reasons discussed in section 1.12b.

Saturated vapour pressures were calculated from the Antoine expression[189] and constants taken from the literature[190]. The second virial coefficients were calculated from the equation and constants listed in reference 190 and the column temperature for most of the probes studied. However, there were no constants listed for the branched heptane isomers. This was circumvented by using the method outlined by DiPaola-Baranyi and Guillet[125]. From literature values[190] for the critical pressure and temperature, A parameters were calculated for the range of temperatures and pressures studied here;

$$\ln(P_c/P) = A(T_c - T)/T \qquad [3.7]$$

where the subscript c denotes the critical value. These were compared to A parameters of a series of n-alkanes at identical temperature and pressure. The n-alkane with the closest A value to a given branched alkane was found to be independent of conditions. *Table 3.1* lists the heptane isomers used in this study and the matching n-alkane. Second virial coefficients were then calculated using the critical volume of the branched alkane with the literature constants of the equivalent n-alkane.

The saturated vapour pressures agreed to well within 1 % for both experimental data points and empirical analytical fits to data, such as obtained from reference 190 and 191 for instance. However, the fluctuations in the measured second virial coefficients from different sources can be considerably larger. Most literature reports cited in this thesis calculate second virial coefficients using the expression due to McGlashan and Potter[192], who describe it in terms of a power series of reciprocal reduced temperature. A number of compilations of critical constants are available, for instance references 193, 194. Although there is some fluctuation in reported constants, there is

Table 3.1: Heptane isomers and the n-alkane with the closest A value as calculated from equation [3.7]

Heptane	Equivalent n-alkane
2-Methylhexane	Heptane
3-Methylhexane	Heptane
2,3-Dimethylpentane	Hexane
2,4-Dimethylpentane	Hexane
2,2,3-Trimethylbutane	Pentane

negligible difference in second virial coefficients calculated from the McGlashan and Potter expression and the expression from reference 190 used in this work. *Figure 3.1* shows values for two typical probes calculated by the former method compared to the method employed in this thesis and experimentally measured values[195].
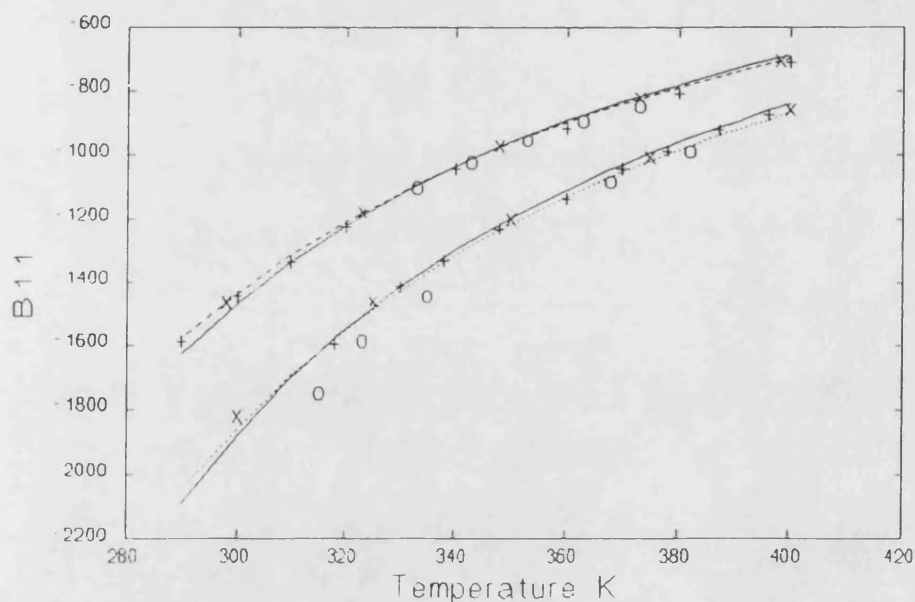

Figure 3.1: Second virial coefficients for benzene (top curves) and hexane (bottom curves) calculated from reference 190 (solid line) and reference 192 (broken line) compared to three of the most recent sets of experimental values from reference 195

Both sets of calculated data offer reasonable descriptions of the experimental results and agree to within 3% of each other at any given temperature. This uncertainty leads to an uncertainty in the activity coefficient, as seen in equations [1.42] and [3.6]. However, the gas phase correction is usually between 1-5 % of the activity coefficient[97], so the uncertainty in B_{11} will only alter values by less than 1 %. The gas phase correction translates to a maximum decrease in the interaction parameter of 0.05 so the uncertainty in B_{11} would be negligible in the systems studied in this work.

The specific retention volumes and corresponding molar or weight activity coefficients were calculated from the retention times and the relevant constants, outlined above, using the BASIC computer program "CHROM", listed in *appendix II*.

Having obtained the activity coefficients as a function of temperature, the partial molar excess enthalpies and partial molar excess entropies were obtained from equation [1.46], or the corresponding equation [3.8] using the linear regression in the "ASEASYAS" spreadsheet;

$$\ln \gamma^\infty = (H^E/R\ T) - (S^E/R) \qquad [1.46]$$

$$\ln \Omega^\infty = (H^E/R\ T) - (S^E/R) + \ln(M_1/M_L) \qquad [3.8]$$

By describing the saturated vapour pressure of the probe using the Clausius-Clapeyron equation[108], and adopting the approximations associated with it, and using equations [1.46] and [3.8], it follows from equation [1.44] and [3.6] that the specific retention volume can be expressed by equation [3.9] and [3.10];

$$\ln V^o{}_g = -\frac{-\Delta H^{vap} + H^E}{R'T} + \frac{-\Delta S^{vap} + S^E}{R'} + \ln\frac{273.15R''}{M_L} \qquad [3.9]$$

$$\ln V^o{}_g = -\frac{\Delta H^{sol}}{R'T} + \frac{\Delta S^{sol}}{R'} + \ln\frac{273.15R''}{M_L} \qquad [3.10]$$

where the superscripts vap, E, and sol refer to the vaporisation, excess, and solution quantities, respectively, for the enthalpy, H, and entropy, S, corresponding to the free

energy changes defined in section 1.6. Note that to account for the units of specific

retention volume and yield enthalpies and entropies in units of J mol^{-1} and

J mol^{-1} K^{-1}, respectively, the gas constant R' is taken as 8.314 J mol^{-1} K^{-1} and R" is

taken as 83.14 bar cm^3 mol^{-1} K^{-1}.

3.4 BINARY SOLUTION PARAMETERS

In chapter 6 the observed solution behaviour is discussed in terms of various models

of a solution, outlined in chapter 1. The thermodynamic parameters obtained from the

calculations in section 3.3 were used to determine these model solution parameters.

3.4a Interaction Parameters

From the equation [1.23], giving the Flory-Huggins equation for the activity of a

solution, it follows that as the probe tends to infinite dilution the interaction parameter,

χ^∞ is given by;

$$\chi^\infty = \ln \gamma^\infty + \ln (\rho_1/\rho_2) + \ln (M_L/M_1) - [1 - (M_1 \rho_2/M_L \rho_1)] \qquad [3.11]$$

where ρ is the density of the probe, 1, and the stationary phase, 2. This was used to

calculate interaction parameters along with the corresponding equation;

$$\chi^\infty = \ln \Omega^\infty + \ln (\rho_1/\rho_2) - [1 - (M_1 \rho_2/M_L \rho_1)] \qquad [3.12]$$

Stationary phase densities were calculated from the equations given in *table 2.3*.

Probe densities were calculated from the expression;

$$\rho_1 = K[(1 - T_r)/(1 - T_{br})]^n \qquad [3.13]$$

where T_r and T_{br} are the reduced temperature and reduced boiling point of the probe,

respectively. K and n are constants. This expression follows the form proposed by

Goldhammer[193] to estimate densities. The constants were found from fits to literature

data[190] and are listed in *table 3.2*. The discrepancy between the literature data and the

calculated value at any given temperature was negligible. This expression allowed

accurate densities to be calculated at any intermediate temperature where experimental

data was not available.

The equation of state interaction parameter tending to infinite dilution was calculated

from similar equations to [3.11] and [3.12] but the molar volumes were replaced by the

characteristic, or hard-core, molar volumes, for instance;

$$\chi^* = \ln \gamma^\infty + \ln (V^*_2/V^*_1) - [1 - (V^*_1/V^*_2)] \qquad [3.14]$$

where V^* is the characteristic molar volume. The exchange interaction parameter,

X_{12}, was calculated from a rearrangement of equation [1.33];

$$X_{12} = \chi^* \, R \, T \, \tilde{v}/V^*_1$$
$$- P^*_1 \, \tilde{v}\left\{3\tilde{T}_1\ln\left[\left(\tilde{v}_1^{1/3} - 1\right)/\left(\tilde{v}^{1/3} - 1\right)\right] + (1/\tilde{v}_1) - (1/\tilde{v})\right\} \qquad [3.15]$$

where P^*_1 is the characteristic pressure of the probe and $\tilde{v}$ is the reduced segment

volume, as defined in section 1.9. The characteristic parameters were assumed to be

independent of temperature in this work and the literature values[196] used are listed in

table 3.2. Where no characteristic parameters were available, such as for the liquid

crystals, values were calculated from the density measurements using the method

outlined in section 1.9 and assuming the coefficient of thermal expansion to be

constant across the temperature range of the mesophases and isotropic phase studied.

As discussed in section 1.10a, the asymmetry of the liquid crystal does not affect the

solution model of Flory-Huggins in the isotropic phase. However, to account for

asymmetry in the mesophase the interaction parameter must be calculated from an

adjustment of equation 3.11;

$$\chi^\infty = \ln \gamma^\infty + \ln (\rho_1/\rho_2) + \ln (M_L/M_1) - [1 - (M_1 \, \rho_2/M_L \, \rho_1)]$$
$$- (2/y) + [1 - \exp(-2/y)] \qquad [3.16]$$

where y is the disorientation parameter and is given by;

$$\exp(-2/y) = 1 - \phi_0^a[1 - (y/\overline{\eta}^a)] \qquad [1.39]$$

The volume fraction of aligned, rigid sequences, ϕ_0^a, was estimated as outlined in

section 3.2 and the average number of segments in aligned portions, $\overline{\eta}^a$, was estimated

from the molecular structure of the liquid crystal, as described in section 3.6.

Table 3.2: Density and characteristic constants, references 60 and 79 ([a] calculated)

	n	K $g\ cm^{-3}$	P* $J\ cm^{-3}$	V* $cm^3 mol^{-1}$	T* K
Pentane	0.232	0.606	426.1	85.42	4151
Hexane	0.287	0.612	425.7	99.43	4427
Heptane	0.292	0.612	430.3	114.63	4647
Octane	0.294	0.609	437.4	127.74	4825
Nonane	0.297	0.605	434.9	141.76	4975
2-Methylhexane[a]	0.289	0.614	379.7	114.77	4698
3-Methylhexane[a]	0.298	0.619	396.0	112.20	4560
2,3-Dimethylpentane[a]	0.292	0.629	388.5	111.32	4579
2,4-Dimethylpentane[a]	0.293	0.615	369.7	113.40	4444
2,2,3-Trimethylbutane[a]	0.287	0.634	362.6	111.52	4533
Cyclohexane	0.295	0.720	526.9	84.39	4657
Benzene	0.306	0.813	618.9	69.41	4666
Toluene	0.296	0.778	560.4	84.58	4941
Ethylbenzene	0.300	0.758	553.7	98.79	5239
p-Xylene	0.297	0.751	531.1	99.10	5112
m-Xylene[a]	0.293	0.754	556.2	99.20	5239
o-Xylene	0.293	0.768	539.5	97.73	5252
PDMS[a]				32420	
LCP S_A[a]				2861	
LCP I[a]				2616	
HCB N[a]				206.0	
HCB I[a]				223.4	
OCB S_A[a]				230.5	
OCB N[a]				236.7	
OCB I[a]				244.4	

3.4b Solubility Parameters

The stationary phase solubility parameters, δ_2, were estimated using the method of Guillet[125], discussed in section 1.12b, from the equation;

$$(\delta_1{}^2/R\ T) - \chi/V^o{}_1 = (\delta_2/R\ T)\delta_1 - [(\delta_2{}^2/R\ T) + \chi^S/V^o{}_1] \qquad [1.54]$$

where χ^S is the entropic contribution to the interaction parameter. The probe interaction parameter, δ_1, was calculated from the molar enthalpy of vaporisation and the molar volume;

$$\delta_1 = [(\Delta H^{vap} - R\ T)/V^o{}_1]^{1/2} \qquad [3.17]$$

where the molar enthalpy of vaporisation was calculated from literature values[191] at 25 °C using the approximation of Watson[193];

$$\Delta H^{vap} = \Delta H^{vap}(25\ °C)[(1 - T_r)/(1 - T_{r(25)})]^{0.38} \qquad [3.18]$$

Values for the left hand side of equation [1.54] were found to approximate to a linear correlation with temperature over a limited temperature range. Thus, values were interpolated to set temperatures within each phase to account for the variation in the measurement temperatures between different probes from which the solubility parameters were obtained. Values of individual χ^S were not computed because of the large degree of uncertainty in the values, as discussed in section 3.7.

3.5 TERNARY SOLUTIONS

Chapter 7 considers the solution behaviour of the probe tending to infinite dilution in a binary stationary phase. The presence of a second stationary phase component requires an extention to the binary solution approach of calculating the interaction parameters. The interaction parameter between probe and the individual components at a given temperature was calculated using the appropriate equation, [3.11] or [3.12]. Denoting the probe as component 1 and the stationary phase components as 2 and 3, the interaction parameter between the probe and the binary stationary phase, $\chi^\infty{}_{1(23)}$, was calculated from a similar expression to those in equation [3.11] and [3.12];

3.4b Solubility Parameters

The stationary phase solubility parameters,δ_2, were estimated using the method of Guillet[125], discussed in section 1.12b, from the equation;

$$(\delta_1{}^2/R\ T) - \chi/V^o{}_1 = (\delta_2/R\ T)\delta_1 - [(\delta_2{}^2/R\ T) + \chi^S/V^o{}_1] \qquad [1.54]$$

where χ^S is the entropic contribution to the interaction parameter. The probe interaction parameter, δ_1, was calculated from the molar enthalpy of vaporisation and the molar volume;

$$\delta_1 = [(\Delta H^{vap} - R\ T)/V^o{}_1]^{1/2} \qquad [3.17]$$

where the molar enthalpy of vaporisation was calculated from literature values[191] at 25 °C using the approximation of Watson[193];

$$\Delta H^{vap} = \Delta H^{vap}(25\ °C)[(1 - T_r)/(1 - T_{r(25)})]^{0.38} \qquad [3.18]$$

Values for the left hand side of equation [1.52] were found to approximate to a linear correlation with temperature over a limited temperature range. Thus, values were interpolated to set temperatures within each phase to account for the variation in the measurement temperatures between different probes from which the solubility parameters were obtained. Values of individual χ^S were not computed because of the large degree of uncertainty in the values, as discussed in section 3.7.

3.5 TERNARY SOLUTIONS

Chapter 7 considers the solution behaviour of the probe tending to infinite dilution in a binary stationary phase. The presence of a second stationary phase component requires an extention to the binary solution approach of calculating the interaction parameters. The interaction parameter between probe and the individual components at a given temperature was calculated using the appropriate equation, [3.11] or [3.12]. Denoting the probe as component 1 and the stationary phase components as 2 and 3, the interaction parameter between the probe and the binary stationary phase, $\chi^\infty{}_{1(23)}$, was calculated from a similar expression to those in equation [3.11] and [3.12];

$$\chi^{\infty}_{1(23)} = \ln [273.2 \, R(w_2 \, v_2 + w_3 \, v_3)/V^0_g \, P^0 \, V^0_1] - P^0 \, B_{11}/R \, T$$

$$- [1 - (V^0_1/V^0_2)]\phi_2 - [1 - (V^0_1/V^0_3)]\phi_3 \qquad [1.57]$$

Instead of the segment volume of the stationary phase, or equivalent expression, the weight average segment volume is now used, $(w_2 \, v_2 + w_3 \, v_3)$, where v and w are the segment volume and weight fraction, respectively, of the designated stationary phase component. The interaction parameter between the stationary phase components was determined using the graphical method of Deshpande and Farooque[138], outlined in section 1.12c, from;

$$(\chi_{1(23)} - \chi_{13})/V^0_1 = \phi_2(\chi_{12} - \chi_{13})/V^0_1 - \phi_2 \, \phi_3 \, \chi_{23}/V^0_1 \qquad [1.59]$$

where the superscript ∞ is dropped for clarity. The terms in bold were plotted as ordinate and abscissa and the interaction parameter obtained from the intercept. As discussed in section 1.12c, this method eliminates the variation in values caused by individual probes interacting differently with the stationary phase. The composition of these stationary phase coatings were taken as the predicted values from preparation conditions. Values are quoted in chapter 7 along with the "effective volume fractions", obtained from the gradient of the above plot. In chapters 5 and 6 the interaction parameters are shown to change linearly with temperature within a given phase. Values were calculated at a set of temperatures in each phase, following the approach outlined in section 3.4b to account for the acquisition of retention measurements at slightly different temperatures for different sets of data.

3.6 MOLECULAR DIMENSIONS

The interaction between probe molecules and stationary phase has often been discussed in terms of the asymmetry of the probe molecules, usually quantified as the length to breadth ratio. This approach to correlating thermodynamic data is discussed in chapter 5. It is also evident from section 3.4a that to estimate the number of segments a rigid mesogen occupies on a hypothetical lattice it is necessary to estimate the molecular dimensions of the liquid crystal. These were obtained from energy

minimised conformations of molecule projections using the computer package
"ALCHEMY II".

Each probe was taken to have three orthogonal dimensions describing the molecule
size. To obtain the length to breadth ratio the longest dimension was assigned to the
length and the molecule was assumed to be cylindrical with a diameter equal to the
second longest dimension. *Figure 3.2* illustrates the energy minimised structure for
octane. *Table 3.3* gives all dimensions of each probe together with the axial ratio, so
defined. It can be seen that for aliphatic probes the approximation to a cylinder is
reasonable, but the aromatic probes are more disc-like.
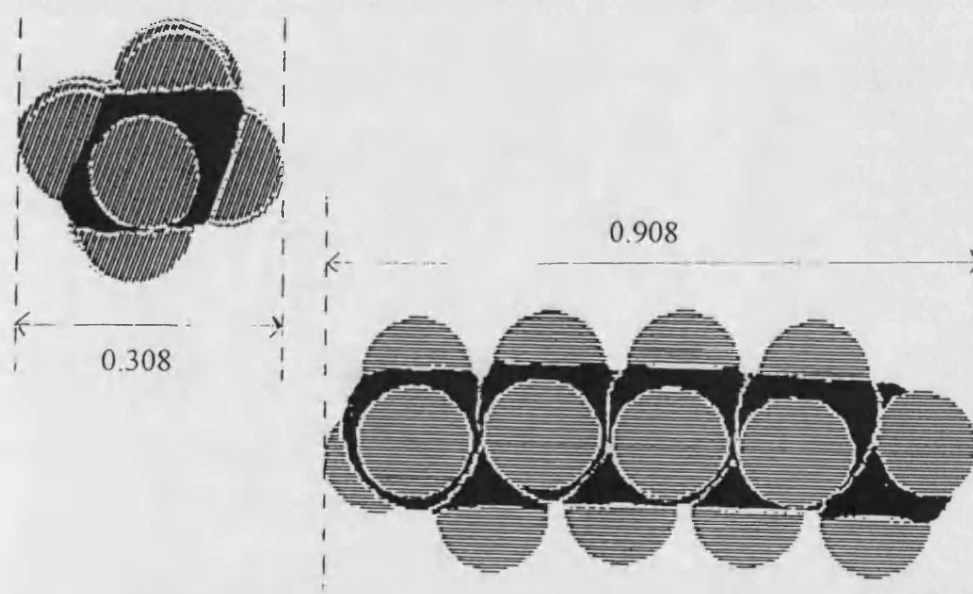
Figure 3.2: Energy minimised structure for octane with molecule dimensions

The number of segments a rigid mesogen occupies on a lattice is simplified to a single
value for the liquid crystals studied in this thesis because they are comprised of
sections that are either clearly rigid or definitely flexible in behaviour. The molecule
dimensions are given in *table 3.4* The torsional angle between the biphenyl rings of
the mesogen was found to be 28 º and 33 º for HCB and OCB, respectively, compared
to literature values[197] of ≈ 45 º for biphenyl.

Table 3.3: Molecular dimensions of the IGC probes

	Length nm	Breadth nm	Depth nm	L:B
Pentane	0.564	0.308	0.308	1.83
Hexane	0.731	0.308	0.308	2.37
Heptane	0.857	0.308	0.308	2.78
Octane	0.908	0.308	0.308	2.95
Nonane	1.107	0.308	0.308	3.59
Decane	1.227	0.308	0.308	3.98
Cyclohexane	0.431	0.431	0.266	1.00
2-Methylhexane	0.685	0.372	0.308	1.84
3-Methylhexane	0.656	0.376	0.308	1.74
2,3-Dimethylpentane	0.613	0.480	0.308	1.28
2,4-Dimethylpentane	0.682	0.364	0.308	1.87
2,2,3-Trimethylbutane	0.499	0.433	0.383	1.15
Benzene	0.497	0.430	0.180	1.16
Toluene	0.587	0.430	0.180	1.37
Ethylbenzene	0.730	0.430	0.180	1.70
p-Xylene	0.676	0.430	0.180	1.57
m-Xylene	0.666	0.500	0.180	1.33
o-Xylene	0.511	0.505	0.180	1.01

Table 3.4: Molecular dimensions of the cyanobiphenyls

	Total Length nm	Mesogen Length nm	Mesogen Breadth nm
HCB	1.771	1.094	0.430
OCB	1.998	1.094	0.430
LCP	-	1.094	0.430

Table 3.3: Molecular dimensions of the IGC probes

	Length nm	Breadth nm	Depth nm	L:B
Pentane	0.564	0.308	0.308	1.83
Hexane	0.731	0.308	0.308	2.37
Heptane	0.857	0.308	0.308	2.78
Octane	0.908	0.308	0.308	2.95
Nonane	1.107	0.308	0.308	3.59
Decane	1.227	0.308	0.308	3.98
Cyclohexane	0.431	0.431	0.266	1.00
2-Methylhexane	0.685	0.372	0.308	1.84
3-Methylhexane	0.656	0.376	0.308	1.74
2,3-Dimethylpentane	0.613	0.480	0.308	1.28
2,4-Dimethylpentane	0.682	0.364	0.308	1.87
2,2,3-Trimethylbutane	0.499	0.433	0.383	1.15
Benzene	0.497	0.430	0.180	1.00
Toluene	0.587	0.430	0.180	1.37
Ethylbenzene	0.730	0.430	0.180	1.70
p-Xylene	0.676	0.430	0.180	1.57
m-Xylene	0.666	0.500	0.180	1.33
o-Xylene	0.511	0.505	0.180	1.01

Table 3.4: Molecular dimensions of the cyanobiphenyls

	Total Length nm	Mesogen Length nm	Mesogen Breadth nm
HCB	1.771	1.094	0.430
OCB	1.998	1.094	0.430
LCP	-	1.094	0.430

3.7 LIMITS OF UNCERTAINTY

The uncertainty for any of the derived parameters outlined in the above sections obviously depends on the accuracy and precision with which the primary datum can be measured. Equation [3.1] conveniently groups the contributions to uncertainty in the specific retention volume;

$$V^o_g = F(t_R - t_M)/W \qquad [3.1]$$

It has already been stated in section 2.2a that the net retention volume was measured to a precision of within ± 1 %. Flowrates at the column outlet were typically measured to within ± 0.2 % and the overall contribution to uncertainty from the corrected flowrate, calculated from the measured uncertainties outlined in section 2.2, is within ± 0.5 %. The major contribution to uncertainty arises from the column loading term, W. The measured column packing was precise to ± 0.05 % to ± 0.2 %, dependent upon the mass of packing used, but the uncertainty in determining the support loading was much larger than the uncertainty due to column packing. In this work the uncertainty in W was typically between ± 0.5 % and ± 1.4 % but values for some of the soxhlet extractions were as high as ± 2 %. The overall uncertainty in the specific retention volume was estimated to be ± 3 % of the measured value. The accuracy of the specific retention volumes was assessed by comparing values measured for PDMS with literature values. These values are reported in the following chapters. Good agreement was found with the more recent reports.

The activity coefficient has two sources of uncertainty, the uncertainty in the specific retention volume and the uncertainty arising from the correction term for a real gas. The latter can be calculated to within ± 4 %, as outlined in section 3.3. However, the correction term only changes the value of the activity coefficient by between 1 % and 5 % so the uncertainty in the activity coefficient is very close to ± 3 %, the uncertainty in the retention volume.

The relatively small uncertainty in activity coefficients and specific retention volumes translates to much larger percentage uncertainties in the enthalpies obtained from the gradients of the van't Hoff plots. The uncertainty in enthalpy can be found from the uncertainty in the ordinate quantity from[30];

$$\delta\Delta H = 2^{1/2} R\ T_1\ T_2\ \delta X / (T_1 - T_2) X \qquad [3.19]$$

where T_1 and T_2 represent the range of temperature over which the gradient is measured. X is the ordinate parameter and ΔH is the enthalpy term derived from the X parameter. The minimum temperature range used to measure enthalpy changes in any mesophase or phase in this work was 10 °C. This corresponds to an absolute uncertainty in the enthalpy value of 3.5 kJ mol⁻¹ to 5 kJ mol⁻¹ for temperatures at the low end or high end of the overall range measured, respectively. This uncertainty becomes particularly large when considering the excess partial molar enthalpy derived from the activity coefficients. The measured uncertainties in the van't Hoff plot slopes are well below the margins quoted above. These are reported alongside individual values in chapter 5 as standard deviations for the enthalpy and entropy terms. The spreadsheet package used calculated the standard deviations in the slopes and intercepts directly. The negligible uncertainty of the oven temperature justifies the application of the linear regression approach.

When calculating the interaction parameter the activity coefficient and the density of the stationary phase were the two main contributors to the uncertainty, following from equation [3.11]. The final quotient in this equation becomes negligible as the stationary phase molecules get larger and the major contributions arise from the first two logarithm terms. The absolute uncertainty in the interaction parameter follows as ± 0.04. The other interaction parameters calculated in equation [3.14] and [3.16] have similar uncertainty limits. Dependent upon probe molecule, this can constitute between 2 % and 20 % of the measured value. However, the results presented in chapter 6 indicate uncertainties are actually towards the lower end of this range. To calculate the exchange interaction parameter requires the characteristic parameters.

The temperature and volume terms are reasonably precise, to within ± 2-3 %, but the characteristic pressure can have a precision of only ± 10 %. This leads to uncertainty in the exchange parameter of a similar order of magnitude.

The solubility parameter uncertainty is dependent on the uncertainty in the interaction parameter. Literature values used to calculate the probe solubility parameters are quoted to sufficient accuracy for this to only form a minor contribution to uncertainty. Using the method of Guillet, section 3.4b, the solubility parameter of the stationary phase is found from a slope and hence only incurs a relatively small standard deviation. The standard deviation was typically ± 0.5 % of the measured value. It is possible to obtain the entropy contribution to the interaction parameter, χ^S, from the intercept of such a plot but the intercept is very sensitive to the fluctuations in the ordinate quantity. Uncertainties orders of magnitude greater than the measured value of χ^S can result and values are not quoted here.

In the ternary system the interaction parameter between the stationary phases was subject to the cumulative uncertainties in the three measured probe-stationary phase interaction parameters, as follows from equation [1.59]. The parameter required is measured from a graphical plot similar to the one described above for the solubility parameter. However, although the slope can be obtained to a precision of ± 2-3 % the parameter of interest this time is obtained from the intercept. Values can suffer uncertainty limits that are up to three times the measured value, as Etxeberria et al.[139] caution (see section 1.12c). Thus, the interaction parameters between the two stationary phase components quoted in this study are only considered in terms of general trends, rather than assigning any great significance to the absolute values.

CHAPTER 4

PHASE TRANSITION BEHAVIOUR

The liquid crystals studied exhibit a variety of mesophases and transitions, as illustrated in *figure 2.1*. The crystalline phase, denoted as K, is the solid form exhibited by the liquid crystal and is not a comment upon the degree or nature of the crystallinity.

As discussed in section 1.1, the nematic phases of OCB and HCB possess orientational order only. The OBIB material exhibits a cholesteric phase where the molecules possess orientational order and are twisted in helices. LCP and OCB exhibit a smectic A phase where the directors of the mesophase are oriented in layers orthogonal to the plane of those layers. OBIB, on the other hand, exhibits a smectic C mesophase where the directors are tilted within the planes.

The solution behaviour of these individual phases will be discussed in detail in the following two chapters. Here the discussion will concentrate on the transition behaviour of these materials. This chapter begins by comparing transition temperatures measured by DSC to those given by the supplier, reported to have been measured by hot-stage microscopy (HSM). There follows a brief discussion of these transitions observed in the density measurements before considering IGC as a method for measuring the transitions. The IGC method is a static method of transition determination, where the temperature is obtained from a set of data obtained under isothermal conditions, as opposed to the dynamic method of DSC. The chapter ends with a look at the crystallisation of these materials focusing on the rate of the nematic to crystalline transition in HCB.

4.1 DIFFERENTIAL SCANNING CALORIMETRY (DSC)

4.1a Effect of Heating Rate

The effect of altering the heating rate was measured for a 12.7 mg sample of the HCB liquid crystal. Heating rates between 2 °C min^{-1} and 20 °C min^{-1} were measured. Uncertainties in the transition temperatures and the associated transition enthalpies were of the same order of magnitude as those reported in section 4.1b. As the heating rate increased the peak maxima shifted to higher temperature and the energy associated with the transition, obtained from the area under the peak, decreased. By comparing the baseline width under the endotherm with the heating rates, the phase transitions were estimated to occur within a time interval of a few minutes. Comparison of the thermograms for other liquid crystals with those for HCB, see figure 2.2, indicate all the transitions measured in this study occur over a similar time interval. *Figure 4.1a* and *4.1b* show the temperature of the peak maxima and endotherm energies for the crystal to nematic and nematic to isotropic transitions on heating. As the heating rate increased more of the energy was lost in the background signal and a linear correlation between heating rate and shift in peak maximum was observed for the crystalline to nematic transition. A near linear relationship existed for the clearing transition. The curvature at high heating rates is due to a contribution from the broad crystal to nematic peak, shifting the peak maxima to lower temperature. As the heating rate decreased the transitions became sharper and the energies closer to the true values. Decreasing the sample size would also sharpen the peaks. In the following work a heating rate of 5 °C min^{-1} was used with sample sizes between 5 mg and 12 mg to give convenient run times with reasonably sharp peaks, giving the transition temperature to within ± 0.5 °C, where the smaller transitions could be detected.
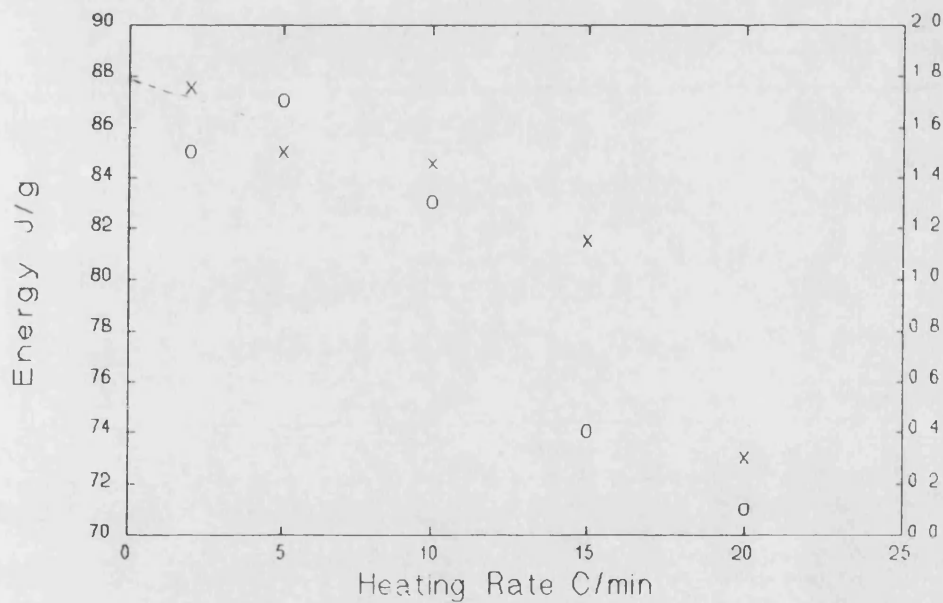
a)
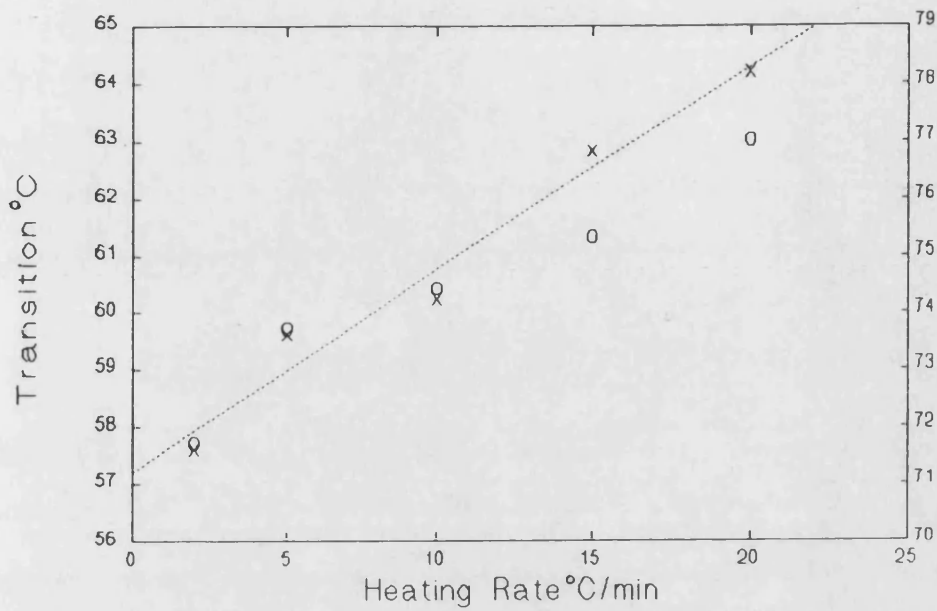
b)

Figure 4.1: a) Transition temperature at different heating rates and b) their respective energies for $T_{K \to N}$, x (left hand scale), and $T_{N \to I}$, o (right hand side) in HCB. The dotted line illustrates the linear dependence on heating rate.

4.1b Mesophase transitions and enthalpies

The transition temperatures and energies obtained from DSC on heating are compared in *table 4.1* to HSM and DSC values quoted by the supplier[198]. The samples were heated to the isotropic region and then cooled at a controlled rate to room temperature. *Table 4.2* lists the corresponding transitions on cooling. Initial and subsequent temperature cycles were identical and the thermograms are illustrated in *figure 2.2*.

The smectic A to isotropic transition for the LCP is considerably lower than the value from the manufacturer. All other values are in good agreement with the suppliers data. In all cases the endotherm of fusion from the crystal phase to the mesophase is considerably larger than subsequent transitions reflecting the considerable disruption of the molecules on forming the liquid phase. In OBIB the smectic C to cholesteric transition is relatively large compared to the clearing transition but in OCB the smectic A to nematic transition is relatively small, and can only be seen on expanding the scale of the thermogram traces. The latter indicates the similarity between the two mesophases in OCB. The degree of ordering in the mesophase decreases with temperature[199] and diminishes rapidly as the clearing temperature is approached. Hence, the relatively low energies associated with this transition compared to the melting transition. In the smectic A phase the arrangement of the directors and the mobility of the individual molecules[200] allows the smectic to nematic transition to be pictured as the sliding of molecules orthogonally out of the smectic layers. This requires little molecular rearrangement and so the associated transition energy was low. The comparatively high energy for the smectic C to cholesteric transition is indicative of a much larger molecular rearrangement.

From a comparison of the measured values in *table 4.1* and *4.2*, it is evident that there was little hysteresis in temperatures for isotropic-mesophase and mesophase-mesophase

Table 4.1: Transition temperatures, in °C, and energies, in kJ mol^{-1}, on heating samples . Uncertainties are the measured differences between duplicate runs.

	Mass mg	Tg	$T_{K\rightarrow S}$ $(T_{K\rightarrow N})$	Energy	$T_{S\rightarrow N}$ $(T_{S\rightarrow C})$	Energy	$T_{N\rightarrow I}$ $(T_{S\rightarrow I})$	Energy
HCB a	5.5		58.6 ±1.3	32.3 ±1.4			75.4 ±0.3	0.54 ±0.04
b			57	29.67			75.5	
			(44.3 ±0.2^c)					
OCB a	10.9		55.4 ±0.5	29.9 ±1.2	66.1 ±0.3	0.03 ±0.01	79.6 ±0.3	0.93 ±0.12
b			54.5	29.5	67		80	
OBIB a	9.4		78.8 ±0.2	20.3 ±0.1	99.4 ±0.4	2.74 ±0.12	122.1 ±0.4	1.18 ±0.17
b			79		100		122	
LCP a	11.6	-6.8 ±1.4^d					73.2 ±0.9	1.82 ±0.07^e
b		-3.9					79.1	

a: measured, b: suppliers data, c: immediately reheating sample, d: -3.4 °C for 10 °C min^{-1}, e: per mole of segments

Table 4.2: Transition temperatures, in °C, and energies, in kJ mol^{-1}, on cooling samples. Uncertainties are the measured differences between duplicate runs.

	Mass mg	Tg	$T_{S \to K}$ ($T_{N \to K}$)	Energy	$T_{N \to S}$ ($T_{C \to S}$)	Energy	$T_{I \to N}$ ($T_{I \to S}$)	Energy
HCB	5.5		34.0 ±0.5	23.8 ±2.6			74.3 ±0.2	0.7 ±0.1
OCB	10.9		22.4 ±0.4	24.1 ±1.8			77.5 ±0.2	0.8 ±0.1
OBIB	9.4		62.8 ±0.0	18.6 ±0.1	97.3 ±0.2	2.9 ±0.2	120.6 ±0.1	1.5 ±0.0
LCP	11.6	-13.4					69.7 ±0.1	1.8 ±0.1[a]

a: per mole of segments

transitions. This was consistent with the short transition times. The difference between duplicate cooling runs were fortuitously small in many cases as the baseline was considerably nosier on cooling than heating and discrepancies in energies given in *tables 4.1* and *4.2* were a result of this. The baseline fluctuations on cooling made identification of the nematic to smectic A transition in OCB impossible. However, the most marked discrepancy between heating and cooling was the differences at the melting/freezing temperature.

If the large hystereses about the crystal-mesophase transition were governed by kinetic factors alone much broader exotherms would be expected on cooling than on heating. However, the peaks are similar for both indicating the liquid crystal is supercooling. As the liquid crystal supercools it loses entropy and the free energy of the system decreases. So when the liquid crystal eventually crystallises the observed exotherm is smaller, similar to the behaviour observed in glassy materials[201]. This behaviour can be seen in the tables. On reheating the OCB and OBIB identical transition temperatures were obtained but HCB behaved differently. If the HCB was reheated immediately a crystal to nematic transition now occurred at 44.3 °C and with a lower endotherm energy, as shown in *table 4.2*. This transition proved to be repeatable on subsequent runs. However, if the sample was left for a few days prior to rerunning the original transition behaviour was observed. This behaviour could be explained by the formation of a second, less organised crystal phase on cooling which reverts slowly back to the more stable crystal form when left at room temperature. The existence of a second crystal phase with a transition to the nematic mesophase at 44 °C is briefly eluded to in the supplier's literature[198]. At the heating rate employed here the liquid crystals supercooled by 23 °C (10 °C), 33 °C, and 17 °C for HCB, OCB, and OBIB, respectively. If the HCB is considered to be supercooling with respect to the high temperature crystal form, the value in brackets, these values are seen to reflect the mobility of the molecules within the mesophase. The more mobile nematic phase is able to rearrange into the crystal phase more easily than the smectic

phases. The greater degree of supercooling for OCB compared to OBIB reflects the lower temperature range of the mesophase where there is less thermal energy for molecular rearrangement.

4.1c Supported liquid crystals

All previously reported data was obtained from bulk materials. However, later in this chapter the transition temperatures are reported from IGC measurements where the liquid crystal is coated upon a Chromosorb P support. There are several reports in the literature[169-171], as discussed in section 1.14, which claim such thin coated films can be affected by the support surface. To establish whether coating altered the phase behaviour in the systems studied here a 12.4 mg sample of HCB coated support, with a 0.1436 mass fraction of HCB, was run. The transition temperatures and energies are given in *table 4.3*. Generally the values agree, to within experimental uncertainty, with

Table 4.3: Comparison of transition temperatures, $^\circ C$, and energies, kJ mol^{-1}, for bulk HCB and a sample coated on Chromosorb P

	Bulk HCB	Coated HCB
$T_{K \rightarrow N}$	58.6 $\pm$ 1.3	57.4 $\pm$ 0.6
Energy	32.3 $\pm$ 1.4	28.7 $\pm$ 2.4
$T_{N \rightarrow I}$	75.4 $\pm$ 0.3	76.1 $\pm$ 0.4
Energy	0.5 $\pm$ 0.04	0.46 $\pm$ 0.19
$T_{I \rightarrow N}$	74.3 $\pm$ 0.2	74.7 $\pm$ 0.4
Energy	0.66 $\pm$ 0.11	0.51 $\pm$ 0.10
$T_{N \rightarrow K}$	34.0 $\pm$ 0.5	30.9 $\pm$ 0.6
Energy	23.8 $\pm$ 2.6	18.0 $\pm$ 0.9
$T_{K \rightarrow N}{}^a$	44.3 $\pm$ 0.2	44.1 $\pm$ 0.5
Energy	25.8 $\pm$ 0.6	18.6 $\pm$ 1.8

a: immediately reheating sample

those reported for the bulk materials. However, the supercooled to crystalline transition was depressed by 3 °C and the exotherm and endotherm associated with cooling and immediately reheating about this transition are lower. This could be a consequence of the constraints the support surface places on the liquid crystal during crystallisation. On the long time scale the initial transition behaviour during heating was restored so it is reasonable to assume there is no significant alteration of the liquid crystal phase behaviour by coating it onto the Chromosorb at the loading employed.

Heating cycles for an 8 % loading of OCB on Chromosorb P have previously been reported[154]. There was good agreement between the transition temperatures of the coated and uncoated liquid crystal.

4.2 DENSITY MEASUREMENTS

For the liquid crystals HCB, OCB, and LCP enough material was available to measure the densities as a function of temperature. The results are shown in *figure 4.2*. For the mesophase transitions the change in density was small and of the order of the uncertainty in the measurements. However, the crystalline to mesophase transitions were accompanied by a decrease in density of around 10 % and the transitions can be obtained. In HCB the change was very abrupt and occurred between 55.5 °C and 56.4 °C. OCB had a much broader change with the density decreasing between 49.6 °C and 53.6 °C. If the higher temperature is taken as the point where no more crystalline phase exists, and is thus the transition temperature, these values are in agreement with those reported from the DSC measurements. OCB is therefore exhibiting a premelting transition. This phenomenon is well known and has been noted in crystal-mesophase and higher temperature mesophase transitions in a series of reports[175] that measured the density of cholesteric liquid crystals by dilatometry, although premelting in the higher temperature transitions only occurred to 1 °C below the transition.

The fact that the density behaviour of HCB was so different from that of OCB was surprising. IGC measurements, reported in section 4.3, showed a premelting "softening" of the crystalline phase for both liquid crystals and so the behaviour would appear to be more involved than just a consequence of the mesophase the material fuses into. An explanation of this discrepancy is that the crystalline region undergoes some form of reordering, prior to entering the nematic phase, creating "soft", less dense regions in equal proportion to higher density regions. However, this will need further study before the behaviour can be fully elucidated.
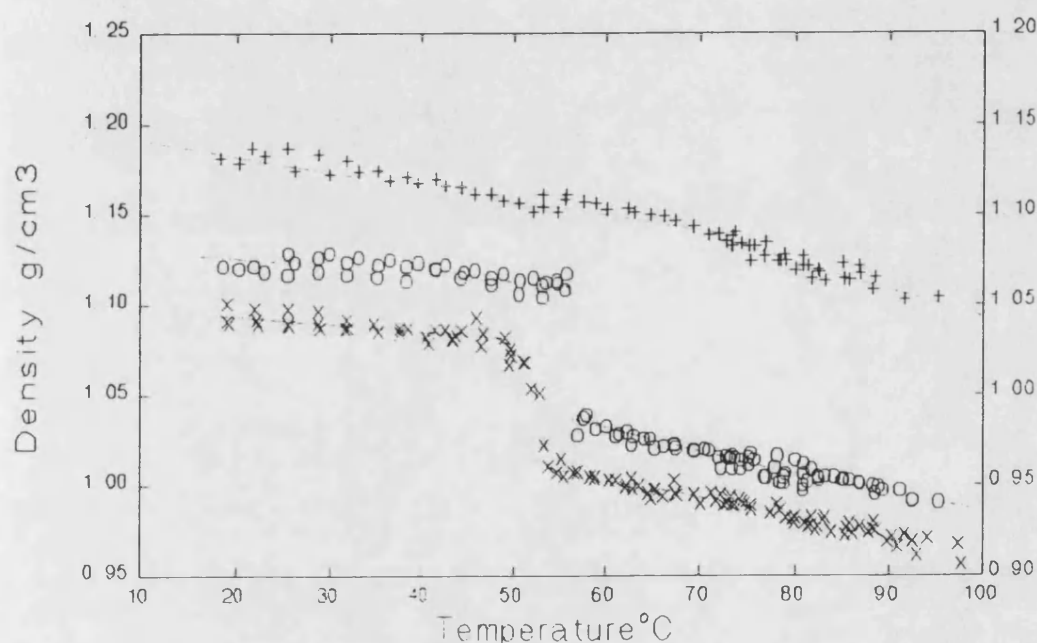
Figure 4.2: Density as a function of temperature for HCB, o, OCB, x, (left hand scale) and LCP, +, (right hand scale).

4.3 INVERSE GAS CHROMATOGRAPHY

The phase behaviour of the liquid crystal stationary phases was studied using a range of hydrocarbon probes with differing shape and polarisability. More polar probes, such as chloroform, are very good solvents for the materials used here. In their studies on polymer transitions, Llorente et al [202] reported that such probes interfere with transitions by dissolving in the lower temperature phase. This implies that hydrocarbon

probes would be less inclined to distort the retention behaviour of the liquid crystals about the transitions.

The van't Hoff plots for all probes in all stationary phases are shown in appendix I. Examples of plots are reproduced in *figure 4.3* to *4.6* for benzene and nonane probes with the four liquid crystals studied. In chapter 5 it will be seen that similar plots of the activity coefficients give more marked changes about a phase transition, but for now discussion will be restricted to the retention volume behaviour. As discussed in section 1.12a, the retention volume generally decreases as the temperature increases. About the crystalline transition temperature retention increased considerably as the probe was able to absorb into the bulk as opposed to just adsorbing on the liquid crystal surface. Retention then decreased again with further, smaller, increases in retention about subsequent phase transitions until the isotropic phase was reached, whereupon retention continued to fall with increasing temperature. This general behaviour has been commonly observed in liquid crystal systems[17,145,158]. This behaviour indicates first order phase transitions, where the first derivative of the change in chemical potential is discontinuous and, hence, is accompanied by an enthalpy change. This has already been seen to be the case from the DSC thermograms, where the phase transitions are accompanied by endotherm or exotherm peaks. There also exists the possibility that the first derivative is continuous but the second derivative is not. This is a second order phase transition and is accompanied by a change in slope of the enthalpy temperature dependence. An example of this behaviour is the glass transition in polymers which was observed as a step in the DSC thermograms. For OCB the smectic A to nematic phase transition was accompanied by a very subtle increase in retention volume indicating that the transition approaches second order. This is a consequence of the similarity between the two phases, as discussed in section 4.1b, where sliding of molecules out of the smectic layer is sufficient to effect a nematic phase. However, although this phase transition
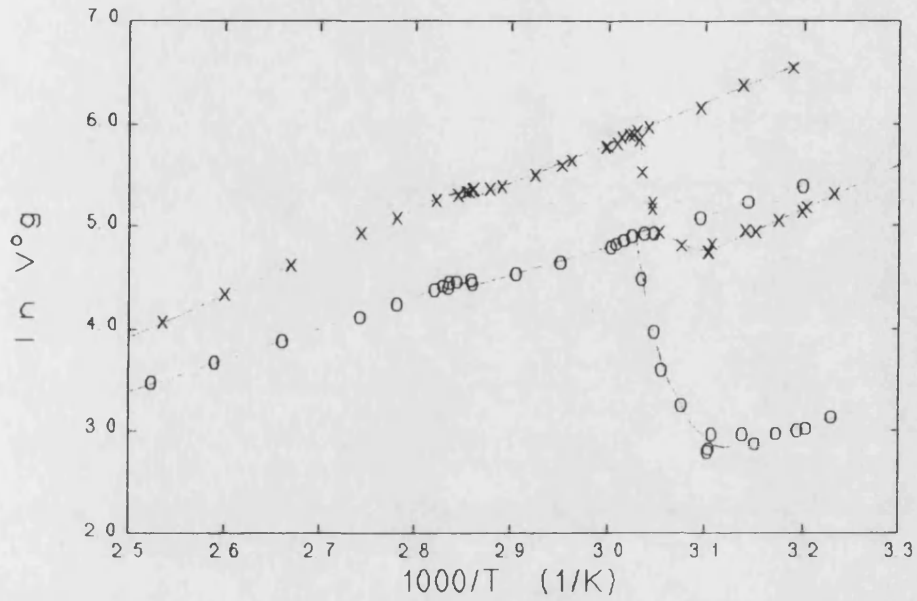
Figure 4.3: Nonane, x, and benzene, o, retention as a function of temperature for HCB.
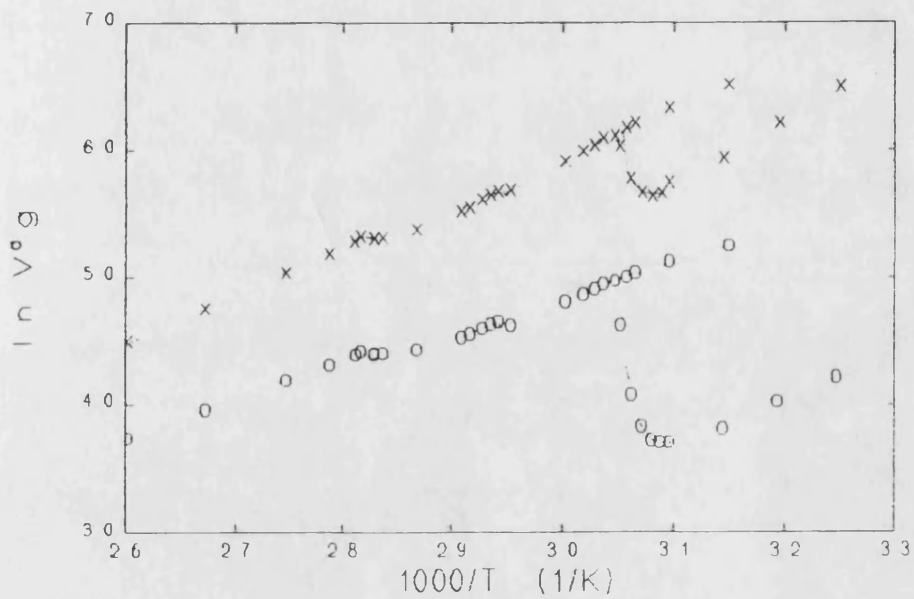

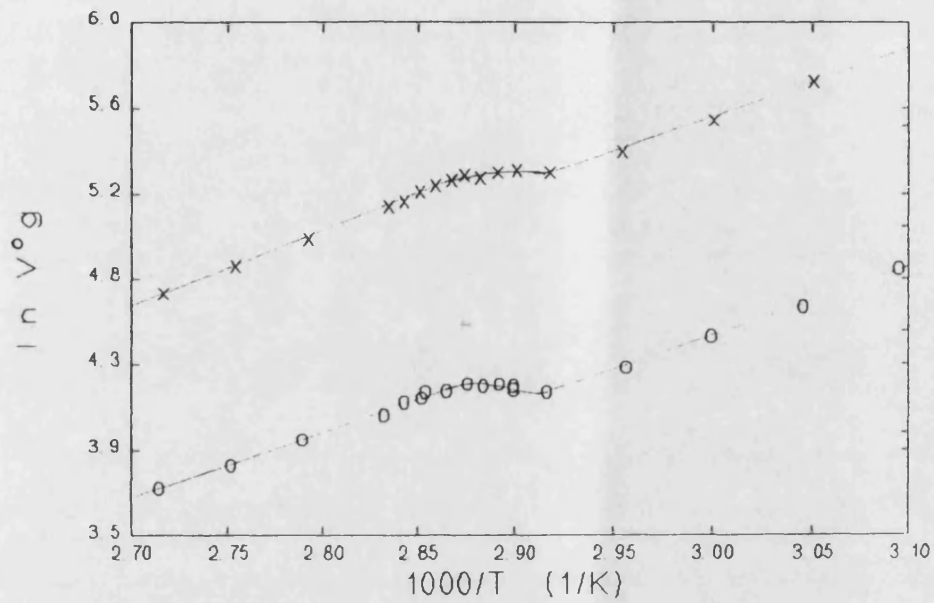**Figure 4.4:** Nonane, x, and benzene, o, retention as a function of temperature for OCB.

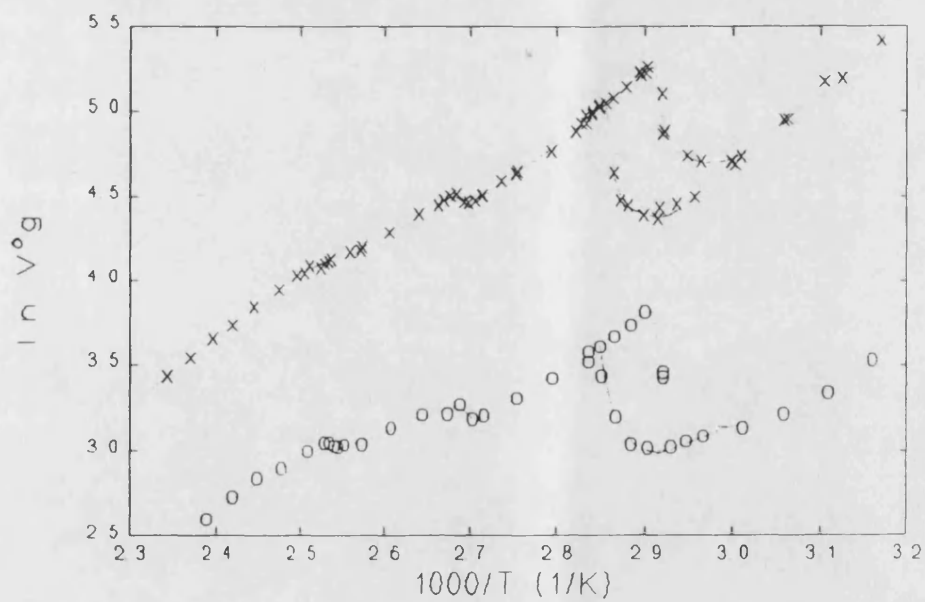**Figure 4.5:** Nonane, x, and benzene, o, retention as a function of temperature for LCP.

Figure 4.6: Nonane, x, and benzene, o, retention as a function of temperature for OBIB.

approaches second order it was shown in section 4.1b that it is accompanied by a small enthalpy change and is thus strictly first order. Several reports on liquid crystals describe such "weakly first order" transitions, for example reference 152, but no true second order liquid crystal phase transition has been reported to date to the knowledge of this author.

Most transitions exhibit some degree of premelting behaviour, manifested as an increase in probe retention volume prior to the transition temperature. However, this only occurs over a significant temperature range for the crystalline to mesophase transition. No hysteresis was observed, within experimental uncertainty, for the higher temperature mesophase transitions but considerable hysteresis occurs about the crystalline transition. Also, as the liquid crystal mesophase is cooled it enters the supercooled phase. Previous reports in the literature[149] consider this to be a continuation of the higher temperature phase. In section 4.3c and chapter 5 evidence will be presented that indicates the supercooled phase is not identical to the higher temperature mesophase and a phase transition temperature can be associated with the cooling process.

4.3a Effect of different probes

The transition temperature is taken as the temperature at which the lower temperature phase no longer exists. This corresponds to the retention maximum about the transition. The transition temperatures for the various probes in the different liquid crystals are listed in *tables 4.4, 4.5, 4.6* and *4.7*. No significant difference was found for the probes used. Comparison with results given in the previous sections of this chapter show the precision and accuracy is comparable to that found from HSM, DSC, or density measurements. The LCP values corroborate those measured by DSC and indicate the data from the supplier does not correctly describe the phase transitions in the sample obtained for this work.

4.3b Retention Volume Profiles

In figure, 4.2 the probe retention with HCB stationary phase shows two classic "Z-profiles", see section 1.12a, about the crystal and isotropic transitions. The crystal transition was considerably more obvious than the isotropic transition. Similar profiles are seen for the other liquid crystals. OBIB showed a more marked change in retention for the smectic C to cholesteric phase than was seen at the clearing

Table 4.4: Transition temperatures, $^{\circ}$C, for HCB measured for different probes. Uncertainties were estimated from the retention plots, the standard deviation is reported for the average value. N' refers to the supercooled phase.

	T_{NI}	$T_{N \to N'}$	$T_{K \to N}$
Pentane	76.9 ±0.9	57.6 ±0.4	57.5 ±0.5
Hexane	76.6 ±0.6	57.6 ±0.7	57.3 ±0.2
Heptane	76.5 ±0.7	57.4 ±0.5	57.2 ±0.1
Octane	76.0 ±0.4	57.6 ±0.7	57.0 ±0.3
Nonane	75.7 ±0.5	58.0 ±0.7	57.3 ±0.5
Benzene	77.0 ±0.6	57.7 ±0.6	57.4 ±0.9
Toluene	76.8 ±0.4	57.1 ±0.4	57.2 ±0.2
Ethylbenzene	76.8 ±0.4	57.5 ±0.8	57.6 ±0.2
p-Xylene	77.0 ±0.5	57.6 ±0.7	57.2 ±0.2
m-Xylene	76.9 ±0.6	57.8 ±0.7	56.9 ±0.5
o-Xylene	76.7 ±0.6	57.3 ±0.8	57.1 ±0.3
Cyclohexane	76.9 ±0.6	57.5 ±0.4	57.1 ±0.2
Average	76.7 ±0.4	57.6 ±0.2	57.2 ±0.2

temperature. OCB shows complementary behaviour. These trends are in agreement with the energy measurements from DSC, given in section 4.1b. *Figures 4.3 to 4.6* show that nonane and benzene retention profiles are generally different and this

Table 4.5: Transition temperatures, °C, for OCB measured for different probes.

Uncertainties were estimated from the retention plots, the standard deviation is reported for the average value. S' refers to the supercooled phase.

	T_{NI}	T_{NS}	$T_{S \to S'}$	$T_{K \to S}$
Pentane	80.0 ±0.6	66.4 ±0.1	53.6 ±0.4	55.1 ±0.5
Hexane	80.5 ±0.7	66.4 ±0.1	53.6 ±0.4	55.1 ±0.5
Heptane	80.5 ±0.7	66.4 ±0.1	53.6 ±0.4	55.3 ±0.3
Octane	80.0 ±0.8	66.4 ±0.1	53.7 ±0.3	55.1 ±0.5
Nonane	80.7 ±0.6	66.5 ±0.4	53.2 ±0.7	54.8 ±0.2
2-Methylhexane		66.5 ±0.2	53.4 ±0.5	55.3 ±0.5
3-Methylhexane		66.5 ±0.2	53.4 ±0.5	55.1 ±0.5
2,3-Dimethylpentane		66.4 ±0.1	53.4 ±0.5	55.5 ±0.5
2,4-Dimethylpentane		66.4 ±0.1	53.4 ±0.5	55.0 ±0.4
2,2,3-Trimethylbutane		66.5 ±0.2	53.4 ±0.5	54.9 ±0.6
Benzene	81.2 ±0.4	66.4 ±0.5	53.5 ±0.5	54.8 ±0.2
Toluene	81.0 ±0.4	66.4 ±0.4	53.5 ±0.5	54.7 ±0.3
Ethylbenzene	81.2 ±0.8	66.5 ±0.5	53.2 ±0.7	55.1 ±0.5
p-Xylene	81.0 ±0.6	66.5 ±0.4	53.3 ±0.6	54.8 ±0.2
m-Xylene	80.2 ±0.6	66.5 ±0.4	53.3 ±0.5	55.1 ±0.5
o-Xylene	80.8 ±0.5	66.5 ±0.6	53.5 ±0.5	55.0 ±0.4
Cyclohexane	81.1 ±0.6	66.7 ±0.1	53.6 ±0.3	55.3 ±0.4
Average	80.7 ±0.4	66.5 ±0.1	53.4 ±0.1	55.1 ±0.2

behaviour is typical between any of the aliphatic and aromatic probes, as seen in *appendix I*. For a given phase transition, the aromatic probes show a more marked increase in retention. The difference is smaller in OBIB.

Table 4.6: Transition temperatures, °C, for LCP measured for different probes. Uncertainties were estimated from the retention plots, the standard deviation is reported for the average value.

	T_{SI}
Pentane	74.3 ± 0.5
Hexane	73.2 ± 0.6
Heptane	73.5 ± 0.8
Octane	73.0 ± 0.5
Nonane	72.8 ± 0.6
2-Methylhexane	75.8 ± 0.5
3-Methylhexane	75.5 ± 1.0
2,3-Dimethylpentane	74.7 ± 0.6
2,4-Dimethylpentane	75.2 ± 0.4
2,2,3-Trimethylbutane	76.0 ± 0.7
Benzene	73.8 ± 0.8
Toluene	74.0 ± 0.6
Ethylbenzene	74.0 ± 0.7
p-Xylene	73.9 ± 1.0
m-Xylene	75.2 ± 0.7
o-Xylene	74.3 ± 0.8
Cyclohexane	75.5 ± 0.7
Average	74.4 ± 1.0

In chapters 5 and 6 it will be seen that the aromatic probes are thermodynamically better solvents for the liquid crystals used here. However, distortion of transition temperatures due to dissolution of the lower temperature phase was not an effect noted in the systems studied, as seen from *tables 4.4* to *4.7*. Indeed, where the pretransition melting is greatest, approaching the crystalline to mesophase transition,

Table 4.7: Transition temperatures, °C, for OBIB measured for different probes.

Uncertainties were estimated from the retention plots, the standard deviation is reported for the average value. S' refers to the supercooled phase.

	T_{CI}	T_{CS}	$T_{S \rightarrow S'}$	$T_{K \rightarrow S}$
Octane	122.5 ±0.5	99.3 ±0.5	77.8 ±0.7	77.2 ±0.3
Nonane	122.1 ±0.7	99.3 ±0.5	77.9 ±0.7	77.1 ±0.4
Decane	121.3 ±0.5	99.3 ±0.5	77.9 ±0.7	77.1 ±0.4
Benzene .	121.6 ±0.5	99.1 ±0.9	78.8 ±0.7	78.3 ±0.2
Toluene	122.0 ±0.7	99.3 ±1.0	78.6 ±0.5	78.0 ±0.5
Ethylbenzene	121.6 ±0.5	99.6 ±0.7	78.6 ±0.6	77.2 ±0.1
p-Xylene	121.6 ±0.5	99.7 ±0.4	78.1 ±0.5	77.4 ±0.3
m-Xylene	121.6 ±0.5	99.6 ±0.4	78.1 ±0.5	77.4 ±0.3
o-Xylene	121.8 ±0.6	99.7 ±0.4	78.2 ±0.3	77.5 ±0.4
Average	121.8 ±0.3	99.4 ±0.2	78.2 ±0.3	77.5 ±0.4

both aliphatic and aromatic probes start to increase in retention at the same temperature, within the bounds of uncertainty.

The retention profiles about the crystalline phase transition can also give an idea of the differences between the relative adsorption and absorption behaviour of the probes. The retention volumes for the OBIB approximately double on entering the mesophase. For OCB the retention of the aliphatic probes increases by 50 % whereas the aromatic probe retentions triple and cyclohexane doubles. In HCB the aliphatic probe retention triples on entering the mesophase and cyclohexane values quadruple but aromatic probes increase by seven or eight times. Clearly the shape of the molecules is important in these trends as molecules with similar shapes exhibit similar increases in retention above a transition temperature. However, the large retention differences about the transition temperature in HCB indicate that the extent to which a probe can

interact is the governing factor. In going from the crystal to nematic phase there is a large loss in molecular order compared to forming a smectic phase. Thus, the probes will have a greater interaction with the mesophase. The much lower retention volume increases accompanying melting into a smectic phase indicate that all the probes have poorer interactions with the mesophase than in the nematic mesophase. The higher increases for the aromatic solvents indicates a better penetration of the smectic layers by these probes. However, differing interaction in the mesophase, whilst likely to be the major factor, is not the only possible contribution. Different degrees of adsorption on the crystal surface will also play a part. Greater aromatic probe affinity for the crystal surface will cause the difference between aliphatic and aromatic probe retention increases to contract whilst greater aliphatic probe affinity for the crystal surface will cause the difference to expand. A more in-depth discussion of the surface properties of the liquid crystals will be given in chapter 5. The elimination of these differences as we go from HCB to OCB to OBIB is indicative of the reduced interaction of any given probe with the stationary phases and increased "liquid crystal-liquid crystal" interactions, either arising from greater dispersion forces between the molecules or increased dipole strength.

4.3c The Supercooled Region

Supercooling in liquid crystals, where the mesophase is retained on cooling below the equilibrium freezing point, has been observed since the inception in gas chromatography work[203]. The supercooled region has been reported[148] to exhibit a reasonable stability such that it can be used to extend the separating power of these materials in analytical applications. This phase has always been regarded as a continuation of the mesophase to lower temperature[149]. However, this supercooled phase exhibits properties which differ significantly from those of the higher temperature phase.

In initial studies on HCB and OCB the columns were cooled from the conditioning temperature of 80 °C to around 40 °C and probe retention measured on increasing temperature. The supercooled region was sufficiently stable in both cases for reproducible measurements, exhibiting a linear van't Hoff plot, to be made. Further study revealed that the supercooled region could be divided into two parts. *Figure 4.7* illustrates these points for heptane with HCB stationary phase. On heating the sample
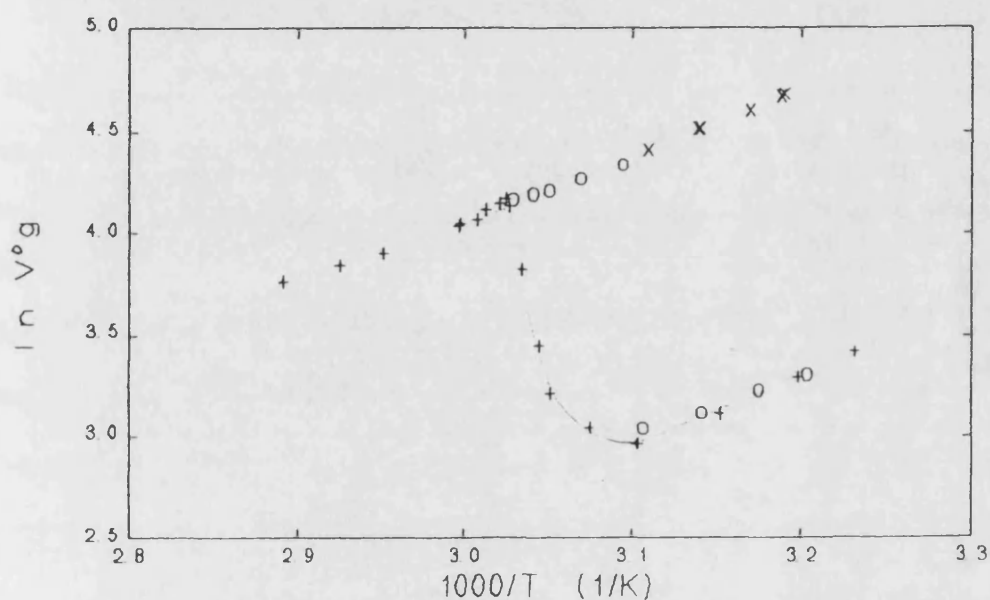

Figure 4.7: Retention volumes for heptane on HCB about the melting transition showing values for heating, +, cooling in the "stable" state, o, and values in the "apparently stable" state, x.

from the crystalline phase the retention increased as the melting transition temperature was approached, peaked at the transition temperature and then decreased at higher temperature. If the stationary phase was cooled from the nematic phase the probe retention followed the higher curve. Above 50 °C the measured retention volumes remained constant on the higher curve. No long term study was undertaken and the retention volumes may well have remained constant over a much longer period of time. Below 50 °C the retention times appeared constant, within the bounds of uncertainty, for up to several minutes but at longer times the retention volume visibly decreased.

After a period of a few days the isothermal retention had again stabilised and values close to those measured in the crystalline phase were obtained. The transition between the two types of behaviour occurred as a sharp change at 50 °C. Similar behaviour was observed for OBIB and OCB. In the former case the change occurred at 71 °C and for the latter the change occurred below 40 °C, but was difficult to ascertain more accurately as this was the limit of reasonable temperature control of the chromatograph oven.

In *figure 4.7* there is an indication of a slope change in the data about the nematic to supercooled region. *Figures 4.8* to *4.10* show examples of expanded van't Hoff diagrams for different probes about the mesophase to supercooled region in HCB, OCB, and OBIB. Data for all probes exhibited different slopes about the supercooled and mesophase regions. The extent of the difference varies from probe to probe but the aromatic probes generally gave the more marked changes. This indicates the supercooled phases in the liquid crystals studied here are not just extensions of the mesophases to lower temperature but constitute a different phase. The thermodynamic
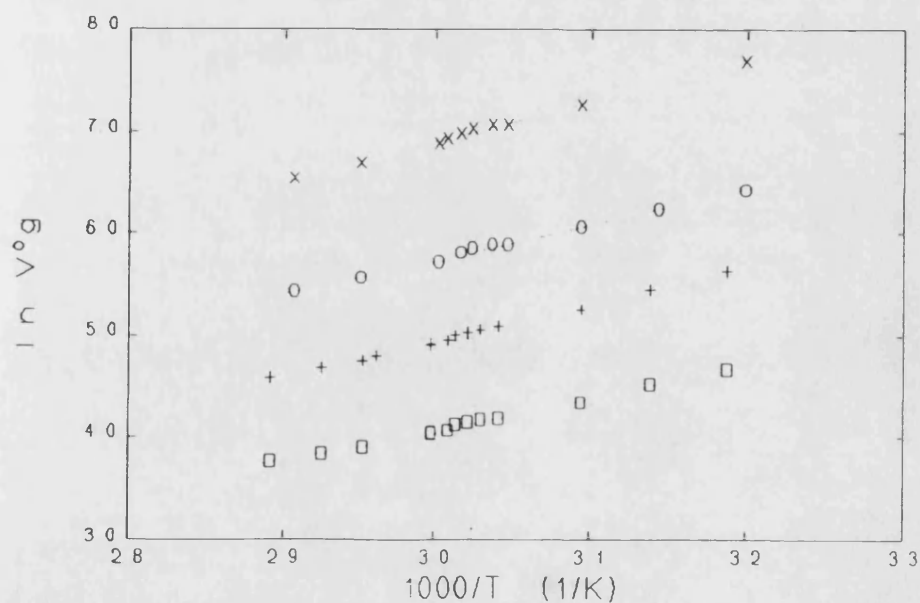

Figure 4.8: Retention about the nematic-supercooled transition temperature in HCB for heptane, , octane, +, toluene, o, and o-xylene, x.
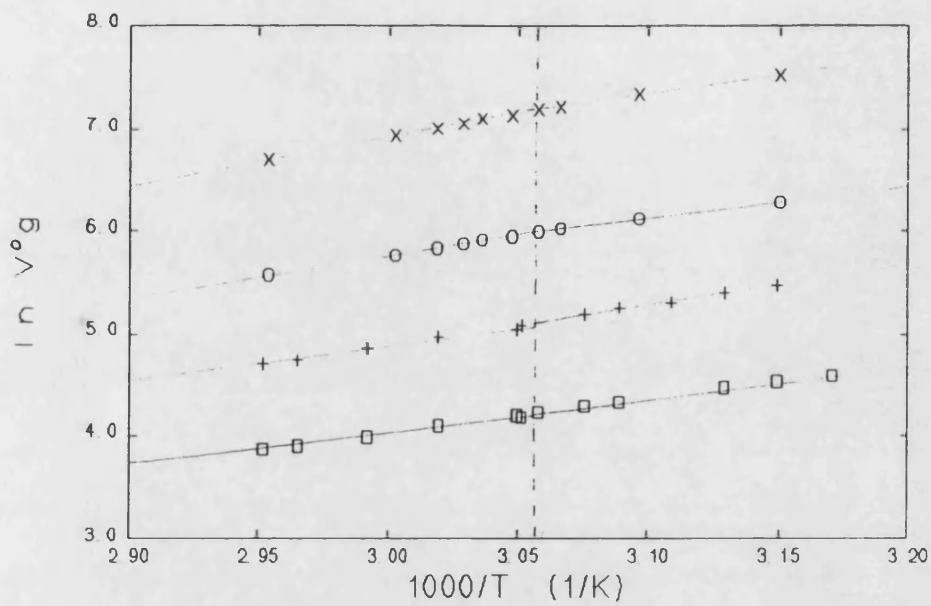
Figure 4.9: Retention about the smectic-supercooled transition temperature in OCB for
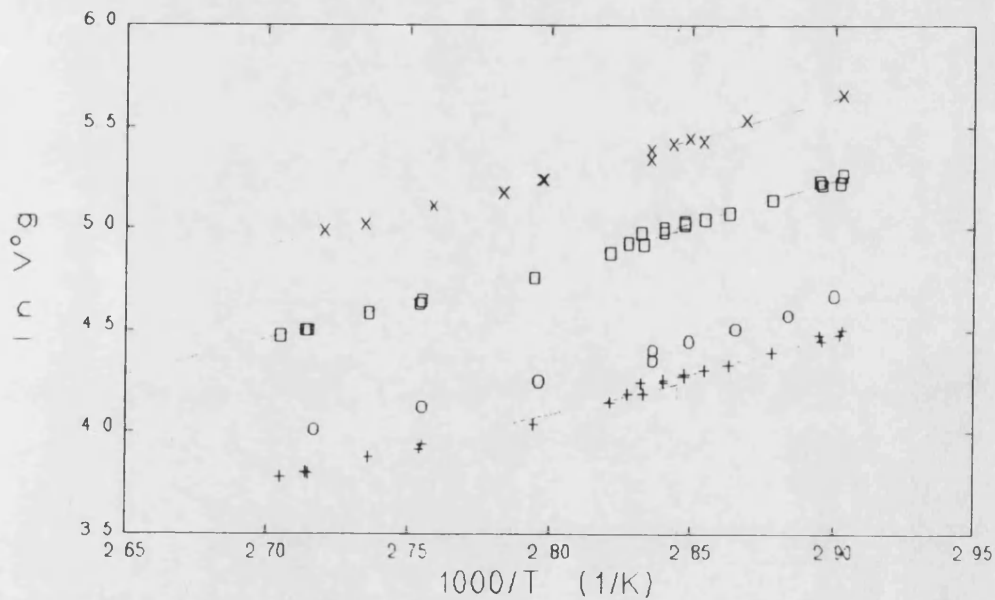
heptane,□ octane, +, toluene, o, and o-xylene, x.

Figure 4.10: Retention about the smectic-supercooled transition temperature in OBIB for

octane, +, nonane, , toluene, o, and o-xylene, x.

inferences of this behaviour will be discussed in chapter 5 and the measured transition

temperatures are given in *tables 4.4, 4.5*, and *4.7*. The transition temperature was

generally less marked than the mesophase transitions and the change in slope was more

discernible for HCB and OBIB than for OCB. The lack of a corresponding exotherm

in the DSC thermograms indicate that these are true second order phase transitions.

The absence of an observable step in the DSC thermograms also infers that the

accompanying change in heat capacity at the transition temperature is much smaller

than that observed for the glass transition temperature in LCP.

4.3d Degree of crystallinity

Before considering the rate of transformation from the unstable supercooled region to

the crystalline phase the degree of crystallinity in the latter will be estimated along with

the "effective crystallinity" of the mesophases, see section 3.2. The "effective

crystallinity" of the mesophase will be used in chapter 6 to estimate the fraction of

aligned liquid crystal in the lattice model of Flory[82]. Estimating the degree of

crystallinity in these materials raises a number of concerns;

> i) Literature reports[112,113] measuring crystallinity using IGC extrapolate
>
> isotropic retention values to an adjacent lower temperature phase. In this work
>
> the extrapolation was over a much wider temperature range and the values
>
> obtained could be considerably more susceptible to any curvature in the van't
>
> Hoff plot.
>
> ii) The solubility of the probe in the bulk liquid crystal could affect values.
>
> iii) The method assumes adsorption on the crystal surface is negligible
>
> compared to bulk absorption.

These points will be considered in the following discussion. Notwithstanding the

above effects, the estimates reported highlight a number of points alluded to in

previous sections. *Figures 4.11* to *4.13* illustrate the results for the three materials
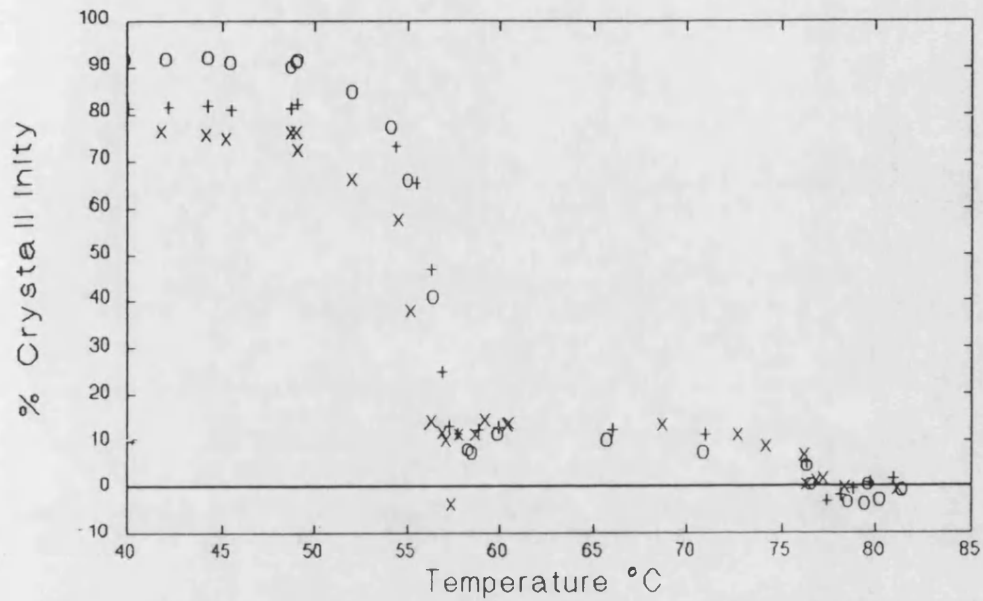
with crystalline phases.

Figure 4.11: Degree of crystallinity and "effective crystallinity" in HCB, as a function of temperature, as measured with toluene, o, cyclohexane, +, and heptane, x, probes.
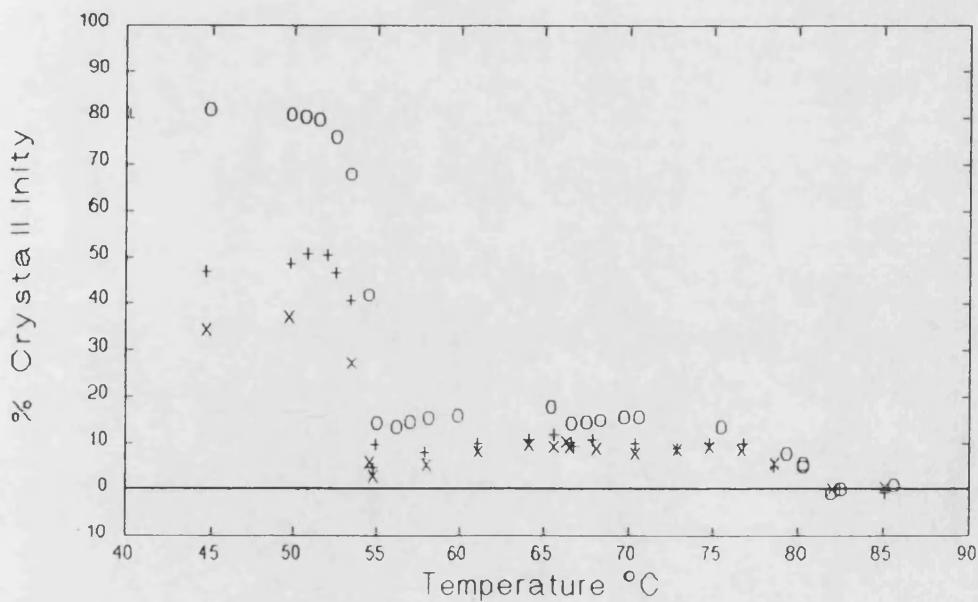

Figure 4.12: Degree of crystallinity and "effective crystallinity" in OCB, as a function of temperature, as measured with toluene, o, cyclohexane, +, and heptane, x, probes.
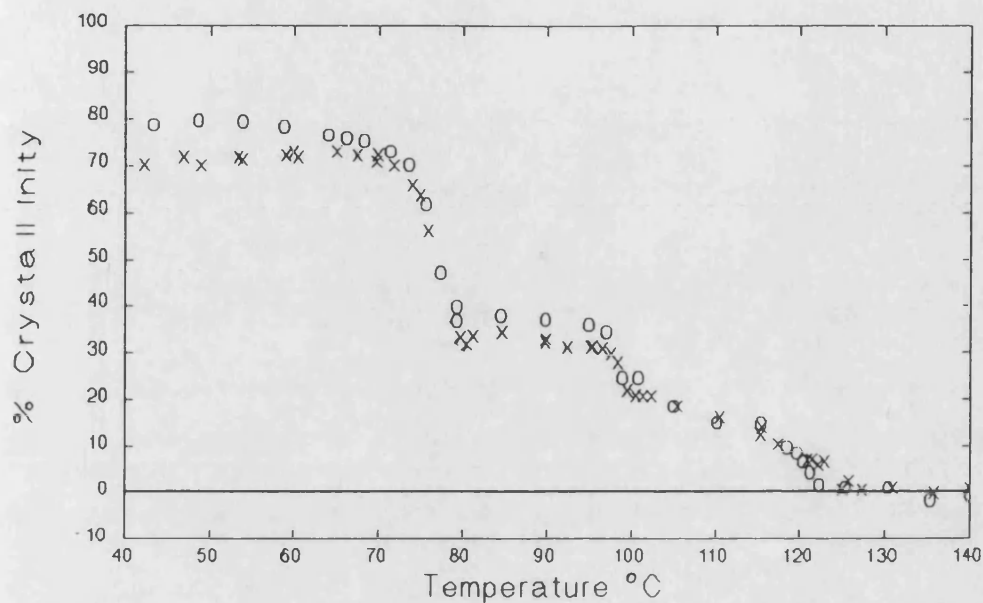
Figure 4.13: Degree of crystallinity and "effective crystallinity" in OBIB, as a function of temperature, as measured with toluene, o, and nonane, x, probes.

All n-alkane probe results agree with the heptane results shown and all aromatic probe results agree with the toluene results shown. Generally, the "effective crystallinity" increases rapidly just below the clearing temperature then increases more slowly as the temperature is lowered. This profile of temperature dependence is in agreement with the form of the order parameter[199]. The difference between values for HCB and OCB are small and the smectic A and nematic phases of OCB are similar. Values for OBIB, however, are considerably higher and there is a significant increase in values in going from the cholesteric to smectic C mesophase. These results reaffirm the trends in the IGC and DSC data already discussed. At the melting temperature values increase rapidly and then level off to a plateau as the temperature is lowered further. It is interesting to compare results for the cyanobiphenyl materials with the density measurements in section 4.2. The premelting "softening" of the crystalline phase agrees closely for OCB but HCB values appear to contradict. The density measurements show a sharp melting point transition whereas the crystallinity results

presented here indicate "softening" up to 8 °C below the melting point. As the density measurements measure an average property of the liquid crystal whereas IGC is more susceptible to the more penetrable portions of the stationary phase, these results can only be reconciled if there is some form of rearrangement occurring within the material forming more dense and less dense regions in equal proportion.

So far the question of curvature in the plots and probe dependence has not been considered. The fact that the aromatic probes levelled off to a constant value at low temperatures indicates curvature was insignificant in the plots. For the other probes, however, there was some decrease in values at lower temperatures, particularly for the OCB stationary phase. The figures also clearly show that values exhibit significant probe dependence, again this is most marked in OCB. In chapters 5 and 6 the aromatic probes are shown to act as better solvents for the liquid crystals studied here. Assuming similar interactions occur between a probe and liquid crystal surface as between the probe and bulk liquid crystal, aromatic probes would be expected to interact more favourably than aliphatic probes with the liquid crystal surface. So it might be assumed that the aromatic probes would interact with the crystal surface to a larger extent than the aliphatic probes. This would reverse the observed trends. Alternatively, the liquid crystals may align in the crystal phase to present an aliphatic surface to the probe. Whilst the small differences between OBIB and HCB may arise from different surface characteristics, it is difficult to envisage such an affect accounting for the large discrepancy in OCB. Thus, the probe dependence is most likely to be governed by the differences of probe interaction with the isotropic phase. The results suggest adsorption of aromatic probes was much less significant than bulk absorption than was the case for the aliphatic probes. Hence, the aromatic probe results are likely to represent crystallinities that a close to the true values. Making this assumption, the figures show that none of the materials studied form a totally crystalline phase and that OCB and OBIB are less crystalline than HCB. These observations can be reconciled by considering the degree of flexibility in the molecular

structure of the individual materials. The rigid portion of HCB is a greater part of the total molecule than the corresponding rigid portion in OCB, see section 3.6.

4.3e Crystallisation Kinetics

The observation of an unstable supercooled region, described in section 4.3c, led to the consideration of IGC to investigate the kinetics of crystallisation to the solid crystal phase. As previously mentioned, OCB crystallised in an inconvenient temperature range to study with the current apparatus. Preliminary studies on OBIB and HCB showed that 90 % of the former had transformed within ten minutes of quenching to the isothermal temperature of interest. HCB, on the other hand, took between one to three days to transform, making it a more suitable material to study with the current apparatus.

Crystallisation was studied at four temperatures below the metastable, supercooled region. *Table 4.8* lists the four temperatures along with the bounds of fluctuation in temperature observed during a run. *Figure 4.14* shows an example plot of the change

Table 4.8: Average temperature and range of temperature, °C, observed during crystallisation.

Average temperature	Temperature range
48.7	48.4→49.0
46.6	46.2→46.9
43.6	43.1→44.0
38.5	38.0→38.9

in specific retention volume with time for five probes at 38.5 °C. Two distinct regions can be seen. The first region occupies around 8-10 hours during which time 30-35 % of the liquid crystal has transformed into the solid state. This is followed by a longer

period of time during which the remainder of the liquid crystal transformed to the solid

state at a rate which slowed as complete crystallisation was approached.

Figure 4.15 shows the mass fraction crystallinity, calculated as outlined in section

3.2, for the four temperatures, as measured by the heptane probe. Note that the

calculation assumes the equilibrium state at infinite time was totally crystalline. The

crystallisation process proceeded faster at higher temperature, as would be expected

because of the greater thermal energy allowing faster rearrangement to the crystal

form. However, the difference in rate between 43.6 °C and 38.5 °C was not

significant. The two transformation regions are clearly visible. The probe to probe

reproducibility was good, as shown by the results for the five probes studied at

38.5 °C in *figure 4.16*. This infers that the retention times of the probes were

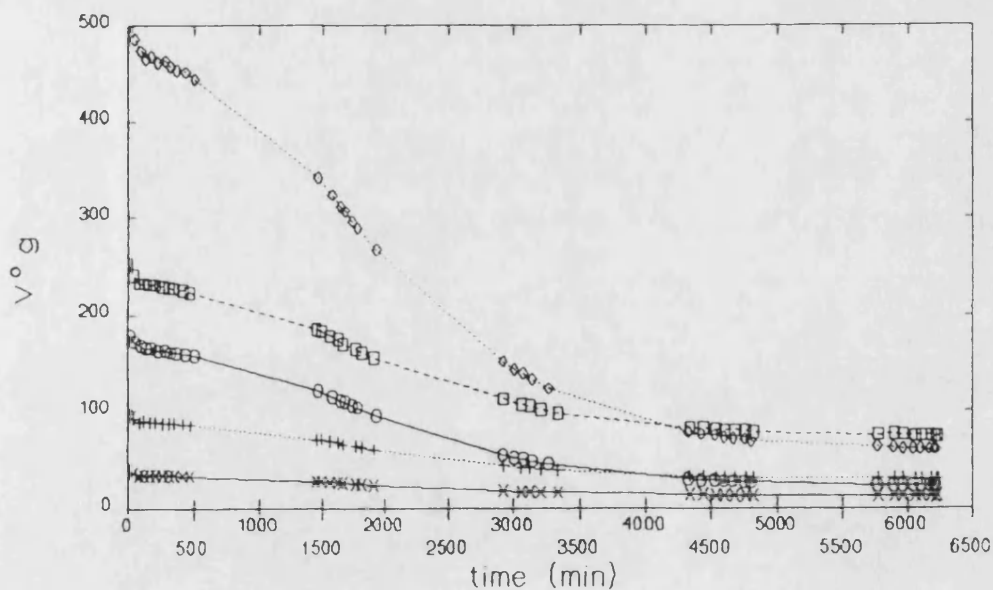insignificant compared to the rate of the transformation.

Figure 4.14: Retention as a function of time for hexane, x, heptane, +, octane, □, benzene, o,
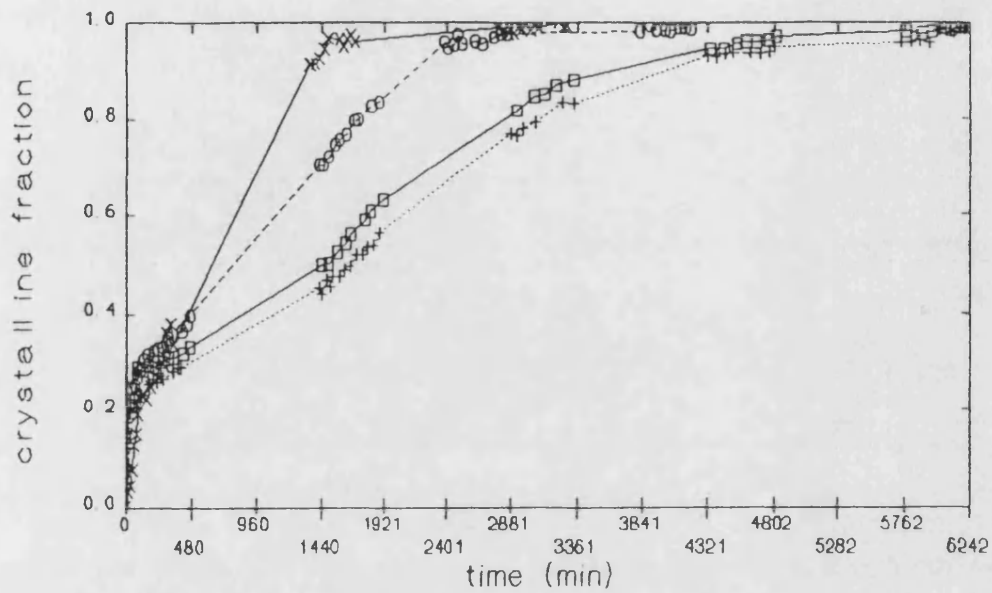
and toluene, ◊, at 38.5 °C in HCB.

Figure 4.15: Degree of crystallinity of HCB measured using heptane as probe at
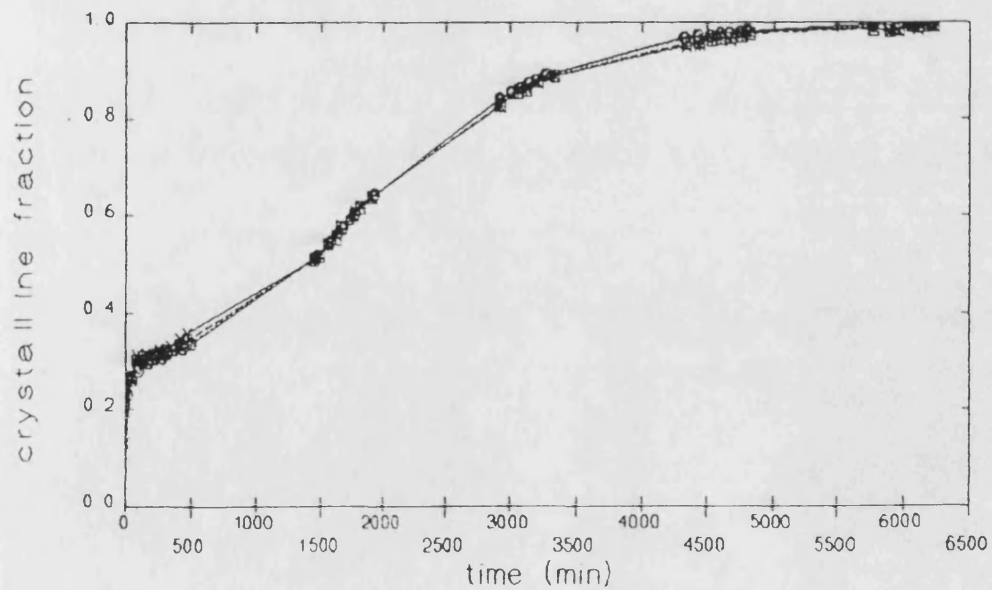
x 48.7 °C, o 46.6 °C, + 43.6 °C, □ 38.5 °C.

Figure 4.16: Degree of crystallinity of HCB using hexane, x, heptane, +, octane, □, benzene,

o, and toluene, ◊, probes at 38.5 °C

The mass fraction crystallinity, F^c was used to obtain the Avrami parameters[176], see section 1.15, from plots of the left hand side of equation 3.5 against the logarithm of the time;

$$\ln [-\ln (1 - F^c)] = \ln K + n \ln t \qquad [3.5]$$

where K and n are the Avrami parameters. *Figure 4.17* gives the plot for the heptane probe results at the four temperatures studied. While there was significant scatter in some of the results, particularly at early times, some general trends emerge. The two crystallisation regions are clearly evident. The results at 48.7 °C differ significantly from those at other temperatures within the first region. The reason for this is unclear but could be a result of the proximity of the temperature to the metastable limit of the supercooled phase, 50 °C. The Avrami plots at long times, and at short times for the other three temperatures studied, showed very similar forms.

Table 4.9 lists the Avrami parameters in each of the two regions. The effective rate constants show that the process in region 1 is several orders of magnitude faster than
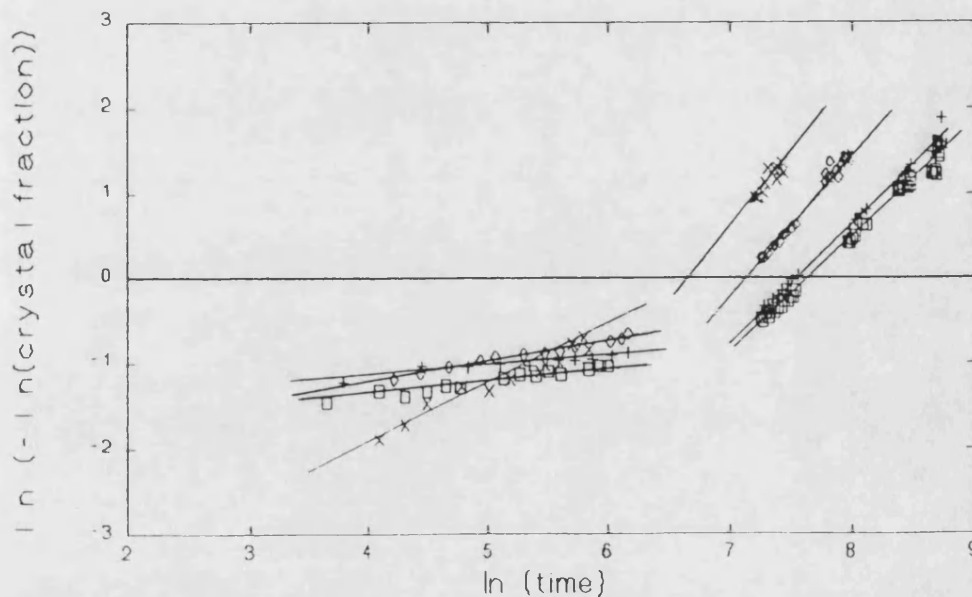

Figure 4.17: Avrami plots for crystallisation of HCB at x 48.7 °C, o 46.6 °C, + 43.6 °C, □ 38.5 °C.

Table 4.9: Avrami constants for the N'→K transition in HCB.

Temperature °C	Region 1*		Region 2*	
	n_1	K_1 min^{-n}	n_2	K_2 min^{-n}
48.7	0.8	3.7×10^{-3}	1.7	1.2×10^{-5}
46.6	0.33	5.3×10^{-2}	1.9	7.0×10^{-7}
43.6	0.21	9.8×10^{-2}	1.4	2.1×10^{-5}
38.5	0.22	6.0×10^{-2}	1.6	3.8×10^{-6}

* The division between region 1 and region 2 was taken as ln [t (min)] = 7

that in region 2, although it should be noted that direct comparison of the values is not possible due to the dependence of units on the value of n. There is no clear trend in K_1 or K_2 with temperature, but the values carry large uncertainties due to the extrapolation procedure and dependence on the values of n_1 and n_2, respectively. The exponent values, n, are very low compared to the values between 2 and 4 for transformations to the mesophase and crystalline state, respectively, measured by Price and co-workers[175] and Jabarin and Stein[204]. It was pointed out in section 1.15 that the rate of crystallisation in polymers also usually gives exponents of 3 and 4. However, in certain polymers, such as some polyesters[179], much lower exponents have been measured.

It is important to note two major differences between this work and previous studies. Firstly, transitions studied here were measured on quenching from the more viscous supercooled mesophase. Secondly, the liquid crystal was spread as a thin coating over a solid support which may have affected the crystal growth.

Cheng[179] suggested that, for similarly viscous systems, very low exponent values could be obtained. The modified Avrami model and subsequent adjusted crystallisation

equation accounting for both the "cold crystallisation" from a viscous medium and the diminishing number of nucleation sites with time was presented in section 1.15. The IGC results presented above can be interpreted qualitatively using this model. Assuming nucleation is heterogeneous, due to the presence of the support surface, initially there would be a large number of nucleation sites. During initial crystallisation, growth would have been restricted by liquid crystal viscosity and steric factors at the support surface. As crystal growth progressed the crystallites would coalesce and the number of nucleation sites would have reduced. After this initial stage, crystallisation would continue in a more conventional manner but would be slow due to the viscosity of the liquid crystal. The n values in *table 4.9* would then indicate diffusion controlled, three dimensional crystal growth, according to this model. Whilst the model offers a self consistent explanation of the crystallisation of supported HCB, this was a preliminary study and the explanation is at present only speculative. The behaviour of HCB during the DSC runs indicates the initial process could be due to an initial solidification process followed by a much longer rearrangement process. Whilst it is clear that more work is necessary to fully elucidate the mechanism of crystallisation in this system, the IGC technique has been shown to provide a useful method of obtaining kinetic data of this type, particularly where the transformations are relatively slow.

In the sections above it has been shown that IGC can be used to measure the temperatures of a range of mesophase transitions in liquid crystals. It may be applied to a wide range of low molar mass or polymeric materials with a precision and accuracy comparable to other techniques. Although IGC is comparatively slow for transition temperature measurements alone, the technique has the potential to discern subtle phase changes that other techniques may not detect. The method also has the advantage of simultaneously measuring other data of interest, such as estimating the degree of crystallisation or measuring thermodynamic parameters of solution within a given phase. The latter application will be the subject of the following chapters in this

thesis. This chapter has also demonstrated the potential of IGC as a method for following kinetic transformations in suitable mesogenic systems.

CHAPTER 5

PHASE BEHAVIOUR

Having measured the specific retention of probes at different temperatures to elucidate the mesophase transition temperatures of the liquid crystals, this chapter now turns the attention to the thermodynamic solution behaviour of the individual phases and mesophases. The different liquid crystals studied will be discussed individually with comparisons between preceding sections. A discussion of the low molar mass liquid crystals will be followed by a look at LCP, comparing solution behaviour with both the low molar mass analogues and PDMS, and the chapter will end with a brief look at adsorption on the crystal phases of the low molar mass materials. But first some general trends in the data are considered.

In section 3.3 it was shown that the activity coefficient of the probe at infinite dilution in the stationary phase solution can be calculated from the specific retention volume and the probe saturated vapour pressure at a given temperature. From a set of values in a given stationary phase the partial molar enthalpy change of solution and partial excess molar enthalpy of solution may be calculated. Having calculated these values, it was shown in section 1.5b that the activity coefficient gives a measure of the strength of interaction between the probe and stationary phase relative to interactions in the pure probe solvent, values larger than 1 indicating poor interaction and values below 1 indicating good interaction. The activity coefficients in the systems studied here showed a marked difference in form within the different mesophases and phases exhibited by a given liquid crystal.

As temperature increased in a particular stationary phase the activity coefficient decreased. This was matched by a decrease in order of the mesophases as temperature increased. Generally the measured activity coefficients were greater than unity indicating the non-mesogenic probes were unfavourable solvents. However, the aromatic probes exhibited lower values than the aliphatic probes and activity

coefficients for these probes became less than unity at high temperatures in the isotropic phase. For OCB and OBIB some aromatic probes even exhibited values below unity into the highest temperature mesophase. Apart from the entropy value for pentane in the smectic A mesophase of OCB, all excess partial molar enthalpies and partial molar entropies of solution were positive. This indicates solution formation depended on the balance between unfavourable interactions between components and favourable disruption of the liquid crystal order.

The simple picture of solution formation outlined above does not account for all the trends observed. Mesophases within a given liquid do not follow the solution behaviour trend such a description would predict, identical mesophases in different materials showed different trends, and the supercooled phases exhibited behaviour that would have been expected of a higher temperature phase. These complications are discussed below in terms of the qualitative approach developed by Chow and Martire[71], and outlined in section 1.10a. Although they only applied the model to the nematic and isotropic phase, similar arguments are applicable to the other mesophases encountered here.

5.1 HEXYLOXYCYANOBIPHENYL (HCB)

The molar activity coefficients for all probes are given in *figure 5.1* and the excess partial molar quantities and partial molar solution quantities are listed in *tables 5.1* and *5.2*, respectively. The reported temperature indicates the average temperature of the regression range. However, it was shown in section 4.3d that there was negligible curvature in the van't Hoff plots and so the gradients, and hence the enthalpies and entropies reported here, are independent of temperature. The trends in the values are listed below where the superscripts sol and E, denoting the solution and excess quantities respectively, have been omitted for clarity and will be omitted in subsequent sections;

$$\gamma^{super} > \gamma^{N} > \gamma^{I} \qquad [1]$$

$$\Delta H^{super} \approx \Delta H^{I} < \Delta H^{N} \qquad [2]$$

$$H^{I} < H^{super} < H^{N} \qquad [3]$$

$$\Delta S^{super} < \Delta S^{I} < \Delta S^{N} \qquad [4]$$

$$S^{I} < S^{super} < S^{N} \qquad [5]$$

For m-xylene the isotropic and supercooled values in [5] are similar and nonane, 2,2,3-trimethylbutane, 2-methylhexane, and 3-methylhexane have close but reversed isotropic and supercooled values in [4].

In chapter 4 the enthalpy changes accompanying transitions between phases and mesophases were shown to be small. Thus the different solution behaviour in each stationary phase form must be governed by differences in probe-liquid crystal interactions and not by the changing liquid crystal-liquid crystal interactions. Trends [4] and [5] show the absorption of probe in the nematic mesophase resulted in a greater disruption of the phase than absorption in the isotropic phase, as would be expected. Whilst trends [1], [2], and [3] show that the probes interact more strongly in the isotropic phase. In *figure 5.2* the activity coefficient plots are extrapolated for some of the probes to allow direct comparison of the values between the different phases under isothermal conditions. It is evident from the figure that solution formation in the isotropic phase is enthalpically driven whereas the nematic solution is governed by entropy effects due to the respective favourability of the activity coefficients at low and high temperatures.

Looking at the thermodynamic values for the supercooled phase, trends [3] and [5] showed the probes exhibited lower partial molar excess enthalpies and partial molar excess entropies of solution in this phase. These observations, along with the extrapolated data in *figure 5.2*, show that the supercooled region was less ordered than the nematic region and was able to form stronger interactions with the probe molecule, from similar arguments to those above. However, the smaller difference in activity
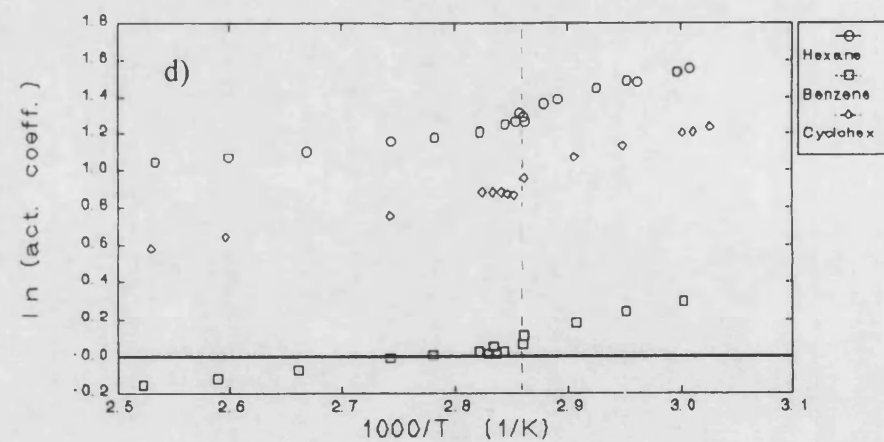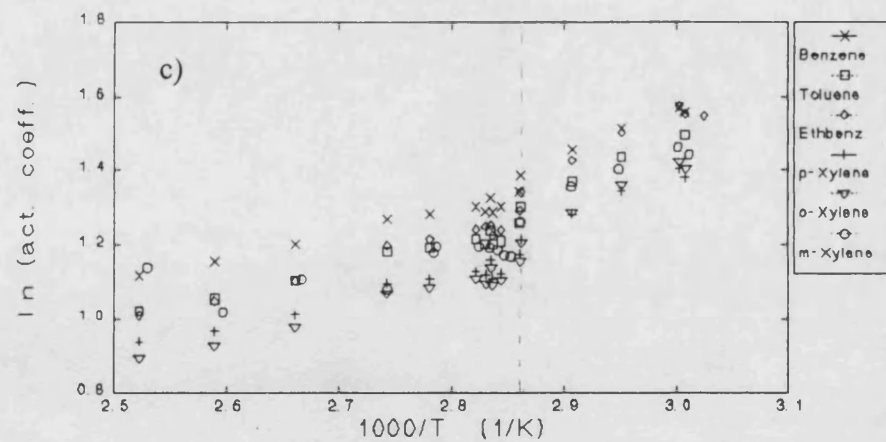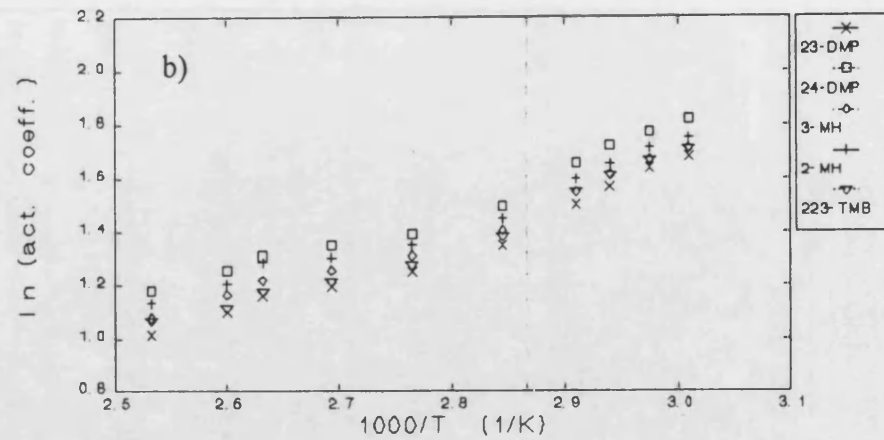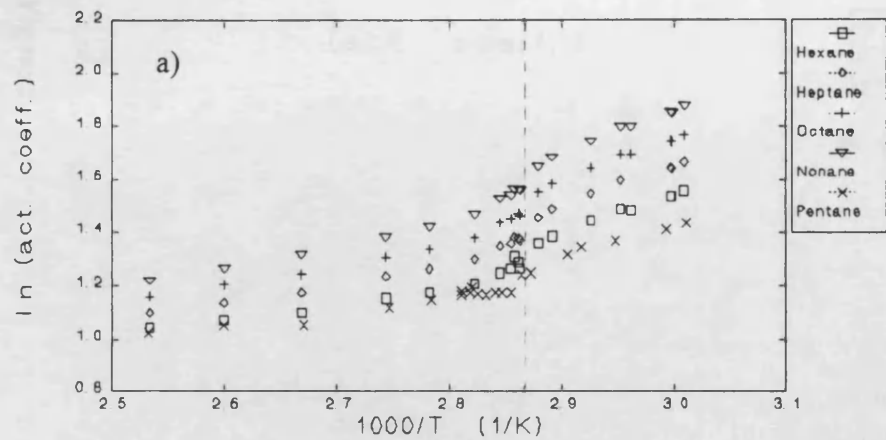
Figure 5.1: Activity coefficients in HCB, a) n-alkanes, b) heptane isomers, c) aromatic probes, d) "six carbon" probes.

Table 5.1: Partial molar excess values for HCB. Enthalpies in kJ mol^{-1} and entropies in J mol^{-1} K^{-1}. Standard deviations in parentheses.

| PROBE	I (100 °C) H^E	S^E	N (66 °C) H^E	S^E	N^{super} (48 °C) H^E	S^E
Pentane	4.0 (0.7)	1.6 (1.5)	10.4 (0.7)	13.9 (0.4)	6.3 (0.3)	6.9 (0.3)
Hexane	4.7 (0.3)	3.4 (0.7)	11.3 (0.6)	21.0 (0.7)	7.3 (1.2)	9.3 (1.2)
Heptane	5.7 (0.2)	5.5 (0.6)	11.8 (0.7)	21.8 (0.7)	8.0 (1.1)	10.3 (1.2)
Octane	6.3 (0.3)	6.4 (0.7)	12.4 (0.7)	22.8 (0.7)	8.6 (1.1)	11.2 (1.2)
Nonane	7.1 (0.3)	7.9 (0.8)	13.2 (0.7)	24.1 (0.7)	9.9 (1.6)	14.2 (1.7)
2-Methylhexane	7.9 (0.8)	10.4 (2.0)	13.3 (1.1)	25.6 (0.8)	11.5 (1.2)	20.4 (1.2)
3-Methylhexane	8.2 (0.5)	11.8 (1.4)	13.8 (1.3)	27.2 (1.0)	11.5 (1.1)	20.6 (1.1)
2,3-Dimethylpentane	8.5 (0.6)	12.9 (1.5)	14.9 (1.2)	30.9 (0.9)	10.7 (1.3)	18.3 (1.4)
2,4-Dimethylpentane	7.9 (0.6)	10.1 (1.4)	13.8 (1.2)	26.5 (0.9)	11.1 (0.8)	18.3 (0.8)
2,2,3-Trimethylbutane	8.2 (0.5)	11.9 (1.2)	13.4 (1.0)	26.1 (0.8)	11.0 (1.0)	18.9 (1.1)
Cyclohexane	8.2 (0.8)	16.1 (2.0)	10.9 (0.5)	22.7 (0.4)	9.4 (0.3)	18.2 (0.4)
Benzene	5.4 (0.2)	15.0 (0.6)	8.0 (1.2)	21.8 (1.1)	7.6 (0.7)	20.6 (0.8)
Toluene	5.7 (0.3)	15.1 (0.8)	10.0 (1.3)	27.0 (1.7)	7.3 (0.5)	19.0 (0.6)
Ethylbenzene	6.8 (0.4)	16.9 (1.0)	10.0 (1.7)	25.2 (1.6)	9.2 (0.9)	22.7 (1.1)
o-Xylene	6.3 (0.4)	16.6 (1.0)	9.1 (1.7)	23.6 (1.7)	8.5 (0.5)	21.9 (0.5)
m-Xylene	6.7 (1.2)	17.0 (1.7)	7.9 (1.4)	19.7 (1.2)	7.0 (0.9)	16.9 (0.8)
p-Xylene	5.7 (0.4)	14.6 (1.0)	8.0 (1.7)	20.7 (1.6)	7.2 (0.4)	18.3 (0.4)
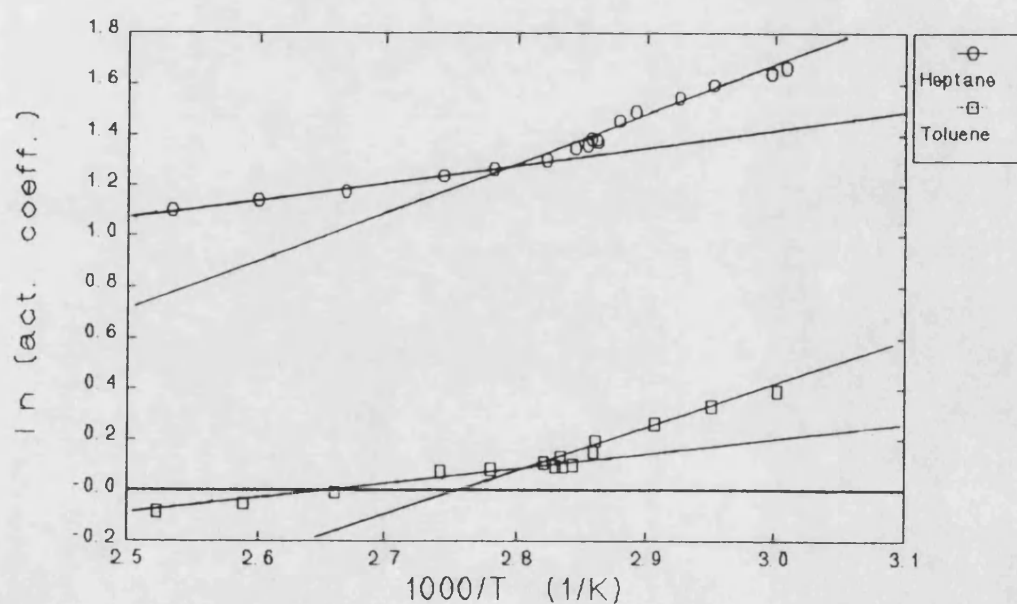
Figure 5.2: Extrapolated activity coefficient data for heptane, x, and toluene, o.

Table 5.2: Partial molar solution values for HCB. Enthalpies in kJ mol^{-1} and entropies in J mol^{-1} K^{-1}. Standard deviations in parentheses.

PROBE	I (100 °C) $-\Delta H^{sol}$	$-\Delta S^{sol}$	N (66 °C) $-\Delta H^{sol}$	$-\Delta S^{sol}$	N^{super} (48 °C) $-\Delta H^{sol}$	$-\Delta S^{sol}$
Pentane	18.6 (0.4)	72.2 (1.5)	16.3 (0.5)	66.4 (0.5)	19.4 (0.3)	75.9 (0.4)
Hexane	23.1 (0.2)	77.9 (0.2)	18.3 (0.7)	65.3 (0.8)	23.2 (1.2)	79.6 (1.6)
Heptane	26.6 (0.2)	81.2 (0.4)	22.5 (0.8)	70.3 (1.0)	27.3 (1.1)	84.9 (1.4)
Octane	30.5 (0.2)	85.6 (0.3)	26.5 (0.7)	75.2 (0.8)	31.5 (1.2)	90.4 (1.5)
Nonane	34 1 (0.2)	89.2 (0.4)	30.5 (0.7)	80.0 (0.9)	33.5 (1.5)	89.0 (2.0)
2-Methylhexane	22.9 (0.8)	74.0 (2.6)	19.3 (1.2)	64.0 (1.0)	21.9 (1.2)	71.8 (1.5)
3-Methylhexane	22.9 (0.7)	73.1 (1.9)	19.1 (1.4)	62.7 (1.3)	22.2 (1.1)	71.9 (1.4)
2,3-Dimethylpentane	22.3 (0.7)	71.5 (2.1)	17.4 (1.3)	58.1 (1.2)	22.4 (1.4)	73.0 (0.2)
2,4-Dimethylpentane	21.4 (0.6)	72.3 (1.9)	17.1 (1.2)	60.8 (1.1)	20.7 (0.8)	71.4 (1.1)
2,2,3-Trimethylbutane	20.8 (0.4)	69.6 (1.4)	17.0 (1.0)	59.5 (0.9)	20.1 (1.1)	68.8 (1.3)
Cyclohexane	21.3 (0.7)	67.1 (2.1)	20.3 (0.5)	65.1 (0.5)	22.5 (0.4)	72.0 (0.6)
Benzene	24.8 (0.3)	70.2 (1.1)	22.9 (1.1)	65.5 (1.1)	25.1 (0.7)	72.2 (0.9)
Toluene	28.6 (0.3)	73.8 (1.2)	25.8 (1.4)	66.5 (2.2)	29.6 (0.4)	77.7 (0.6)
Ethylbenzene	31.2 (0.4)	75.9 (1.2)	30.1 (1.7)	73.3 (1.9)	31.9 (0.8)	79.0 (1.1)
o-Xylene	33.1 (0.3)	77.6 (1.2)	32.3 (1.7)	76.2 (2.0)	33.1 (1.1)	78.5 (1.6)
m-Xylene	35.7 (1.7)	86.9 (5.4)	32.6 (1.4)	79.3 (1.5)	36.2 (1.0)	90.0 (1.2)
p-Xylene	32.7 (0.4)	78.4 (1.2)	32.2 (1.7)	77.8 (2.0)	34.1 (0.2)	83.3 (0.4)

coefficients than observed about the clearing temperature implies that the effect of probe-liquid crystal interaction was not as dominant in the supercooled phase as it was in the isotropic phase. This is supported by extrapolation of isotropic activity coefficients to the supercooled region. That a lower temperature mesophase should exhibit characteristics that imply a lower ordered phase than a higher temperature mesophase is surprising. Such behaviour has been noted in other systems[205] and the resulting mesophase termed a "re-entrant" phase. The phenomenon was explained as a necessary disruption of order to allow the molecules of the mesophase to realign in the crystalline form. However, such behaviour is usually associated with liquid crystals that exhibit a tendency to dimerise, creating a "fat" central portion, but no reports of such behaviour in HCB have been found by this author and re-entrant phases are

usually observed[206] under applied pressures significantly removed from ambient conditions.

Whilst the partial molar excess quantities of the probes can be used to compare the solution behaviour between different liquid crystal phases, these values may not be used for a direct comparison of solution behaviour between different probes. The partial molar excess quantities are relative to the pure probe solvent. For instance, as interactions between benzene molecules in pure solvent will be different from those between hexane molecules in pure solvent these thermodynamic quantities will express deviations from different reference states. The partial molar enthalpy and entropy changes of solution, as defined in section 3.3, are measured from the reference state of an infinitely dilute vapour at one bar[207]. Thus, these values are a measure of the solution behaviour for different probes from a common reference state. The values contain a contribution from liquid crystal-liquid crystal interaction but this will be constant for each system. Thus, according to the model of Chow and Martire[71], large and negative partial molar enthalpy changes of solution are the result of strong interactions (due to low potential energy between any molecule pair) and/or severe restriction on probe movement within the solution. Low values of activity coefficient are a result of strong interactions and/or little restriction of the probe molecule in solution. The partial molar entropy change of solution describes the loss of entropy the probe suffers on transferring from the gas phase to the infinitely dilute solution. Large, negative values indicate a large restriction on probe movement in the infinitely dilute solution but strong interactions between probe and liquid crystal will also lower this entropy. Thus the individual contributions can be disseminated from the overall thermodynamic solution behaviour and in the following discussion this approach will be used to consider the trends in the different types of probes studied.

n-alkanes: As the alkane chainlength increases the polarisability increases (see data in reference 191) allowing stronger dispersion interactions between the probe and HCB. However, a more elongated molecule suffers a greater restriction on becoming solvated and hence the partial molar entropy change of solution would decrease. This

does indeed occur in both the isotropic phase and the mesophases of HCB. For instance, in the nematic phase the partial molar entropy change of solution decreased from -66.4 J mol^{-1} K^{-1} for pentane to -80.0 J mol^{-1} K^{-1} for nonane whilst the partial molar enthalpy change of solution decreases from -16.3 kJ mol^{-1} to -30.5 kJ mol^{-1}. Figure 5.1 shows the activity coefficient also increases as chainlength increases in these phases and mesophases. If we now consider the two extreme cases of thermodynamic parameters reflecting either the predominance of the interaction potential or the restrictive nature of the solution we can predict the trend we would expect between mesophases and the isotropic phase. Both cases would result in the observed activity coefficient trends. The potential energy dominated partial molar enthalpy change of solution would predict that values for a given probe would increase from the isotropic phase to nematic to supercooled mesophase whereas the dominance of restricted probe movement would predict the opposite. The actual observed values indicate the potential energy term is the dominant contribution with the restrictive nature of the liquid crystal solution causing a perturbing effect. The dominance of the interaction term is supported by the partial molar entropy changes of solution which followed the trend in the partial molar enthalpy changes of solution.

branched-alkanes: Comparing the thermodynamic parameters of the heptane isomers between different phases and mesophases of HCB reveals very similar trends to those observed for the n-alkanes above. This indicates that the solution behaviour is again governed by interaction between probe and liquid crystal molecules rather than restriction of the probe molecule by the stationary phase. However, within a given phase or mesophase the trend between different probes is not immediately clear. In the isotropic phase the spread in activity coefficients between probes is similar to that observed in the n-alkanes but in the mesophases the spread is considerably less, indicating the difficulty the mesophases have in distinguishing between the different probes. The isomers present a variety of molecular shapes from the globular 2,2,3-trimethylbutane to the flexible heptane chain. In table 3.3, section 3.6, the molecular dimensions for the heptane isomers are given, see also below. As branching increases the molecules become more globular, 2,4-dimethylpentane proves to be the

exception with a length to breadth ratio between that of heptane and 2-methylhexane. Also, the number of conformations the molecule can access will decrease with branching. Thus, if the solution behaviour was governed by the potential energy between components the partial molar enthalpy change of solution would follow the observed trend, apart from the 2,4-dimethypentane value which was higher, but the activity coefficients would exhibit the opposite trend to the observed values. However, if restriction of probe movement was the major factor governing the parameters the greater the branching within the probe the lower the activity coefficient should be and the higher the partial molar enthalpy change of solution. However, the measured values for heptane were lower than the prediction and the activity coefficient of 2,4-dimethylpentane was higher than predicted. It is tempting to ascribe the discrepancy to an interplay between both factors resulting in the observed trends. However, both effects predict activity coefficients that are too low for 2,4-dimethylpentane so it is difficult to see how any combined effect would raise the value.

At this point it is worth considering the length to breadth ratio of these probes. Firstly, if the simple rule of thumb of "like dissolves like" is assumed, the greater the length to breadth ratio the more favoured the solution formation should be. The measured values show that this simple picture does not apply here and the measured trend was almost opposite to the prediction. However, consider the interaction between a rigid rod probe and the rigid rod liquid crystal molecules, similar to liquid crystal-liquid crystal interaction discussed in section 1.1. At a given temperature the system will have a certain amount of thermal energy which it cannot use to adopt different conformations and so the two molecules must rotate relative to each other greatly decreasing the interaction between the two molecules. If the probe were totally flexible some portion of this energy would be used to access different conformations enabling more of the probe to remain closer to the liquid crystal molecule than with the rigid probe. In the present case the two factors to consider are the length to breadth ratio, larger values being more susceptible to thermal motion, and the degree of

branching, greater branching reducing the accessible conformations. The following are the trends in the two contributions;

i) *branching:* 2,2,3-trimethylbutane > 2,3-dimethylpentane/2,4-dimethylpentane >

2-methylhexane/3-methylhexane > heptane

ii) *length:breadth:* heptane > 2,4-dimethylpentane > 2-methylhexane >

3-methylhexane > 2,3-dimethylpentane > 2,2,3-trimethylbutane

Thus it can be seen why there is no evident trend. However, the above discussion shows that by considering the molecular shape contribution to interaction between components, rather than accounting for the effect of probe molecule shape just in terms of the lost probe freedom on solution formation, it is possible to account for the observed trend. The high values of 2,4-dimethylpentane can now be seen as a consequence of the molecules high degree of branching and large length to breadth ratio.

aromatic probes: Ethylbenzene was the only probe studied that possessed a flexible portion in its molecular structure and is therefore the only probe likely to possess any significant vibrational energy contributions to the solution behaviour. Thus the solvency will be governed by potential energy and rotational energy effects. As the length to breadth ratio of the probe increases the probe will lose more rotational energy upon forming a solution. In *figure 5.3a* the partial molar enthalpy changes of solution in the isotropic phase are plotted against length to breadth ratio. In *figure 5.3b* the same quantities are plotted against probe polarisability. Similar plots were obtained for values in the two mesophases. The latter plot offers a more compatible fit to the measured values and presents much closer agreement between the aromatic and n-alkane probes. This indicates that the potential energy of the interaction between probe and liquid crystal is, again, the governing factor. The trend in values between the isotropic and other two mesophases was identical to the n-alkane probes but the increase in the partial molar enthalpy and entropy values was smaller. This reflects the lower flexibility of the aromatic probes and hence smaller loss of probe molecule freedom when dissolving in the nematic phase. The trend in the activity coefficients follow from the above arguments apart from m-xylene which exhibited higher activity
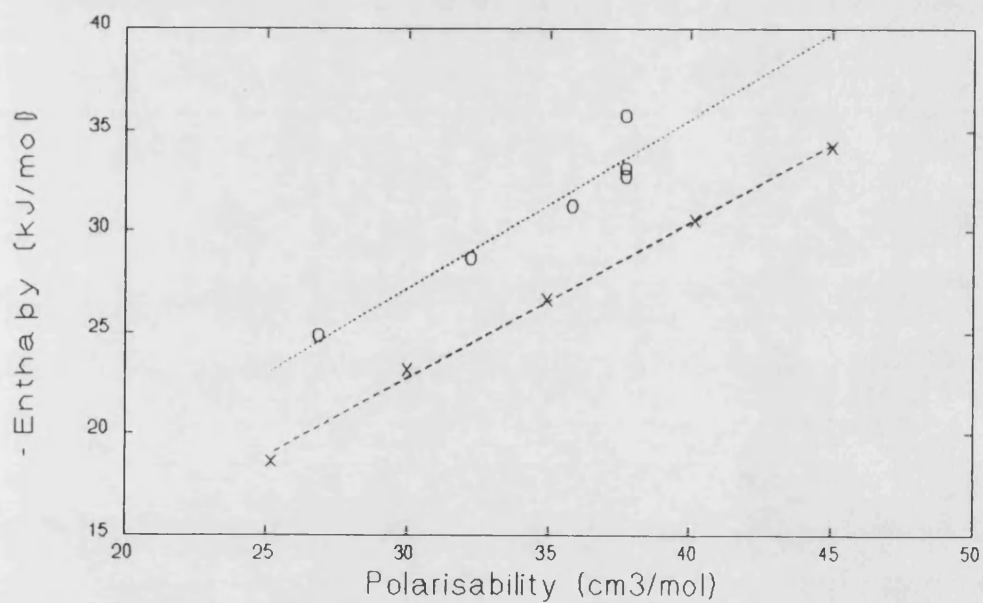
a)
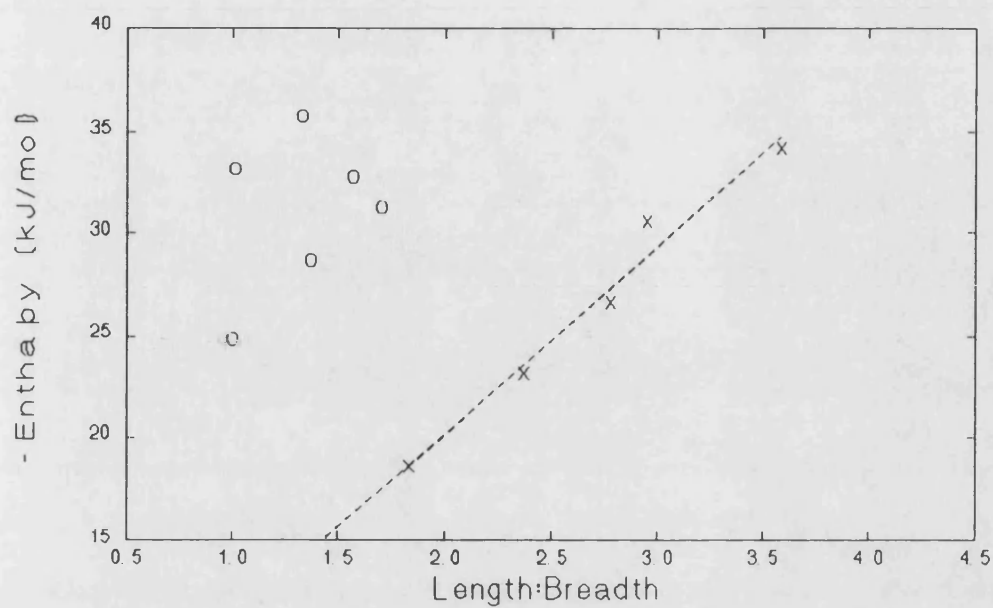
b)

Figure 5.3: The partial molar enthalpy change of solution for n-alkane, x, and aromatic, o, probes against a) length to breadth ratio and b) polarisability.

coefficient values and larger partial molar quantities than would be expected, particularly in the isotropic region. The reason for this is unclear but the xylene trends are likely to be the result of the combined effects of molecular geometry and the lower symmetry of *ortho* and *meta* xylenes. These trends cannot be explained by the dipole moments of the xylenes, indeed the dipole moments appear to have little effect on the solution thermodynamics.

C6 probes: The polarisability increases according to the order benzene < cyclohexane < hexane and the rigidity of the molecules increases in the opposite direction. In the isotropic phase and mesophases the partial molar enthalpy change of solution for benzene was lower than that for hexane with the greatest difference in the nematic phase. The values for cyclohexane might be expected to fall between these two probes. This occurs in the nematic phase but in the other two phases the spread of values was smaller and cyclohexane values were close, but higher, than those for hexane. *Table 5.2* shows the partial molar entropy changes of solution are very similar in the nematic phase for all three probes whereas the values increase from hexane < benzene < cyclohexane in the isotropic phase. These trends indicate a fine balance between contributing factors to the solution behaviour. The activity coefficients are considerably different for all the probes, increasing from benzene to hexane, so the molecular geometry must be a more important factor for these three probes than in any of the above sets of probes. This does not mean that the liquid crystal restriction of probe movement has become a governing factor. Indeed, this contribution does not explain the above enthalpy trends, although it would account for the trends in the activity coefficients. However, the potential energy governed prediction, based on the polarisability of the probes, does not account for either the observed activity coefficients or the enthalpies. Thus, the model for predicting solution behaviour appears to no longer apply. However, if the molecular geometry is considered it is seen that the rigidity increases from hexane to benzene and the two ring probes have length to breadth ratios of unity. In fact, the benzene molecule approximates to a rigid disc. Thus, a rigid probe with a small length to breadth ratio must be capable of forming stronger interactions than a more flexible, elongated probe and the measured

values are governed by the potential energy of interaction between the solution components. The observed values cannot be governed by restriction of probe movement because the enthalpy values would not be so similar. Benzene also offers the possibility of improved solvency due to specific interaction between the probe and the biphenyl rings.

The discussions for the different types of probe above have highlighted the number of different factors that can affect the solution behaviour of a system. The arrangement of the liquid crystal molecules is obviously important in governing the solution behaviour. The shape, rigidity, and degree of branching of the probe molecule all contribute to the solution characteristics. However, it is the probe-liquid crystal interaction that governs behaviour and the major effect of probe molecule geometry is that of augmenting or decreasing the strength of this interaction. The effects of liquid crystal restriction of probe movement on solution formation are a minor perturbation. If these effects appear to govern solution behaviour it is due to a decrease in interaction effects more than an increase in the restrictive nature of the liquid crystal.

5.2 OCTYLOXYCYANOBIPHENYL (OCB)

The molar activity coefficients for the probes are given in *figure 5.4* and the excess partial molar quantities and partial molar solution quantities are listed in *tables 5.3* and *5.4*, respectively. The trends in these values are summarised below;

$$\gamma^{super} > \gamma^{S} > \gamma^{N} > \gamma^{I} \qquad [1]$$

$\Delta H^{S} < \Delta H^{I} < \Delta H^{super} < \Delta H^{N}$	aromatic	[2a]
$\Delta H^{S} < \Delta H^{super} < \Delta H^{I} < \Delta H^{N}$	aliphatic	[2b]
$\Delta H^{super} < \Delta H^{I} < \Delta H^{S} < \Delta H^{N}$	branched alkanes	[2c]

$\Delta S^{S} < \Delta S^{I} < \Delta S^{super} < \Delta S^{N}$	aromatic	[3a]
$\Delta S^{S} < \Delta S^{super} < \Delta S^{I} < \Delta S^{N}$	aliphatic	[3b]
$\Delta S^{super} < \Delta S^{I} < \Delta S^{S} < \Delta S^{N}$	branched alkanes	[3c]

$$H^S < H^I < H^{super} < H^N \qquad \text{aromatic} \qquad [4a]$$

$$H^S < H^{super} < H^I < H^N \qquad \text{aliphatic} \qquad [4b]$$

$$S^S < S^I < S^{super} < S^N \qquad \text{aromatic} \qquad [5a]$$

$$S^S < S^{super} < S^I < S^N \qquad \text{aliphatic} \qquad [5b]$$

In [2b] isotropic and nematic values are similar for pentane and the supercooled and smectic values for cyclohexane and heptane are reversed. In [3b] the supercooled and isotropic values of nonane are similar but reversed. In [4b] the supercooled value is lowest for 2,3-dimethylpentane and 3-methylhexane and is higher than the isotropic value for nonane.

An obvious difference between OCB and HCB is the absence of one set of trends for all probes. This is partly a consequence of the similarity of values for different phases in OCB. The arguments put forward in the previous section that the change in liquid crystal-liquid crystal interaction between mesophases and phases do not determine the observed trends also hold for OCB. Also, the nematic phase and isotropic phase exhibit identical trends to those seen in HCB. However, extrapolation of the activity coefficients from the nematic phase to the isotropic region, as illustrated in *figure 5.5*, shows that the isotropic phase retains the more favourable values for several degrees above the clearing point, whereas HCB gave favourable extrapolated activity values above the clearing point. This indicates either the isotropic phase of OCB retains some order on heating from the nematic mesophase to the isotropic phase or the nematic phase of OCB is less ordered than that of HCB. The effective crystallinity values given in section 4.3d indicate the former.

Figure 5.5 shows the smectic phase exhibited activity coefficients between those of the extrapolated values of the nematic mesophase and isotropic phase. The partial molar excess enthalpies were lower than both the isotropic phase and nematic mesophase values and the corresponding entropies exhibited the same trend. These trends indicate the solution behaviour in the smectic phase is more enthalpically driven
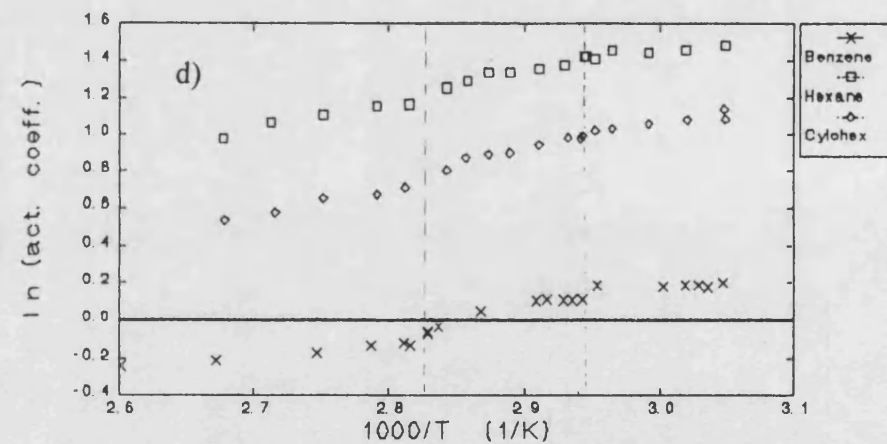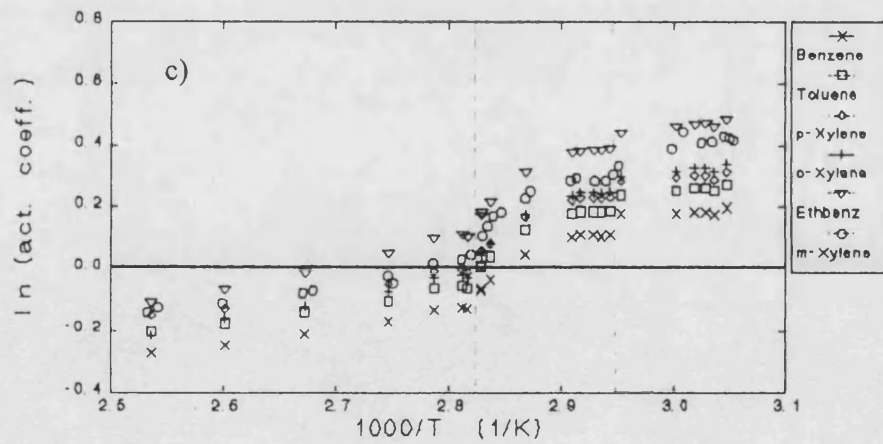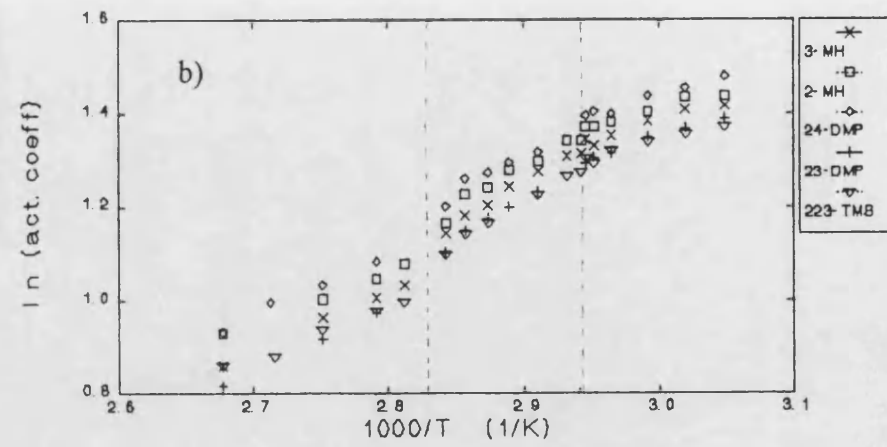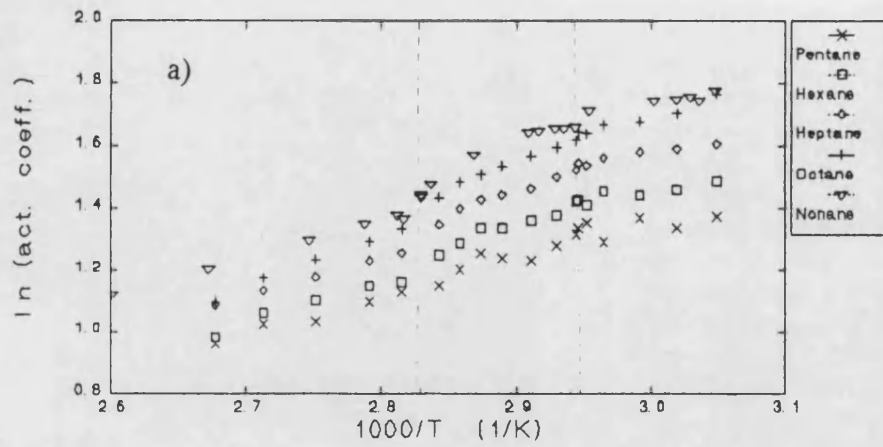
Figure 5.4: Activity coefficients in OCB, a) n-alkanes, b) heptane isomers, c) aromatic probes, d) "six carbon" probes.

Table 5.3: Partial molar excess values for OCB. Enthalpies in kJ mol^{-1} and entropies in J mol^{-1} K^{-1}. Standard deviations in brackets.

PROBE	I H^E	(90 °C) S^E	N H^E	(73 °C) S^E	S_A H^E	(60 °C) S^E	S_A^{super} H^E	(48 °C) S^E
Pentane	8.9 (1.8)	15.7 (1.5)	9.5 (3.2)	17.3 (2.3)	1.7 (3.6)	-6.0 (1.9)	6.5 (1.8)	8.5 (1.3)
Hexane	9.7 (0.6)	17.4 (0.3)	11.5 (1.7)	22.1 (1.2)	4.4 (1.5)	1.1 (0.7)	7.4 (1.3)	10.2 (1.0)
Heptane	10.3 (1.3)	18.5 (0.2)	13.1 (1.4)	26.1 (1.0)	6.7 (1.5)	7.0 (0.7)	8.2 (0.2)	11.8 (0.3)
Octane	12.6 (0.2)	24.3 (0.2)	14.5 (1.1)	29.3 (0.8)	7.8 (1.5)	9.4 (0.7)	8.9 (1.4)	13.0 (0.8)
Nonane	10.6 (0.3)	18.4 (0.2)	16.0 (1.9)	35.5 (1.4)	8.9 (1.0)	14.9 (0.6)	12.0 (1.5)	22.1 (0.4)
2-Methylhexane	9.2 (0.5)	17.1 (0.6)	14.8 (1.6)	32.3 (1.2)	7.3 (0.6)	10.2 (0.3)	8.0 (0.6)	12.4 (0.3)
3-Methylhexane	10.8 (0.4)	21.7 (0.5)	15.2 (0.7)	33.8 (0.5)	8.4 (1.2)	13.8 (0.7)	7.7 (0.7)	11.8 (0.4)
2,3-Dimethylpentane	11.5 (0.3)	23.9 (0.2)	15.1 (1.6)	33.7 (0.8)	8.2 (0.5)	13.4 (0.3)	7.7 (0.8)	12.0 (0.5)
2,4-Dimethylpentane	11.3 (0.3)	22.5 (0.2)	13.2 (2.4)	27.3 (1.3)	7.0 (1.1)	9.2 (0.7)	7.2 (0.7)	9.8 (0.4)
2,2,3-Trimethylbutane	9.0 (0.8)	17.1 (0.9)	13.9 (0.5)	30.3 (0.2)	6.6 (1.1)	8.5 (0.7)	7.9 (1.1)	12.7 (0.6)
Cyclohexane	10.6 (1.1)	23.8 (1.2)	15.1 (1.9)	36.3 (1.4)	7.0 (0.6)	12.3 (0.3)	8.9 (0.8)	18.1 (0.7)
Benzene	5.4 (0.5)	16.3 (0.5)	12.0 (1.8)	34.1 (1.6)	4.1 (1.8)	10.8 (1.8)	10.8 (1.0)	31.4 (0.7)
Toluene	5.4 (0.6)	15.6 (0.6)	12.3 (1.8)	34.4 (1.6)	4.8 (1.3)	12.4 (1.3)	11.1 (1.0)	31.9 (0.7)
Ethylbenzene	7.7 (0.5)	20.7 (0.6)	14.2 (2.0)	38.4 (1.7)	5.8 (1.3)	13.8 (1.3)	12.4 (1.0)	34.0 (0.7)
o-Xylene	6.2 (0.6)	17.6 (0.7)	13.7 (2.0)	38.0 (1.7)	5.4 (1.3)	13.6 (1.3)	12.0 (0.9)	34.1 (0.6)
m-Xylene	6.5 (1.0)	18.1 (1.2)	11.4 (1.7)	30.9 (1.4)	6.1 (1.2)	15.2 (0.5)	12.8 (2.7)	35.9 (0.7)
p-Xylene	5.9 (1.6)	16.7 (0.7)	12.0 (1.9)	33.2 (1.7)	4.5 (1.5)	11.1 (1.5)	11.3 (1.0)	32.0 (0.7)

Table 5.4: Partial molar solution values for OCB. Enthalpies in kJ mol^{-1} and entropies in J mol^{-1} K^{-1}. Standard deviations in brackets.

| PROBE	I (90 °C) $-\Delta H^{sol}$	$-\Delta S^{sol}$	N (73 °C) $-\Delta H^{sol}$	$-\Delta S^{sol}$	S_A (60 °C) $-\Delta H^{sol}$	$-\Delta S^{sol}$	$S_A{}^{super}$ (48 °C) $-\Delta H^{sol}$	$-\Delta S^{sol}$
Pentane	14.9 (1.8)	61.5 (1.5)	15.0 (3.2)	62.0 (2.4)	21.5 (3.4)	81.5 (0.2)	18.3 (1.3)	71.5 (1.5)
Hexane	20.0 (0.9)	68.8 (0.7)	17.7 (1.8)	63.1 (0.1)	24.4 (1.7)	82.7 (1.4)	22.0 (2.0)	75.3 (1.2)
Heptane	23.0 (0.2)	70.7 (0.1)	20.7 (1.4)	64.9 (0.0)	26.9 (1.1)	83.1 (0.8)	26.9 (0.5)	82.8 (0.4)
Octane	24.9 (0.2)	69.6 (0.1)	23.9 (1.2)	67.3 (0.0)	31.2 (0.9)	88.8 (0.7)	27.1 (2.9)	75.9 (0.2)
Nonane	31.2 (0.2)	79.9 (0.2)	28.2 (1.8)	72.0 (1.7)	39.4 (1.0)	105.1 (0.7)	30.8 (0.7)	78.5 (0.5)
2-Methylhexane	21.0 (1.0)	65.8 (0.4)	17.3 (1.6)	56.0 (1.2)	18.6 (3.2)	59.4 (2.5)	24.7 (0.4)	77.3 (0.4)
3-Methylhexane	20.7 (0.5)	64.3 (0.7)	17.2 (0.7)	54.9 (0.5)	16.4 (3.5)	52.1 (2.0)	25.9 (1.0)	80.5 (1.1)
2,3-Dimethylpentane	19.6 (0.2)	61.4 (0.1)	16.8 (1.7)	54.0 (0.9)	17.4 (3.6)	55.4 (2.7)	24.6 (0.5)	76.9 (0.5)
2,4-Dimethylpentane	18.8 (1.4)	62.2 (1.2)	17.3 (2.5)	58.7 (1.3)	17.7 (3.2)	59.5 (2.6)	23.9 (0.7)	77.9 (0.7)
2,2,3-Trimethylbutane	20.3 (0.8)	65.4 (0.9)	15.2 (0.8)	51.7 (0.6)	15.8 (3.7)	53.3 (3.1)	22.4 (0.6)	72.6 (0.6)
Cyclohexane	19.4 (1.1)	60.6 (1.2)	15.6 (1.9)	50.5 (0.1)	21.8 (1.3)	68.6 (1.1)	23.2 (0.0)	72.8 (0.0)
Benzene	25.6 (0.2)	71.4 (0.4)	18.2 (1.8)	51.2 (1.4)	31.4 (0.9)	90.2 (0.6)	21.9 (1.0)	61.1 (0.7)
Toluene	29.7 (0.2)	75.6 (0.5)	22.2 (2.0)	55.2 (0.2)	33.8 (0.7)	89.4 (0.6)	25.7 (1.0)	64.5 (0.7)
Ethylbenzene	31.3 (0.2)	74.6 (0.6)	24.1 (2.2)	55.1 (0.2)	36.9 (0.8)	92.8 (0.6)	28.6 (1.0)	67.4 (0.7)
o-Xylene	33.6 (0.2)	77.8 (0.7)	25.9 (2.2)	56.8 (0.2)	38.6 (0.8)	94.0 (0.6)	30.3 (0.9)	68.6 (0.7)
m-Xylene	34.2 (0.9)	81.1 (1.7)	28.9 (0.2)	67.3 (0.1)	35.7 (1.2)	87.6 (0.6)	30.1 (1.8)	70.3 (0.5)
p-Xylene	33.8 (0.2)	80.2 (0.6)	26.6 (2.0)	60.4 (0.2)	38.7 (0.9)	96.0 (0.6)	29.9 (0.9)	69.3 (0.7)
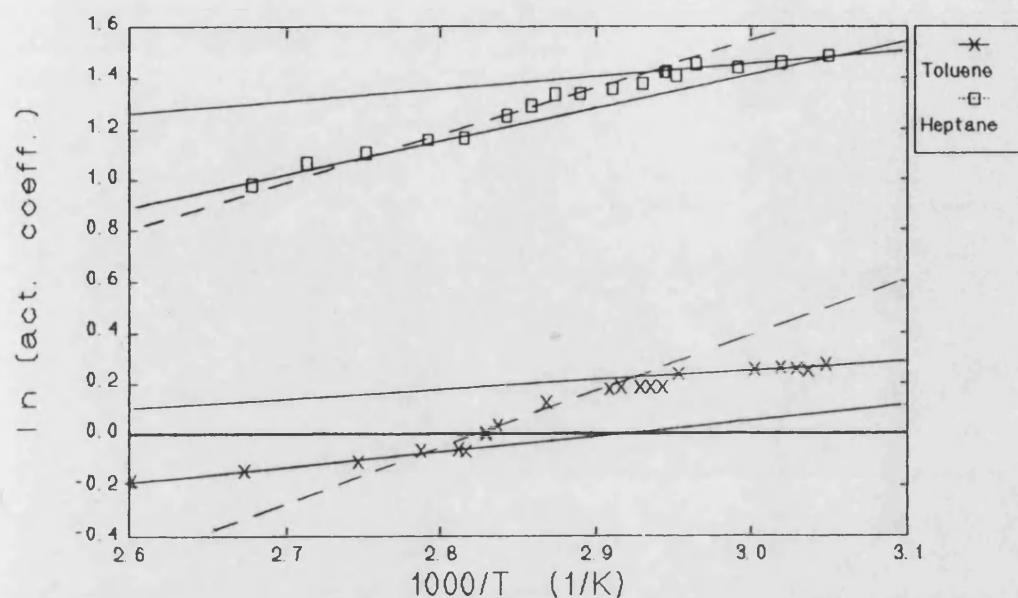
Figure 5.5: Extrapolated activity coefficient data for heptane, x, and toluene, o.

than in the nematic phase. Surprisingly, the partial molar excess enthalpy and entropy also indicate the smectic phase is more like a given probe than the isotropic phase. One might expect the more ordered smectic phase would require higher excess enthalpies to form a solution which would create a greater disruption of the layered phase. That this does not occur, and the measured activity coefficients in the smectic mesophase indicate more favourable solution formation in the isotropic phase, indicates that the probes spend a comparatively short time in the part of the layered smectic structure that would give unfavourable interactions. That is, the aromatic probes spend more time within a smectic layer, where the biphenyls are, whilst the aliphatic probes spend more time between layers, where the alkyl chains are. In a similar manner to HCB, the supercooled region exhibited values intermediate between the smectic phase and the nematic phase. Again, the behaviour indicates re-entrant behaviour for OCB. This has been observed[205] and the cause was discussed in the previous section. The following discussion will look at the trends between different sets of probes in OCB.

n-alkanes: The trends amongst the n-alkanes are similar to those reported for HCB where longer chains result in greater potential energy interactions and greater restrictions on the probe molecule. The enthalpies and entropies can also be fitted to linear correlations with molecular polarisability. This illustrates the importance of the potential energy contributions to solvation. However, the activity coefficients at all temperatures are lower than those exhibited by HCB. Hence, OCB has a greater affinity for the probes. The lower magnitudes of the enthalpy and entropy indicate this increased affinity results from a more favourable entropic term. The longer alkyl chain in OCB is obviously more important because of the greater flexibility it allows the probe to have rather than an increased similarity of potential energies of the liquid crystal and probe. Comparing *figures 5.1* and *5.4*, the activity coefficients at a given temperature in an identical phase were lower for OCB but the decrease in value was reduced when the temperature was lowered. This behaviour is comparable to that observed in other liquid crystals, such as the homologous series of alkylcyanobiphenyls[152] which also exhibit smaller reductions in activity coefficient values on adding extra methylene units to the alkyl chain as the chain gets longer.

branched alkanes: The enthalpies and entropies of solution follow very similar trends in all the liquid crystal phases and the trends in OCB are similar to those in HCB, governed by the delicate balance between increased rigidity, resulting in stronger interactions, and the disruption of the liquid crystal molecules. The activity coefficients also show a similar trend, decreasing from 2,4-dimethylpentane to 2,2,3-trimethylbutane. However, the most striking difference is the n-heptane values which are higher than the branched isomers in OCB but were lower than most of them in HCB. Looked at another way, the decrease in activity coefficients for heptane in going from HCB to OCB was smaller than the decreases observed for the branched alkanes. This reflects the greater effect the extra alkyl chainlength has on reducing unfavourable interaction with the liquid crystal molecules.

aromatic probes: In the nematic and isotropic region the behaviour of OCB is similar to HCB with the presence or absence of strong interaction between the probe and

liquid crystal governing whether the solution formation was entropically or enthalpically driven. The smectic A phase of OCB exhibited identical thermodynamic solution parameter trends to those in the nematic mesophase, apart from *meta*-xylene which exhibited a relatively higher partial molar enthalpy change of solution and lower partial molar entropy change of solution. The activity coefficients in the smectic region exhibited an identical trend to the nematic and isotropic phases and all values were significantly lower than in HCB. The values for *para*-xylene were larger than the other xylenes in OCB as opposed to *meta*-xylene in HCB. These above trends indicate that OCB offers a more flexible environment for the probes than HCB. The importance of the polarisability is thus reduced while the length to breadth ratio has become the governing factor over symmetry for the rotational energy contribution to the solution behaviour. This was particularly prevalent in the smectic phase where the mesophase structure was considerably more restrictive. In the supercooled phase the enthalpies and entropies are very similar for all xylene isomers.

C6 probes: In HCB the values for cyclohexane were intermediate to those of hexane and benzene in the nematic phase and higher than both in the isotropic phase. With OCB the second trend predominates for all phases. The partial molar entropy change of solution decrease for benzene in OCB is greater than in HCB in the isotropic phase reflecting the influence of the longer alkyl chain on the liquid crystal. Whilst, again, the corresponding entropies for solution formation in the nematic phase were similar for benzene and cyclohexane and the lowering in entropy from HCB to OCB was smaller than for hexane. Thus molecular shapes compatible with the two-dimensional environment of the nematic phase are even more important than in HCB, as might be expected from the results in section 4.3d which indicate the nematic mesophase of OCB is more ordered than in HCB. The trends in the smectic phase revert to those of the isotropic phase, but the differences are even more marked. The observations here follow the same explanations given for HCB. The large differences in the activity coefficients again illustrates that, although OCB offers a generally more flexible environment for the probes than HCB, the interaction strength still dominates the solution behaviour.

The above two sections have shown that there are many similarities between the two cyanobiphenyl probes, as might be expected for two stationary phases with similar molecular structures. However, the presence of the longer alkyl chain in OCB had a significant influence on the interaction between probe and liquid crystal and this resulted in an overall improvement of the favourability of solution formation over that observed in HCB.

5.3 OCTYLOXYBIPHENYL iso-OCTYLOXYBENZOATE (OBIB)

The molar activity coefficients for the probes are given in *figure 5.5* and the partial molar excess quantities and partial molar solution quantities are given in *tables 5.5.* and *5.6* respectively are shown below;

$$\gamma^{super} > \gamma^S > \gamma^C > \gamma^I \qquad [1]$$

$$\Delta H^{super} < \Delta H^I < \Delta H^S < \Delta H^C \qquad [2]$$

$$\Delta S^{super} < \Delta S^I < \Delta S^S < \Delta S^C \qquad [3]$$

$H^C > H^S > H^I > H^{super}$	aromatic	[4a]
$H^C > H^S > H^{super} > H^I$	aliphatic	[4b]

$S^C > S^S > S^I > S^{super}$	aromatic	[5a]
$S^C > S^S > S^{super} > S^I$	aliphatic	[5b]

In [3] and [4a] the isotropic and supercooled region values for *para*-xylene are reversed.

As seen with OCB the trends are different for aliphatic and aromatic probes. However, the excess properties alone are affected. Another difference between this chiral material and the cyanobiphenyls is the larger enthalpy changes that accompany the phase transitions, particularly between the mesophases. Thus there will be a greater perturbation to the solution behaviour due to the stronger interactions in the cholesteric and smectic C phases relative to the adjacent higher temperature phases. However, the transition enthalpies, shown in chapter 4, are still reasonably small so the

major solution effects are still likely to be governed by the probe-liquid crystal interactions.

The trends above show that the highest temperature mesophase, that is the cholesteric phase, exhibited the highest partial molar entropy and enthalpy changes of solution and highest partial molar excess quantities. This behaviour follows the trends observed for the two cyanobiphenyl materials. Trends [2] and [4] show solution formation is more enthalpically favourable in the isotropic phase than in the cholesteric mesophase and trend [3] and [5] illustrate the entropically favourable nature of the cholesteric phase. With OBIB the smectic C mesophase is not as enthalpically favoured as the isotropic phase. This is opposite to the smectic A mesophase behaviour in OCB and is indicative of the influence of the twisted nature of this smectic C phase. The trend in [3] shows that the smectic mesophase offers a favourable entropic environment to the probe compared to the isotropic phase. Above, it has already been stated that the smectic mesophase exhibited stronger interactions with a given probe than the isotropic phase and the smectic mesophase also has positional and orientation order which the isotropic phase does not. Thus the disordering effect of the probe on the liquid crystal must have a much greater influence over solution behaviour than was found with the non-chiral liquid crystals. Despite this, trend [1] indicates the isotropic phase was the thermodynamically more stable at the lower temperatures so the probe-liquid crystal potential energy contributions were the governing factor again.

The partial molar excess properties given in trends [4] and [5] follow the order C > S_C >I. Thus, the isotropic phase was most like a given probe liquid and the cholesteric phase was the most dissimilar. This trend is easily visualised on the grounds of the increased liquid crystal order in the mesophases and a greater interaction between probe and smectic mesophase than probe and cholesteric mesophase. Interestingly, for OBIB the supercooled region exhibited values which do not fall between the smectic and cholesteric region as found for OCB. Instead values are considerably closer to those of the isotropic phase which could indicate a loss of any sense of twist in the
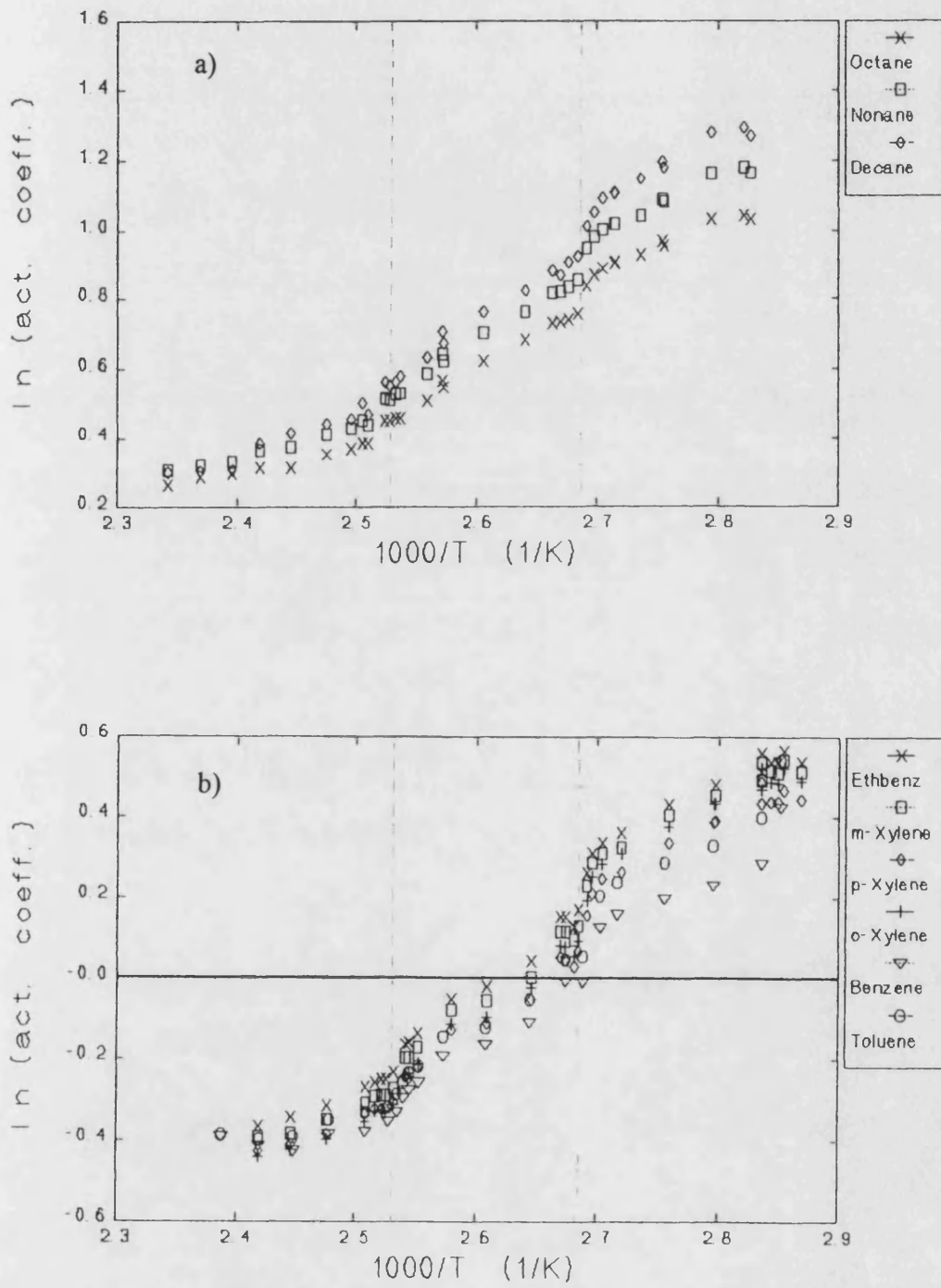
Figure 5.5 Activity coefficients in OBIB. a) n-alkanes, b) aromatic probes.

Table 5.5: Partial molar excess parameters for OBIB. Enthalpies in kJ mol⁻¹ and entropies in J mol⁻¹ K⁻¹. Standard deviation in parentheses

PROBE	I H^E	(133 °C) S^E	C H^E	(110 °C) S^E	S_C H^E	(90 °C) S^E	S_C^{super} H^E	(75 °C) S^E
Octane	6.7 (0.7)	13.6 (0.7)	16.9 (1.0)	38.9 (0.9)	11.9 (0.7)	24.7 (0.8)	8.4 (0.5)	15.4 (0.2)
Nonane	8.2 (0.7)	17.0 (0.7)	17.5 (1.0)	39.7 (1.0)	13.7 (0.7)	28.9 (0.7)	9.5 (1.5)	17.3 (0.6)
Decane	8.8 (1.7)	18.1 (1.3)	18.5 (1.5)	42.0 (1.3)	16.3 (1.0)	35.2 (1.2)	11.2 (2.0)	21.0 (0.9)
Benzene	4.4 (0.7)	14.1 (0.6)	13.9 (0.4)	37.6 (0.3)	9.3 (0.7)	24.0 (0.7)	3.1 (1.6)	6.4 (0.6)
Toluene	6.1 (0.2)	18.0 (0.2)	15.0 (0.3)	40.1 (0.2)	11.4 (0.7)	29.2 (0.7)	4.8 (0.3)	10.3 (0.2)
Ethylbenzene	8.2 (0.5)	26.2 (0.5)	16.7 (0.5)	43.8 (0.5)	14.1 (0.5)	35.5 (0.7)	7.3 (2.7)	16.4 (1.1)
o-Xylene	9.5 (1.1)	26.7 (0.9)	17.4 (0.4)	46.3 (0.4)	14.9 (0.6)	38.0 (0.7)	8.3 (2.2)	19.8 (0.9)
m-Xylene	9.0 (0.8)	25.1 (0.7)	16.3 (0.7)	43.2 (0.6)	14.3 (0.6)	36.2 (0.7)	5.9 (2.1)	12.7 (0.7)
p-Xylene	8.9 (0.7)	25.1 (0.7)	15.8 (0.5)	42.2 (0.4)	15.1 (0.7)	38.9 (1.0)	9.6 (2.8)	9.6 (1.1)

Table 5.6 Partial molar changes of solution for OBIB. Enthalpies in kJ mol^{-1} and entropies in J mol^{-1} K^{-1}. Standard deviation in parentheses

PROBE	I (133 °C)		C (110 °C)		S_C (90 °C)		S_C^{super} (75 °C)	
	$-\Delta H^{sol}$	$-\Delta S^{sol}$	$-\Delta H^{sol}$	$-\Delta S^{sol}$	$-\Delta H^{sol}$	$-\Delta S^{sol}$	$-\Delta H^{sol}$	$-\Delta S^{sol}$
Octane	28.1 (0.6)	77.7 (0.6)	19.3 (1.0)	56.1 (1.5)	25.6 (0.7)	73.6 (0.8)	31.7 (2.0)	86.0 (0.9)
Nonane	30.7 (0.7)	79.0 (0.7)	23.1 (1.1)	60.3 (1.0)	28.2 (0.7)	74.9 (0.9)	34.8 (2.1)	88.7 (0.9)
Decane	32.0 (1.7)	76.9 (1.7)	26.4 (1.5)	63.3 (1.2)	30.2 (1.1)	74.4 (1.2)	37.5 (2.4)	90.2 (1.1)
Benzene	27.1 (1.9)	74.3 (1.7)	14.4 (2.0)	43.0 (2.0)	22.2 (0.5)	64.9 (0.4)	28.2 (1.6)	81.6 (0.5)
Toluene	28.3 (1.4)	71.1 (1.5)	17.6 (2.1)	44.7 (2.0)	24.0 (0.7)	63.0 (0.6)	30.6 (0.4)	86.0 (0.7)
Ethylbenzene	30.4 (1.0)	75.8 (1.5)	21.7 (1.3)	50.0 (1.2)	25.3 (0.8)	61.3 (0.9)	34.5 (4.0)	87.1 (1.5)
o-Xylene	33.1 (1.1)	79.9 (1.5)	23.1 (1.6)	51.0 (1.5)	25.8 (0.7)	59.9 (0.9)	35.1 (4.5)	86.0 (1.6)
m-Xylene	31.9 (1.0)	78.5 (1.4)	22.7 (1.6)	51.7 (1.5)	25.3 (1.1)	60.1 (1.1)	36.4 (2.9)	91.4 (1.3)
p-Xylene	31.6 (1.1)	77.6 (1.5)	23.5 (1.6)	53.5 (1.5)	24.1 (0.9)	56.5 (1.0)	32.2 (2.8)	75.0 (1.5)

supercooled phase to allow rearrangement into a non-twisted crystalline structure. The relative solution behaviour of the probes is discussed below.

n-alkanes: Within each phase the partial molar enthalpy changes of solution exhibited a linear correlation with chainlength. This follows the pattern seen in the previous liquid crystals where the increase in chainlength increases the restriction of molecular flexibility whilst increasing potential energy contributions due to the greater polarisability. The activity coefficients generally increased from octane to decane indicating the importance of the contribution of liquid crystal restriction of probe movement in a given phase. However, the lower values in the isotropic phase compared to the mesophases reflect that this is a perturbation of the values which were mainly determined by the potential energy contribution arising from probe-liquid crystal interactions. The length of the alkane chain becomes even more important to the overall solution behaviour in the smectic C phase, as seen by the increased difference in activity coefficient values between probes.

aromatic probes: The aromatic probes exhibited similar trends relative to the n-alkanes as observed with HCB and OCB. Partial molar enthalpy changes of solution correlate well with the polarisability of the probe molecule and there was no evidence that there was any significant contribution to the solution behaviour from the permanent dipoles within the probe molecules. Indeed, the observed activity coefficient values showed that *para*-xylene formed the most favourable solution with OBIB of all the xylene isomers yet it is the only one without a permanent dipole. Partial molar enthalpies for aromatic probes in the cholesteric and isotropic phase are lower than values for the n-alkanes but become higher for the smectic C phase. The corresponding entropies are similar in the isotropic phase but become progressively higher than the aliphatic probes as the temperature is reduced. This supports the premise that the potential energy of the interactions is the governing factor. Amongst the xylene isomers the enthalpy and entropy values increase from *ortho<meta<para* for the isotropic and smectic phases. In the cholesteric phase the *para*-xylene values are

lowest. These trends indicate the importance of the length to breadth ratio in the cholesteric mesophase due to twisted nature of this mesophase.

In all the low mass liquid crystals discussed there remain size and shape perturbations to the solution behaviour of the probe-liquid crystal system even in the isotropic phase. This reflects the rod-like nature of the molecules. Although the phase is comprised of a disordered array of liquid crystal molecules the nature of the shape of an individual molecule would appear sufficient to impose an asymmetrical environment on the probe molecules solvated.

5.4 POLYMER LIQUID CRYSTAL

5.4a Polydimethylsiloxane (PDMS)

Before discussing the solution behaviour of the probes with the polymeric liquid crystal the behaviour of the same probes with PDMS will be discussed to allow comparison. PDMS was studied because it is often used for gas chromatographic separations and also forms the polymer backbone from which the mesogen side-groups are suspended.

The entropies associated with the solution process are reported but the significance of the values is limited due to the polydispersity the polymer, see sections 1.12b and 3.3. Connected with this was a need to present weight activity coefficients as opposed to the molar activity coefficients reported for low molar mass systems. This adds a complication to their interpretation. *Figure 5.6* highlights this point by showing the weight activity coefficients for n-alkanes in HCB. Comparison with the previously discussed molar activity coefficients in *figure 5.1* shows the trend has been reversed. The differences in probe molar masses would be sufficient to reverse the trends in PDMS and LCP as well. Presumably the increase in the proportion of end-groups per unit mass in going from nonane to pentane is responsible for the reversal in trends between molar and weight activity coefficients. The upshot is that the relative
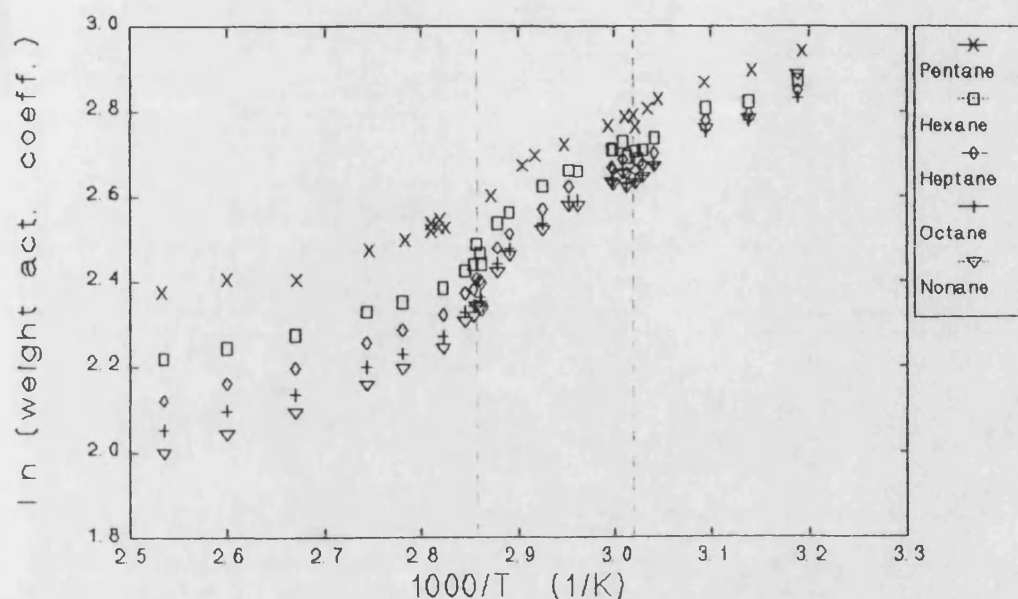
Figure 5.6: Weight activity coefficients for the n-alkanes in HCB.

deviations from the ideal are not given by the order of the weight activity coefficients unless isomers are being discussed.

The activity coefficients are given in *figure 5.7* and the partial molar excess and partial molar solution change quantities are listed in *table 5.7*. The striking feature is the small partial molar excess enthalpy values compared to those previously reported in the liquid crystal systems. The values for the n-alkanes decrease to favourable interactions as this chainlength reduces. The less flexible branched isomers of heptane exhibit larger partial molar excess enthalpies but the difference is very small. Values for the aromatic probes indicate poorer interaction with PDMS than the aliphatic probes show. This is not unreasonable considering the aliphatic sidechains of the polymer. Similar arguments to those given above could be proposed to account for the relative solution parameter changes. However, the much closer agreement found between the xylene isomers and clearer trend in the heptane isomers are a strong indication that energetic factors dominate the solution behaviour almost exclusively. The activity coefficients for the heptane isomers support this and the xylene isomers indicate that the dipole moment may be the governing perturbation factor rather than shape and size. The rigidity of the aromatic probes still enable stronger interactions to occur with
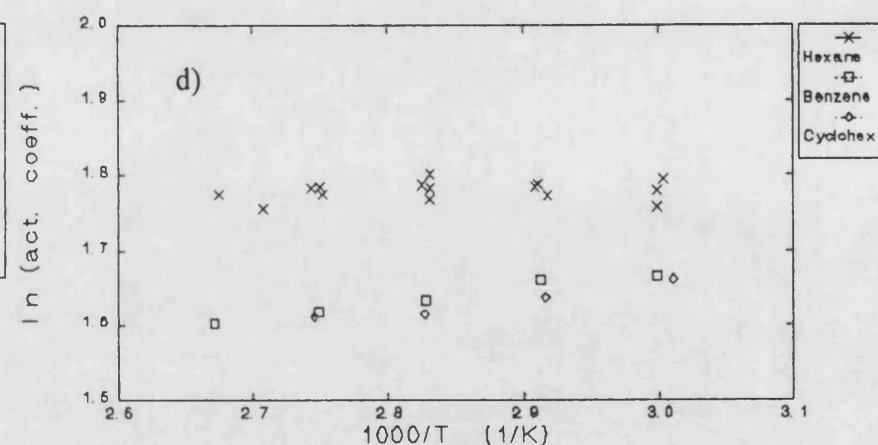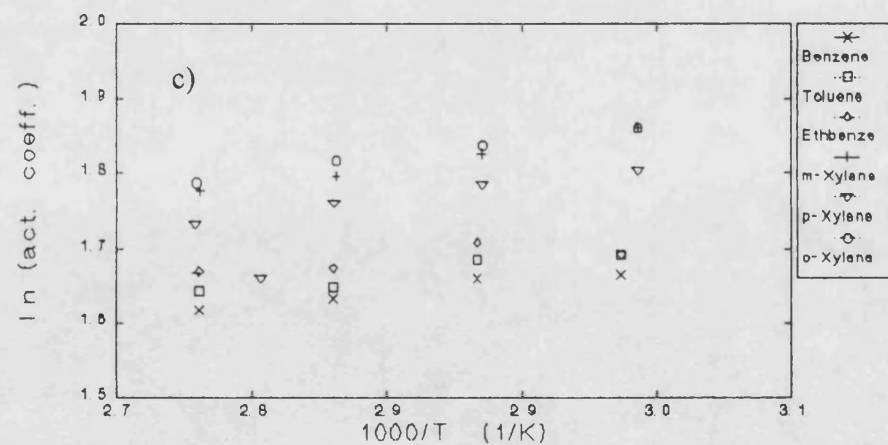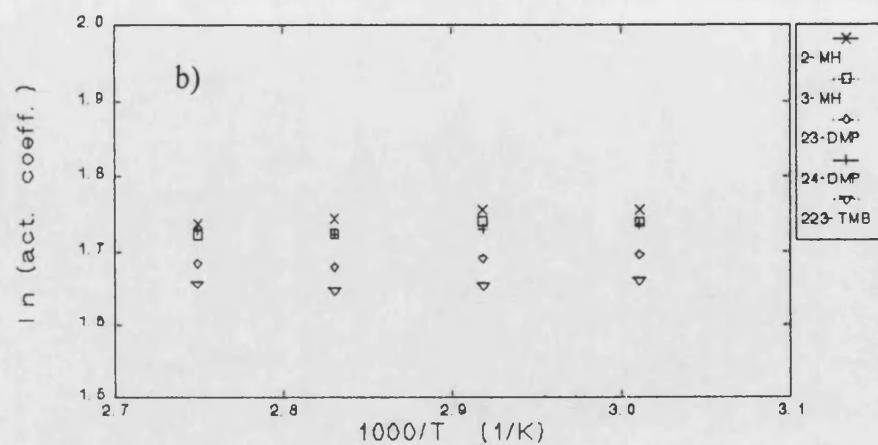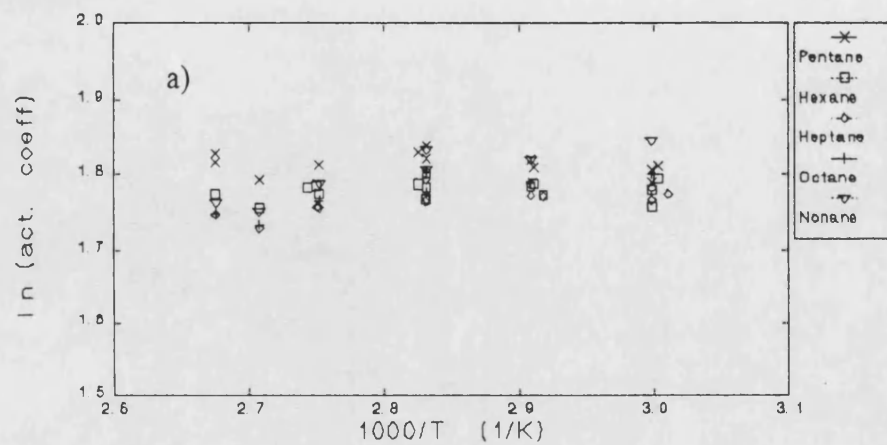
Figure 5.7: Weight activity coefficients in PDMS, a) n-alkanes, b) heptane isomers, c) aromatic probes, d) "six carbon" probes.

Table 5.7: Partial molar excess quantities and partial molar changes of solution parameters for

PDMS. Enthalpies in kJ mol^{-1}and entropies in J mol^{-1} K^{-1}. Standard deviations in parentheses.

PROBE	(78 °C) H^E	S^E	$-\Delta H^{sol}$	$-\Delta S^{sol}$
Pentane	-0.3 (0.3)	-68.0 (1.2)	24.5 (0.4)	42.2 (1.4)
Hexane	0.2 (0.3)	-65.0 (1.1)	28.8 (0.3)	48.2 (1.3)
Heptane	0.8 (0.3)	-61.8 (1.1)	32.8 (0.3)	53.2 (1.3)
Octane	1.6 (0.5)	-58.4 (1.3)	36.4 (0.6)	57.3 (1.6)
Nonane	2.4 (0.5)	-55.7 (1.3)	40.3 (0.6)	62.1 (1.7)
2-Methylhexane	0.6 (0.1)	-62.1 (0.3)	31.5 (0.3)	51.5 (0.6)
3-Methylhexane	0.6 (0.2)	-61.9 (0.4)	31.8 (0.3)	51.7 (0.7)
2,3-Dimethylpentane	0.5 (0.2)	-62.1 (0.4)	31.4 (0.2)	51.0 (0.3)
2,4-Dimethylpentane	0.3 (0.2)	-62.9 (0.4)	30.2 (0.1)	50.1 (0.3)
2,2,3-Trimethylbutane	0.2 (0.3)	-62.5 (0.5)	29.8 (0.2)	48.3 (0.3)
Cyclohexane	1.6 (0.3)	-59.7 (0.6)	29.1 (0.2)	44.6 (0.3)
Benzene	1.7 (0.2)	-60.2 (0.4)	29.4 (0.3)	45.3 (0.8)
Toluene	1.8 (0.3)	-58.8 (0.7)	33.5 (0.3)	50.4 (0.8)
Ethylbenzene	1.3 (0.4)	-59.2 (1.0)	37.9 (0.5)	57.5 (1.3)
o-Xylene	4.5 (0.8)	-51.0 (3.2)	35.8 (0.8)	49.9 (3.2)
m-Xylene	4.2 (0.7)	-51.7 (2.4)	35.3 (0.6)	49.9 (2.4)
p-Xylene	3.8 (0.7)	-52.6 (2.5)	35.5 (0.7)	50.2 (2.5)

PDMS but this is not as marked as in the liquid crystals and the activity coefficients are

much closer.

5.4b Polymer Liquid Crystal (LCP)

The weight activity coefficients are illustrated in *figure 5.8* and the partial molar

enthalpies are listed in *table 5.8*. The general trends are listed below;

$$\Omega_I < \Omega_S \qquad\qquad [1]$$

$$\Delta H^S < \Delta H^I \qquad\qquad [2]$$

$$H^S < H^I \qquad\qquad [3]$$

The partial molar excess enthalpy and partial molar enthalpy change of solution for cyclohexane were anomalous, exhibiting values in the smectic A and isotropic phase that were opposite to the trend observed for the other probes. The glass transition falls considerably below the region studied here and should have little influence on results. Also, there was no crystalline region of LCP and hence no supercooling of the material.

The energy of the mesophase to smectic transition per repeat unit of the polymer, reported in chapter 4, was of a similar order to the low molecular mass cyanobiphenyl materials. This indicates the differences in phase behaviour observed were again due to the probe-liquid crystal interactions. Unlike the OCB analogue, this material does not exhibit a nematic phase. However, the general trends observed for the smectic A and isotropic phases were identical for LCP and OCB, the only difference was that the branched alkanes also agreed with this general trend in LCP. Hence, it is likely that the trends in the thermodynamic parameters for LCP were governed by the interaction strengths between probes and liquid crystal. For instance, the higher weight activity coefficients in the smectic phase would thus be a consequence of the entropy lost by strong interaction.

The partial excess molar enthalpies were of a similar magnitude to the OCB values in the smectic A phase and generally considerably higher than those reported for PDMS. This is indicative that the mesogen was governing the solution behaviour in the mesophase with PDMS acting as a moderator to this behaviour. In the isotropic phase this was also found to be true except for cyclohexane which now exhibits an excess enthalpy much closer to that observed in PDMS. This appears to be the cause of the reversal in trend and may be due to the probe spending most of the time interacting with the polymer backbone in the isotropic phase, but the reason is unclear. Below, discussion reverts to the more robust method of comparing the solution parameters.
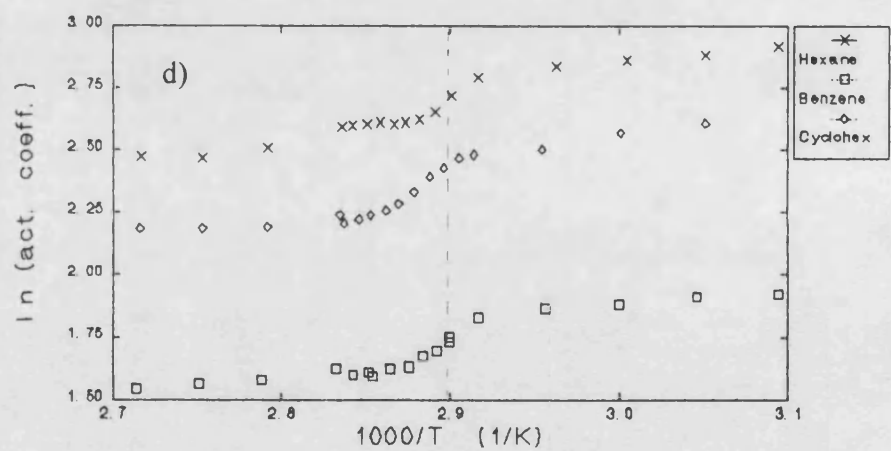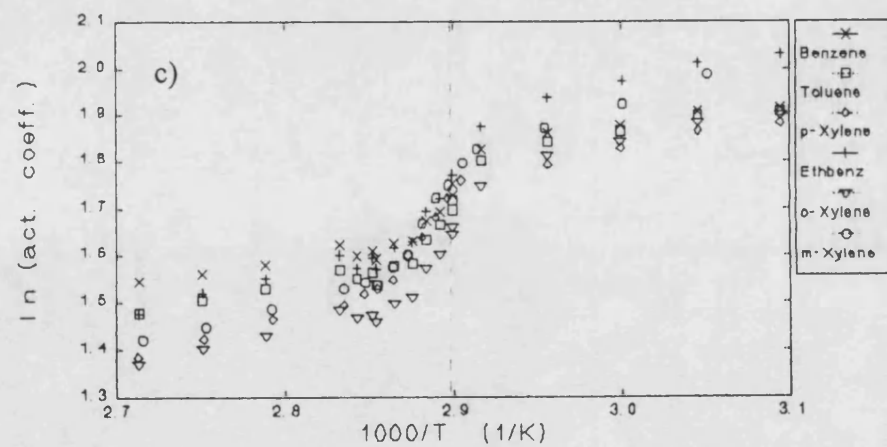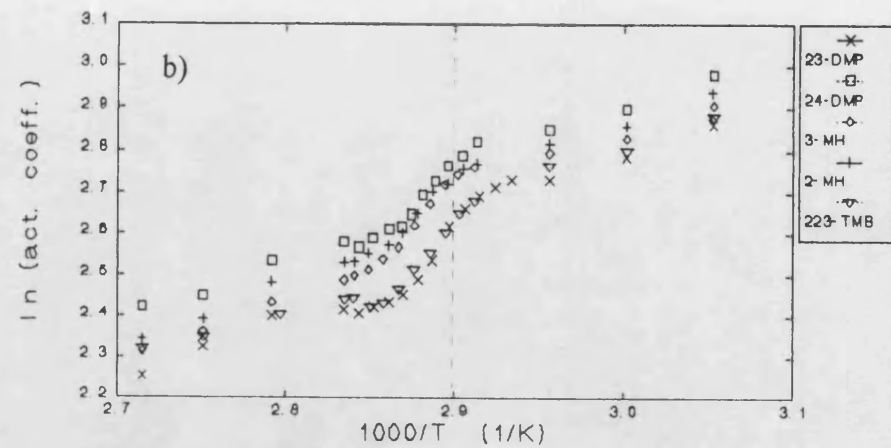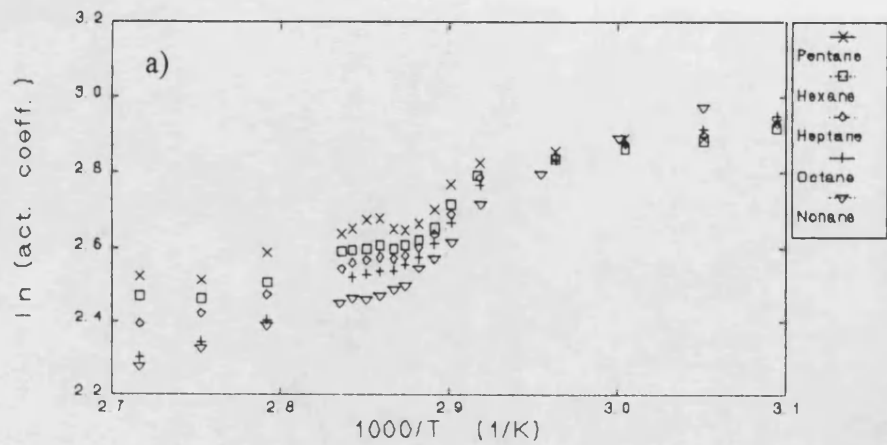
Figure 5.8: Weight activity coefficients in LCP, a) n-alkanes, b) heptane isomers, c) aromatic probes, d) "six carbon" probes.

Table 5.8: Partial molar excess quantities and partial molar changes of solution for LCP. Enthalpies in kJ mol⁻¹ and entropies in J mol⁻¹ K⁻¹. Standard deviations in parentheses.

PROBE	S_A (57 °C) H^E	S^E	$-\Delta H^{sol}$	$-\Delta S^{sol}$	I (88 °C) H^E	S^E	$-\Delta H^{sol}$	$-\Delta S^{sol}$
Pentane	4.2 (1.1)	-44.4 (1.1)	21.1 (1.1)	58.6 (0.9)	8.3 (0.6)	-29.4 (2.2)	14.9 (2.5)	38.0 (1.8)
Hexane	4.9 (0.4)	-40.6 (0.4)	25.1 (0.4)	62.7 (0.7)	9.4 (1.2)	-28.3 (2.3)	19.9 (2.6)	46.8 (1.7)
Heptane	5.5 (0.4)	-37.7 (0.3)	29.3 (0.4)	67.1 (1.0)	11.2 (0.5)	-21.3 (0.9)	22.5 (1.0)	47.9 (0.8)
Octane	7.3 (0.6)	-31.1 (0.6)	32.2 (0.7)	68.8 (1.2)	11.4 (0.6)	-8.77 (1.4)	25.3 (0.5)	44.3 (1.1)
Nonane	12.9 (0.7)	-10.3 (0.8)	31.7 (0.8)	56.7 (1.4)	12.4 (0.3)	-13.5 (0.2)	29.6 (0.2)	56.7 (0.2)
2-Methylhexane	8.2 (1.4)	-29.6 (1.7)	24.9 (1.6)	58.7 (1.5)	13.6 (1.2)	-12.7 (1.1)	17.8 (1.2)	40.6 (1.0)
3-Methylhexane	6.8 (2.2)	-33.6 (1.8)	26.8 (2.3)	63.3 (1.6)	12.4 (0.6)	-15.9 (0.5)	19.4 (0.6)	42.1 (0.4)
2,3-Dimethylpentane	7.9 (1.8)	-29.6 (2.2)	24.9 (1.9)	59.9 (1.8)	11.1 (2.5)	-5.6 (1.3)	20.2 (2.5)	50.8 (2.2)
2,4-Dimethylpentane	7.9 (1.7)	-30.6 (2.1)	23.5 (1.8)	58.3 (1.7)	11.6 (1.4)	-18.9 (1.2)	18.3 (1.4)	45.9 (1.2)
2,2,3-Trimethylbutane	7.3 (1.6)	-31.5 (1.9)	23.4 (1.6)	52.8 (2.3)	8.7 (0.4)	-26.0 (0.3)	17.6 (4.3)	51.8 (1.2)
Cyclohexane	8.7 (0.8)	-26.7 (0.9)	22.8 (0.9)	53.4 (0.9)	3.6 (1.4)	-40.0 (1.2)	29.0 (0.0)	63.0 (1.1)
Benzene	3.5 (0.6)	-37.6 (0.6)	28.8 (0.7)	61.7 (0.9)	5.5 (0.8)	-30.1 (0.7)	25.3 (0.7)	56.3 (1.0)
Toluene	4.2 (0.6)	-33.8 (0.7)	32.2 (0.7)	64.1 (1.0)	6.4 (0.4)	-25.9 (0.4)	28.5 (0.4)	58.2 (0.8)
Ethylbenzene	5.9 (0.7)	-28.3 (0.7)	34.5 (0.7)	64.1 (1.4)	8.6 (0.6)	-18.8 (0.4)	30.2 (0.5)	58.9 (1.2)
o-Xylene	7.8 (0.6)	-28.6 (0.7)	36.3 (0.8)	65.3 (1.6)	5.5 (0.7)	-19.8 (0.5)	32.2 (0.5)	60.1 (0.9)
m-Xylene	9.6 (0.3)	-17.0 (0.3)	31.4 (0.3)	57.6 (0.3)	7.5 (0.5)	-21.1 (0.4)	31.8 (0.4)	57.5 (0.4)
p-Xylene	5.5 (0.7)	-28.4 (0.7)	35.2 (0.8)	67.8 (0.7)	7.5 (0.5)	-20.9 (0.4)	31.5 (0.6)	54.9 (0.5)

n-alkanes: In the isotropic phase the alkanes follow a linear dependence with polarisability as seen previously with the low molecular mass materials, see *figure 5.9*. In the smectic phase the trend was similar but nonane and octane had similar values. This could be a result of the liquid crystal restriction of the probe being compensated by the disruption of the mesophase or due to there being no free alkane chain, the tetherered chain not permitting the same degree of interaction as the probe chain gets longer. For the reasons outlined in section 5.4a, the weight activity coefficients have to be interpreted with care. However, it is clear that an account of the different molecular masses of the probes would result in the smectic values spreading from less favourable solutions with nonane to more favourable solutions with pentane. The range of activity coefficient values in the isotropic phase would contract, and while pentane values would again be lowest, the spread of values would be considerably smaller. Comparison with the activity coefficients for OCB and PDMS, *figures 5.4* and *5.7* respectively, shows that the isotropic phase appears to allow a stronger influence on solution properties of the polymer backbone.


branched alkanes: Here weight and molar activity coefficients trends can be compared directly. The enthalpy of solution increases as branching increases. Increased branching results in lower molecular flexibility and stronger interaction. The enthalpy trend in the smectic phase implies the loss in flexibility is the governing factor in the solution process but the activity coefficients show there is a more involved interplay between the two effects. In fact, the activity coefficients follow the same trend as OCB and not PDMS so the observed parameters would be expected to result from the effects discussed in section 5.2. The agreement with OCB for activity coefficients illustrates that the entropy gain from poorer interaction must be offset by an entropy loss due to a restrictive environment. This is another indication of the "tethering" effect the polysiloxane backbone has on the mesogen. The implication is a greater sense of order on the solution. In the isotropic phase the same activity coefficient trend occurs as in the smectic phase. However, the trend in the partial molar enthalpy of solution has changed. In each phase the trend correlates with that found in PDMS.

aromatic probes: The aromatic probes generally have higher enthalpies than the aromatic probes. In *figure 5.9a* the partial molar enthalpy changes of solution in the isotropic phase are plotted against the polarisability, values taken from reference 191. Similar plots were obtained for the mesophases. In *figure 5.9b* the same values for the aromatic probes are plotted against the polarisability as calculated from the Debye[208] expression. This also accounts for the permanent dipole contribution to the polarisability. Most values correlate with the polarisability given in *figure 5.9a* but a possible improved fit to the observed values was possible when the effect of the permanent dipole was accounted for. However, the activity coefficients show that effects arising from the liquid crystal restriction of probe movement, discussed for OCB, also contribute. Thus the interaction governs the behaviour but both dipole and size/shape effects perturb the trend significantly, as opposed to OCB where size/shape effects alone were adequate to account for the perturbations.

C6 probes: In PDMS cyclohexane and benzene activity coefficients were almost identical but in LCP the values followed the behaviour of OCB. The partial molar enthalpies in the smectic phase were similar for benzene and cyclohexane and increased for hexane whilst the isotropic phase exhibits intermediate behaviour for cyclohexane to that of the other two probes. The smectic trend is indicative of a greater contribution to this enthalpy from molecular restraint of rotational/vibrational motion for cyclohexane. The high activity coefficient values for hexane indicate much poorer interaction for hexane and the high enthalpy shows that this, and not loss of flexibility, governed solution properties. In the isotropic phase flexibility loss is not as critical as the phase has a higher entropy. Thus the rigidity of the molecule becomes most important and would appear to solely govern the trend in solution behaviour.

Thus, the solution behaviour of the liquid crystal polymer was mainly governed by the properties of the mesogen it contained. Also, the behaviour closely follows the behaviour of the low molecular mass analogue in the mesophase. However, the polymer backbone does exert some influence on the solution properties and this becomes most marked in the isotropic phase of the liquid crystal.
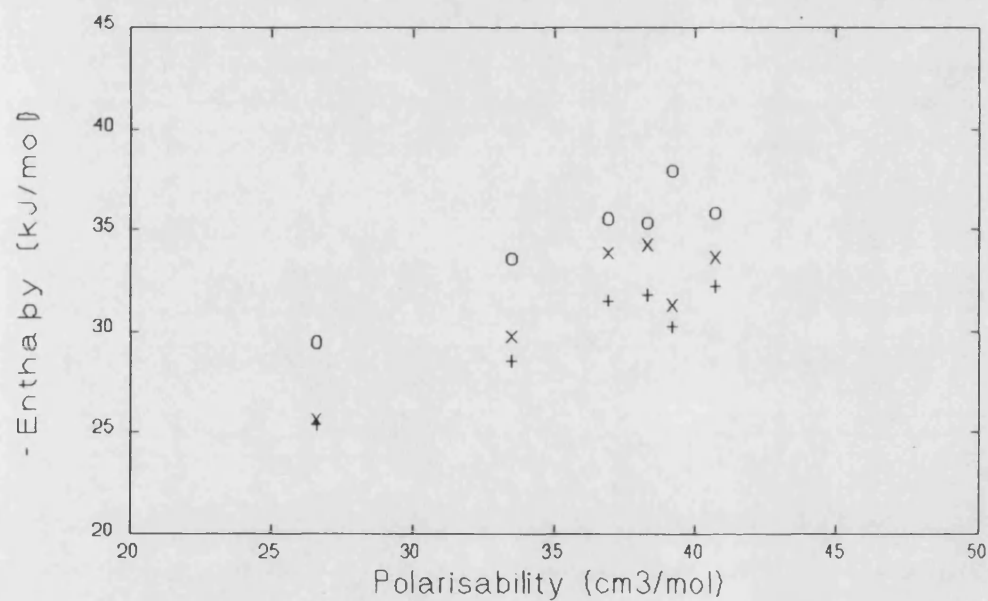
a)
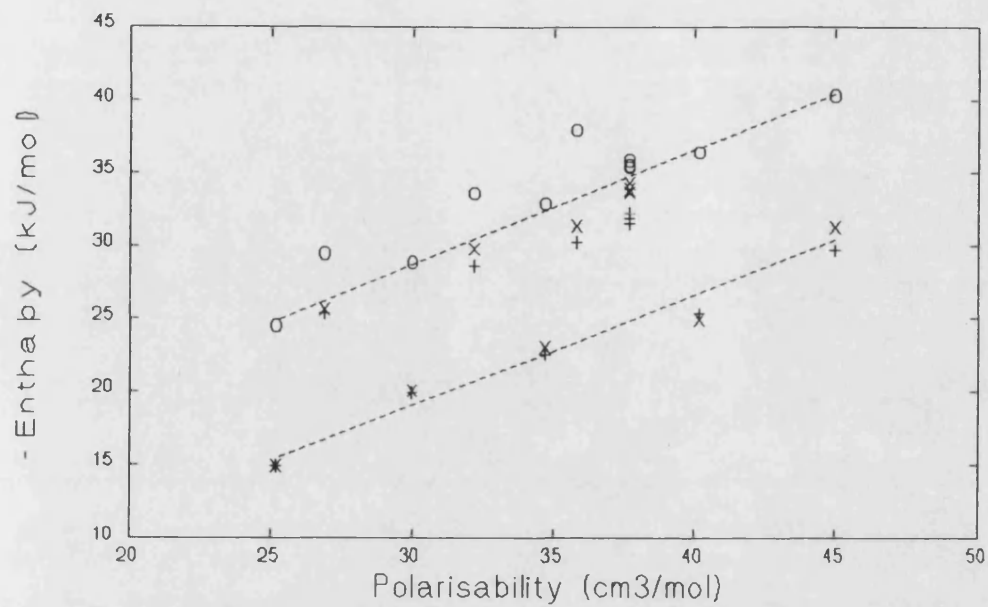
b)

Figure 5.9: Partial molar enthalpy changes of solution, kJ mol^{-1}, for aromatic and n-alkane probes in OCB, x, PDMS, o, and LCP, +, against polarisability. a) Without the permanent dipole contribution, b) with the permanent dipole contribution.

5.5 THE SURFACE OF THE CRYSTAL PHASE

In the above sections interactions between probe and liquid crystal have been discussed for solution formation due to probe absorption and the observed thermodynamic nature of the solution used to elucidate the cause of this interaction. In the next chapter this observed behaviour will be fitted to solution models and discussed in terms of the model parameters. But before that probe interactions with the liquid crystal whilst adsorbing on the crystalline surface will be considered briefly.

Adsorption measurements present a difficulty of ensuring the probe is at infinite dilution at a surface. In chapter 1 it was pointed out that the adsorption isotherm may not be linear at probe injection sizes used for infinite dilution bulk measurements. Thus it may be necessary to work with very small injection volumes of probe and to fully characterise a surface requires the measurement of the adsorption isotherm. However, several reports have shown it is possible to gain useful interpretations of surfaces without prior determination of the full isotherm[124]. In this study the constancy of retention volumes for the probes studied over the limited range of sample injections used, and small amount of peak tailing were taken as an indication of a near linear adsorption isotherm. However, it was observed that peak tailing was significantly greater for adsorption measurements than observed in the absorption experiments. Discussion here will be limited to the qualitative observations of the liquid crystal surface through the partial molar enthalpy change of adsorption.

If a surface were to act as a totally inert support the molar enthalpy change of adsorption would be identical to the molar enthalpy change of condensation, which is just the reverse of the molar enthalpy change of vaporisation. Where the surface interacts with the probe the molar enthalpy change of adsorption refers to the process of condensation from the probe saturated vapour followed by interaction with an infinitely large surface area. Although the choice of reference state is not ideal for IGC work[30] it is adequate for the preliminary investigation undertaken in this thesis. Thus, the adsorption term, ΔHa, can be measured from the slope of the equivalent of the

van't Hoff plot and the extra energy required for the probe to interact with the surface, Hi, can be found from the difference between the former and the enthalpy of vaporisation, similar to the partial molar excess enthalpy of mixing. The size of the interaction enthalpy contribution thus gives a measure of the surface character relative to pure probe solvent. The trends in these parameters for different probes and their inferences are considered for HCB, OCB, and OPPB but first the adsorption behaviour of the Chromosorb P support will be considered.

5.5a Chromosorb P support

The adsorption enthalpies and interaction enthalpies of a variety of probes onto uncoated support are given in *table 5.9* and the enthalpy change for the adsorption of these probes are plotted against the normal boiling point in *figure 5.10*.
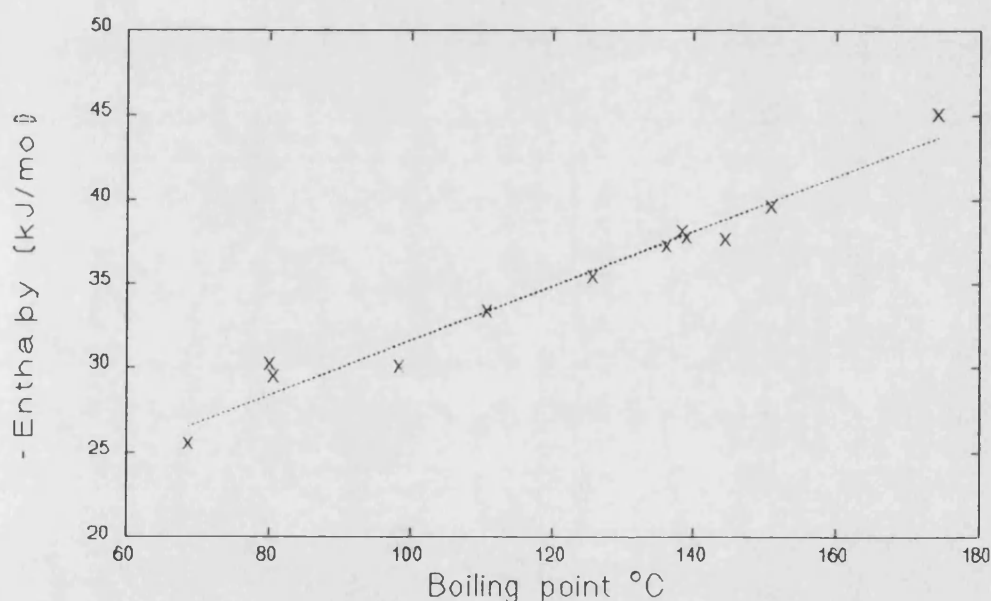

Figure 5.10: Enthalpy of adsorption, kJ mol^{-1}, for a variety of probes against normal boiling point.

Table 5.9 shows that a small amount of energy must be lost upon condensation to permit interaction with the surface. Cyclohexane and the aromatic probes required less energy than the alkane probes to form interactions at the Chromosorb surface, but the values only differ by small amounts. The boiling point was taken as a reasonable parameter to model interaction strength within liquid probe and hence model the

Table 5.9: Adsorption enthalpies and surface interaction enthalpies, kJ mol⁻¹, in for

Chromosorb P. Standard deviations in parentheses.

PROBE	$-\Delta H^a$	H^i
Hexane	25.5 (3.0)	3.4
Heptane	30.0 (1.1)	3.9
Octane	35.4 (0.7)	3.4
Nonane	39.5 (1.1)	4.2
Decane	45.0 (1.3)	3.4
Benzene	30.2 (1.2)	1.5
Toluene	33.3 (0.7)	2.3
Ethylbenzene	37.2 (0.7)	2.8
o-Xylene	37.6 (0.9)	3.4
m-Xylene	37.7 (0.7)	2.6
p-Xylene	38.1 (1.0)	1.8
Cyclohexane	29.4 (1.2)	1.4

readiness of a probe to condense on a surface. *Figure 5.10* shows that all probes studied can be fitted to a single linear correlation with the boiling point. These results show that Chromosorb P does not act as a totally inert support. However, the effect it has on different probes is small enough for the effect to be constant for different probes.

It should be noted that the Chromosorb P had been treated with a DMCS coating to reduce active sites on the surface. These silane molecules reduce the active site density at the surface and hence create a low energy surface. Thus interaction between surface and probe would be expected to be smaller than for the pure probe solvent and so extra energy is needed, relative to condensation onto pure solvent, for the probe to condense on the Chromosorb surface.

5.5b Liquid Crystal Surfaces

Table 5.10 lists the adsorption enthalpies and interaction enthalpies of adsorption and *figure 5.11a* shows the enthalpy changes of adsorption plotted against the normal boiling point. The slopes of the equivalent of the van't Hoff plots appear to be constant with temperature but results were obtained over a comparatively small temperature range. The average temperature of this range is quoted in *table 5.10* and *figure 5.11b* shows the logarithm of the specific retention volume at these average temperatures plotted against the normal boiling point. The first thing that is apparent

Table 5.10: Adsorption enthalpies and surface interaction enthalpies, kJ mol^{-1}, in for the crystalline surfaces of HCB, OCB, and OBIB. Standard deviations in parentheses.

PROBE	HCB $-\Delta H^a$	(44 °C) H^i	OCB $-\Delta H^a$	(40 °C) H^i	OBIB $-\Delta H^a$	(49 °C) H^i
Pentane	21.9 (2.7)	3.7	28.8 (0.2)	-2.9		
Hexane	25.4 (2.0)	5.2	32.8 (0.6)	-2.0		
Heptane	28.1 (1.7)	7.4	37.5 (0.2)	-1.7		
Octane	32.7 (1.7)	7.7	41.5 (2.2)	-0.8	33.5 (1.0)	6.6
Nonane	36.3 (1.8)	9.1	45.0 (1.2)	-0.6	37.8 (1.2)	7.2
Decane					41.7 (1.2)	8.2
2-Methylhexane	28.4 (1.0)	5.3	36.2 (2.5)	-2.3		
3-Methylhexane	28.2 (0.7)	5.8	35.4 (2.4)	-1.2		
2,3-Dimethylpentane	27.4 (1.1)	5.8	34.5 (2.2)	-1.1		
2,4-Dimethylpentane	27.3 (1.4)	4.5	34.0 (1.9)	-1.9		
2,2,3-Trimethylbutane	26.3 (0.5)	4.8	33.7 (1.7)	-2.4		
Cyclohexane	25.1 (0.6)	7.1	33.9 (0.5)	-1.6		
Benzene	19.7 (1.5)	13.3	33.6 (1.6)	-0.5	22.3 (2.4)	10.4
Toluene	23.7 (1.4)	13.3	37.7 (0.7)	-0.4	30.1 (1.7)	6.7
Ethylbenzene	27.5 (1.3)	13.8	42.2 (1.1)	-0.7	34.6 (3.8)	6.4
o-Xylene	26.6 (0.9)	15.9	40.1 (1.0)	2.6	38.9 (2.7)	3.3
m-Xylene	27.3 (0.5)	14.4	37.7 (0.2)	4.2	36.2 (2.0)	5.2
p-Xylene	26.5 (0.6)	14.9	41.4 (1.9)	0.2	36.7 (2.4)	4.4

is the lack of a common curve for all probes. The values are split into aliphatic and aromatic probes. This reflects the nature of the liquid crystal surface.

The values in *figure 5.11b* illustrate that the crystalline surfaces for each liquid crystal have different properties. Whilst the different temperature range studied for each liquid crystal could affect the adsorption enthalpies obtained, the linear retention volume plots and relatively small differences in the average temperature of each range indicate that any such effects are small. In section 2.2 it was pointed out that the support has a high surface area and that coatings did not tend to cover the highly porous regions of the surface effectively. However, the constancy of retention volumes above a 5 % loading[209] indicate that probe retention on the uncoated support was negligible. An alternative explanation is that the support and liquid crystal surface have the same adsorption characteristics. This cannot be so otherwise the retention values in *figure 5.11b* would fall on an identical linear plot for different probes and the adsorption enthalpies in *figure 5.11a* would agree with those for Chromosorb P in *figure 5.10*.

For HCB the adsorption enthalpies for the aromatic probes were considerably lower than the aliphatic probes whereas the values were considerably closer in OCB. The OCB values were also considerably lower than HCB values. The adsorption enthalpy values for OBIB exhibited alkane values similar to HCB but the aromatic probe values were higher than HCB. These values show that the different liquid crystals form surfaces with different energetic adsorption sites even when the molecules are similar in structure. The variation in interaction enthalpy between probes was larger than for the Chromosorb support and in all systems more energy was required to effect adsorption as the alkane chainlength increased. The interaction enthalpy for aromatic probes was generally higher than the alkanes and values increased as the normal boiling point of the probe increased for the cyanobipenyls but OBIB exhibited the opposite trend. All interaction enthalpies for a given probe decreased from HCB to OBIB to OCB.
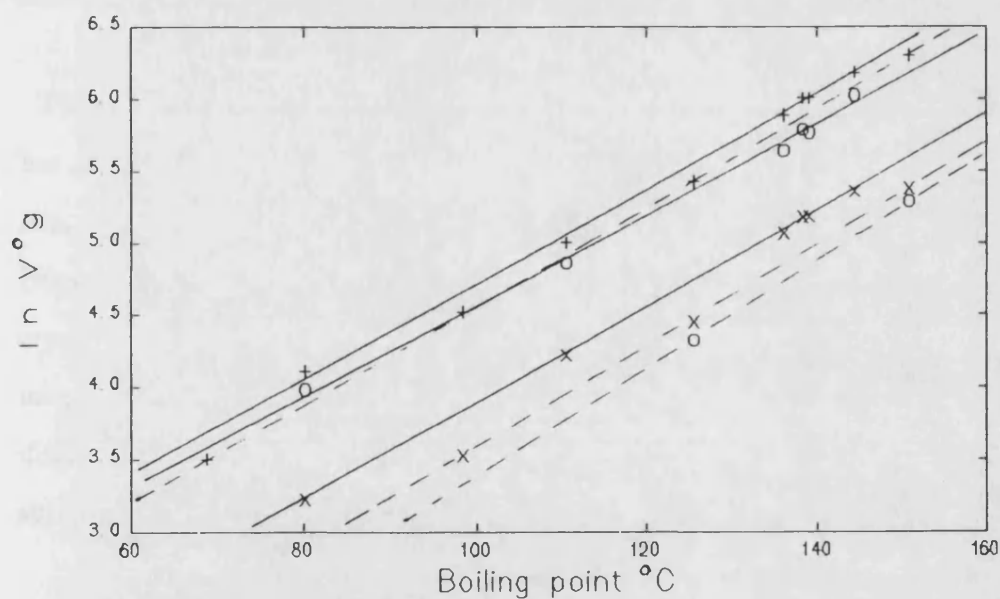
a)
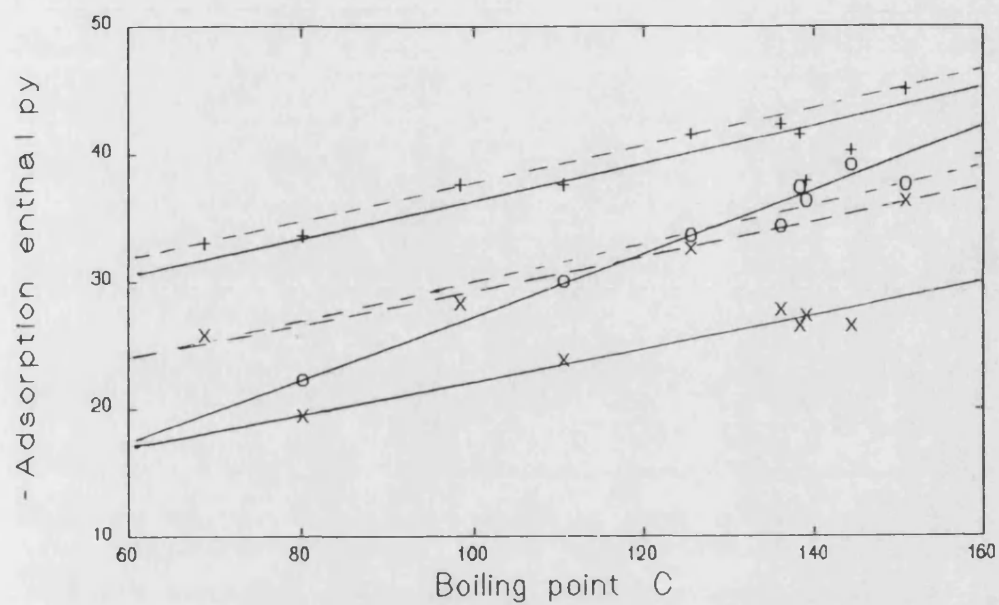
b)

Figure 5.11: a) adsorption enthalpies, kJ mol^{-1}, and b) logarithm of specific retention volumes at 40 °C against the normal boiling point of each probe; x HCB, + OCB, o OBIB, alkanes given by dashed line and aromatic probes by solid line.

The logarithm of specific retention volume was plotted against the normal boiling point because this will be governed by the surface size of a probe molecule and the work of cohesion between probe molecules. Figure 5.11b shows that the difference between aromatic and aliphatic probes was small in OCB indicative of small non-dispersion energies present at the surface. With HCB the retentions are generally considerably lower indicative of poorer interaction between the probe and the surface. The aromatic probe retentions in HCB are now considerably larger than the aliphatic ones. This is indicative of non-dispersive interactions. With OBIB there was a large difference between retentions for the two types of probes. The graphs indicate the proportion of liquid crystal surface that is aliphatic in nature increases from OBIB < HCB < OCB. This does not appear unreasonable upon consideration of the molecular structures of the liquid crystals. Also, the closeness of values in OCB could be indicative of the molecular pairing within the crystal structure, as discussed in section 5.2.

This has only been a preliminary look at the behaviour of the liquid crystal surface. It has shown that the crystalline surface behaves differently from that of the Chromosorb support and that similar liquid crystals may form different crystalline surfaces. However, the different extent of interaction for a given probe between different liquid crystal surfaces observed here cannot be discussed without a more detailed investigation of the nature of these surfaces. They may arise from such effects as different surface areas of the liquid crystals or different crystalline shapes but further study is needed on these materials before the full picture can be elucidated.

CHAPTER 6

MODELLING SOLUTION BEHAVIOUR

In chapter 5 the solution behaviour at infinite dilution was discussed in terms of the deviations from the ideal solution, manifest as the activity coefficient, and the trends used to infer the behaviour of the solvent and the stationary phase. In this chapter the results are used to calculate interaction parameters for different solution models. These values are compared with the trends observed in the previous chapter and the inferences made from them.

To date, few liquid crystalline systems have been fitted to solution models so comparison will necessarily be made with non-mesogenic low mass and polymeric systems reported in the literature. The data will initially be fitted to the classical Flory-Huggins solution model, outlined in section 1.8. Although reports in the literature[151] state that Flory-Huggins interaction parameters have been calculated for liquid crystal systems none have thus far been published, to the knowledge of this author. The interaction parameters obtained are then used to calculate the solubility parameter, as outlined in section 3.4b, and the inferences of this robust, but semi-quantitative approach are discussed. The chapter will then proceed to apply a more rigorous equation of state approach and discuss the results in terms of the improvement on the classical theory. The chapter will finish with a discussion of a recent advancement in the interaction parameter approach to account for anisotropy of the liquid crystal systems.

In order to obtain the above parameters it is seen from the equations given in chapter 3 that the density of each material must be known. As only a small quantity of the chiral liquid crystal, OBIB, was available the density could not be measured with the current apparatus available and discussion will be confined to the cyanobiphenyl materials. Also, data is only given for the normal liquid crystal phases and mesophases

as the current density measurement procedure was unable to take measurements upon cooling into the supercooled region.

6.1 FLORY-HUGGINS INTERACTION PARAMETERS

It was seen in sections 1.8 and 1.8a that once we have accounted for the athermal combinatorial effects of mixing molecules of differing sizes, the remaining deviations can be assigned as a reduced residual free energy of mixing term, due to interactions between the different components. Tending to infinite dilution of solvent, this so called "interaction parameter" can be calculated from the activity coefficient using the expression given in chapter 3;

$$\chi^{\infty} = \ln \gamma^{\infty} + \ln(V^o_2/V^o_1) - (1-(V^o_1/V^o_2)) \qquad [1.43]$$

$$\chi^{\infty} = \ln \Omega^{\infty} + \ln(\rho_1/\rho_2) - (1-(V^o_1/V^o_2)) \qquad [3.12]$$

Figures 6.1 and *6.2* illustrate the temperature dependence of the interaction parameters for a selected number of the probes in the two liquid crystals. *Tables 6.1* and *6.2* list the interaction parameter at a given temperature within the nematic and isotropic phases of HCB and *tables 6.3* to *6.5* list the values at given temperatures in the smectic A, nematic and isotropic phases of OCB, respectively.

From *figures 6.1* and *6.2*, the interaction parameter is seen to have a linear dependence on temperature in each of the phases of the low mass materials and can be fitted to the following relationship;

$$\chi = b - a/T \qquad [6.1]$$

Comparison with equations [1.24] and [1.25] in section 1.8a shows that this empirical fit to data is commensurate with the idea that the interaction parameter represents a free energy of interaction and is not a consequence of enthalpic terms alone. Although a linear fit with temperature can be obtained in all the phases and mesophases studied,
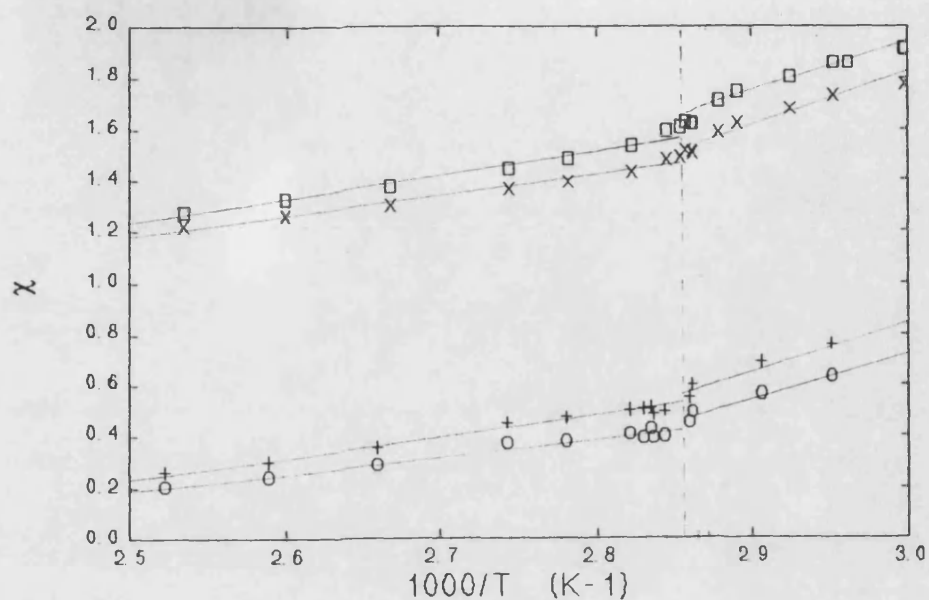
Figure 6.1: Interaction parameters against 1000/T for heptane, x, nonane,□,toluene, o, and
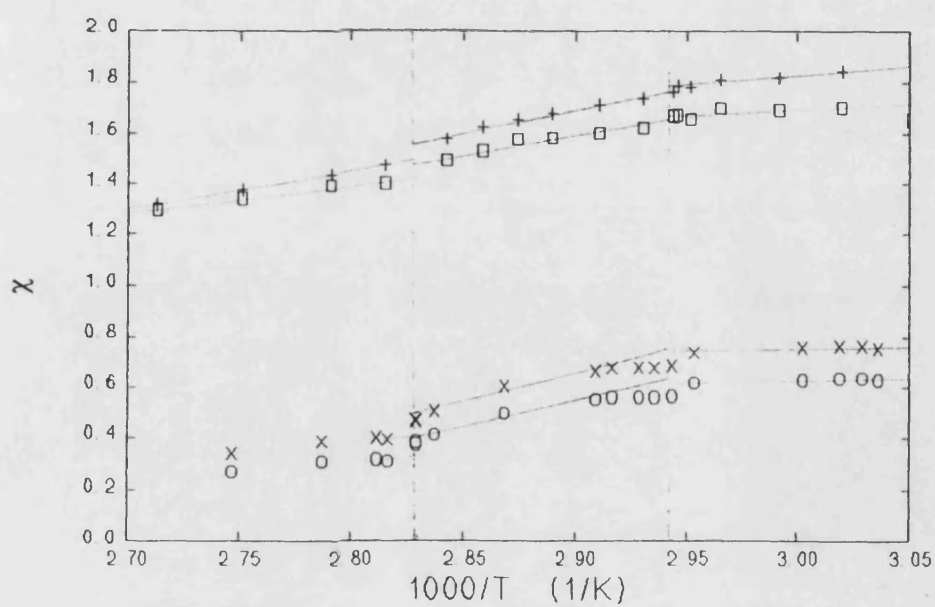
ethylbenzene, +, in HCB.

Figure 6.2: Interaction parameters against 1000/T for hexane,□,octane, +, toluene, o, and

ethylbenzene, x, in OCB.

Table 6.1: Flory-Huggins interaction parameters, hard-core interaction parameters and exchange interaction parameters at 68 °C in the nematic mesophase of HCB.

Probe	χ^{∞}	χ^{*}	X_{12} (J cm^{-3})
Pentane	1.58	1.65	68.9
Hexane	1.61	1.65	61.0
Heptane	1.68	1.69	55.1
Octane	1.73	1.74	51.3
Nonane	1.80	1.80	48.1
2-Methylhexane	1.75	1.79	58.2
3-Methylhexane	1.78	1.77	58.2
2,3-Dimethylpentane	1.70	1.72	57.3
2,4-Dimethylpentane	1.84	1.87	60.5
2,2,3-Trimethylbutane	1.73	1.75	58.2
Cyclohexane	1.40	1.40	62.0
Benzene	0.62	0.63	33.7
Toluene	0.59	0.59	26.44
Ethylbenzene	0.72	0.71	26.9
p-Xylene	0.56	0.55	21.1
m-Xylene	0.63	0.62	23.4
o-Xylene	0.58	0.57	21.8

the aromatic-OCB systems exhibit a region at the low temperature end of the nematic phase where the interaction parameter is constant with temperature. In general, the nematic phase exhibits the greatest dependence upon temperature and the smectic phase the least dependence. The interaction parameter increases as the temperature decreases, so the interaction between probe and liquid crystal is endothermic. This behaviour is observed for all stationary phase-probe systems reported in the literature, both mesogenic[151] (as implied from the activity coefficient values) and

Table 6.2: Flory-Huggins interaction parameters, hard-core interaction parameters and exchange interaction parameters at 86 °C in the isotropic phase of HCB.

Probe	χ^{∞}	χ^*	X_{12} (J cm^{-3})
Pentane	1.37	1.44	63.5
Hexane	1.35	1.43	43.2
Heptane	1.39	1.44	39.6
Octane	1.42	1.46	37.3
Nonane	1.48	1.51	35.6
2-Methylhexane	1.50	1.55	44.4
3-Methylhexane	1.46	1.52	42.7
2,3-Dimethylpentane	1.41	1.47	41.7
2,4-Dimethylpentane	1.53	1.60	43.8
2,2,3-Trimethylbutane	1.42	1.49	42.2
Cyclohexane	1.10	1.16	42.6
Benzene	0.37	0.48	16.5
Toluene	0.38	0.43	13.2
Ethylbenzene	0.47	0.50	15.9
p-Xylene	0.36	0.39	11.0
m-Xylene	0.43	0.46	14.3
o-Xylene	0.35	0..38	11.6

non-mesogenic[221], and so is likely to be a consequence of the dominant effect of the poor enthalpic contribution at low temperature compared to high temperature, although the increasing order within liquid crystals as the temperature cools may also raise the interaction parameter due to an increase in the unfavourable entropy of interaction and a further reduction in the enthalpic interaction arising from probe exclusion.

Table 6.3: Flory-Huggins interaction parameters, hard-core interaction parameters and exchange interaction parameters at 58 °C in the smectic mesophase of OCB.

Probe	χ^{∞}	χ^*	X_{12} (J cm^{-3})
Pentane	1.65	1.70	69.8
Hexane	1.70	1.73	62.5
Heptane	1.78	1.78	56.6
Octane	1.84	1.84	52.7
Nonane	1.85	1.84	47.5
2-Methylhexane	1.62	1.63	51.7
3-Methylhexane	1.60	1.61	52.1
2,3-Dimethylpentane	1.56	1.58	51.4
2,4-Dimethylpentane	1.63	1.65	52.5
2,2,3-Trimethylbutane	1.55	1.56	50.8
Cyclohexane	1.44	1.45	62.4
Benzene	0.67	0.68	35.5
Toluene	0.56	0.63	27.1
Ethylbenzene	0.76	0.74	26.9
p-Xylene	0.58	0.57	20.8
m-Xylene	0.70	0.68	24.4
o-Xylene	0.62	0.60	22.0

In the smectic phase of OCB the aromatic probes exhibited near constant interaction parameters as a function of temperature whereas the aliphatic probes exhibited a much greater temperature dependence. This suggests the probes interact differently with different parts of the liquid crystal molecule. The aromatic probes would be expected to favour interaction with the biphenyl ring whereas the aliphatic probes would be expected to favour interaction with the alkyl chain. The biphenyl rings have a larger probability of being found within a rigid smectic layer[210] than between layers and

Table 6.4: Flory-Huggins interaction parameters, hard-core interaction parameters and exchange interaction parameters at 75 °C in the nematic mesophase of OCB.

Probe	χ^{∞}	χ^*	X_{12} (J cm^{-3})
Pentane	1.56	1.63	66.5
Hexane	1.57	1.62	58.9
Heptane	1.61	1.63	52.7
Octane	1.65	1.66	48.7
Nonane	1.64	1.65	44.0
2-Methylhexane	1.42	1.45	46.9
3-Methylhexane	1.39	1.42	46.4
2,3-Dimethylpentane	1.37	1.40	46.0
2,4-Dimethylpentane	1.45	1.49	47.3
2,2,3-Trimethylbutane	1.35	1.39	45.4
Cyclohexane	1.25	1.28	55.8
Benzene	0.54	0.57	29.1
Toluene	0.50	0.51	22.6
Ethylbenzene	0.61	0.60	23.3
p-Xylene	0.46	0.46	17.5
m-Xylene	0.53	0.53	20.4
o-Xylene	0.48	0.47	18.5

would thus be more confined than the alkyl chains and would not be as susceptible to thermal disruption. Hence, the environment within a layer would be much less temperature sensitive as would be observed from interaction parameters with probes that interact to a greater extent with the biphenyl rings, that is the aromatic probes. The tendency for OCB molecules to align forming a quadrupole arrangement between adjacent molecules in the smectic phase[211] would enhance this. The small temperature dependence of the aromatic probe interaction parameters a few degrees above the

Table 6.5: Flory-Huggins interaction parameters, hard-core interaction parameters and exchange interaction parameters at 90 °C in the isotropic phase of OCB.

Probe	χ^∞	χ^*	X_{12} (J cm^{-3})
Pentane	1.33	1.43	54.9
Hexane	1.33	1.40	49.0
Heptane	1.36	1.40	43.9
Octane	1.37	1.40	40.4
Nonane	1.41	1.43	37.7
2-Methylhexane	1.18	1.23	38.7
3-Methylhexane	1.14	1.20	37.4
2,3-Dimethylpentane	1.10	1.15	36.4
2,4-Dimethylpentane	1.20	1.26	38.3
2,2,3-Trimethylbutane	1.12	1.16	39.9
Cyclohexane	1.00	1.05	44.2
Benzene	0.28	0.37	16.4
Toluene	0.27	0.31	11.8
Ethylbenzene	0.35	0.25	9.1
p-Xylene	0.24	0.26	9.0
m-Xylene	0.24	0.26	9.3
o-Xylene	0.23	0.24	9.1

smectic to nematic transition temperature could be a result of the prevalence of such pairing of adjacent molecules even when the smectic layer structure no longer exists. The lack of an obvious parallel in behaviour for the HCB system at the low temperature end of the nematic mesophase implies that the molecules do not exhibit such a tendency to pair up. Alternatively, the HCB molecules form a less ordered mesophase and are thus more susceptible to thermal motion. Either or both could be true but evidence in section 4.3d infers there was a lower degree of order in HCB than in OCB.

The trends in the interaction parameters are identical to those already discussed for the activity coefficients in chapter 5. This corroborates the general observations that the longer chain alkane probes are able to undergo stronger interactions with the liquid crystal than the shorter chain alkanes but suffer from a greater constraint in the conformations they can adopt. The more rigid heptane isomers are able to interact more strongly with the liquid crystal than the n-alkanes. The aromatic probes are generally better at interacting with the liquid crystal resulting in lower interaction parameters. This is indicative of the dominance of the rigid, aromatic portion of the liquid crystal molecule in the solution behaviour. However, care must be exercised when comparing absolute interaction parameter values, as outlined below.

To form a thermodynamically favourable solution at constant temperature and pressure the free energy of solution must be negative, see section 1.6. If the solution is thermodynamically unfavourable it has a positive free energy of solution and so there must exist a critical point where the free energy of solution is zero. This has a corresponding critical interaction parameter which for small molecule probes in long chain polymers tends to a value of 0.5, from equation [1.24]. However, in the liquid crystal systems here the difference between probe and stationary phase molecular size was much smaller than for polymer stationary phases. This results in different critical interaction parameters with different probes in the same stationary phase. For instance, nonane-HCB has a critical value of 1.6 whereas pentane-HCB has a critical value of 1.1. The observed values for the liquid crystal systems here show that the aliphatic probes form unfavourable solutions whereas the aromatic probes form favourable solutions with the liquid crystal. However, the aliphatic probes are not as unfavourable as they may first appear.

Another consideration when dealing with low mass materials in solution with small molecules is the applicability of the Flory-Huggins approach. The combinatorial entropy contribution conforms to the same expression, given in section 1.7b, for

polymer-polymer, polymer-solvent, and solvent-solvent systems[212] for a lattice theory. However, the free energy term arising from the interaction between segments on a lattice could result in additional terms in the theory. A consideration is the increased influence of the end-groups. During the derivation of the Flory-Huggins expression the effect of an additional interaction site at each end of a molecule is usually neglected due to the large number of interaction sites in total. Following the derivation outlined by Lovell and Young[213] without making such an approximation yields the following expression for the activity coefficient at infinite dilution;

$$\ln\gamma^{\infty} = \ln(V^o_2/V^o_1) + (1-(V^o_1/V^o_2)) + \chi + 2.\chi.V^o_1/(V^o_2(z-2)) \qquad [6.2]$$

where z is the number of first neighbour cells on the lattice and the other parameters are as defined in chapter 3. The true Flory-Huggins interaction parameter, χ, is related to the measured value, χ^m, by;

$$\chi = \chi^m.[V^o_2.(z-2)/(2.V^o_1 + V^o_2(z-2))] \qquad [6.3]$$

For polymer-solvent systems the molar volume of the solvent is much smaller than that of the polymer and the measured interaction parameter tends to the true value but in the liquid crystal systems in this thesis the factor in the brackets becomes significant. The measured interaction parameter can alternatively be considered as the Flory-Huggins interaction parameter as the number of first neighbour cells approaches infinity[45]. However, in a real liquid the number of nearest neighbours will be between 6 and 10[214].

The effect of a finite number of first neighbour cells is most marked for HCB because it was the smallest liquid crystal molecule studied. *Figure 6.3* shows the effect of different z values on the interaction parameter for benzene and nonane in HCB whilst *table 6.6* illustrates the trend in probe-HCB systems with different z values at 59 °C. For a given z value the decrease in the interaction parameter for a given system from the measured value is in the same proportion at all temperatures; for z equal to 6 the true interaction parameter would be 66% of the measured value for nonane and 83%
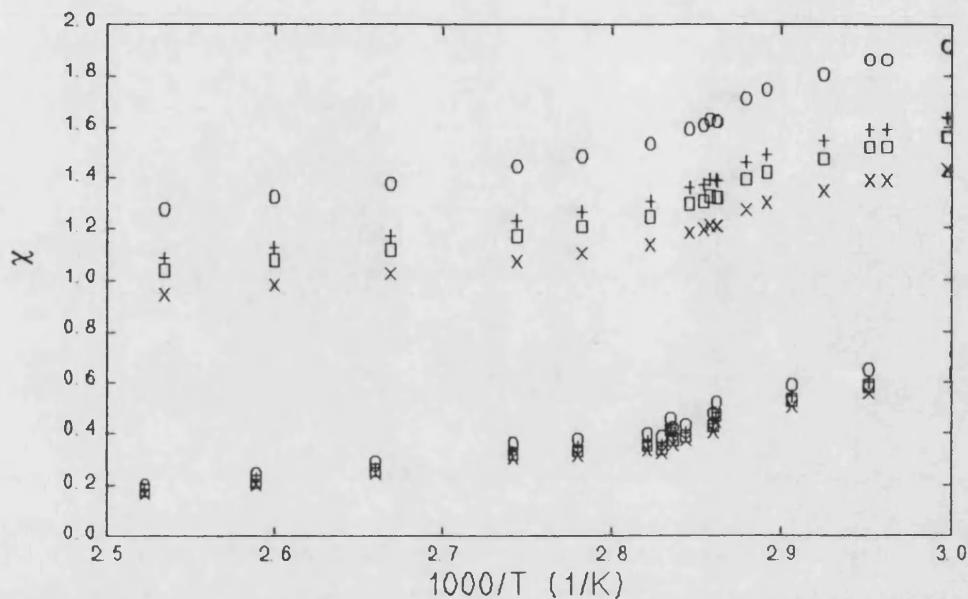
Figure 6.3: Interaction parameters for nonane (top) and benzene (bottom) in HCB calculated assuming z = 6, x, z=8,□ z=10, +, and z=∞, o.

for benzene. Thus, the trends in probe interaction parameters will remain constant at all temperatures. The table illustrates that the change in the number of first neighbour cells does not alter the trends observed between those probes studied here. As a liquid crystal can form semi-ordered fluid phases the number of first neighbour cells is likely to be closer to 10 than 6. Also, the effect of the dissimilar segments comprising the liquid crystal may have a substantial effect on the interaction parameter and does not benefit from having a large number of repeat units to average out such dissimilarities. As the z values are not known at present for the liquid crystal fluid phases studied, the application of any correction would be arbitrary and, whilst noting these possible complications, the assumption of an infinite value for z is adopted in this thesis.

OCB contains two more methylene units in the alkyl chain than HCB. Therefore, it would be reasonable to assume that the change in the interaction parameter for a given probe would arise from the addition of these units. If the interaction parameter can be

determined by summation of contributions of the different units comprising the liquid

Table 6.6: Interaction parameters in HCB at 59 °C for different z values.

Probe	z=6	z=8	z=10	z=∞
Pentane	1.36	1.45	1.50	1.67
Hexane	1.37	1.47	1.53	1.72
Heptane	1.40	1.51	1.57	1.79
Octane	1.41	1.53	1.60	1.85
Nonane	1.44	1.57	1.65	1.93
2-Methylhexane	1.46	1.58	1.64	1.88
3-Methylhexane	1.44	1.55	1.62	1.85
2,3-Dimethylpentane	1.42	1.53	1.59	1.82
2,4-Dimethylpentane	1.51	1.63	1.70	1.94
2,2,3-Trimethylbutane	1.43	1.55	1.61	1.84
Cyclohexane	1.18	1.27	1.32	1.49
Benzene	0.59	0.62	0.64	0.69
Toluene	0.56	0.59	0.61	0.67
Ethylbenzene	0.65	0.70	0.73	0.81
p-Xylene	0.51	0.54	0.56	0.63
m-Xylene	0.54	0.60	0.59	0.66
o-Xylene	0.56	0.57	0.62	0.70

crystal molecule the effect of adding two methylene units should be independent of the rest of the molecule. This is the basis of the UNIFAC technique[215] used with some success for predicting activity coefficients. On the other hand, the interaction parameter may be an average of contributions over the whole liquid crystal molecule where the contribution of individual units vary according to their position within the structure of the molecule. In an attempt to further this line of reasoning the effect of adding two methylene groups to long chain alkanes is compared to the liquid crystals.

The interaction parameters for octadecane and hexadecane at 30 °C and 40 °C were calculated using the activity coefficient data of Laub *et al.*[216] and values are listed in *table 6.7*. In these systems the interaction is favourable for all four probes measured. The interaction parameter becomes more favourable as the alkane chain lengthens. The

Table 6.7: Interaction parameters in Hexadecane and Octadecane at 30 °C and 40 °C.

Probe	n-C16		n-C18		Difference	
	30 °C	40 °C	30 °C	40 °C	30 °C	40 °C
Hexane	-1.46	-1.47	-1.64	-1.64	0.18	0.17
Heptane	-1.27	-1.29	-1.46	-1.46	0.19	0.17
Cyclohexane	-1.85	-1.89	-2.05	-2.06	0.20	0.17
Benzene	-1.84	-1.89	-2.04	-2.07	0.20	0.18

table shows there are only small temperature and probe effects on the difference in interaction parameter between the two long chain alkanes and the contribution of the two methylene units is approximately constant. Values were also calculated for a series of C20 to C30 alkanes with C5 to C8 alkane probes using the activity coefficients of Parcher and Harbison[217] at 100 °C. No clear trend emerged as the probe alkane chain length increased by two methylene units for two given stationary phases that differed by two methylene units and there was no clear trend in going to longer chainlength stationary phases. Differences for the addition of two methylene units were between 0.11 and 0.20 with an average of 0.14. This wide variation may be a consequence of the activity coefficients being reported as averages over the temperature range 80 °C to 120 °C. Thus, it appears that extending an alkyl chain by two methylene units results in a reduction of between 0.14 and 0.21 in the interaction parameter for long chain alkane stationary phases.

Table 6.8 lists the interaction parameters for probes with HCB and OCB at

temperatures where both exhibit isotropic and nematic phases. Note that in section 3.7

the uncertainty in the interaction parameter was given as ± 0.04. In the isotropic phase

the values for the n-alkane systems are comparable in both liquid crystal systems with

only nonane exhibiting any marked decrease for the OCB system. The cyclohexane

system shows a small decrease. The decrease in interaction parameter is more marked

for the aromatic probes but still significantly lower than the results on the long chain

alkane systems would predict. In the nematic phase values for OCB and HCB are very

similar and the alkane probes actually show a small, but significant, increase in the

values for OCB. These trends agree with those that would be predicted from activity

coefficient data in other liquid crystal systems[152], discussed in chapter 5. Clearly the

addition of two methylene groups to the alkyl chain of the liquid crystal is

comparatively insignificant compared with the alkane systems discussed above. The

results suggest that it is the rigid biphenyl portion of the molecules that is governing

the interactions in

Table 6.8: Interaction parameters at three temperatures in HCB and OCB.

Probe	97 °C		84 °C		72 °C	
	HCB	OCB	HCB	OCB	HCB	OCB
Pentane	1.29	1.30	1.40	1.39	1.52	1.55
Hexane	1.27	1.28	1.37	1.37	1.53	1.59
Heptane	1.29	1.30	1.40	1.41	1.62	1.65
Octane	1.34	1.30	1.42	1.43	1.66	1.69
Nonane	1.40	1.35	1.48	1.46	1.75	1.70
Cyclohexane	1.00	0.94	1.10	1.04	1.33	1.29
Benzene	0.30	0.23	0.40	0.29	0.58	0.56
Toluene	0.32	0.23	0.42	0.29	0.54	0.52
Ethylbenzene	0.38	0.31	0.50	0.38	0.68	0.64

solution. This is particularly true in the mesophase where the additional order, and thus enhanced interaction between adjacent liquid crystal molecules, is detrimental to the biphenyl-alkane interactions. That there is not a large increase in values for nematic OCB is indicative that there is interaction with the alkyl chain despite it not being dominant in the interaction parameter. The greater reduction in values for aromatic probes in the isotropic phase arises because of the increased importance of the alkyl chain once the order of the liquid crystal has been removed. The probe has less probability of interacting in an environment where the majority of the nearest neighbour segments are aromatic.

6.1a Polydimethylsiloxane (PDMS)

Although there are several reports on PDMS systems in the literature, studied both by IGC and static methods, there are few that give interaction parameters at temperatures comparable with the present work. *Table 6.9* lists interaction parameters and

Table 6.9: Comparison of interaction parameters and characteristic interaction parameters with literature values at 60 °C.

Probe	χ ref. a	ref. b	χ^* ref. b	ref. c	ref. d	This work χ	χ^*
Pentane	0.45	0.43	0.56	0.48		0.33	0.47
Hexane	0.43	0.45	0.54	0.47	0.48	0.37	0.48
Heptane	0.45	0.48	0.56	0.49	0.50	0.42	0.49
Octane	0.47	0.54	0.54	0.51		0.47	0.53
Benzene	0.62	0.75	0.81	0.75	0.78	0.55	0.63
Toluene		0.76	0.79	0.72	0.76	0.57	0.62
Ethylbenzene		0.79	0.81	0.73	0.78	0.57	0.61
Cyclohexane	0.44			0.47		0.43	0.50

a) Patterson *et al.*[218] b) Summers *et al.*[101] c) Lichtenthaler *et al.*[103] d) Galin[219]

Table 6.10: Comparison of specific retention volumes for PDMS, gcm^{-3}, at 60 °C.

Probe	Literature values[220]	This work
Pentane	24.8-26.6	26.0
Hexane	59.9-61.3	60.3
Heptane	137.0-144.3	138.1
Octane	310.6-332.1	313.1
Benzene	91.6-105.5	106.8
Toluene	212.8	245.6
Ethylbenzene	446.1	531.0
Cyclohexane	101.2-106.1	105.4

characteristic interaction parameters for PDMS at 60 °C and *table 6.10* lists specific

retention volumes measured for probes with PDMS. The first thing to note is the large

spread of results reported in the literature. Values measured in this work agreed more

closely with the higher specific retention volumes reported in more recent work[220].

However, the majority of interaction parameters have only been quoted in the older

reports. The estimated uncertainty in the interaction parameter for this work, given in

section 3.7, was ± 0.04. The aliphatic probes agree with some reports within this limit

but the aromatic probes exhibited values outside of this limit. Although, the use of

different second virial coefficients would contribute to a discrepancy in values, it was

shown in chapter 3 that such an effect would not be large enough to account for the

discrepancy. However, as the collation of data by Tseng and Lloyd[221] illustrates, there

is are large fluctuations in the reported values.

Interaction parameters measured in this work for PDMS-probe systems are shown as

a function of temperature in *figures 6.4*. As observed with the liquid crystal systems,

the plots conform to a linear dependence on temperature. The main difference with

PDMS is the lower values for aliphatic-PDMS systems compared to the aromatic

system. This favoured solution formation with aliphatic probes has already been noted

for the activity coefficient data and the trends here are identical. The interaction

parameters exhibited little temperature dependence with the probes studied which was

in agreement with the behaviour reported in the literature.
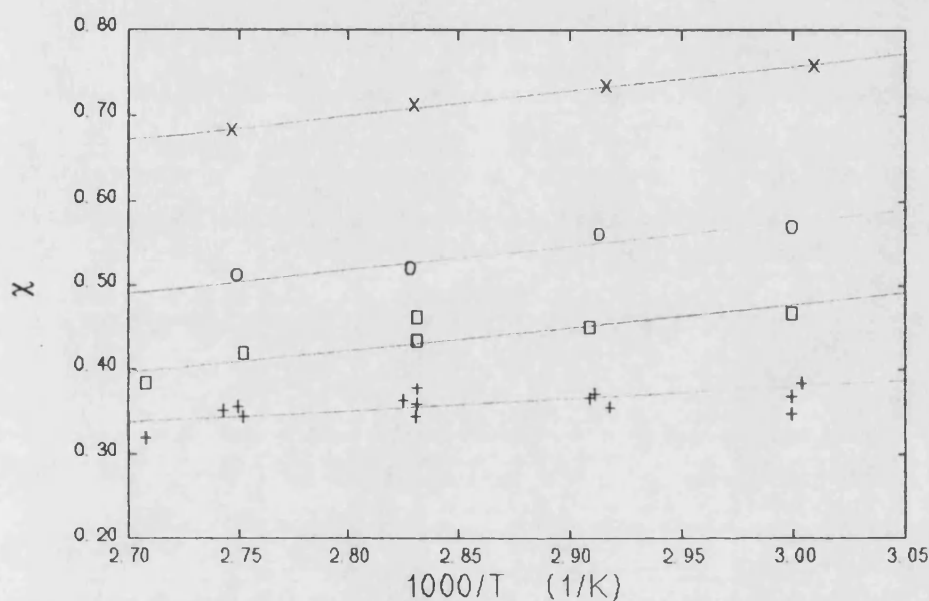
Figure 6.4: Interaction parameters in PDMS as a function of temperature for hexane, +,

octane, □, toluene, o, and o-xylene, x.

6.1b Liquid Crystal Polymer (LCP)

Figure 6.5 shows the variation of the interaction parameter with temperature for

various LCP-probe systems. As with the other systems discussed above, there is a

linear dependence with temperature. The major difference to the systems discussed

previously is the greater temperature dependence in the isotropic phase compared to

the mesophase. This is a direct consequence of the higher thermal coefficient of

expansion of isotropic LCP. This can be seen from density measurements as a function

of temperature, given in chapter 4. Cyclohexane behaves differently to the other

probes exhibiting less temperature dependence in the isotropic phase than the nematic

phase. Why this should occur is unclear at present but could be due to a preferred interaction with the polymer backbone acting as a poor mesogen probe and hence exhibiting values closer to the PDMS-probe behaviour than other probes studied.
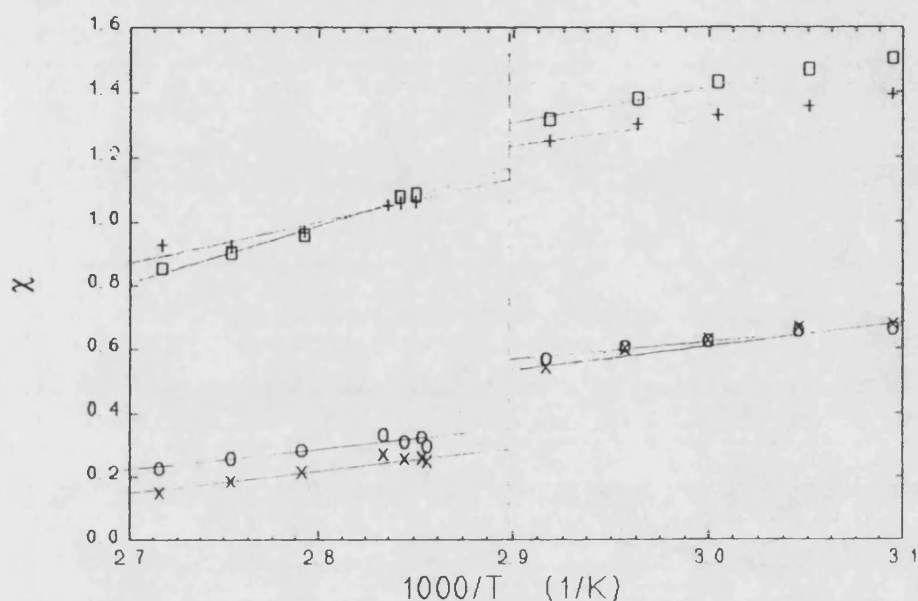
Figure 6.5: Interaction parameters in LCP as a function of temperature for hexane, +, octane, □, toluene, o, and o-xylene, x.

Table 6.11 and *6.12* lists the interaction parameters for LCP, PDMS and OCB at a temperature in the isotropic phase and smectic phase of the liquid crystals, respectively. The values for LCP are higher for aliphatic probes than for aromatic probes. This implies the LCP-probe solution is governed by the mesogen both in the mesophase and the isotropic phase. However, the PDMS backbone exerts greater influence in the isotropic phase. This is evident from the greater similarity of the alkane probes in the isotropic phase. LCP is an oligomer and so there will be differences in the critical interaction parameters between different probe systems, as discussed above for the low molar mass systems. However, the effect will be considerably smaller.

Table 6.11: Interaction parameters, hard-core interaction parameters, and exchange interaction parameters for LCP in the smectic mesophase at 70 °C and interaction parameters for PDMS and OCB.

Probe	LCP χ	χ^*	X_{12} (Jcm⁻³)	PDMS χ	OCB χ
Pentane	1.22	1.40	40.3	0.34	1.53
Hexane	1.25	1.39	37.3	0.37	1.60
Heptane	1.29	1.40	34.1	0.40	1.65
Octane	1.31	1.41	31.9	0.45	1.70
Nonane	1.29	1.37	28.5	0.51	1.71
2-Methylhexane	1.27	1.38	35.1	0.37	1.48
3-Methylhexane	1.27	1.39	34.6	0.37	1.46
2,3-Dimethylpentane	1.21	1.33	33.3	0.33	1.42
2,4-Dimethylpentane	1.30	1.44	34.7	0.34	1.49
2,2,3-Trimethylbutane	1.19	1.32	32.9	0.29	1.41
Cylclohexane	1.10	1.21	39.9	0.40	1.30
Benzene	0.57	0.68	22.2	0.54	0.59
Toluene	0.54	0.62	18.7	0.56	0.55
Ethylbenzene	0.62	0.69	20.2	0.59	0.66
p-Xylene	0.43	0.47	13.7	0.66	0.50
m-Xylene	0.57	0.64	18.3	0.70	0.57
o-Xylene	0.52	0.57	16.7	0.73	0.53

The above discussion has shown that the interaction parameter model of a solution corroborates the inferences made from the thermodynamic parameters in chapter 5. However, the model also suggests that the observed behaviour is governed mainly by the rigid mesogen and only moderated by the presence of the flexible end groups of these cyanobiphenyl. Hence, OCB and HCB exhibited similar interaction parameters

Table 6.12: Interaction parameters, hard-core interaction parameters, and exchange interaction parameters for LCP in the isotropic phase at 85 °C and interaction parameters for PDMS and OCB.

Probe	LCP χ	χ^*	X12 (Jcm^{-3})	PDMS χ	OCB χ
Pentane	0.97	1.09	45.4	0.32	1.40
Hexane	0.96	1.04	39.4	0.35	1.39
Heptane	0.98	1.02	34.6	0.38	1.41
Octane	0.95	0.98	30.3	0.44	1.43
Nonane	0.97	0.98	27.5	0.50	1.45
2-Methylhexane	0.98	1.03	35.1	0.36	1.22
3-Methylhexane	0.95	1.00	34.3	0.35	1.19
2,3-Dimethylpentane	0.92	0.98	33.8	0.31	1.16
2,4-Dimethylpentane	1.02	1.10	36.5	0.32	1.26
2,2,3-Trimethylbutane	0.92	0.98	33.6	0.27	1.16
Cylclohexane	0.82	0.86	39.4	0.36	1.03
Benzene	0.27	0.40	22.6	0.44	0.31
Toluene	0.28	0.29	13.4	0.52	0.31
Ethylbenzene	0.31	0.30	12.1	0.55	0.39
p-Xylene	0.22	0.21	8.6	0.62	0.27
m-Xylene	0.24	0.23	9.3	0.66	0.30
o-Xylene	0.21	0.19	7.8	0.70	0.27

for the same probe in the same type of mesophase at identical temperature. The polymeric liquid crystal also exhibited behaviour suggesting the mesogen governed the interaction between probe and liquid crystal but the polymer backbone appeared to exert a greater perturbation on the behaviour than the flexible alkyl chain exerted on

the low molar mass cyanobiphenyls. This was especially so in the isotropic phase of the liquid crystal polymer.

The "hard-core" interaction parameters and exchange interaction parameters will be discussed in section 6.4. First, discussion of the solution behaviour will continue with the more classical solution model description afforded by the regular solution theory.

6.2 REGULAR SOLUTION THEORY

In chapter 1 it was shown that the best solvent for a material could be evaluated by using the semi-empirical regular solution approach introduced by Hildebrand. The theory requires the calculation of the solubility parameter of a material and matching the solubility parameter of a solvent to it. Whilst this theory is not as refined as the Flory-Huggins approach, taking no account of entropic effects, it is none the less a useful and widely used method of determining good solvents.

Probe solubility parameters were calculated as outlined in section 3.4b and these were used along with probe interaction parameters to obtain the liquid crystal solubility parameters using the method developed by Guillet[125] from;

$$\delta_1^2/R\,T - \chi/V^o{}_1 = (2\,\delta_2/R\,T)\delta_1 - (\delta_2^2/R\,T + \chi^S/V^o{}_1) \qquad [1.52]$$

where the parameters have been previously defined in sections 1.12b and 3.4b. A plot of the function in bold on the lefthandside against the probe solubility parameter allows the solubility parameter for the high molar mass material to be calculated from the slope.

Most literature values for solubility parameters have been reported at 25 °C. These were obtained either from extrapolation of interaction parameter data to this temperature[222] or, more recently, by direct measurement[223]. Low temperature chromatography measurements often suffer from poor temperature control and

considerable effort is necessary to ensure an apparatus has adequate stability whilst extrapolation of interaction parameters can suffer from significant error due to the relatively large uncertainty in these values. The temperature dependence of the solubility parameter is considerably smaller than that of the corresponding interaction parameter, as will be seen below. Hence, extrapolation of solubility parameter data obtained at elevated temperatures to ambient temperature should introduce less error in the extrapolated value than calculating solubility parameters from extrapolated interaction parameter data. This variation of the Guillet method was used in the following discussion.

To obtain the temperature dependence of the solubility parameters in the systems studied in this thesis values were calculated at four different temperatures in each phase and mesophase. A typical plot is given in *figure 6.6* for PDMS. Although the figure shows a good linear correlation with solvent solubility parameter different slopes and intercepts are obtained for the aliphatic and aromatic probes. This is to be
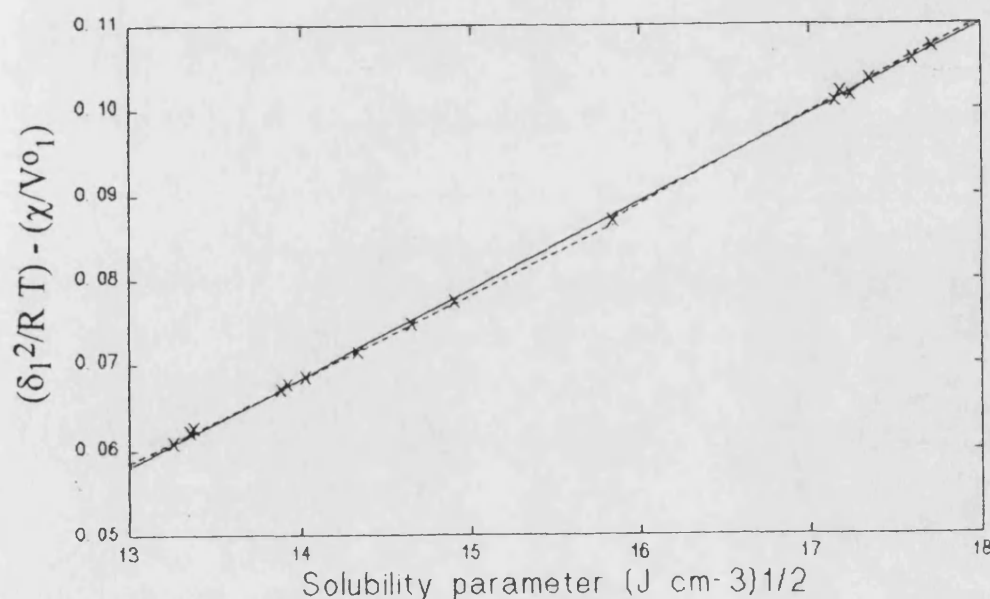
Figure 6.6: Estimation of PDMS solubility parameter at 60 °C, solid line gives regression for all data and dotted line gives regressions for aliphatic and aromatic probes.

expected from the extension of the basic theory introduced by Hansen ,and discussed in section 1.10, where he accounted for the non-dispersion forces between the probe and stationary phase. Similar behaviour was observed in the liquid crystal systems and *figure 6.7* gives three plots for OCB at a temperature in each of the different phases. All the liquid crystals studied exhibit similar behaviour to OCB and *table 6.13* lists the solubility parameters at each temperature. Values calculated from all the probes are plotted as a function of temperature in *figure 6.8*. As can be seen for other systems[54,126] the solubility parameter changes little with temperature compared to the interaction parameter and an empirical relationship can be fitted to the data;

$$\delta = K - D/T \qquad\qquad [6.4]$$

where T is temperature and K and D are constants. The extrapolated value of PDMS at 25 °C of 15.2 ±0.2 $(J.cm^{-3})^{1/2}$ is in good agreement with the literature[224] values which range between 14.9 and 15.5 $(J.cm^{-3})^{1/2}$. With the liquid crystal systems the solubility parameters could equally be fitted to a single linear relationship through all phases and mesophases without incurring a significanterror in the solubility parameter in the respective phases. The regression equations for these linear relationships in the

a)
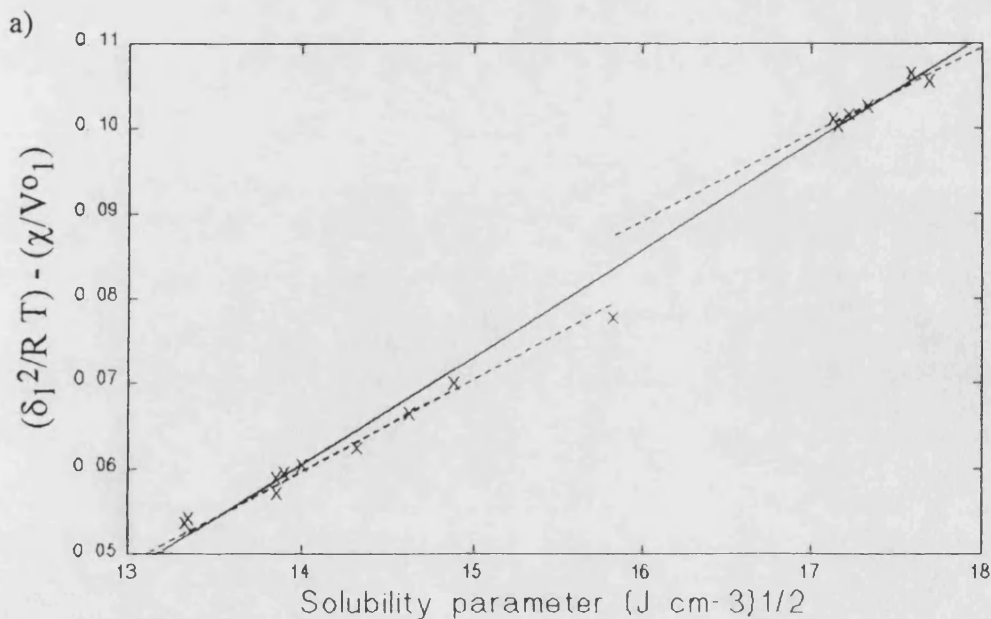
Figure 6.7: Estimation of OCB solubility parameter at a) 61 °C in the smectic mesophase

b)
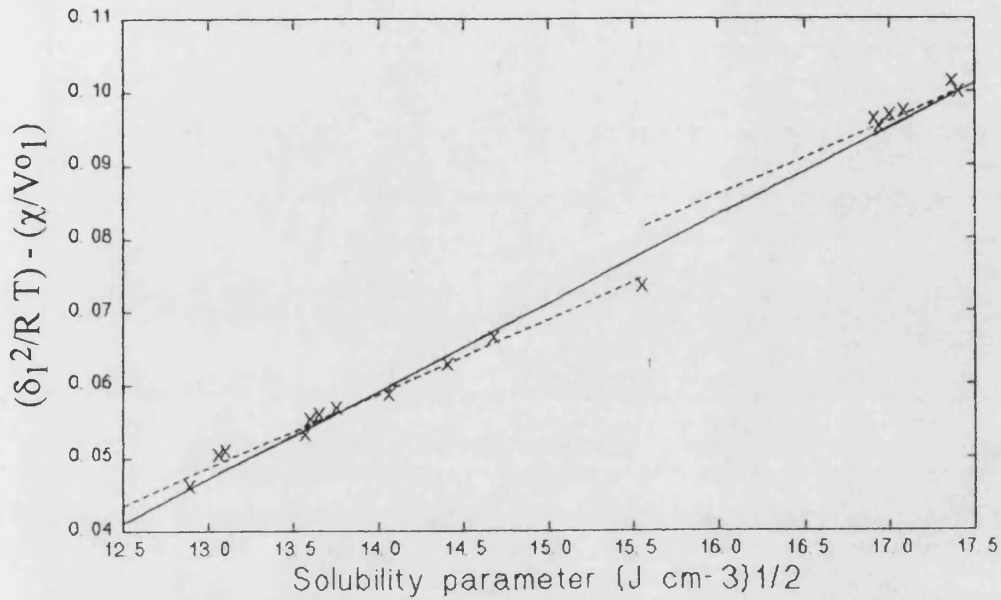
c)
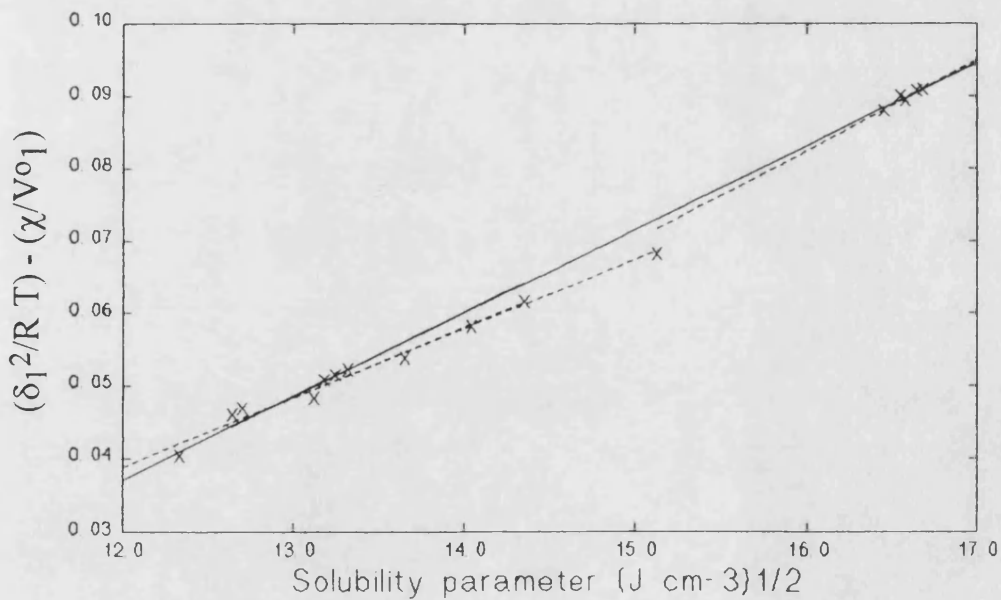
Figure 6.7: Estimation of OCB solubility parameter at b) 70 °C in the nematic mesophase, and c) 85 °C in the isotropic phase; solid line gives regression for all data and dotted line gives regressions for aliphatic and aromatic probes.

Table 6.13: Solubility parameters, δ, and the dispersion, δd, and polar, δp, contributions at different temperatures, $^{\circ}C$. Values in $(Jcm^{-3})^{1/2}$ and standard deviations in parentheses. δd was obtained from alkane values and the result used to calculate δp from aromatic values.

Phase	$^{\circ}C$	δ	δd	δp	Phase	$^{\circ}C$	δ	δd	δp
HCB N	60.4	17.7 (0.3)	15.5	-	OCB S	58.0	17.6 (0.4)	14.9	-
	64.5	17.7 (0.3)	15.9	-		61.1	17.5 (0.4)	15.0	-
	68.7	17.5 (0.3)	15.4	-		64.1	17.4 (0.4)	14.7	-
	72.7	17.4 (0.3)	15.1	-		65.6	17.3 (0.4)	14.9	-
HCB I	81.1	17.0 (0.3)	14.8	10.9	OCB N	68.1	17.3 (0.4)	14.8	-
	91.3	17.0 (0.3)	14.7	11.0		70.4	17.1 (0.4)	14.6	-
	101.5	16.7 (0.3)	14.2	11.2		72.9	17.1 (0.4)	14.7	-
	111.5	16.6 (0.3)	13.6	10.9		74.8	17.2 (0.4)	14.6	-
LCP S	50.0	17.1 (0.3)	15.5	-	OCB I	82.0	17.3 (0.3)	14.4	12.2
	54.6	17.2 (0.4)	15.4	-		85.1	17.1 (0.5)	14.3	11.7
	59.7	16.7 (0.3)	15.2	-		90.3	16.9 (0.5)	14.1	12.2
	64.3	16.8 (0.3)	15.6	-		95.4	16.6 (0.3)	14.1	13.4
LCP I	79.4 .	79.4 (0.3)	14.7	2.9	PDMS	60.3	14.4 (0.1)	13.6	6.6
	85.0	16.4 (0.3)	14.6	11.6		69.5	14.1 (0.1)	13.4	5.6
	90.0	16.2 (0.3)	14.3	11.6		80.1	13.9 (0.1)	13.1	4.0
	94.9	16.0 (0.3)	14.2	11.8		90.5	13.6 (0.1)	13.5	4.6
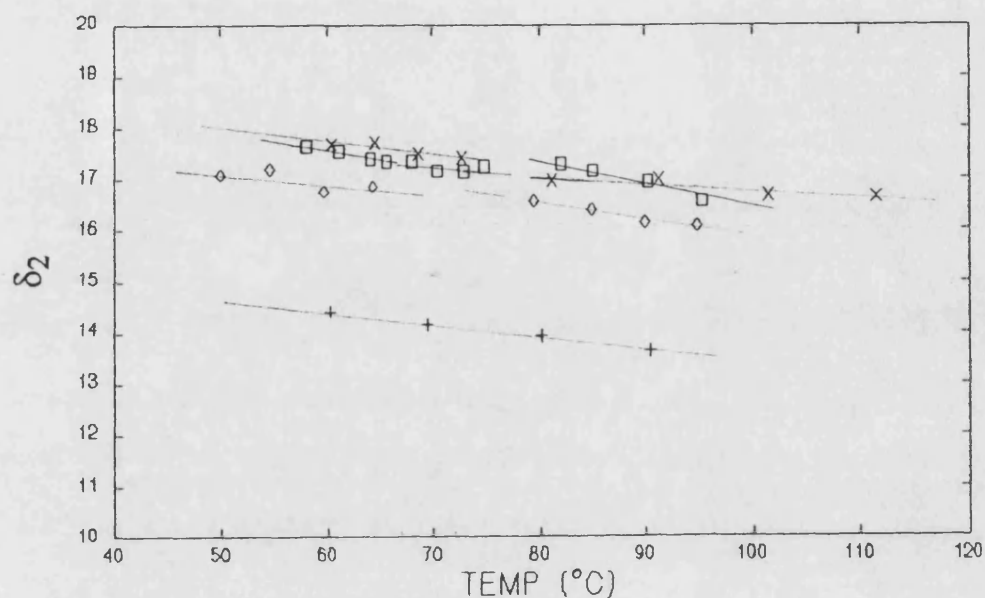
Figure 6.8: Solubility parameters as a function of temperature for PDMS +, HCB x, OCB □, and LCP ◊.

different stationary phases are listed below;

$$HCB: \quad \delta = 19.02 - 0.0225 \ T$$

$$OCB: \quad \delta = 18.76 - 0.0210 \ T$$

$$LCP: \quad \delta = 18.27 - 0.0228 \ T$$

This illustrates that the enthalpic interactions between the liquid crystal molecules of a given material are very similar regardless of the mesophase formed. This is hardly surprising considering the molecular structure of the material does not change between phases.

The most striking feature of the liquid crystal plots, illustrated by *figure 6.7* for OCB, was the change in behaviour of the aromatic probes in going from the mesophase to the isotropic phase. In the isotropic phase the behaviour was similar to PDMS where the aromatic probes form a steeper slope than the aliphatic probes. This is the behaviour that would be expected. The aliphatic probes interact through dispersion

forces alone whilst the aromatic probes can additionally interact by more specific interactions, arising from the π orbitals within the molecules, enabling them to probe the polar component of the stationary phase resulting in the solubility parameter for that phase being higher. The uncertainty in the solubility parameter from the aromatic probes alone is considerably higher than the aliphatic probes due to the comparatively narrow range of the probe solubility parameters. However, the change in slope to one that is less steep than the aliphatic probe slope occurs consistently for all systems studied on going to the mesophase. This is difficult to rationalise but has been observed in a number of polymer systems[126]. The values imply that the cohesive energy density contribution is negative but this seems very unlikely. Stronger forces between molecules should result in the need for more energy to pull them apart. One explanation could be that the aromatic solvents were not effectively probing the liquid crystal mesophase whereas the aliphatic probes were. This also seems unlikely and contradicts the conclusions of previous sections. However, if the aromatic probe had a preferential interaction over aliphatic probes with the rigid mesogen the solubility parameters would be more susceptible to competitive interaction from adjacent mesogens. These adjacent mesogens are already favourably aligned in the mesophase and are in close proximity to the liquid crystal mesogen being probed. Thus, the behaviour in these systems may be rationalised as a consequence of competitive interaction where as the solubility parameter of the probe increased the effect would become more severe. However, further work on systems capable of ordering is required to investigate the possibility of a correlation between the extent of the effect noted here and the degree of ordering within the stationary phase.

In the isotropic liquid phases of all the systems studied the polar contribution to the solubility parameter is generally constant, within the bounds of uncertainty. The dispersion contribution generally decreases as temperature is raised. This would be expected due to the smaller effect thermal disruption of the molecules would have on more polar interactions. Also, PDMS exhibits considerably smaller polar contributions

than the liquid crystal systems at all temperatures. The overall solubility parameter for PDMS varies between 13.5-14.5 $(Jcm^{-3})^{1/2}$ as temperature decreases from 90 °C to 60 °C whereas the liquid crystal systems all exhibit values between 16.5-17.5 $(Jcm^{-3})^{1/2}$. The results corroborate previous observations that PDMS favours aliphatic solvents whilst these liquid crystals favour aromatic solvents. Heptane gives the closest match with PDMS, over the temperature range studied, and benzene and *ortho*-xylene present the close matches in solubility parameter for the liquid crystals.

Figure 6.8 shows that there is little difference between the low molar mass liquid crystals and the LCP, the last exhibiting slightly lower values. This model is a crude description of solution behaviour and the validity of any conclusions drawn from the detail of the results should be viewed with caution. However, the results presented here suggest that the enthalpic interactions in these cyanobiphenyls are very similar for both the low molar mass and polymeric materials. This suggests that the different liquid crystal mesophases do not form primarily as a consequence of the enthalpic interactions between liquid crystal molecules.

Although the solubility parameter model allows the determination of a favourable, rather than unfavourable solvent for a given material it does not necessarily predict the solvent that will yield a solution closest to an ideal solution. For instance, the activity coefficients given in chapter 5 for PDMS show that all alkanes exhibit very similar solution behaviour. This is not reflected in the solubility parameters where there is a growing mismatch in values for the polymer and solvent as the solvent chainlength varies from heptane. On inspection of the corresponding interaction parameters, given in *table 6.11*, the alkanes have closer values and follow the observed trend in the activity coefficients. Whilst the solubility parameter gives a reasonable interpretation of the attraction between molecules in the liquid it takes no account of the entropic behaviour of the interaction.

The solubility model implies that the large differences in the interaction parameters between different liquid crystal phases, observed in the extrapolated plots in chapter 5, result from entropic effects. This is illustrated in table 6.14 which gives examples of the enthalpic and entropic contributions to the interaction parameter as defined in section 1.8a, χ^H and χ^S respectively. The table clearly illustrates that the solubility parameter model predicts a large contribution to the measured interaction parameter from entropic interaction effects.

In this section the solubility parameter model has been shown to yield stationary phase solubility parameters which are in general agreement with the observed solution behaviour of the studied systems. However, the model has been shown to be only semi-quantitative in these systems. The enthalpic interactions within the liquid crystal fluid for both low molar mass and polymeric liquid crystals were similar and imply the different mesophases formed depend mainly upon the entropy of interaction. However, inspection of values in *table 6.14* shows that this is not necessarily the case

Table 6.14: Enthalpic and entropic contributions to the interaction parameter for hexane and benzene at different temperatures.

Phase	°C	Hexane		Benzene	
		χ^H	χ^S	χ^H	χ^S
PDMS	80.0	0.02	0.36	0.26	0.19
LCP S	60.0	0.45	0.88	0.02	0.60
LCP I	85.0	0.51	0.45	0.00	0.27
HCB N	66.0	0.74	0.91	0.00	0.65
HCB I	86.0	0.72	0.63	0.01	0.36
OCB S	58.0	0.68	1.02	0.00	0.67
OCB N	70.0	0.66	0.94	0.00	0.59
OCB I	85.0	0.78	0.61	0.02	0.29

and highlight the need for high accuracy solubility parameter values. But it should be noted that the solubility parameter theory is a semi-empirical theory.

6.3 EQUATION OF STATE THEORY

As discussed in chapter 1, the drawback of the classical approach to solution behaviour is that the different thermal expansions of the segments in a multicomponent system are not accounted for. The equation of state approach is to combine segments and not volumes of a component, as described in section 1.9. The resulting "hard-core" interaction parameter comprises a "free-volume" contribution and an interaction contribution;

$$\chi^* \, R \, T = P_1^* \, V_1^* [3 \, \tilde{T}_1 \ln((\tilde{v}_1^{1/3}-1)/(\tilde{v}_2^{1/3}-1)) + (1/\tilde{v}_1)-(1/\tilde{v}_2)]$$
$$+ X_{12}.V_1^*/\tilde{v}_2 \tag{3.15}$$

where X_{12} is the exchange interaction parameter and the term in the square brackets is the "free-volume" contribution. All parameters were calculated as described in section 3.4a.

The "hard-core" interaction parameters and exchange interaction parameters are listed at a given temperature in each phase for all systems studied in the tables in section 6.1. *Figure 6.9* illustrates the temperature variation of the "hard-core" interaction parameter for the OCB system with examples of the probes studied. Generally the trends and behaviour are very similar to the classical interaction parameters already discussed. The main differences are that the alkane probes exhibit a smaller range of values at a given temperature and benzene values are higher compared to toluene and ethylbenzene, resulting in a change in the trend with benzene exhibiting the highest values in the liquid crystal systems. These changes are a consequence of the different rates of expansion of the probes. As the interaction parameter now accounts for all non-combinatorial entropy effects the values are higher than in the

the different rates of expansion of the probes. As the interaction parameter now

accounts for all non-combinatorial entropy effects the values are higher than in the
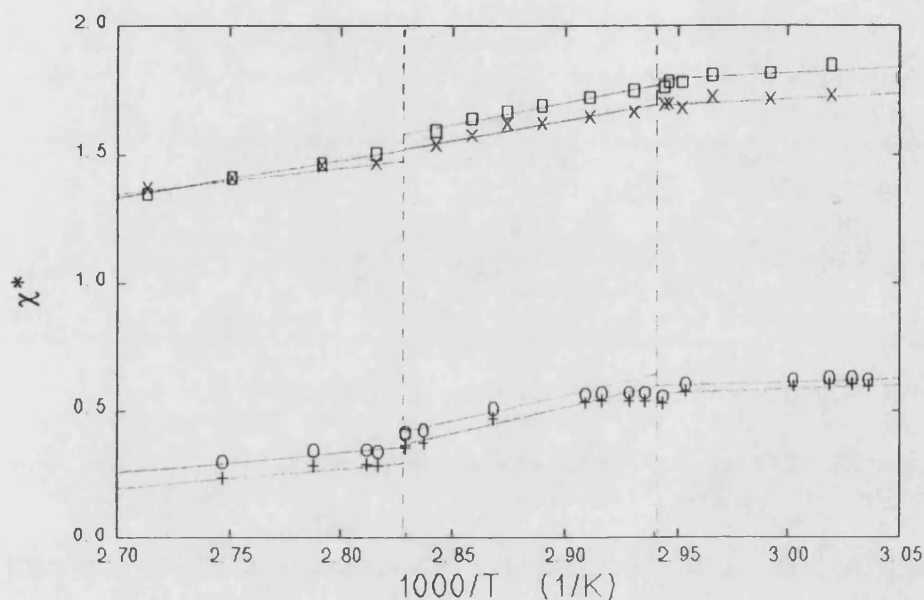
Figure 6.9: "Hard-core" interaction parameters for hexane, x, octane, □, toluene, o, and o-xylene, +, in OCB.

classical theory. As end groups will have a higher "free-volume"[224] the probes with

the greater proportion of end groups will experience the greater increase in the

interaction value from interaction parameters reported in section 6.1, that is the lower

n-alkanes and branched alkanes as opposed to the higher n-alkanes. Thus the alkane

values occur over a narrower range. A similar argument applies to the aromatic probes

but because the interaction parameters reported in section 6.1 exhibited a narrow range

of values the effect is large enough to alter the trend.

Equation [3.15] illustrates that a low exchange interaction parameter implies a

solution with interactions similar to those within the pure solvent. The results given in

the tables in section 6.1 show that the difference in interaction between the

components of the solution are significant for all systems. As the exchange interaction

parameter is theoretically the value between the "hard-core" segments it should not be

subject to thermal disturbances and thus exhibit a constant value as temperature increases. This is not strictly true for any system that has been studied. A further adjustable parameter has been introduced in some systems to account for such behaviour[68];

$$X_{12} = X_{12}{}^T - T Q_{12} \, \bar{v}_2 \qquad\qquad [1.33]$$

where $X_{12}{}^T$ is now the true exchange interaction parameter and Q_{12} is an entropic term. The extra term implies there is some form of ordering occurring within the solution. This would lead one to expect positive values of Q_{12} which would reduce the contribution of the exchange interaction parameter to the solution behaviour. In fact both positive and negative values have been measured, dependent upon the system studied[225]. Also the accuracy of the fit to experimental data when the concentration of the solvent is allowed to increase to finite concentrations has been found to be poorer with the additional parameter[225]. Thus the validity of such a term is dubious and in this thesis values are not calculated for this entropic term but the possible effects are discussed qualitatively.

Figure 6.10 shows the exchange interaction parameters at different temperatures in PDMS for some of the probes studied. Although the graphs show some temperature dependence giving negative entropy contributions, the graphs show almost constant values with temperature for all probes. The variation with temperature was at least an order of magnitude lower than the variation in the interaction parameters, χ and χ^*, previously shown. The alkanes exhibited a comparatively narrow range of values indicating the chainlength was not too critical on the interaction strength. The heptane isomers were similar and showed a clear trend of decreasing exchange interaction parameter as the branching increased with the more rigid molecules having lower values. An explanation for this could be that the loss of interacting surface as a molecule becomes more spherical is outweighed by the increased strength of interaction with adjacent molecule segments, as was inferred from previous results

above. Cyclohexane, however, had significantly higher values. This shows that forming a flexible chain into a ring is not as favourable as introducing branching
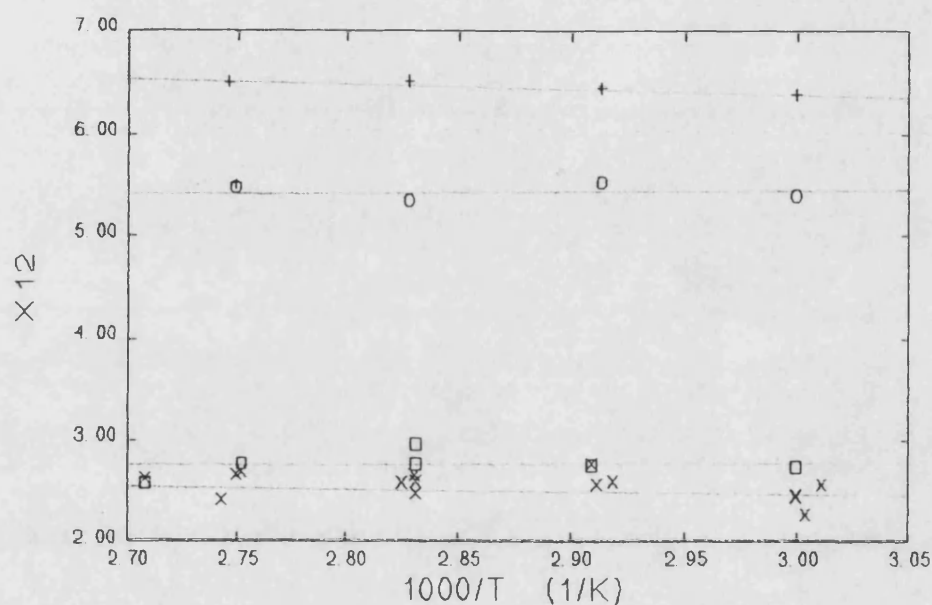
Figure 6.10: Exchange interaction parameters for hexane, x, octane, □, toluene, o, and o-xylene, +, in PDMS.

suggesting that alkyl end-groups interact more favourably with PDMS than the alkyl chains. Alternatively, this could arise because the chain retains most of the flexibility but excludes interaction with PDMS by the "self-shielding" effect of the ring. That is, forming a ring introduces branching but effectively increases molecular width increasing the distance between the PDMS segments and segments of the probe. With the aromatic probes the interactions the pure components undergo are clearly more mismatched than seen with the alkanes. As the alkyl chainlength decreases from ethylbenzene to benzene the values rise. The xylene probes also exhibit differences with values rising as the strength of the dipole rises within the molecule. These results are consistent with the methyl side-groups governing the interaction behaviour of the PDMS molecule.

The trends in the exchange interaction parameters for probe-PDMS systems noted here agree with those reported in the literature[101,103,218,219]. The reported values were given at 25 °C or 60 °C. Theoretically the parameter should be independent of temperature and the values directly comparable to those reported in this work. However, it has already been shown that some temperature dependence does exist in practice. The values reported by Lichtenthaler *et al.* ere considerably lower than values in this work which are close to, but less than the values of Summers *et al.* and Galin.

The temperature behaviour of the exchange interaction parameter in the liquid crystal systems is illustrated for some example probes in HCB and OCB, in *figure 6.11* and *6.12*, respectively. With these systems the temperature dependence was generally greater than in PDMS and would yield positive entropy contributions to the apparent exchange parameter. The exception being the smectic phase of OCB which exhibited negative Q_{12} values. The variation in exchange interaction parameter with temperature was still lower than seen for the interaction parameter. Both liquid crystals exhibited a clear divide between different phases and mesophases for any given probe with values higher in the lower temperature phases.

In the HCB-alkane systems the exchange interaction parameters were about three or four times larger than seen for alkane probes in the PDMS stationary phase. At this point the effect of adopting the approximation of infinite nearest neighbour should be considered. The "true" "hard-core" interaction parameter values would be lower than those reported, following the behaviour discussed in section 6.1 and illustrated by *table 6.6* and *figure 6.3*. From equation [3.15], given at the beginning of this section, it follows that the exchange interaction parameter would also be lower. However, the effect of the different "free-volume" of the probes would be to increase the difference in values between different probes, as opposed to the decrease observed for interaction parameters in section 6.1, and the values would not be lowered from those measured

alkane chainlength increased. It is unclear why the values should be so high for pentane in the isotropic phase but in both phases the reduction in the exchange interaction parameter became smaller with increasing chainlength. This might be explained by

a) an unfavourable interaction between chain ends and HCB compared to chain centres leading to smaller contributions from the chain ends in longer molecules when interaction is averaged over the whole chain

or b) An increasing ability to access linear conformations as the chainlength increases allowing better interaction which would increase less at longer chainlengths than at shorter chainlengths.

In reality both effects were probably affecting the overall interaction behaviour. The higher values in the nematic phase show the greater dissimilarity between the interactionsof the two components and are indicative of the lower flexibility of the liquid crystal molecules and reduction in the time the solvent spends probing the rigid portion of the mesogen. That these values do not increase considerably more from
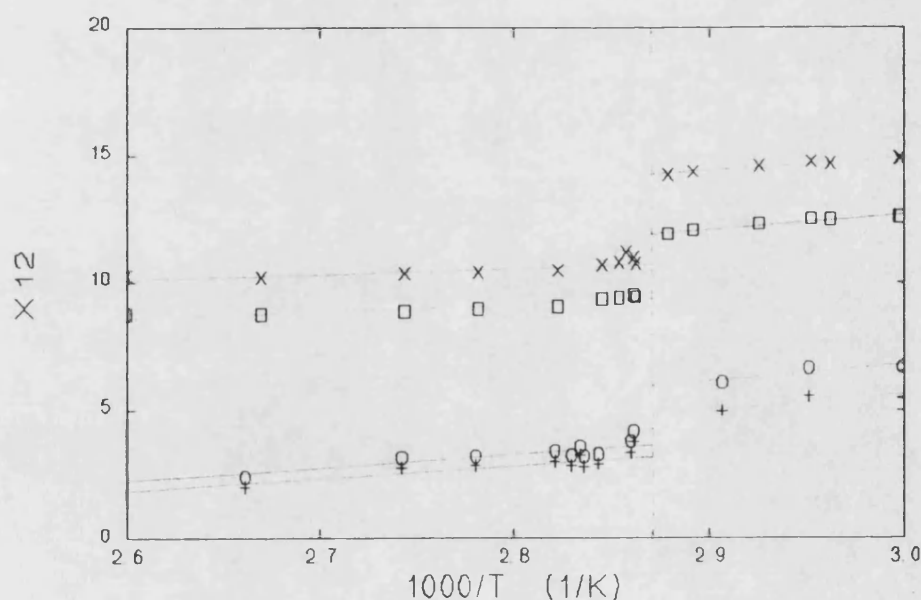
Figure 6.11: Exchange interaction parameters for hexane, x, octane, □, toluene, o, and o-xylene, +, in HCB.
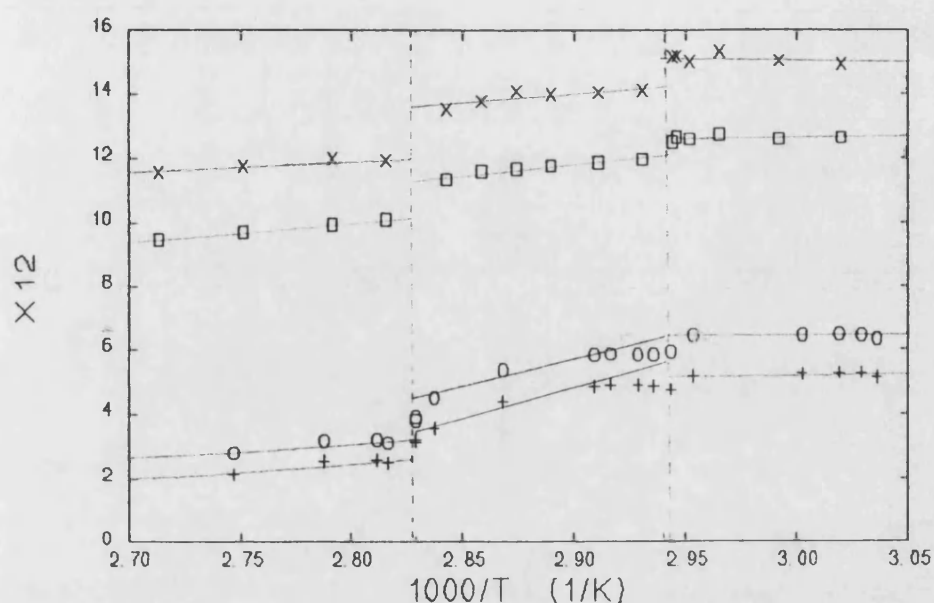
Figure 6.12: Exchange interaction parameters for hexane, x, octane, □, toluene, o, and o-xylene, +, in OCB

those found in the isotropic phase and that they do not have a much higher temperature dependence show that the probe was able to access all of the molecule in the nematic phase.

The heptane isomers exhibited similar behaviour in isotropic HCB to that observed in PDMS. In the nematic phase all values except 2,4-dimethylpentane have practically identical exchange interaction values. This indicates that the gain in interaction branching affords the molecule is negated by the reduced ability to probe between the ordered portions of the molecule. Clearly 2,4-dimethylpentane is particularly poor. In chapter 5 the observed behaviour implied that molecule shape effected the trends in thermodynamic parameters through changing interactions. The close exchange interaction parameters reported here indicate that this is manifest through the changing "free-volume" of the isomers.

In HCB cyclohexane exchange interaction parameters agree closely with the n-alkane values. In the isotropic phase values are close to those for hexane whereas the values are nearer pentane in nematic phase. In PDMS cyclohexane exhibited significantly more unfavourable values than the n-alkanes. The temperature dependence of the exchange interaction parameters in both stationary phases show that the probe is able to access all the stationary phase. Thus, the relatively unfavourable values in PDMS must arise from the inability of PDMS to interact with the probe as well as with n-alkanes. This was discussed above as a "self-shielding" effect in cyclohexane. In HCB the rigidity of the liquid crystal molecule results in poorer interaction with probe generally and hence less discrimination between similar probes.

Interaction between aromatic probes and HCB was more favourable than observed in alkane-PDMS systems. The discrimination between different probes was thus greater than observed in the aliphatic-HCB systems. In the isotropic phase values were close for all aromatic probes and there was considerable temperature dependence. This indicates that the anisotropy of the liquid crystal molecule was able to confer some degree of ordering on the solution above the clearing temperature. In the nematic phase temperature dependence of the exchange interaction parameter was greater with values dropping sharply just below the clearing point. This is consistent with the ordering within the pure liquid crystal and shows that the order parameter alters little until the temperature rises close to the clearing temperature. The difference between nematic values and isotropic values were much higher for the aromatic probes than aliphatic probes which indicates the preference of aliphatic probes to avoid the rigid portion of the mesogen in the mesophase. This supports earlier conclusions that the rigid portion of the mesogen governs interaction between the liquid crystal and probe. Also, the similarity in xylene isomer values reinforces the dominance of dispersion forces on interactions in these solutions as opposed to dipole interactions.

Exchange interaction parameters for OCB and HCB were similar supporting the argument in section 6.2 that the rigid mesogen governs the inter-liquid crystal interactions. The n-alkane values were spread over a wider range than in HCB but the contraction of values at longer chainlength was still evident. In the smectic mesophase the values were almost constant indicating the order of the mesophase changes little with temperature. This is supported by the behaviour of the aromatic probes in the smectic mesophase. Some aromatic probes show a slight increase in values with temperature but the significance of this is unclear. With the heptane isomers the values were lower than in HCB which indicates the importance of molecule rigidity in OCB-probe systems. In the nematic mesophase the aromatic probes again exhibit a drop to low values as the clearing temperature is approached. The most striking difference between OCB and HCB was the higher benzene-OCB exchange interaction parameters. The tendency for OCB to arrange to form quadrapoles, and thus decrease the aromatic nature of the mesogen, would explain this. However, the fact that the other aromatic probes are not affected to any great extent and the persistence of high benzene values at elevated temperatures make this dubious and further work is necessary before this behaviour can be explained satisfactorily.

The exchange parameters in LCP are given in *table 6.12*. Comparing these to OCB and PDMS values shows that they do not directly correlate with either of the other two systems but are generally closer to the OCB system. For aliphatic probes the exchange interaction parameters increased in going from the smectic phase to the isotropic phase whereas aromatic probes exhibited a decrease in values. *Figure 6.13* illustrates the temperature dependence for some example probes in LCP. For any given probe in the smectic mesophase there was a greater temperature dependence than was measured in OCB. As with the low molar mass system, the gradient of the alkane probes becomes more negative as the carbon chainlength increases but the gradient is more positive for the LCP system than the OCB system. In the isotropic phase the temperature dependence of the exchange interaction parameter is greater than in the smectic phase.

This agrees with the values observed in OCB and the magnitude is also similar. The decrease in values compared to OCB could be a result of the influence of favourable interaction with the polysiloxane backbone but the discrepancy could equally be a result of the approximations of the theory discussed in section 6.1. The aromatic probes exhibit similar behaviour to that observed in OCB. However, the xylene isomers are more spread in the smectic phase and toluene was significantly favoured over ethylbenzene. Also, benzene does not show such a marked increase in the smectic mesophase values over the other aromatic probes as was seen in the OCB mesophases. In the isotropic phase values agree closely with those in OCB and benzene now exhibits the large discrepancy with other aromatic probes. Cyclohexane has values close to those of hexane in both phases. The results indicate there was a definite contribution to the interaction from the presence of the polymer backbone. This contribution was greater in smectic-alkane interactions than in the isotropic-alkane interactions. In the aromatic-LCP systems the effect was much less marked but results in an increase in exchange
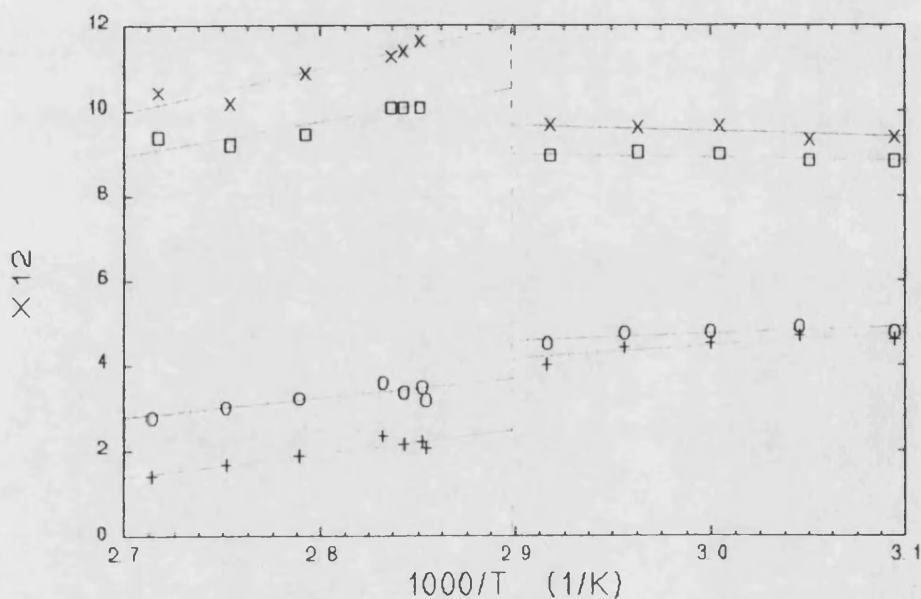
Figure 6.13: Exchange interaction parameters for hexane, x, octane, □, toluene, o, and o-xylene, +, in LCP.

interaction parameters in the isotropic phase. These observations are consistent with the interactions of the different probes with PDMS and illustrate that the rigid portion of the mesogen dominates interaction with contributions from the linking chain or backbone only becoming significant when a probe has sufficiently poor interaction with the rigid liquid crystal mesogen.

The equation of state model of solution behaviour has allowed the interaction behaviour to be disseminated into an enthalpic contribution and a "free-volume" contribution. Exchange interaction parameters for the liquid crystal systems imply that the enthalpic interactions are very similar for all the cyanobiphenyls studied and the differences observed in the interaction parameters arise largely from "free-volume" effects. The application of this more rigorous solution model does not alter trends in the interaction parameters between probes and the results support earlier conclusions that solution behaviour is governed by the rigid mesogen and not by the flexible end groups of the liquid crystal molecule.

6.4 ANISOTROPY EFFECTS ON THE SOLUTION PARAMETERS

In the above sections various solution models were employed to elucidate the cause of the observed solution behaviour but no account of the anisotropy of the liquid crystal molecules was accounted for. In this section the correction to the interaction parameter arising from the liquid crystal model developed by Flory and co-workers[76-82], and discussed in section 1.10a, is considered.

The interaction parameter is unaffected by molecular anisotropy in the isotropic phase. In the mesophase, the structure of which was unspecified by the theory, an extra parameter, y, has to be introduced. This is the "disorientation parameter" and represents the number of adjacent rows in a lattice required to accommodate the rigid mesogen, and is illustrated shematically in *figure 1.10* (section 1.10a). The true

interaction parameter, χ^T, is then related to the interaction parameter measured in section 6.1, χ, by;

$$\chi = \chi^T + (2/y) - [1 - \exp(-2/y)] \qquad [6.5]$$

where y can be obtained by solving the rearranged form of equation [1.37] below;

$$\exp(-2/y) - 1 + \phi_0{}^a[1 - (y/\overline{\eta}{}^a)] = 0 \qquad [6.6]$$

if appropriate estimates of the length of the rigid mesogen, $\overline{\eta}{}^a$, and volume fraction of aligned mesogens, $\phi_0{}^a$, are available. Thus, any correction would result in a constant shift in values for all probes and the trends in the interaction parameters between different probes discussed above would remain the same. Only the temperature dependence of values in the mesophases would change. *Figure 6.14* plots the function of y in equation [6.6], $f(y) = \exp(-2/y) - 1 + \phi_0{}^a[1 - (y/\overline{\eta}{}^a)]$, against y for a mesogen length of 20 lattice segments for various volume fractions of aligned mesogen. A number of points arise from the figure. The value of y is strictly an integer number but it can be treated as a continually varying parameter[82] and when y equals the mesogen
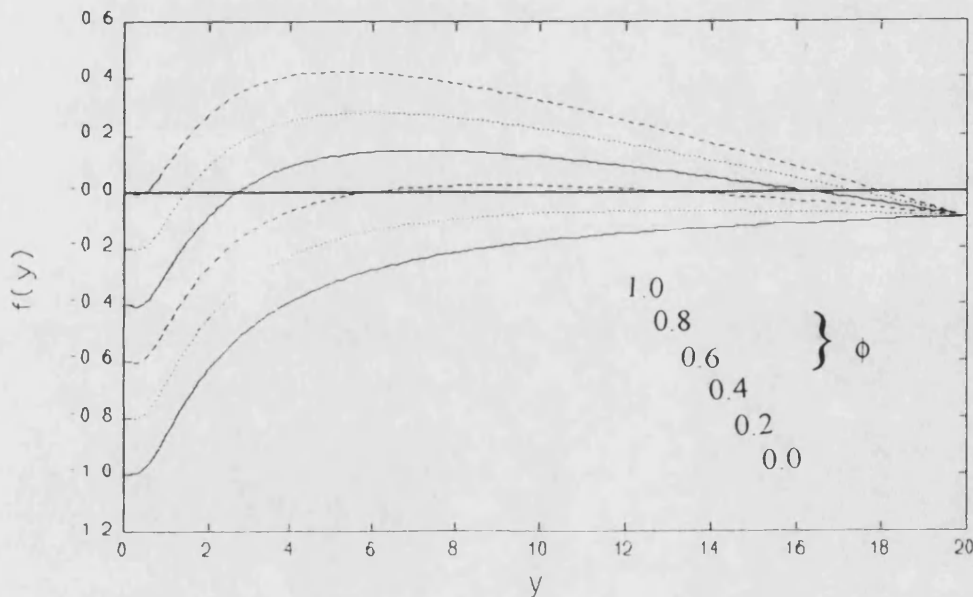
Figure 6.14: The function of the disorientation parameter against increasing disorientation for a theoretical mesogen of 20 lattice segments. Higher lines indicate larger volume fraction of the aligned mesogens.

length in segments, or when there is no ordered mesogen fraction, equation [6.6] has

no solutions, as would be expected because no mesophase exists. As the volume

fraction of aligned mesogen increases the equation becomes solvable and of the two

solutions the lower one is the one with physical significance[82]. Hence, as the volume

fraction of aligned mesogens decreases from unity the liquid crystal molecules become

less ordered and require more lattice rows to accommodate the rigid mesogen. At a

volume fraction of 0.2 equation [6.6] has no solutions implying the rigid mesogen has

negligible effect on the interaction parameter at this low volume fraction.

In the cyanobiphenyl systems studied the volume fraction of the aligned mesogens

was taken as the effective degree of crystallinity of the mesophases, presented in

section 4.3d. Values increased from 0 at the clearing temperature to between 0.1 and

0.2 for HCB and OCB at the melting temperature. As this fraction denotes the portion

of the mesophase acting as if it were totally aligned the values are a low estimate of the

volume fraction of aligned mesogens. The size of a lattice segment is taken as a cube

of side equal to the molecular diameter of the liquid crystal and the solvent assumes the

value of unity. A system such as cyanobiphenyl with benzene would be expected to fit

this model closely. The model only requires the dimensions of the aligned rigid

mesogen, which in this case is equivalent to the dimensions of any mesogen. From the

molecular dimensions in section 3.6 the rigid mesogen occupies 2.5 lattice segments.

As a lattice segment is either occupied or not 3 segments are required to accommodate

the mesogen. The function of y for various volume fractions of aligned mesogens are

shown in *figure 6.15*. Again all curves converge as the disorientation parameter

approaches the segment length of the mesogen. However, for the cyanobiphenyl

systems there are no solutions of equation [6.6] at any concentration. In fact no

mathematical solution of the equation is possible until the number of mesogen

segments, or axial ratio of the liquid crystal, is 5.44, or 6 segments in terms of the

model. By comparison with the above case for an axial ratio of 20, the result implies
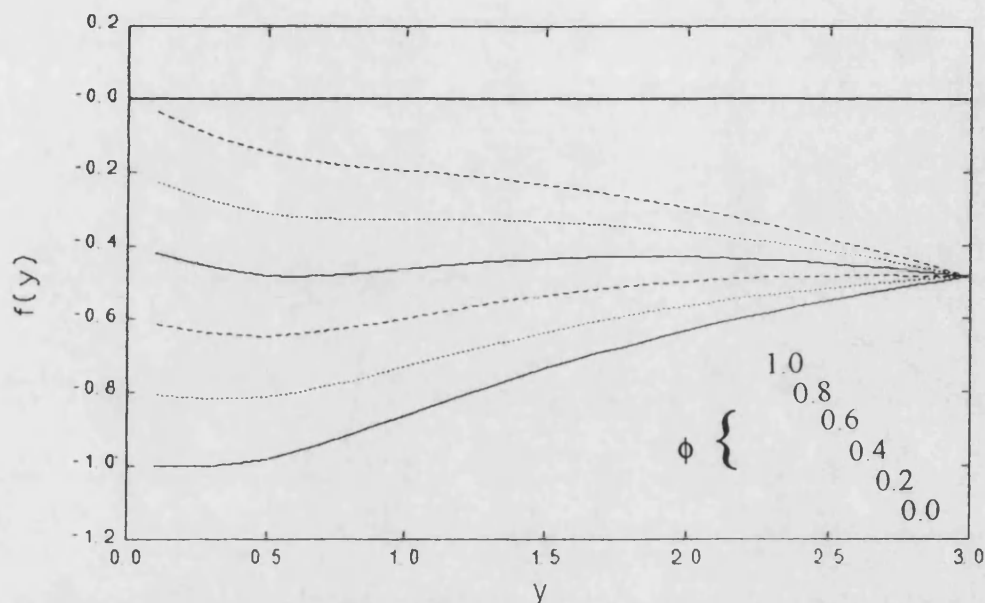
Figure 6.15: The function of the disorientation parameter against increasing disorientation for cyanobiphenyls with 3 lattice segments. Higher lines indicate larger volume fraction of the aligned mesogens.

that the mesogen is not long enough to require any correction to the interaction parameters calculated without accounting for the anisotropy of the liquid crystal molecules.

So in this section it has been shown that, according to this model, the liquid crystal mesophases of the cyanobiphenyls are sufficiently disordered for the anisotropy of the molecules to have an insignificant effect on the interaction parameters. As the disorientation parameter was introduced to modify placement of liquid crystal molecules on a lattice, this result does not imply that the anisotropy does not effect the interactions between solvent and liquid crystal. It should be noted that the model is best applied to more ordered systems but the inference is that a more refined description of interactions in solution than the Flory-Huggins theory, or developments based upon it, would need to be employed before the anisotropy of small mesogens needs to be considered explicitly.

CHAPTER 7

TERNARY SOLUTIONS

In the previous chapters the stationary phases were single components and a binary solution was formed with the probe at infinite dilution. The IGC technique is useful for studying ternary solutions where the probe still tends to infinite dilution but the stationary phase is now comprised of two components at finite concentrations. As pointed out in chapter 1, binary stationary phases also have considerable practical importance in chromatographic separations of analytes. However, the main concern of this chapter will be to investigate the thermodynamic behaviour of the stationary phase.

Small molar mass materials have been discussed in terms of their solution properties and compared to PDMS and an oligomeric LCP. This chapter considers the effect of preparing a stationary phase from HCB and PDMS and the thermodynamic solution behaviour with a series of probes. How incorporation of PDMS alters the transition temperatures in HCB is considered and the chapter ends with a discussion of the interaction between the two stationary phases. The solution behaviour is compared and contrasted to that of the polymeric liquid crystal, LCP.

7.1 PROBE RETENTION

Before considering the retention behaviour of a series of probes in different PDMS-HCB compositions it should be noted that the PDMS sample studied in this thesis is of a reasonably high molecular mass. Previous studies[118,128,219] have shown that the retention behaviour of probes in PDMS exhibits some dependence upon the molar mass of the sample. However, at sufficiently large molar masses the effect of chainlength becomes negligible, so in these systems the contribution of polymer chain end-groups to the interaction measured between HCB and PDMS were negligible.

The retention volumes of all probes studied are given in *appendix I*. Example van't Hoff plots are shown for toluene and heptane in the binary stationary phases in *figures 7.1* to *7.4*. Stationary phase composition was determined on the basis of weight fraction.
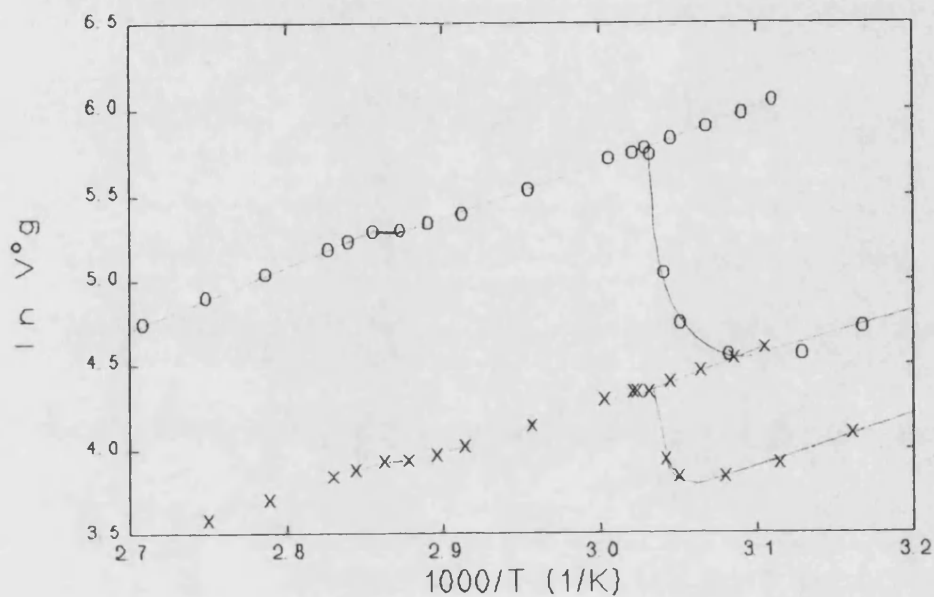
Figure 7.1: Retention of heptane, x, and toluene, o, in 8:2 (w:w) HCB:PDMS as a function of temperature, lower curve on heating higher curve on cooling.
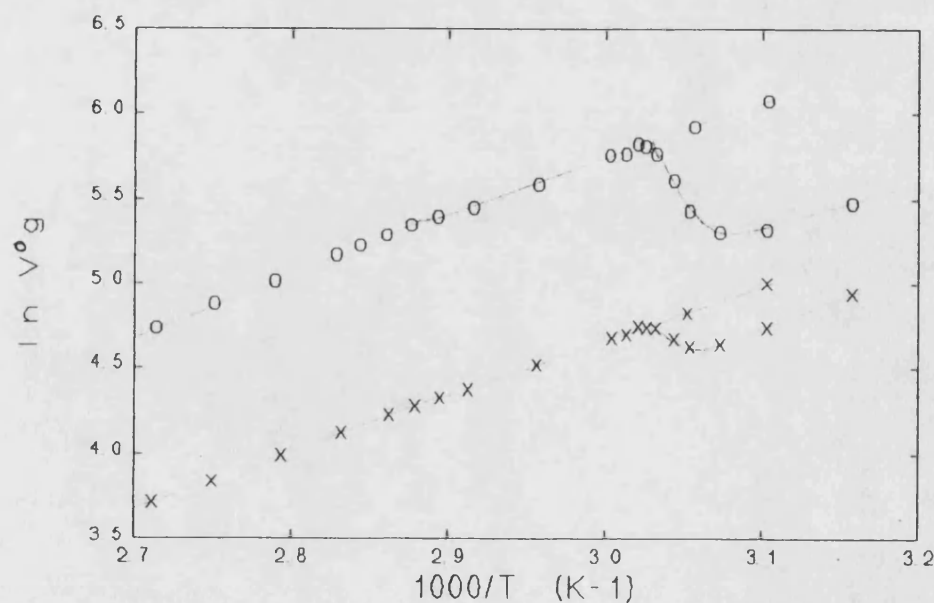
Figure 7.2: Retention of heptane, x, and toluene, o, in 6:4 (w:w) HCB:PDMS as a function of temperature, lower curve on heating higher curve on cooling.
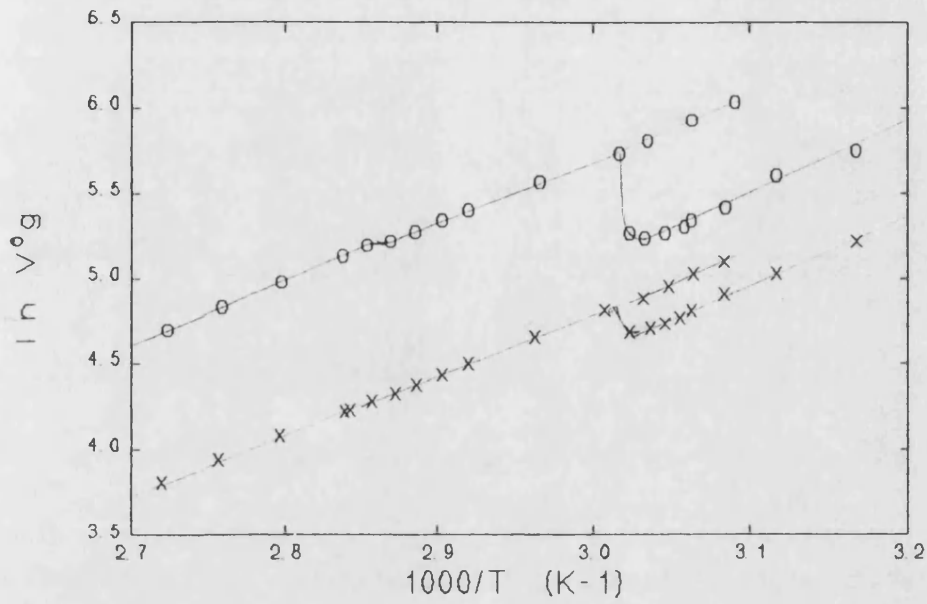
Figure 7.3: Retention of heptane, x, and toluene, o, in 4:6 (w:w) HCB:PDMS as a function of temperature, lower curve on heating higher curve on cooling.
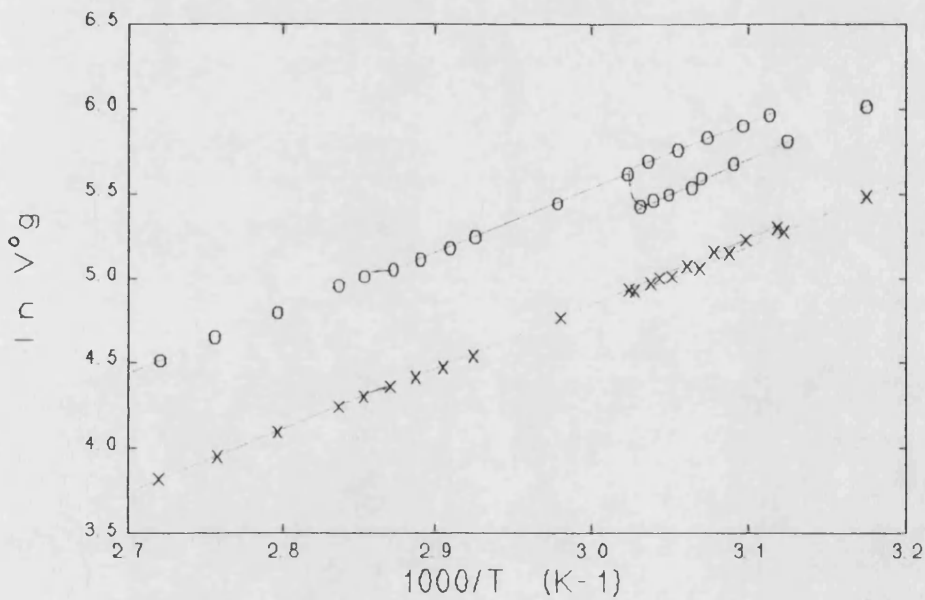
Figure 7.4: Retention of heptane, x, and toluene, o, in 2:8 (w:w) HCB:PDMS as a function of temperature, lower curve on heating higher curve on cooling.

Comparing these plots with those given in chapter 4 for the pure components reveals a predictable pattern in behaviour. The retention volume is reported per gram of stationary phase. As the fraction of HCB in the stationary phase decreased the change in the specific retention volume about a phase transition temperature became less pronounced. In *figure 7.5* retention volumes for benzene and octane are plotted against composition at various temperatures in the isotropic phase and mesophase of HCB. The variation from a weight averaged retention volume was within the limits of uncertainty, about 3 % of the measured values, for the compositions containing 80 % ($^w/_w$) and 20 % ($^w/_w$) HCB. However, specific retention volumes were significantly higher in compositions containing 60 % ($^w/_w$) and 40 % ($^w/_w$) HCB. The results imply the two stationary phase components were acting independently for the 80 % ($^w/_w$) and 20 % ($^w/_w$) HCB compositions. However, the other two compositions appear to be interacting unfavourably to give higher specific retention volumes. Analysis of *figures 7.1* to *7.4* reveals that the clearing temperature of HCB was lowered by the presence of PDMS where this unfavourable interaction was observed. This will be discussed further in section 7.3.

It is interesting to compare the specific retention volumes observed for LCP compared to the binary stationary phase results. As an approximation of the effective composition of mesogen in LCP in relation to a binary HCB-PDMS mixture the oligomer was considered to be composed of repeat segments only. These are divided into "PDMS" portions of formula $Si_2O_2C_4H_{11}$ and "mesogen" portions of formula $C_{16}H_{14}ON$ (see figure 2.1). This leads to an effective composition of 62 % ($^w/_w$) mesogen. *Figure 7.5* shows how the specific retention volumes for octane and benzene compare with those measured for the binary stationary phase. Clearly the values for LCP are considerably lower than those for the binary stationary phase. This reflects the structure of LCP where the mesogen and polysiloxane backbone are compelled to interact more intimately than the individual components, HCB and PDMS, because the mesogen is now chemically bonded to the polysiloxane backbone.

a)
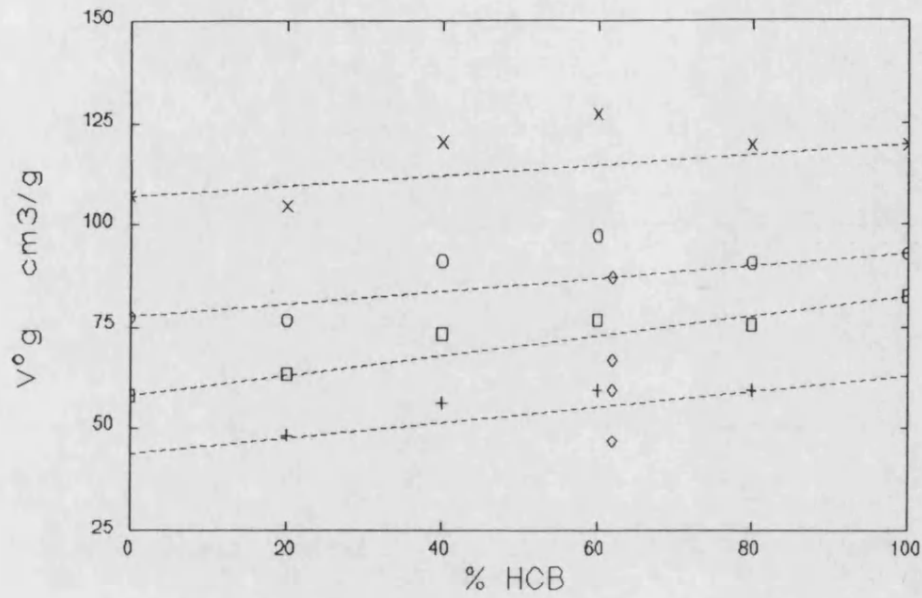
b)
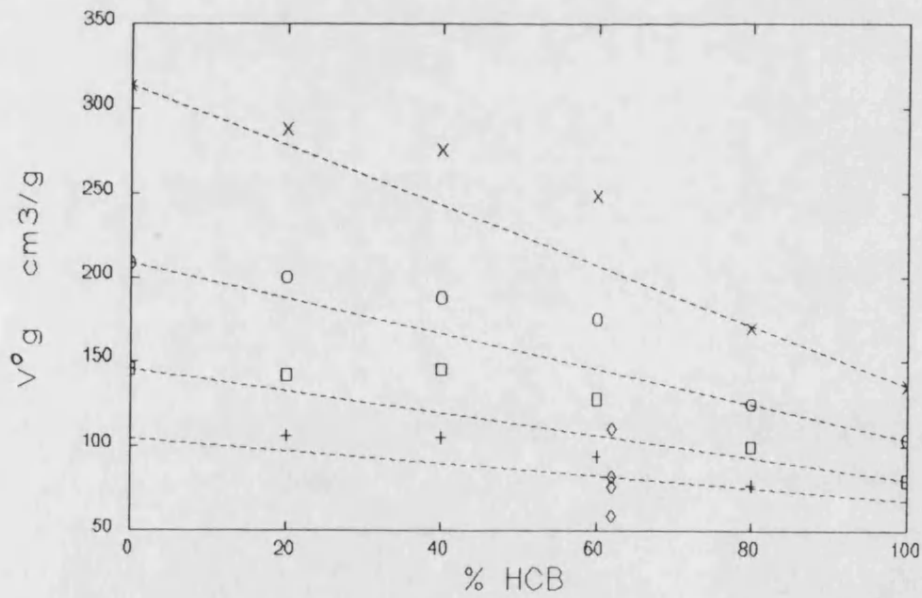
Figure 7.5: Specific retention volume against composition for a) benzene and b) octane at 60 °C, x, 70 °C, o, 80 °C, □, and 90 °C, +. The dashed lines show the calculated weight averaged value. Values, ◊, at 62 % ($^w/_w$) are the corresponding values for LCP

Although this discussion is mainly concerned with the solution thermodynamics and phase behaviour of the binary stationary phase it is worth briefly considering the effect a two component stationary phase has on separation of similar probe molecules. The separation factor is defined as the ratio of the specific retention volumes of two probes;

$$\alpha = V^o_{g1}/V^o_{g2} \qquad\qquad [7.1]$$

Generally HCB separates a given pair of probes better than PDMS. Of the probes studied, the n-alkanes and aromatic probes exhibited reasonable separation in both pure PDMS and HCB stationary phases. Generally the separation factor followed one of two patterns as composition changed and these are exemplified by the plots in *figure 7.6a* and *7.6b* for benzene-toluene and 2.3-dimethylpentane-2,4-dimethylpentane, where the two highest temperature values were in the isotropic region of HCB and the two lower temperatures were in the nematic region of HCB. In the benzene-toluene example the probes are separated by the individual components of the stationary phase and the probes have large differences in boiling point and saturated vapour pressures at a given temperature. The separation factor exhibited a linear dependence with composition for such probe pairs, well within the limits of uncertainty which follow from the discussion in section 3.7 as ± 6 % of the separation factor. However, when the boiling points and saturated vapour pressures of the probe pair were similar the separation factor followed a dependence on the composition exemplified by 2,3-dimethylpentane-2,4-dimethylpentane. The separation behaviour appears to be split into two regions, although a linear dependence is just possible if the limits of uncertainty are considered. As the PDMS fraction was increased separation decreased quite sharply down to 60% HCB. At higher PDMS fractions the separation factor decreased more slowly and the dependence approximates well to linear dependence on HCB fraction. In some liquid crystal gas chromatography systems the presence of a second component has been reported to have little effect upon the separating power of the liquid crystal[160], even down to an 80% composition of the liquid crystal. However, in this system the presence of polymer has a more dramatic effect. Below

a)
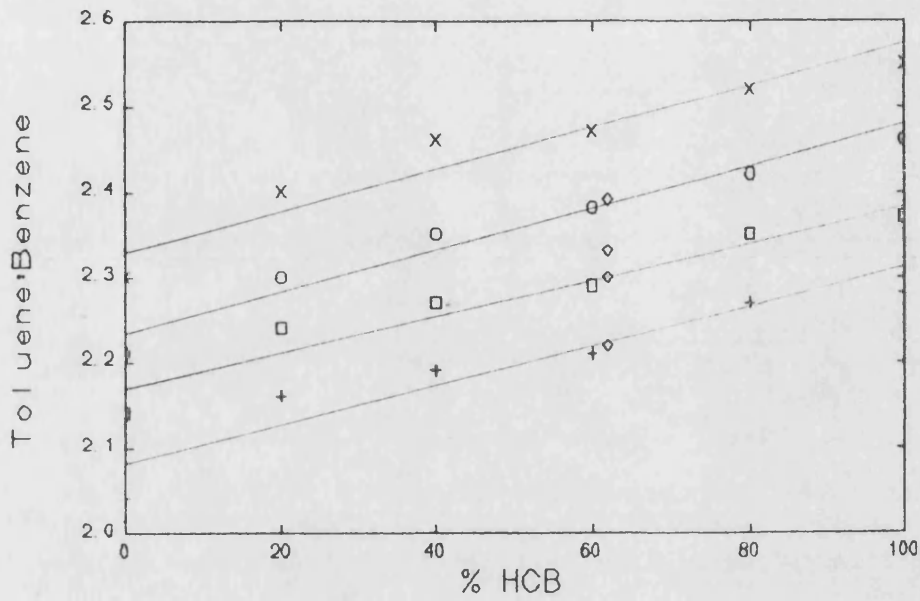
b)
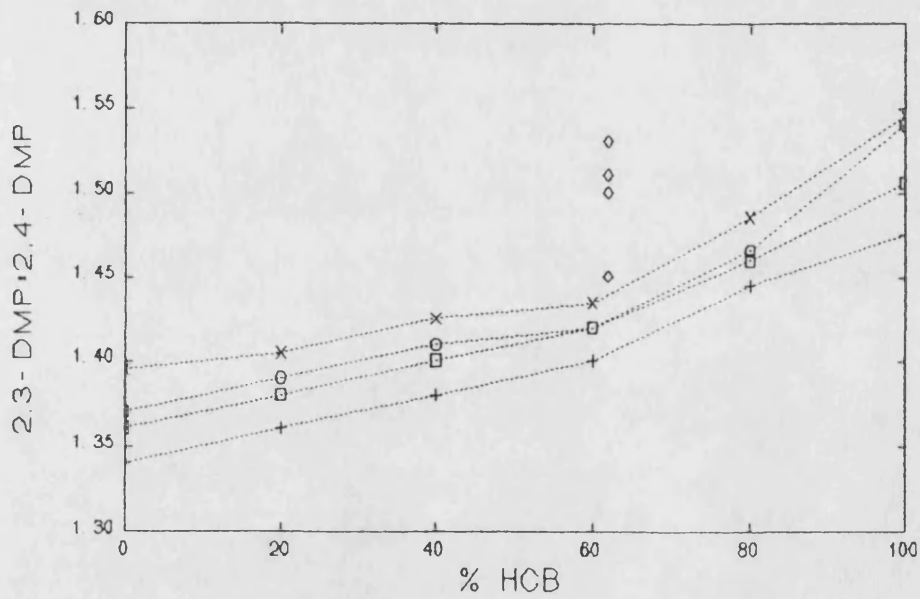
Figure 7.6: Separation factor against composition for a) benzene-toluene and

b) 2,3-dimethylpentane-2,4-dimethylpentane at 60 °C, x, 70 °C, o, 80 °C, □, and 90 °C, +.

Values, ◊, at 62 % ($^w/_w$) are the corresponding values for LCP

60 % HCB the PDMS had a greater influence on the separation factor than the weight fraction would indicate.

Also shown on the figure are the separation factors for LCP. Again the two highest temperatures are in the isotropic phase whilst the lowest two temperatures are in the mesophase and separation improves within a phase as the temperature lowers. In the benzene-toluene case values agree closely in the isotropic phase with those that would be predicted from the effective composition but values became lower as the temperature decreased in the mesophase, but they still agreed within the limits of uncertainty. For 2,3-dimethylpentane-2,4-dimethylpentane all values are higher than would be predicted and are right on the limit of uncertainty. The separation of probe pairs in the oligomeric liquid crystal, LCP, was similar to or better than the equivalent composition of PDMS and mesogen whilst retention volumes were considerably lower than those for probes retained on the binary stationary phase. Thus, whilst this particular system does not optimise separation properties it does illustrate the potential synergy of incorporating the mesogen into the polymer molecule.

7.2 CRYSTALLINITY WITHIN THE STATIONARY PHASE

If the two components of the stationary phase act independently the degree of crystallinity would be expected to agree with the known HCB composition of the stationary phase. However, should the PDMS interact significantly with HCB the observed crystallinity would be expected to deviate from that predicted from the composition.

IGC was used to measure the crystallinity in pure HCB in section 4.3d. The presence of the mesophase, curvature in the van't Hoff plots, and differing solubility of the probes employed may effect measured values but such effects were insignificant for aromatic probes in the pure liquid crystal. However, the poor solubility of aliphatic

probes resulted in significantly lower values for the degree of crystallisation. In a binary stationary phase the presence of the second component may also effect results.

Figure 7.7 shows the degree of crystallinity or "effective crystallinity" of the whole stationary phase for the compositions studied using aromatic probes. The "effective crystallinity" in 80 % ($^W/_w$) HCB was similar to values in pure HCB but lower HCB compositions exhibited smaller values. This indicates PDMS only effects the mesophase behaviour significantly below 80 % HCB. Crystallinity tended to a limiting value as the temperature was lowered apart from 20 % ($^W/_w$) HCB which exhibited a small temperature dependence in the values. This is an artefact of the IGC technique. It could have been due to increased curvature in the van't Hoff plots with a binary stationary phase but section 7.1 showed these were linear over the temperature range studied so the cause is most likely to arise from the relative interaction of the probe between the two stationary phase components. Aliphatic probe values were calculated but are not shown because of their dubious significance, as outlined in section 4.3d. However, they did exhibit greater temperature dependence in the crystalline region and all values were lower than those found for the aromatic probes. In fact, values exhibited identical profiles to the aromatic probe plots but were negative for 20 % HCB, which does not have any physical significance. This behaviour supports the argument that probes with similar solubility in each component of the stationary phase, such as the aromatic probes in the system studied, will give crystallinity values closer to the true values than probes with vastly different solubilities in each component.

Figure 7.8 shows the degree of crystallinity at 50 °C for each composition. Values generally agree closely with the predicted crystallinity expected from the composition of the stationary phase. The low value for 100 % HCB can be explained as a consequence of the greater significance of adsorption due to the lack of another bulk phase for the probe to interact with. Why 40 % HCB should exhibit greater crystallinity than would be predicted is unclear.
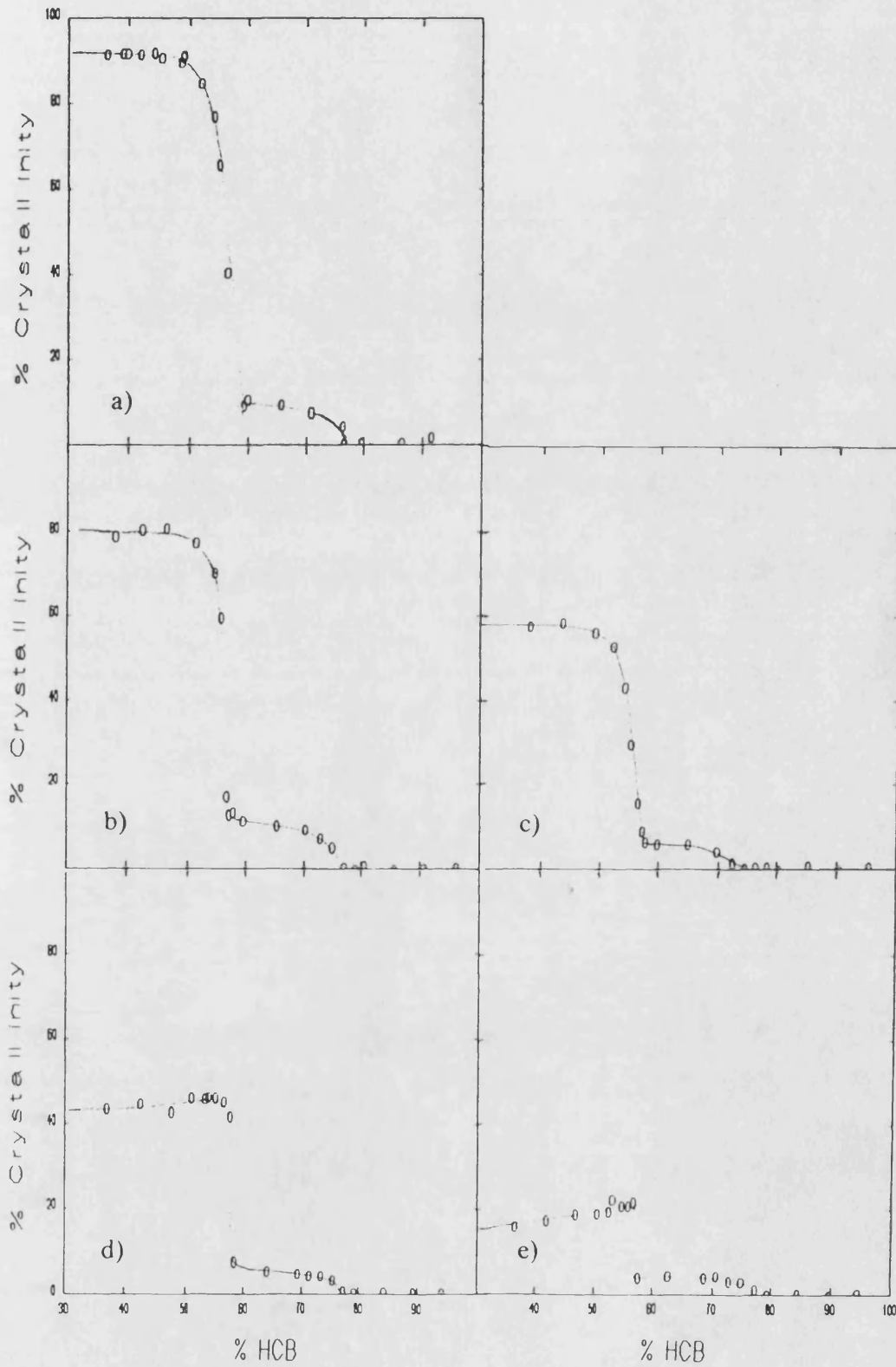
Figure 7.7: Degree of crystallinity per gram of stationary phase against temperature, °C, for

a) 100 % HCB, x, b) 80 % HCB, , c) 60 % HCB, o, d) 40 % HCB, +, and e) 20 % HCB, ◊.
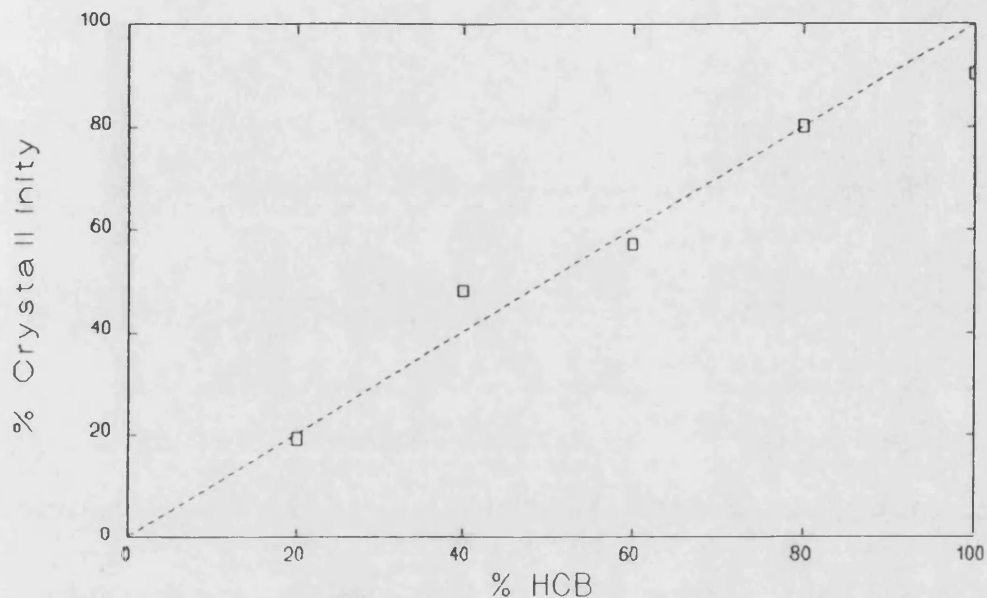
Figure 7.8: Degree of crystallinity at 50 °C against stationary phase composition. Dashed line gives the predicted values.

Figure 7.7 also shows a change in behaviour about the melting point as composition changes. A "softening" of the crystalline phase, starting 8 °C below the melting temperature, has previously been noted for the pure HCB stationary phase. As the composition became PDMS rich the crystallinity profile about the melting temperature exhibited less pre-melting "softening". This could be due to the formation of smaller crystallites as the PDMS composition increased resulting in a higher surface free energy opposing melting until a higher temperature was reached. Alternatively, it may just be a consequence of the greater solubility of the probe in PDMS masking the behaviour of HCB.

The above results indicate that PDMS does not appear to have an effect on the amount of crystal phase formed by HCB but does affect the mesophase formation above a limiting composition of PDMS. PDMS does not appear to be blending with the liquid crystal so, if the observed sharper melting transition behaviour of HCB is

genuine, it must be a result of the constraints in size and shape that the polymer imposes upon the crystallites. In the following section it will be seen that, although PDMS does not appear to be blending with HCB, it does have an effect on the transition temperatures.

7.3 TRANSITION TEMPERATURES

If PDMS blended with HCB in the stationary phase the transition temperatures of the liquid crystal would be expected to be lowered. If the transition temperatures were independent of composition it would be more probable that the two stationary components were immiscible. The liquid crystal transition temperatures were measured using two programs. In the first the material under study was heated to the isotropic phase from ambient temperature. In the second the liquid crystal was equilibrated in the isotropic phase, cooled to 0 °C, held isothermally for 10 minutes and reheated to the isotropic phase.

i) Transition temperatures on heating:

Figure 7.9 shows the results obtained from the heating cycle at the various compositions. Uncertainties are of the same order of magnitude as reported in chapter 4 with results for separate runs agreeing to within ± 1 °C. Generally the results for both coated and uncoated samples are in reasonable agreement with some discrepancy in values at high PDMS composition. Values for coated stationary phases measured by IGC and DSC in very good agreement. For the crystalline-nematic transition there was little composition dependence. The values for the uncoated samples did show a slight decrease in the transition temperature as the PDMS composition increased. At the nematic-isotropic transition the value remains constant down to 60 % HCB fraction then exhibits a marked dip in value. Below 60 % the transition then increases again prior to falling off as PDMS fraction increases. This is considerably more marked in the bulk samples.
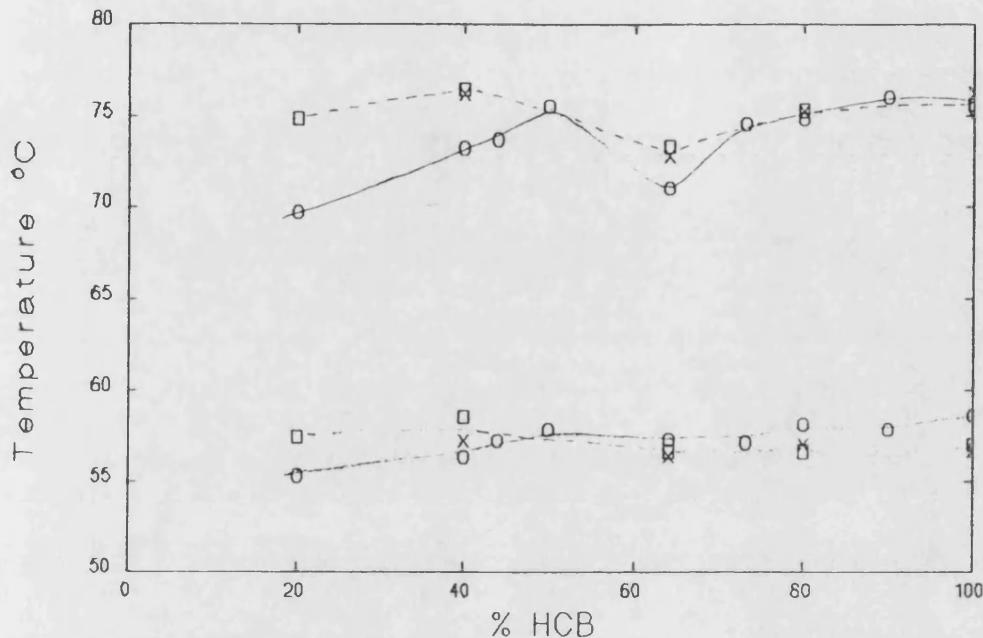
Figure 7.9: Liquid crystal transition temperatures against HCB composition measured by IGC, □, and DSC; x coated, o uncoated.

ii) Cycling transition temperatures:

Figure 7.10 shows the transition temperatures of bulk samples following the second heat program. The clearing transition temperature shows a small degree of supercooling for all compositions. This was seen for the pure HCB in chapter 4 and is a kinetic supercooling effect which depends only on the cooling/heating rate. Both the cooling and heating values exhibited a significant dip in the results for the 60 % HCB composition. About the mesophase to crystalline transition the behaviour was more complicated. All transition temperatures exhibited supercooling but above 60 % HCB the degree of supercooling depended upon the sample with some samples showing a much greater degree of supercooling than others. As each result was the average of duplicate runs with similar uncertainties to those already discussed, it is difficult to reconcile the observed differences. These differences must be due to sample
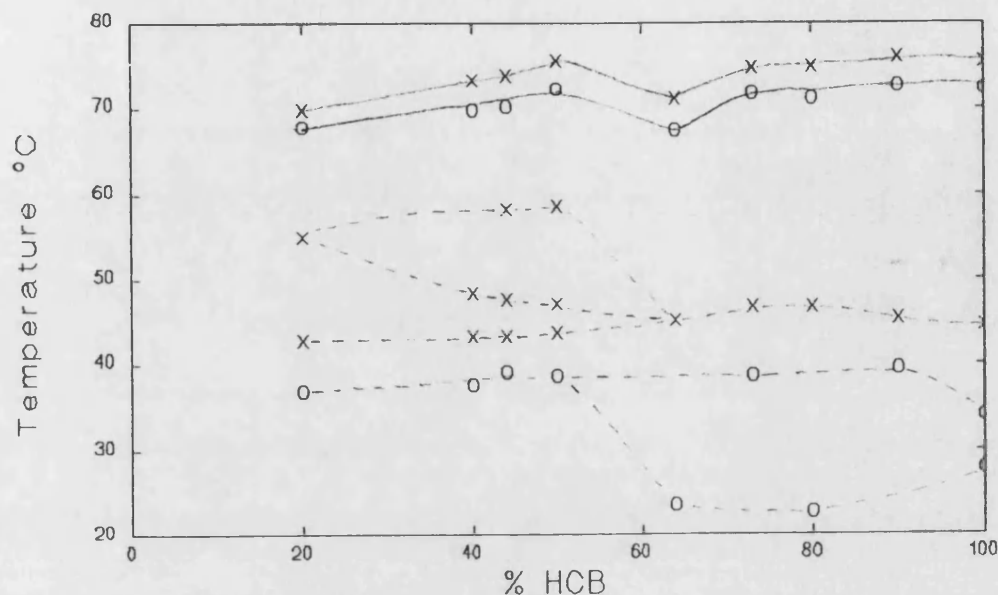
Figure 7.10: Transition temperatures against composition for uncoated PDMS-HCB on cooling, o, and reheating, x.

preparation and on reheating the results did not show any such discrepancies. When the HCB content was above 60 % the liquid crystal remelted at a temperature close to 44 °C, as previously noted in the pure liquid crystal. Below 60 % a number of endotherms were observed between 44 °C and 58 °C with a greater predominance at the higher temperature as the PDMS content increased.

The above results indicate PDMS has some effect on the transition temperature behaviour of HCB but this was too small to be a result of blending interactions between the two components. Also, in systems where two similar liquid crystals interact strongly and a eutectic is formed at given composition the clearing temperature is usually unaffected while the melting temperature exhibits a characteristic dip[171]. If we adopt the hypothesis that the presence of PDMS causes smaller crystals to form, the rate at which liquid crystal molecules would rearrange to form the crystallites would increase as the crystallites became smaller. This is a consequence of the greater

surface area for heat transfer. Hence, small crystals would not be expected to supercool to the extent that larger crystals would under the kinetic conditions of the DSC. The fact that all samples exhibited endotherms about 44 °C on reheating illustrates that they form the second crytalline HCB phase on cooling. Smaller crystallites would be expected to rearrange to the thermodynamically stable form faster than large crystallites due to the larger surface to volume ratio allowing faster dissipation of heat and a greater proportion of the sample would melt at 58 °C. These trends were indeed observed implying that PDMS does cause smaller crystallites to form. However, these are only preliminary observations and a more detailed study is required to elucidate the observed transition temperature behaviour fully.

7.4 SCANNING ELECTRON MICROGRAPHS (SEMs)

If the presence of PDMS caused the size of HCB crystallites to change there should be an observable difference in the surface morphology of the coated supports used in the IGC experiments as the composition of the coating changed. The samples were heated in an oven to 80 °C then removed and allowed to stand at room temperature for several days prior to obtaining the micrographs.

Figure 7.11 shows the series of micrographs for different coating compositions. There was little difference between PDMS coated support and uncoated support which suggests the polymer formed a thin layer over the surface that was thin enough to retain the surface features of the support. For the pure HCB the SEMs of the coated support surface looks different. There were fewer ragged edges to the micrograph and the surface has a "chunky" texture. The HCB appears to form a thicker coating and there were large areas of highly porous uncovered support, as discussed in chapter 2. At 80 % HCB the individual crystals are clearly discernible but as the composition became PDMS rich the crystals were no longer discernible. This is either because the HCB is interacting with the PDMS or the crystals are becoming much smaller and

Figure 7.11: SEMs for a) uncoated support, and b) 100 % PDMS, c) 100 % HCB, d) 80 %

HCB, e) 60 % HCB, f) 40 % HCB g) and 20 % HCB compositions on Chromosorb P.

blending in with the features of the surface. The observations in previous sections would favour the latter.

The SEMs raise concern about surface coverage of the support by the stationary phase coating. It has been noted previously that large areas of support were observed to be uncoated with pure HCB. The SEM experiment was carried out, by necessity, at ambient temperatures so the sample preparation may determine coverage. A further sample of HCB was prepared by placing the coated support in an oven at 80 °C and cooling to 58 °C over the space of an hour. The sample was then further cooled at a degree every half hour down to 45 °C, the limit of the oven. The micrographs obtained are illustrated in *figure 7.12*. The micrograph in a) was much more common and fewer uncovered porous areas existed. Clearly HCB has formed a much more
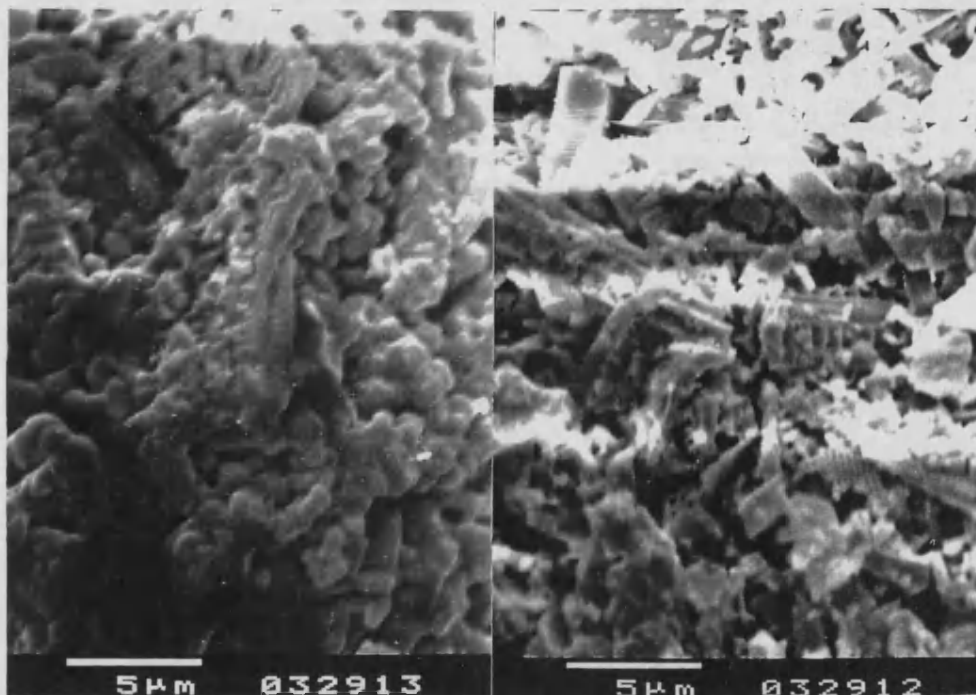
Figure 7.12: SEMs for HCB coated Chromosorb P cooled slowly from the mesophase showing the two types of surface present.

uniform coating indicating that near total coverage is achieved in the fluid state. It appears that the slower cooling allows more uniform crystal growth whereas fast cooling of the sample causes HCB to concentrate on the rougher areas of the support.

This could be due to the faster nucleation and growth on the rougher support sites. The presence of more defined crystals at 80 % HCB than with the pure HCB sample indicates a reduction in the number of nucleation sites leading to more defined, large crystals. This could occur if the PDMS preferentially covered the rough surface, which would occur as PDMS is likely to have a lower interfacial tension than the liquid crystal.

This section has illustrated the difference PDMS makes to the crystallisation behaviour of HCB. Results corroborate the preceding sections by indicating the size of the crystallites becomes small as the composition of PDMS increases. In the following section the behaviour of the PDMS-HCB system will be discussed in terms of the interaction parameter and the results discussed in terms of their compatibility with the above inferences that PDMS and HCB act independently on the support.

7.5 PDMS-HCB INTERACTION PARAMETERS

As discussed in chapter 1, the interaction between two components of a mixture can be quantitatively assessed using an extension of the Flory-Huggins approach and the IGC method can be used to obtain this parameter. However, a number of considerations should be taken into account. The interaction parameters obtained often show a dependence on the probe used. The two components do not have to interact favourably, but the mixture should be reasonably homogenous for the theory to apply and the probe must interact with all of the individual components. In previous sections the crystalline phase of HCB was shown to be inhomogenous with PDMS so the nematic and isotropic phases may also be inhomogenous but calculating an interaction parameter assumes the two components do actually form an homogenous mixture. If the two components were completely homogenous the mesophase behaviour would be lost at high PDMS composition. This does not occur but partial inclusion of PDMS within the mesophase is a possibility and calculating the interaction

parameter on the basis of assuming an homogenous system will allow an evaluation of the plausibility of such a model. Another potential problem is preferential solvent probing of the polymer component especially when HCB is nematic. Thus, if any composition conforms to the requirements of the model it is likely to occur when HCB is in the isotropic phase and more approximate results be obtained as the temperature is lowered through the nematic mesophase.

The interaction parameters were measured using the method of Deshpande and Farooque[138], outlined in section 1.12c, to avoid the problem of probe dependence. From measurements of retention in the binary stationary phase and stationary phases of the pure components, the interaction parameter between the stationary phase components, χ_{23}, can be extracted from the following expression;

$$(\chi_{1(23)} - \chi_{13})/V^o_1 = \phi_2[(\chi_{12} - \chi_{13})/V^o_1] - (\chi_{23}/V^o_2)\phi_2\,\phi_3 \qquad [1.57]$$

where the interaction parameters between probe and different stationary phases are denoted by the subscripts and V^o_i and ϕ_i are the molar volume and volume fractions of the i component. Here subscript 2 denotes the HCB component, subscript 3 denotes the PDMS component and subscript 1 denotes the probe. In the literature the interaction parameter is not usually reported directly. The normalised interaction parameter, χ'_{23}, or energy density parameter, B_{23}, are usually reported where;

$$B_{23} = (\chi_{23}/V^o_2).R\,T = \chi'_{23}\,R\,T \qquad [7.1]$$

In this section the normalised interaction parameter is reported. The method may be applied to obtain "hard-core" interaction parameters but the simpler model is convenient and adequate for the present discussion. The method also allows the effective volume fraction of HCB the solvent probes to be measured.

Probe-binary stationary phase interaction parameters were calculated from the retention volume data shown in section 7.1 and example plots for toluene and octane are shown for the 60 % HCB composition in *figure 7.13*. As observed for the pure components, the plots conform to a linear dependency with reciprocal temperature.
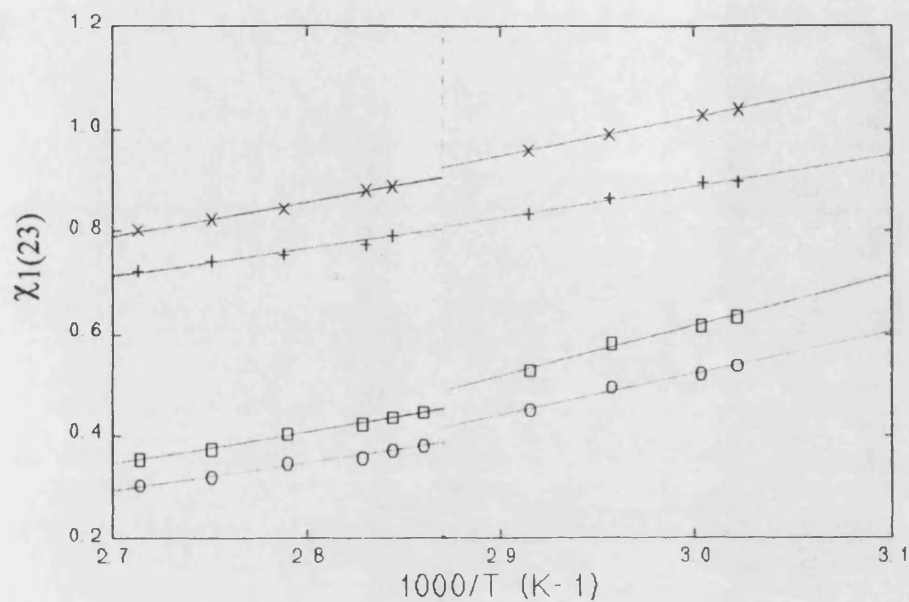
Figure 7.13: Probe interaction parameters against temperature for toluene, o, ethylbenzene, □,

hexane, +, and octane, x, in 60 % HCB: 40 % PDMS ($^{w}/_{w}$)
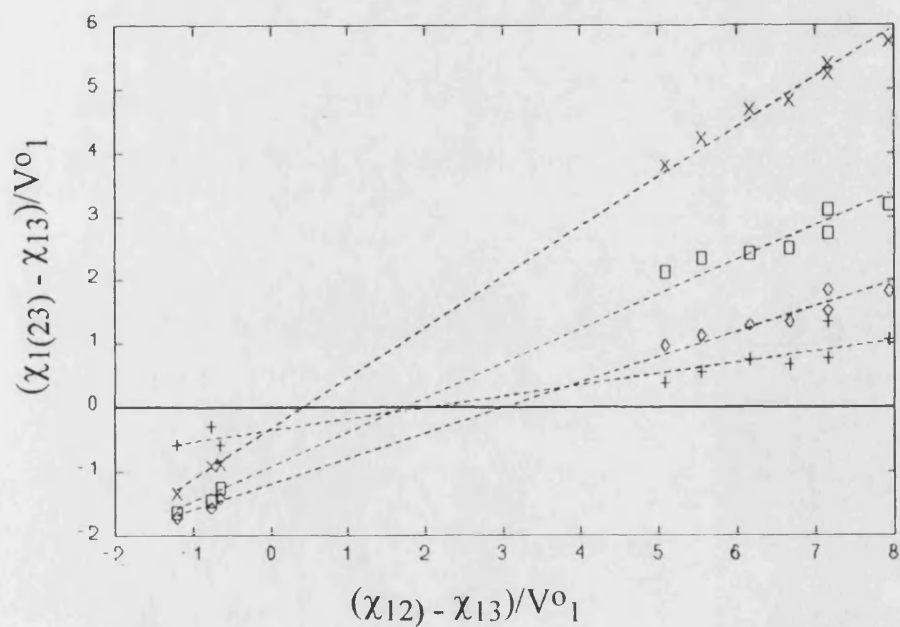
Figure 7.14: Deshpande-Farooque plots for 80 % ($^{w}/_{w}$) HCB, x, 60 % ($^{w}/_{w}$) HCB, □ 40 %

($^{w}/_{w}$) HCB, ◊, 20 % ($^{w}/_{w}$) HCB, +, at 90 °C.

Table 7.1: Interaction parameters measured between HCB and PDMS. Standard error of the intercept and compositions as weight percents

Phase	°C	80 % HCB	60 % HCB	40 % HCB	20 % HCB
I	95.0	0.49 (0.17)	1.04 (0.24)	1.39 (0.14)	0.68 (0.44)
	90.0	0.57 (0.21)	1.57 (0.32)	2.01 (0.21)	0.62 (0.33)
	85.0	0.45 (1.15)	1.41 (3.98)	1.81 (1.55)	0.41 (0.98)
	80.0	0.38 (0.21)	1.48 (0.34)	1.62 (0.17)	0.16 (0.35)
N	72.0	0.12 (0.11)	1.71 (0.26)	1.34 (0.25)	-0.42 (0.30)
	70.0	-0.01 (0.12)	1.43 (0.26)	1.33 (0.21)	-0.52 (0.24)
	65.0	0.11 (0.15)	1.23 (0.24)	1.30 (0.21)	-0.64 (0.20)
	60.0	0.13 (0.14)	1.29 (0.27)	1.00 (0.19)	-0.77 (0.16)
	58.0	-0.40 (0.29)	0.94 (0.32)	0.65 (0.20)	-0.87 (0.16)
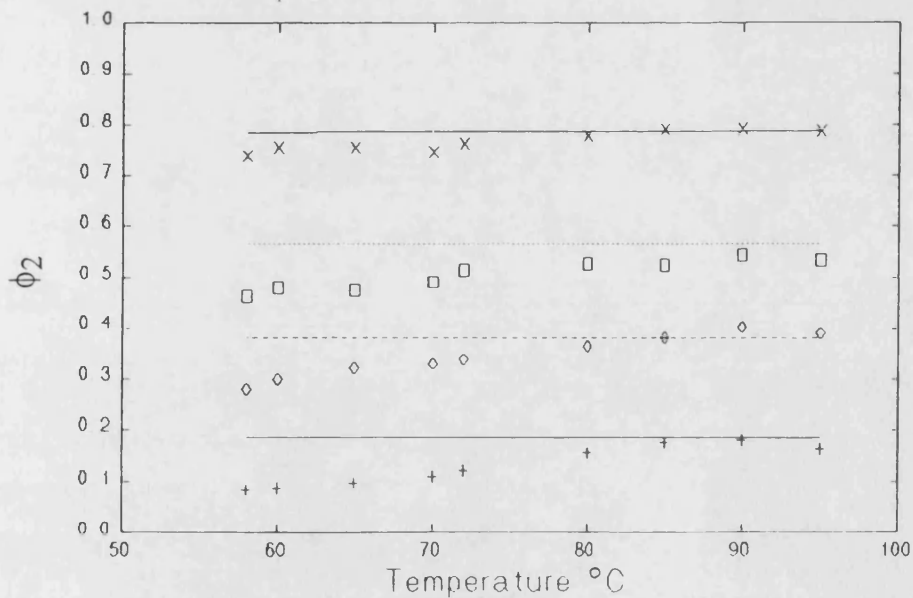
Figure 7.15: Effective volume fraction of HCB measured from the Deshpande-Farooque method. the dashed line is the calculated volume fraction predicted from the prepared composition

The sets of data were used along with data for the pure components, reported in chapter 6, to construct the appropriate plots from equation [1.57] at four temperatures in the isotropic phase and five temperatures in the nematic mesophase. *Figure 7.14* shows examples of these plots and illustrates that there was a good linear correlation for the data. The normalised interaction parameters between the stationary phase components, extracted from the intercept of these plots, are listed in *table 7.1* and the effective volume fraction of HCB the solvent probes is shown as a function of temperature in *figure 7.15*.

In the isotropic phase the predicted and measured volume fraction of HCB were in good agreement indicating that the solvent probes all the liquid crystal component. In the nematic mesophase the measured volume fraction of HCB decreased as temperature decreased and the effect became more prominent as the composition of PDMS increased. This indicates the probe was preferentially dissolving in the polymer component and the nematic phase results should be viewed with caution. However, the majority of the HCB component was probed for all systems and values will approach the true interaction parameter as the temperature is raised and the composition of HCB increased.

In *figure 7.16* the interaction parameters listed in *table 7.1* are plotted as a function of temperature and as a function of composition. The critical value for thermodynamically favourable interaction between the two components, calculated using the expression of Scott[212] given in equation [1.24], is also shown in the figure. There was a maximum in the interaction parameter as the composition changed exhibiting thermodynamically favourable interactions as HCB or PDMS became the minor component of the stationary phase. The observed trend was independent of temperature. The nematic phase exhibited lower values than the isotropic phase, generally. This could be a genuine effect but could equally be a consequence of the reduced portion of the HCB phase the solvent was probing. In the nematic phase the

a)
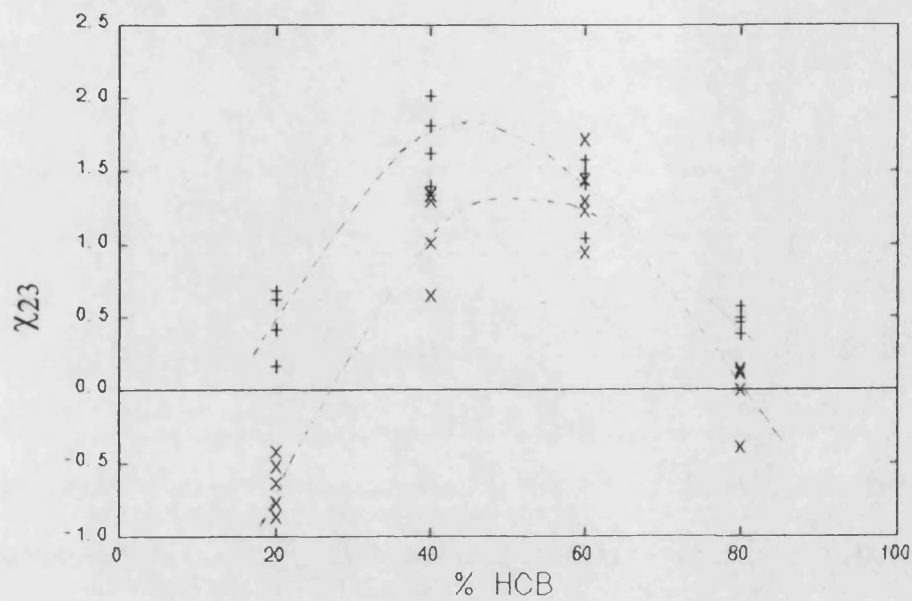
b)
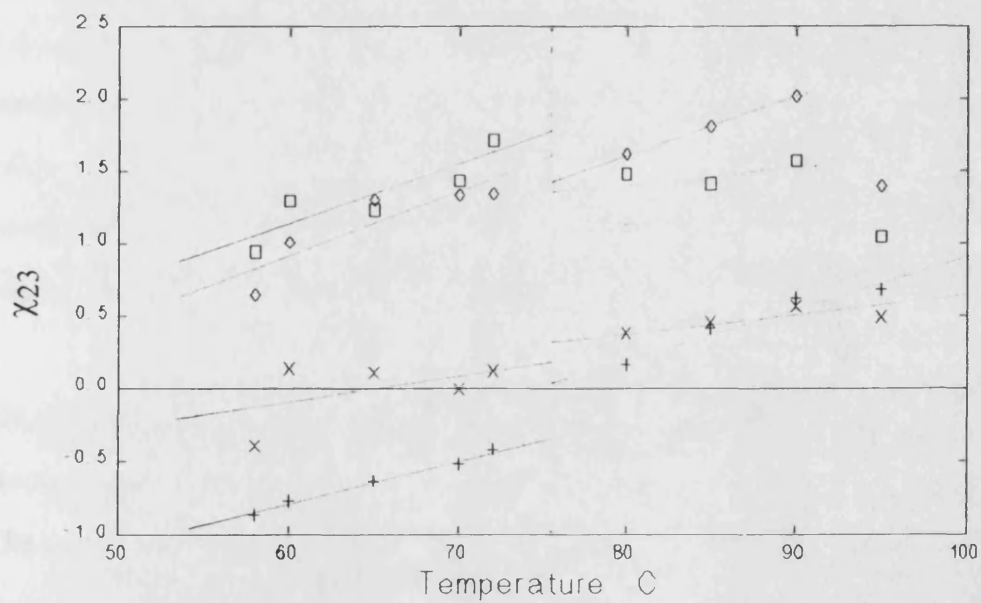
Figure 7.16: Interaction parameters between binary stationary phase components a) as a function of composition (+ isotropic phase, x nematic mesophase) and b) as a function of temperature (80 % HCB x, 60 % HCB □, 40 % HCB ◊, 20 % HCB)

interaction parameter increases with temperature for all compositions. This behaviour indicates the interaction between the two components became more favourable as the temperature decreased, which was contrary to the values between probe and stationary phase. This would suggest a specific orientation dependent interaction between HCB and PDMS. In the isotropic phase the interaction parameter shows no clear trend with temperature but values may have increased with temperature then decreased above 90 °C. The temperature dependence of values in the nematic mesophase, the lack of similar clear behaviour in the isotropic phase, and the negative values for some compositions in the nematic mesophase all suggest the presence of specific interactions between the two components. However, conclusions from the absolute values measured in this system must be treated sceptically, for reasons discussed above. The low values could alternatively be an artefact of the measuring technique. Indeed, such a phenomenon has been reported in systems where one component forms a glass[133]. The reason for such behaviour is unknown at present, but in glassy systems it is attributed to the enhanced interaction between the probe and the pure glassy state due to sorption at the dislocations within the glass[226]. From equation [1.57] it follows that this would lead to low interaction parameters between the stationary phase components. Whilst a possibility in the present system, it seems unlikely to apply here due to the greater fluidity of the mesophase than is found in a glass.

In this section the interaction parameter data suggest that thermodynamically favourable solutions between HCB and PDMS are possible at low PDMS composition. The solutions became unfavoured as the compositions became equivalent and then favoured again as the solution became PDMS rich. The implication is that fluid phases of HCB can interact with PDMS at certain compositions. Unlike the crystalline phase of HCB which phase separates from PDMS at all compositions. However, it is not clear why the observed phase behaviour occurs. Where HCB and PDMS interact the transition temperature would be expected to be lower than where the two components act independently. A possible explanation is that the size of the HCB crystallites

played an important role in the phase behaviour. First consider the two components acting independently with the HCB crystallites becoming smaller as the PDMS fraction increases. The crystalline region would be little effected by the polymer and the melting temperature would remain constant as the composition of the solution changed. However, the fluid mesophase could be constrained by the surrounding polymer. As the crystallites become smaller the effect becomes larger resulting in an increased mesophase order and consequently a higher clearing temperature. This effect would cause the clearing temperature to rise as the PDMS fraction increased. Second, consider the effect of PDMS interacting with HCB. As the fraction of PDMS increased the clearing temperature would be expected to become lower. However, if there was less interaction between the two components the lowering of the clearing temperature would be less. Considering these two effects of crystallite size and interaction it is possible to rationalise the observed behaviour as the result of the two competing effects. Down to 60 % ($^W/_w$) HCB the governing effect is the interaction between components with the lowering of the clearing temperature as PDMS fraction increased being lessened by the decreasing interaction. Below 60 % ($^W/_w$) HCB the crystallite size is significantly small enough for this to be the governing factor and the clearing temperature at first increased as the PDMS fraction increased and then lowered slightly as the interaction between components became favoured again. This picture is consistent with the observed interaction parameter data and the SEMs. The argument is also supported by the constancy of "effective degree of crystallinity" data between different compositions of HCB and PDMS below 60 % ($^W/_w$) HCB, reported in section 7.2. However, the investigation presented here was only in a preliminary form and the trends presented are fairly crude. Thus the above argument is, at present, conjecture that is self consistent with these crude preliminary observations of the binary stationary phase and further investigation is needed before the behaviour of this binary stationary phase is fully elucidated.

CHAPTER 8

CONCLUSIONS

Inverse gas chromatography has been shown to be a useful tool for studying the solution behaviour of liquid crystal systems, both as single component stationary phases and when the liquid crystal is combined with a second stationary phase component. Conclusions drawn from the observed results have been made throughout the previous chapters and in this chapter only the main points will be reiterated.

IGC is a technique capable of measuring transition temperatures within liquid crystals with a precision equal to that obtained by other methods such as DSC and HSM. In the systems studied the effect of coating the liquid crystal onto Chromosorb support had no significant effect on the observed transition temperatures. Although not necessarily the method of choice for transition temperature measurement, due to it being relatively slow compared to other methods, the technique has the advantage of also providing other data such as crystallinity or thermodynamic parameters. However, in the liquid crystal systems considered here there is evidence from IGC of a second order phase transition from the lowest temperature mesophase to a supercooled phase. Although the DSC results suggested the presence of a supercooled phase there was no evidence of a transition accompanying the onset of the supercooled phase. The DSC results did indicate the degree of supercooling was linked to the mobility of the molecules and that less mobile molecules would be likely to exhibit a greater degree of supercooling.

The IGC results about the melting transition allowed an estimation of the degree of crystallinity in the crystalline phases of the liquid crystals. The solid phases were shown to contain a portion of non-crystalline regions where materials with a larger rigid portion of the molecular structure formed more crystalline solid phases. It was also demonstrated that IGC has potential as a method for following kinetic transformations. The technique was used to monitor the rate of crystallisation of HCB

coated as a thin layer on Chromosorb. The crystallisation process occurred in two stages. Initially nucleation governed the process but as the Chromosorb surface became covered the number of nucleation sites diminished and the process proceeded by a slower process governed by the viscosity of the crystallising mesophase.

Within the isotropic phase or mesophase the IGC method was used to study the solution thermodynamics of solvent molecules tending to infinite dilution. The type of liquid crystal phase, and hence the molecular arrangement of the liquid crystals, played an important part in the solution behaviour observed. The nematic or cholesteric mesophase exhibited the greatest temperature dependence, consistent with these being the mesophases where the majority of the liquid crystal order is lost as temperature increases. These mesophases were influenced more than the isotropic phases by the entropic contributions to solution formation whilst the enthalpic interactions between probe and liquid crystal governed phase behaviour in the isotropic phases. Shape, rigidity, and branching within a probe all contributed to the solution behaviour with the liquid crystal but the effects arose mainly from changes in the strength of interaction between probe and liquid crystal molecules. The effect of liquid crystalline restriction on probe movement was a minor perturbation to the solution behaviour. Comparing OCB to HCB the observed trends are similar but OCB exhibited more favourable solution behaviour than HCB indicating the more favourable solution with the probes studied arises due to the increase in the alkoxy chainlength. The thermodynamic parameters follow similar trends in OBIB as well but the chirality increases the order within the mesophases of OBIB. The molecular shape of the probe became more important and the results indicate the increased order of OBIB reduces the interaction of a probe with the stationary phase. All low molar mass liquid crystals exhibited probe size and shape perturbations to the solution behaviour in the isotropic phase. This indicates the rod-like nature of the liquid crystal still imposed a degree of anisotropy to the probe molecule environment even when all liquid crystal order was lost.

Results for PDMS showed that the more favourable solutions were formed with the alkanes rather than the aromatic probes. This trend was opposite to that observed for the low molar mass liquid crystals. Hence, the similar trends in thermodynamic parameters between LCP and the low molar mass liquid crystals clearly indicate the mesogen governed the properties observed in LCP. However, in the isotropic phase of LCP thermodynamic parameters did not agree as closely with the low mass liquid crystal analogues. This indicates the polymer backbone had a greater effect on solution parameters in the isotropic phase.

Applying regular solution theory to the cyanobiphenyl liquid crystal systems showed that the theory is useful for determining potentially good solvents for liquid crystalline materials. However, the theory is semi-empirical and does not necessarily give the most thermodynamically ideal solvent. The theory suggests that both the low molar mass and polymeric cyanobiphenyls exhibit similar enthalpic interactions to each other within a liquid crystal phase at a given temperature. However, different cyanobiphenyls exhibit different mesophases. Regular solution theory implies that these arise due to the different entropy of interaction in different materials. Although the theory is only semi-quantitative the solubility parameters it yields for the liquid crystals are in general agreement with the observed solution behaviour.

Applying Flory-Huggins theory to the cyanobiphenyl systems yielded interaction parameters that corroborated the conclusions drawn from the activity coefficient data. The interaction parameter followed a reciprocal dependence with temperature and the nematic or cholesteric mesophase exhibited the greatest temperature dependence. The interaction parameters support the conclusion that the rigid mesogen governs the solution behaviour of a system and that the observed thermodynamic parameters are not governed by a preferential interaction with part of the liquid crystal molecule but by whether there is favourable or unfavourable interaction with the rigid mesogen.

However, results do not support the idea that probe molecules are excluded from any portion of the liquid crystal but indicate that all of the stationary phase is probed by the solvent.

In OCB the interaction parameters are independent of temperature for a few degrees above the smectic A to nematic transition temperature indicating the quadrupole formation, known to occur in the smectic phase, persists to some degree in the nematic phase. The extra chainlength of OCB compared to HCB has little effect on the interaction parameter indicating the more favourable solution formation between probe and OCB over that between probe and HCB arises from the effect of the longer chain on the entropy of mixing. In LCP the mesogen governs the solution behaviour but the interaction parameters imply the polymer backbone has a greater effect on the interaction between liquid crystal and probe than seen for the alkyl chains of HCB and OCB. This effect is greater in the isotropic phase and implies the presence of the polymer backbone has a greater influence on the phase behaviour of the mesogen than experienced by the presence of the alkyl chain in the low molar mass analogues.

In applying the Flory-Huggins theory to liquid crystal systems, in particular to the low molar mass materials, values and trends between probes could be affected by the approximations inherent in the theory. Although the values may be affected results presented here show that the trends between probes and the interpretations drawn from them are unaffected in the systems studied here. In fact a more rigorous description of solution behaviour based upon an equation of state approach yielded the same trends and corroborated results and conclusions from the Flory-Huggins theory. The equation of state approach allowed the interaction term to be disseminated into an enthalpic contribution and a "free-volume" effect. The results showed all the cyanobiphenyls had similar enthalpic contributions for a given liquid crystal-probe system suggesting differences between different liquid crystal systems arose from "free-volume" effects. A recent liquid crystal theory, based on the Flory-Huggins

theory, was also considered and the anisotropy of the liquid crystal molecules considered in this thesis was found to have a negligible effect on the interaction parameters measured by the simpler Flory-Huggins theory. This does not imply the anisotropy had no effect upon the interaction in solution between probe and liquid crystal, merely that according to the theory the rigid mesogen was not long enough or ordered enough to affect the combinatorial entropy of mixing.

The IGC method has also been used to briefly consider the behaviour of the solid surfaces of the liquid crystals and the Chromosorb support. It was shown that the Chromosorb support was not acting as an inert surface. However, the support did not exhibit any preferential adsorption of a particular type of probe. The liquid crystalline surfaces were shown to adsorb differently to the Chromosorb support and there was some evidence of differentiation between different probes. It was also shown that the liquid crystals studied formed different solid surfaces, even where the liquid crystal molecules were similar, in OCB and HCB. At present it is not clear whether this is due to differing surface areas or the chemical nature of the surface but the results indicate that IGC has potential for studying the solid surfaces of liquid crystal systems.

The results also show that IGC can be used to obtain information about binary stationary phase solutions containing liquid crystals. The brief study of separation properties of binary HCB-PDMS stationary phases shows that there is little advantage in mixing HCB with the polymer to effect separations in the systems studied here. The incompatible nature of the two components leads to a tendency for phase separation. However, by chemically "tethering" the mesogen to the polymer, as in LCP, improved characteristics are possible, though the systems considered here are far from optimum for chromatographic separation work. Of more relevance in the present system is the crystallisation behaviour and thermodynamics of solution formation.

IGC can be used to obtain estimates of crystallinity in binary stationary phases in a similar manner to the determinations in a pure liquid crystal stationary phase. To obtain good estimates the probe must be a good solvent for the mesophase and have comparatively poor adsorption on the crystalline surface, as for the pure liquid crystal measurements. With a binary stationary phase the probe must additionally be equally soluble in both components of the stationary phase. In the HCB-PDMS system the polymer was found to have a negligible effect on the degree of crystallinity but at high composition the PDMS appeared to be constraining the mesophase increasing the nematic order. DSC and IGC values for the transition temperatures indicate that PDMS does not blend with HCB and does not affect the melting temperature. However, as the composition of PDMS increased HCB appeared to form smaller crystallites. The SEM data support this conclusion. Although the crystalline HCB appears to phase separate from PDMS, the interaction parameters between PDMS and HCB indicate that the fluid liquid crystal phases do interact favourably with PDMS when the composition of PDMS is low. As the composition of PDMS increased the interaction became unfavourable up to the composition where the two components were 50:50 mix and then the interaction became favourable again as the PDMS composition increased. The changing interaction parameter and changing crystallite size result in the observed decrease in clearing temperature as the HCB composition approaches 60 % ($^w/_w$).

Thus, this thesis has shown that IGC is a technique that can be extended to study a range of properties in liquid crystal systems. Although the method is slow for transition temperature measurements compared to techniques such as DSC, it has been shown that IGC has the potential to detect subtle transition behaviour other techniques might miss. The work has also shown that IGC retention data for liquid crystal systems can be used to obtain solution theory parameters which usefully describe the solution behaviour of these systems and the method enables this data to be collected more quickly than other more traditional methods for studying solutions.

REFERENCES

REFERENCES

1   Collings, P. J. *"Liquid crystals: Nature's delicate phase of matter"*, Hilger Bristol, (1990)

2   Frank, F. C. *Disc. Farad. Soc.*, **25**, 19, (1958)

3   Reinitzer, F. *Monatsh. Chem.*, **9**, 421, (1888)

4   Lehmann, O. *Z. Phys. Chem. (Leipzig)*, **4**, 462, (1889)

5   *Disc. Farad. Soc. "Configurations and interactions of macromolecules and liquid crystals"*, **25**, (1958)

6   Gray, G. W., Harrison, K. J., and Nash, J. A., *Electron. Lett.*, **9**, 130, (1973)

7   a) Jackson, W. J. Jnr., and Kuhfuss, H., *J. Polym. Sci. Polym. Chem. Ed.*, **14**, 2043, (1976); b) Roviello, A., Sirigu, A., *J. Polym. Sci. Polym. Lett. Ed.*, **13**, 455, (1975)

8   Finkelmann, H., Ringsdorf, H., and Wendorff, J. H., *Makromol. Chem.*, **179**, 273, (1978)

9   McArdle, C. B. *"Side chain liquid crystal polymers"*, Blackie London, (1989)

10   Williams, D. J., *Advances in Polym. Technology*, **10**(3), 173, (1990)

11   Noël, C., and Patrick, N., *Progress in Polym. Sci.*, **16**, 55, (1991)

12   *Merck liquid crystal polymers catalogue*, MerckUK (Poole)

13   a) Dutta, D., Fruitwala, H., Kohli, A., and Weiss, R. A., *Polym. Eng. and Sci.*, **30**(17), 1005, (1990); b) reference 9, *Chapter 14*

14   Freidel G., *Ann. Physique*, **18**, 273, (1922)

15   Gray, G. W., and Goodby, J. W. G., *"Smectic liquid crystals"*, Leonard Hill London, (1984)

16   Gray, G.W. *"Thermotropic liquid crystals"*, Wiley Chichester, (1987)

17   Witkiewicz, Z., *J. Chromatography Chromatogr.Rev.*, **251**, 311, (1982)

18   Young, R. J., and Lovell, P. A., *"Introduction to polymers"* 2nd ed., Chapman Hall London, (1991)

19   Reference 9, Chapter 4

20   Reference 9, Chapter 3.3

21   Reference 9, Chapter 3.4

22   Atkins, P. W., *"Physical chemistry"* 3rd ed. Chapter 8, Oxford University Press Chichester, (1986)

23   Raoult, F. M., *Z. Physik. Chem.*, **2**, 353, (1888)

24   Guggenheim, E. A., *Trans. Farad. Soc.*, **33**, 151, (1936)

25   Stern, O., *Ann. Physik.*, **49**(4), 823, (1916)

26   Henry, W., *Phil. Trans. Roy. Soc. (London)*, **29**, 274, (1803)

27   Hildebrand, J. H., and Scott, R. L., *"Regular solutions"* Chapter 3, Prentice Hall New Jersey, (1962)

28   Everett, D. H., *"Chemical Thermodynamics"* 2nd ed., Longmann London, (1971)

29   Lewis, G. N., *Z. Physik. Chem.*, **61**, 129, (1908)

30   Conder, J. R., and Young, C. L., *"Physicochemical measurement by gas chromatography"* Chapter 5, Wiley Chichester, (1979)

31   Rowlinson, J. S., and Swinton, F. L., *"Liquids and liquid mixtures"* 3rd ed. *p.176*, Butterworths London, (1982)

32   Tompa, H., *"Polymer solutions"* Chapter 2, Academic Press London, (1956)

33   Hildebrand, J. H., *J. Amer. Chem. Soc.*, **51**, 66, (1929)

34   Reference 27, Chapter 1, *p4*

35   *ibid.*, Chapter 7

36   Scatchard, G., *Chem. Rev.*, **8**, 321, (1931)

37   van Laar, J. J., *Z. Physik. Chem.*, **83**, 599, (1913)

38   Guggenheim, E. A., *"Mixtures"* Chapter 4, Clarendon Press Oxford, (1952)

39   London, F., *Z. Physik.*, **63**, 245, (1930)

40   a) Reference 38, Chapter 3; b) Reference 27, Chapter 3

41   Fowler, R. H., and Rushbrooke, G. S., *Trans. Farad. Soc.*, **33**, 1272, (1937)

42   Reference 18, Chapter 3.2

43 a) Huggins, M., *J. Chem. Phys.*, **9**, 440, (1941); b) Ann. N. Y. Acad. Sci., **43**, 1, (1942)

44 a) Flory P. J., *J. Chem. Phys.*, **9**, 660, (1941); b) *ibid*, **10**, 51, (1942)

45 Reference 32, Chapter 4

46 Guggenheim E. A., *Proc. Roy. Soc. A*, **183**, 203, (1944)

47 a) Scott, R. L., *J. Chem. Phys.*, **17**(3), 268, (1949); b) *ibid.* 279

48 Reference 38, Chapter 12

49 Flory, P. J., *Disc. Farad. Soc.*, **49**, 7, (1970)

50 a) Reference 32, Chapter 5; b) Reference 53b

51 Freeman, P. I., and Rowlinson, J. S., *Polymer*, **1**, 20, (1957)

52 Reference 27, Chapter 5

53 a) Huggins, J., *Phys. Chem.*, **52**, 248, (1948); b) Hildebrand, J. H., *Disc. Farad. Soc.*, **15**, 9, (1953); c) Longuet-Higgins, H. C., *ibid.*, **15**, 73, (1953)

54 Ito, K., and Guillet, J. E., *Macromolecules*, **12**, 1163, (1979)

55 Lipson, J. E. G., and Guillet, J. E., *"Macromolecular solutions: solvent-property relationships in polymers"*, eds. Seymour, R. B., and Stahl, G. A., Pergamon Press New York, (1982)

56 a) Prigogine, I., Mathot, V., and Trappeniers, N., *J. Chem. Phys.*, **21**, 559, (1953); b) *ibid.*, *Disc. Farad. Soc.*, **15**, 93, (1953)

57 Lennard-Jones, J. E., *Proc. Roy. Soc.(London) A*, **112**, 214, (1926)

58 a) Bhattacharya, S. N., and Patterson, D., *Polymer*, **6**, 455, (1965); b) Patterson, D., *Macromolecules*, **2**, 672, (1969); c) Patterson, D., Tewari, Y. B., and Schreiber, H. P., *J. Chem. Soc. Farad. II*, **70**, 837, (1974)

59 Dee, G. T., and Walsh, D. J., *Macromolecules*, **21**, 815, (1988)

60 a) Flory, P. J., Orwoll, R. A., and Vrij, A., *J. Amer. Chem. Soc.*, **86**, 3507, (1964); b) *ibid.*, **86**, 3515, (1964)

61 Dee, G. T., and Walsh, D. J., *Macromolecules*, **21**, 811, (1988)

62   Tan, Z., (1993), private communication citing; a) Lipson, J. E. G., and

     Andrews S. S., *J. Chem. Phys.*, **96**, 1426; b) Simha, R., and Somcynsky, T.,

     Macromolecules, **2**, 342, (1969); c) Sanchez, I. C., and Balazs, A. C.,

     Macromolecules, **22**, 2326, (1989)

63   a) Nies, E., and Cifra, P., *Macromolecules*, **27**, 6033, (1994); b) Jonah, D. A.,

     Brostow, W., and Hess M., *Macromolecules*, **26**, 76, (1993); c) Blonski, S.,

     Brostow, W., Jonah, D. A., and Hess, M., *ibid.*, **26**, 84, (1993)

64   a) Fujisawa, K., Shiomi, T., Hamada, F., and Nakajima, A., *Polymer J.*, **13**(11),

     993, (1981); b) references 61 and 62

65   Reference 27, Chapter 6, p81

66   Hansen, C. M., *J. Paint Technol.*, **39**, 104, (1967)

67   a) Voelkel, A., and Janas, J., *J. Chromatography A*, **669**, 89, (1994);

     b) Munk, P., and Tian, M., *"A.C.S. Symposium series"*, **207**, March (1994),

     460

68   Eichinger, B. E., and Flory, P. J., *Trans. Farad. Soc.*, **64**, 2035, (1968)

69   Maier, W., and Saupe A., *Z. Naturforsch.*, **15a**, 287, (1960)

70   Chandrasekhar, S., *"Liquid crystals" 2nd ed.*, Cambridge University Press

     Cambridge, (1992)

71   Chow L. C., and Martire D. E., *J. Phys. Chem.*, **75**, 2005, (1971)

72   a) Willey, D. G., and Brown, G. H., *J. Phys. Chem.*, **76**, 99, (1972);

     b) Oweimreen, G. A., *J. Solution Chem.*, **11**, 105, (1982)

73   a) Martire, D. E., and Yan C., *J. Phys. Chem.*, **96**, 7510, (1992); b) *ibid.*, **96**,

     3489, (1992)

74   Cotter, M. A., and Martire, D. E., *Mol. Cryst. Liq. Cryst.*, **7**, 295, (1969)

75   Martire, D. E., *J. Chromatography*, **406**, 27, (1987)

76   Flory, P. J., *Proc. Roy. Soc. A*, **234**, 73, (1956)

77   Flory, P. J., and Ronca, G., *Mol. Cryst. Liq. Cryst.*, **54**, 289, (1979)

78   *ibid.*, **54**, 311, (1979)

79   Flory, P. J., and Abe, A., *Macromolecules*, **11**, 1119, (1978)

80   Flory, P. J., and Irvine, P. A., *J. Chem. Soc. Farad. Trans. 1*, **80**, 1807, (1984)

81   References 63b and 63c

82   Matheson, R. R. Jnr., and Flory, P. J., *Macromolecules*, **14**, 954, (1981)

83   Reference 63c

84   Orwoll, R. A., *Rubber Chem. Technol.*, **50**, 451, (1977)

85   Bonner, D. C., *J. Macromol. Sci. Revs. Macromol. Chem. C*, **13**(2), 263, (1975)

86   Nehage, G., and Meys, H., *J. Polym. Sci.*, **30**, 271, (1958)

87   Ashworth, A. J., and Price, G. J., *Thermochimica Acta.*, **82**, 161, (1984)

88   Price, G. J., Ph. D. Thesis, *University of Bath*, (1984)

89   a) Conder, J. R., and Purnell, J. H., *Trans. Farad. Soc.*, **64**, 1505, (1968); b) *ibid.* **64**, 3100, (1968); c) *ibid.*, **65**, 824, (1968)

90   a) Brockmeier, N. F., Mc Coy, R. W., and Meyer, J. A., *Macromolecules*, **5**, 130, (1972); b) *ibid.*, **5**, 464, (1972)

91   Tswett, M., *Ber. Deutsch. Botan. Ges.*, **24**, 316, (1906)

92   Glueckauf, E., *J. Chem. Soc. (London)*, 1302, (1947)

93   James, A. T., and Martin, A. J. P., *Biochem. J.*, **50**, 679, (1952)

94   Lipson J. E. G., and Guillet, J. E., *"Developments in polymer characterisation 3"* Chapter 2, ed. Dawkins, J. V., Applied Science Publishing Barking, (1982)

95   Munk, P., *"Modern methods of polymer characterisation"* Chapter 5, eds. Barth, H. G., and Mays, J. W., Wiley Chichester, (1991)

96   Schreiber, H. P., and Lloyd, D. R., *"Inverse gas chromatography A.C.S Symposium series"* Chapter 1, **391**, eds. Lloyd, D. R., Ward, T. C., and Schreiber, H. P., (1989)

97   Reference 30, Chapter 8

98   Ashworth, A. J., and Everett, D. H., *Trans. Farad. Soc.*, **56**, 1609, (1960)

99   McGlashan, M. L., and Williamson, A. G., *Trans. Farad. Soc.*, **57**, 588, (1961)

100   Ashworth, A. J., *J. Chem. Soc. Farad. 1*, **69**, 459, (1973)

101   Summers, W. R., Tewari, Y. B., and Schreiber, H. P., *Macromolecules*, 5, 12, (1972)

102   Hammers, W. E., and de Ligny, C. L., *J. Polym. Sci. Phys. Edn.*, 12, 2665, (1974)

103   Lichtenthaler, R. N., Liu, D. D., and Prausnitz, J. M., *Berichte der Bunsen-Gesellshaft*, 78(5), 470, (1974)

104   Cheng, Y. L., and Bonner, D. C., *Macromolecules*, 7, 687, (1974)

105   Ashworth, A., J., Chein, C.-F., Furio, D. L., Hooker, D. M., Kopecni, M. M., Laub, R. J., and Price, G. J., *Macromolecules*, 17, 1090, (1984)

106   Littlewood, A. B., Phillips, C. S. G., and Price, D. T., *J. Chem. Soc.*, 1480, (1955)

107   Everett, D. H., *Trans. Farad. Soc.*, 61, 1637, (1965)

108   Reference 22, Chapter 7

109   Aspler, J. S., and Gray, D. G., *Macromolecules*, 12, 562, (1979)

110   Moegel, H. J., Kraus, G., and Novak, M., *J. Chromatography*, 324, 29, (1985)

111   Smidsrod, O., and Guillet, J. E., *Macromolecules*, 2, 272, (1969)

112   Gray, D. G., and Guillet, J. E., *Macromolecules*, 4, 129, (1971)

113   Braun, J-M., and Guillet, J. E., *Macromolecules*, 10, 101, (1977)

114   Guillet, J. E., A.C.S. Symposium, (March 1994), San Diego, Introduction to IGC section; Reference 94

115   Stein, A. N., Gray, D. G., and Guillet, J. E., *British Polym. J.*, 3, 175, (1971)

116   Al Saigh, Z., *Polymer preprints A.C.S. Symposium*, Washington D.C., 33, 367 (August 1992)

117   Patterson, D., Tewari, Y. B., Schreiber, H. P., and Guillet, J. E., *Macromolecules*, 4, 356, (1971)

118   Ashworth, A. J., and Price, G. J., *Macromolecules*, 19, 358, (1986)

119   Parcher, J. F., Hansborough, J. R., and Koury, A. M., *J. Chromatogr. Sci.*, 16, 183, (1978)

120   Lichtenthaler, R. N., Liu, D. D., and Prausnitz, J. M., *Macromolecules*, 7, 565, (1974)

121   de Vries, M. J., and Smit, J. H., *J. S. African Chem. Inst.*, 20, 11, (1967)

122   Sa, M. M., and Sereno, A. M., *J. Chromatography*, 600, 341, (1992)

123   Kontominas, M. G., Gavara, R., and Giacin, J. R., *Eur. Polym. J.*, 30(2), 265, (1994)

124   a) Panzer, U., and Schreiber, H. P., *Macromolecules*, 25, 3633, (1992);

        b) Mukhopadhyay, P., and Schreiber, H. P., *Macromolecules*, 26, 6391, (1993)

125   a) DiPaola-Baranyi, G., and Guillet, J. E., *Macromolecules*, 11, 228, (1978);

        b) references 54 and 55

126   Price, G. J., *"Inverse gas chromatography A.C.S Symposium series"*

        Chapter 5, 391, eds. Lloyd, D. R., Ward, T. C., and Schreiber, H. P., (1989)

127   a) Choi, P., Kavassalis, T., and Rudin, A., *"A.C.S. Symposium series"*, 207,

        March (1994), 472; b) Reference 67a

128   Deshpande, D. D., Patterson, D., Schreiber, H. P., and Su, C. S.,

        Macromolecules, 7, 530, (1974)

129   Mandel, B. M., Bhattacharya, C., and Bhattacharyya, S. N., *J. Macromol. Sci.*

        Chem. A, 26(1), 175, (1989)

130   Price G. J., *"Advances in chromatography"* Chapter 3, 28, eds. Giddings J. C.,

        Grushka, E., and Brown, P. R., New York Marcel Dekker, (1989)

131   Laub, R. J., and Purnell, J. H., *Analytical Chem.*, 48, 799, (1976)

132   Riedl, B., and Prud'homme, R. E., *Polym. Eng. Sci.*, 24(17), 1291, (1984)

133   Su, C. S., and Patterson, D., *Macromolecules*, 10, 708, (1977)

134   Shi, R. H., and Schreiber, H. P., *Macromolecules*, 24, 3522, (1991)

135   Prolongo, M. G., Masegosa, R. M., and Horta, A., *Macromolecules*, 22, 4346, (1989)

136   Sanchez, I. C., *Polymer*, 30, 471, (1989)

137   Chee, K. K., *Polymer*, 31, 1711, (1990)

138   Farooque, A. M., and Deshpande, D. D., *Polymer*, 33, 5005, (1992)

139 Etxeberria, A., Uriarte, C., Fernandez-Berridi, N. J., and Iruin, J. J., *Polymer*, **35**, 2129, (1994)

140 Galin, M., and Rupprecht, M. C., Macromolecules, **12**, 506, (1979)

141 Hinshaw, J. V., *LC-GC INT.*, **6**(10), 604, (1993)

142 Haky, J. E., and Muschik, G. M., *J. Chromatography*, **214**, 161, (1981)

143 a) Reference 142 and citations therein; b) Citations in reference 17

144 a) Martire, D. E., Blasco, P. A., Carone, P. F., and Chow, L. C., *J. Phys. Chem.*, **72**, 3489, (1968); b) Chow, L. C., and Martire, D. E., *ibid.*, **73**, 1127, (1969); c) Reference 71

145 Marciniak, W., and Witkiewicz, Z., *J. Chromatography*, **207**, 333, (1981)

146 Kelker, H., *Ber. Bunsenges J. Phys. Chem.*, **67**, 698, (1963)

147 Janini, G. M., Muschik, G. M., and Hanlon, C. M., *Mol. Cryst. Liq. Cryst.*, **53**, 15, (1979)

148 Jawdosiuk, M., and Czarnecka, E., *Wiad. Chem.*, **31**, 329, (1977)

149 a) Wasik, S., and Chester, S., *J. Chromatography*, **122**, 451, (1976);
b) Janini, G. M., Sato, R. I., and Muschik, G. M., *Analytical Chem.*, **52**, 2417, (1980)

150 a) Bocquet, J. F., and Pommier, C., *J. Chromatography*, **205**, 239, (1981);
b) *ibid.*, **205**, 251, (1981); c) *ibid.*, **261**, 11, (1983)

151 a) Coca, J., Medina, I., and Langer, S. H., *Chromatographia*, **25**(9), 825, (1988); b) Coca, J., Medina, I., Langer, S. H., *Liquid Cryst.*, **4**(2), 175, (1989)

152 a) Ghodbane S., Oweimreen, G. A., Lin, G. C., and Martire, D. E., *J. Phys. Chem.*, **83**, 2111, (1979); b) Oweimreen, G. A., *Mol. Cryst. Liq. Cryst.*, **68**, 257, (1981); c)reference 72b; d) Ghodbane, S., Oweimreen, G. A., and Martire, D. E., *J. Chromatography*, **556**, 317, (1991)

153 Oweimreen, G. A., and Shihab, A-K. I., *J. Chem. Eng. Data*, **39**, 266, (1994)

154 Price, G. J., and Shillcock, I. M., *Polymer*, **34**, 85, (1993)

155 Gray, G. W., Harrison, K. J., and Nash, J. A., *Proc. Inf. Conf. Liq. Cryst. 1973 Pramana Suppl.*, ed. Chandrasekhar S., (1), 381, (1975)

156   Reference 9, Chapter 14

157   Rokushika, S., Naikwadi, K. P., Jadhav, A. L., and Hatano, H., *J. High Res. Chromatogr. Chromatogr. Commun.*, **8**, 480, (1985)

158   a) Romansky, M., and Guillet, J. E., *Polymer*, **35**, 584, (1994);

       b) Romansky, M., Smith, P. F., Guillet, J. E., and Griffin, A. C.,

       Macromolecules, **27**, 6297, (1994)

159   a) Szulc, J., Witkiewicz, Z., and Ziolek, A., *J. Chromatography*, **262**, 161,

       (1983); b) Reference 13

160   Janini, G. M., Muschik, G. M., Issaq, H. J., and Laub, R. J., *Analytical Chem.*,

       60, 1119, (1988)

161   Martin, R. L., *Analytical Chem.*, **33**, 347, (1961)

162   Martire, D. E., Pecsok, R. L., and Purnell, J. H., *Trans. Farad. Soc.*, **61**, 2496,

       (1965)

163   Conder, J. R., Locke, D. C., and Purnell, J. H., *J. Phys. Chem.*, **73**, 700, (1969)

164   Lipson J. E. G., and Guillet, J. E., *"Developments in polymer characterisation*

       3" Chapter 2, ed. Dawkins, J. V., Applied Science Publishing Barking, (1982)

165   a) Card, T. W., Al-Saigh, Z. Y., and Munk, P., *Macromolecules*, **18**, 1030,

       (1985); b) Reference 95

166   Reference 30, Chapter 11

167   Witkiewicz, Z., *J. Chromatography*, **200**, 65, (1980)

168   Conder, J. R., Ibrahim, N. K., Rees, G. J., and Oweimreen, G. A., *J. Phys.

       Chem.*, **89**, 2571, (1985)

169   Chow, L. C., and Martire, D. E., *J. Phys. Chem.*, **73**, 1127, (1969)

170   Witkiewicz, Z., *J. Chromatography*, **188**, 107, (1980)

171   Haky, J. E., and Muschik, G. M., *J. Chromatography*, **238**, 367, (1982)

172   Adamski, P., Dylik-Gromiec, A., Klimczyk, S., and Wojceichowski, M., *Mol.

       Cryst. Liq. Cryst.*, **35**, 171, (1976)

173   Liu, X., Hu, S., Shi, L., Xu, M., Zhou, Q., and Duan, X., *Polymer*, **30**, 273,

       (1989)

174 Cheng, S. Z. D., *Macromolecules*, **21**, 2475, (1988)

175 a) Price, F. P., Wendorff, J. H., *J. Phys, Chem.*, **75**, 2839, (1971); b) *ibid.*, **75**, 2849, (1971); c) Price, F. P., and Fritzche, A. K., *ibid.*, **77**, 396, (1973)

176 a) Avrami, M., *J. Chem. Phys.*, **7**, 1103, (1939); b) *ibid.*, **8**, 212, (1940)

177 Alger, M. *"Polymer science dictionary"*, Elsevier New York, (1990)

178 Campoy, I., Marco, C., Gomez, M. A., and Fatou, J. G., *Macromolecules*, **25**, 4392, (1992) and references cited therein

179 a) Cheng, S. Z. D., and Wunderlich, B., *Macromolecules*, **21**, 3327, (1988); b) Reference 174

180 Reference 18, Chapter 3.17

181 *"Polymer handbook"* 3rd. ed., eds. Brandrup, J., and Immergut, E. H., Wiley Chichester, (1989)

182 Peterson, M. L., and Hirsch, J., *Lipid Res.*, **1**, 132, (1959)

183 Bolvari, A. G., Ward, T. C., Koning, P. A., and Sheehy, D. P., *"Inverse gas chromatography A.C.S Symposium series"* Chapter 2, **391**, eds. Lloyd, D. R., Ward, T. C., and Schreiber, H. P., (1989)

184 Brunauer, S., Emett, P. H., and Teller, E., *J. Am. Chem. Soc.*, **60**, 309, (1938)

185 Shaw, D. J. *"Introduction to colloid and surface chemistry"* 3rd ed., Butterworths London (1986), p125

186 Reference 145

187 Flory, P. J., *Macromolecules*, **1**, 285, (1969)

188 reference 30, *Chapter 2*

189 Reference 31, Chapter 2, p20

190 *"Selected values of the properties of hydrocarbons and related compounds"*, TRC Data project, College Station Texas, (1965), and subsequent revisions

191 CRC *"Handbook of chemistry and physics"* 52nd ed., Chemical Rubber Co., Cleveland, (1971)

192 McGlashan, M. L., and Potter, D. J. B., *Proc. Roy. Soc. London A*, **267**, 478, (1962)

193   Reid, R. C., Prausnitz, J. M., and Sherwood, T. K., *"The properties of gases and liquids"* 3rd. ed., McGraw-Hill New York, (1977)

194   a) Dreisbach, R. R., *"Physical properties of chemical compounds"* Adv. Chem. Ser. A.C.S., 15, Washington, (1955); b) ibid. 22, (1959)

195   Dymond, J. H., and Smith, E. B., *"The virial coefficients of pure gases and mixtures, a critical compilation"*, Clarendon Press Oxford, (1980)

196   a) Abe, A., and Flory, P. J., *J. Am. Chem. Soc.*, 87, 1838, (1965);

       b) Reference 60

197   Streitweiser, A. Jnr., and Heathcock, C. H., *"Introduction to organic chemistry"* 3rd. ed. Chapter 30, Macmillan London, p971

198   *Merck liquid crystals catalogue*, MerckUK (Poole)

199   Reference 70, Chapter 2

200   Cladis, P. E., Bogardus, R. K., and Aadsen, D., *Phys. Rev. A*, 18(5), 2292, (1978)

201   West, A. R. *"Solid state chemistry and its applications"* Chapter 18.2, Wiley Chichester, (1986)

202   Llorente, M. A., Menduina, C. and Horta, A., *J. Polym. Sci. Polym. Phys. Edn.*, 17, 189, (1979)

203   Kelker, H., *Z. Anal. Chem.*, 198, 254, (1963)

204   Jabarin, S. A., and Stein, R. S., *J. Phys. Chem.*, 77, 409, 1973

205   Reference 70, Chapter 5.6

206   Cladis, P. E., Bogardus, R. K., Daniels, W. B., and Taylor, G. N., *Phys. Rev. Lett.*, 39, 720, 1977

207   Meyer, E. F., *J. Chem. Educ.*, 50(3), 191, 1973

208   Reference 22, Chapter 24.1

209   Shillcock, I. M., Project report, 527, *University of Bath*, (1991)

210   a) reference 70, *Chapter 5*; b) reference 9, *Chapter 2*

211   a) Gray, G. W., Lydon, *Nature*, 252, 221, (1974); b) reference 200

212   Reference 47b)

213   Reference 18, Chapter 3.2

214   Reference 32, Chapter 3

215   Price, G. J., and Dent, M. R., *J. Chromatography*, **585**, 83, (1991)

216   Chein, C.-F., Kopecni, M. M., Laub, R. J., and Smith, C. A., *J. Phys. Chem.*,
        85, 1864, (1981)

217   Parcher, J. F., Weiner, P. H., Hussey, C. L., and Westlake, T. N., *J. Chem.
        Eng. Data*, **20**, 145, (1975)

218   Deshpande, D. D., Patterson, D., Schreiber, H. P., and Su, C. S.,
        Macromolecules, **7**, 531, (1974)

219   Galin, M., *Macromolecules*, **10**, 1239, (1977)

220   a) Roth, M., and Novak, J., *Macromolecules*, **19**, 364, (1986) and references
        cited therein; b) References 101, 218, 219, and 221

221   Tseng, H.-S., and Lloyd, D. R., *J. Applied Polym. Sci.*, **30**, 307, (1985)

222   Reference 125a

223   Price, G. J., and Guillet, J. E., *J. Solution Chem.*, **16**, 605, (1987)

224   Reference 18, Chapter 4.4

225   Chahal, R. S., Kao, W.-P., and Patterson, D., *J. Chem. Soc. Farad. Trans. I*,
        69, 1834, (1973)

226   Kambour, R. P., Ramagosa, E.-E., and Gruner, C. L., *Macromolecules*, **5**, 335,
        (1972)

APPENDICES

APPENDIX I

Van't Hoff plots (ln V^o_g vs 1000/T) for all systems studied:

HCB: n-Alkanes
ln V^og vs 1000/T

HCB: Aromatic probes
ln V^og vs 1000/T
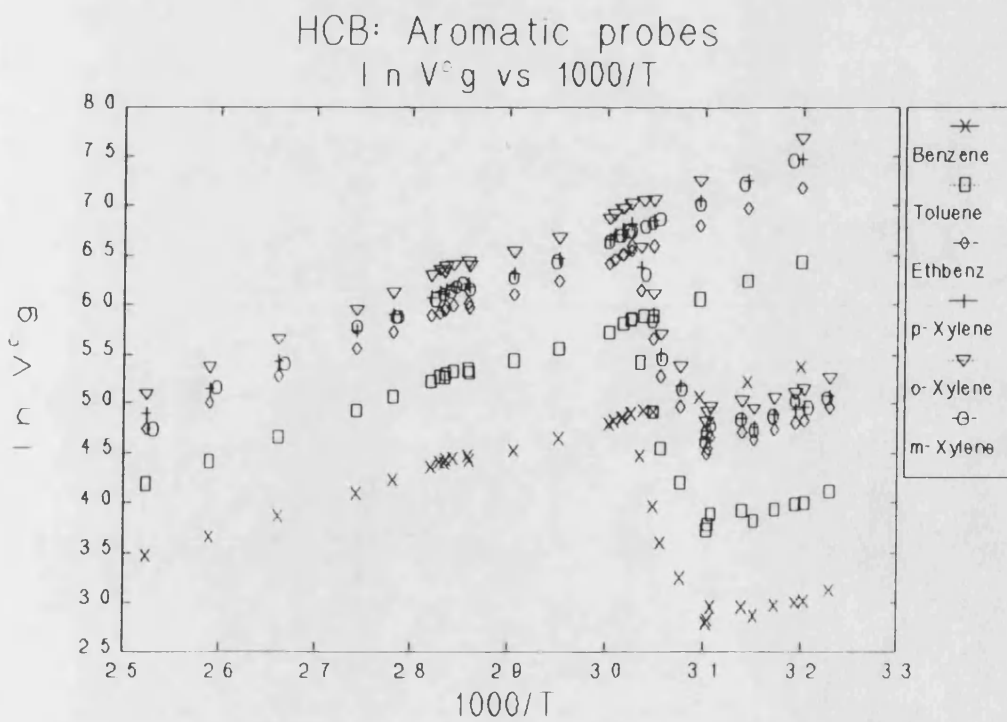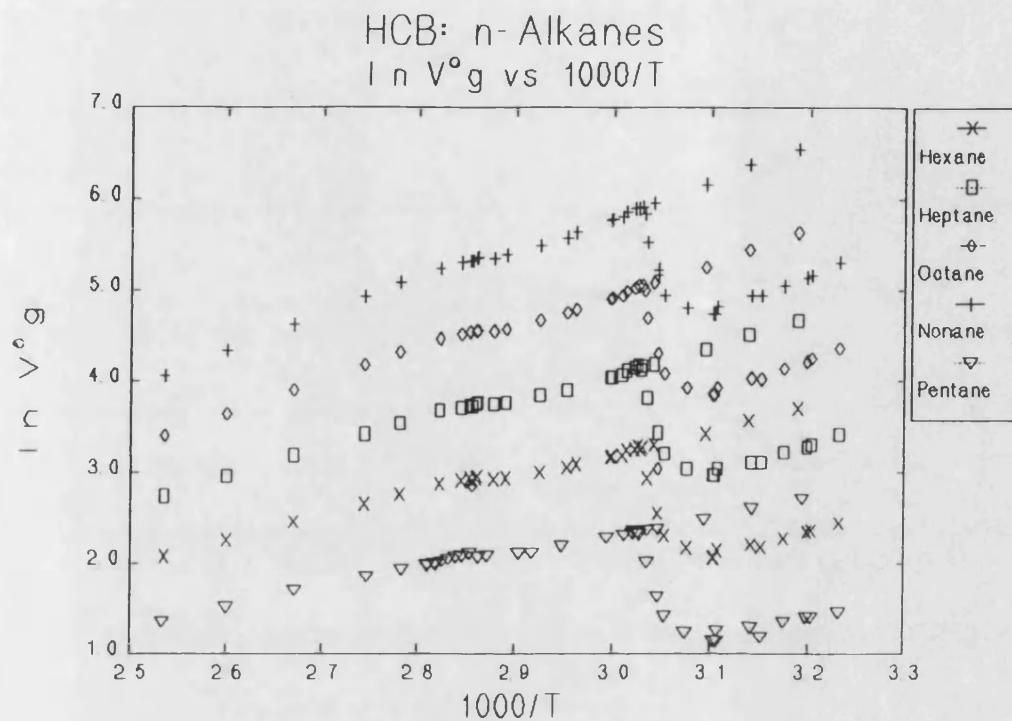
HCB: "C6" probes
l n V°g vs 1000/T
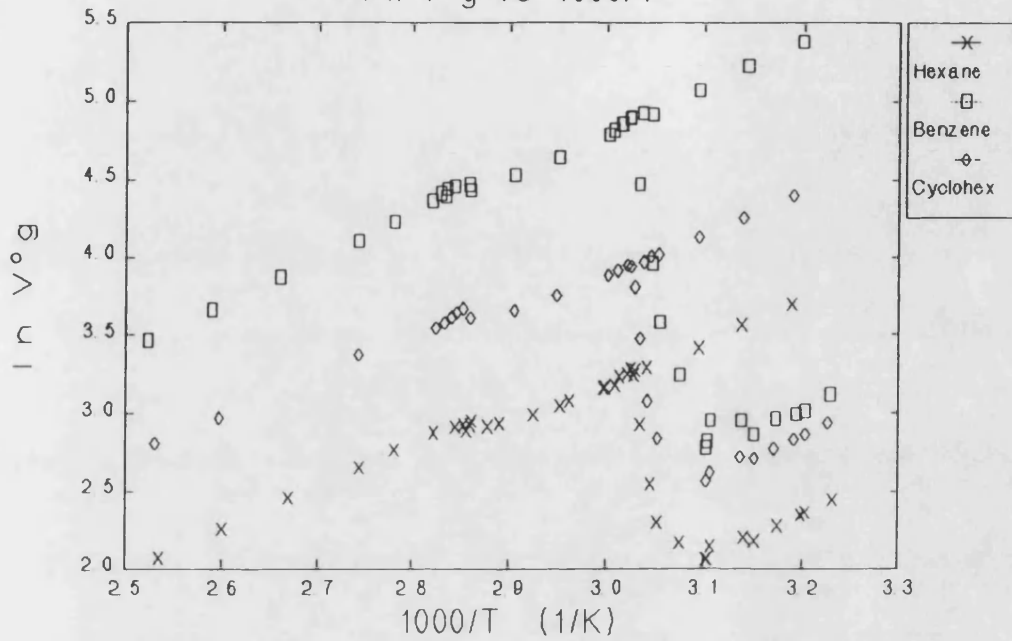
HCB: Heptane isomers
l n V°g vs 1000/T
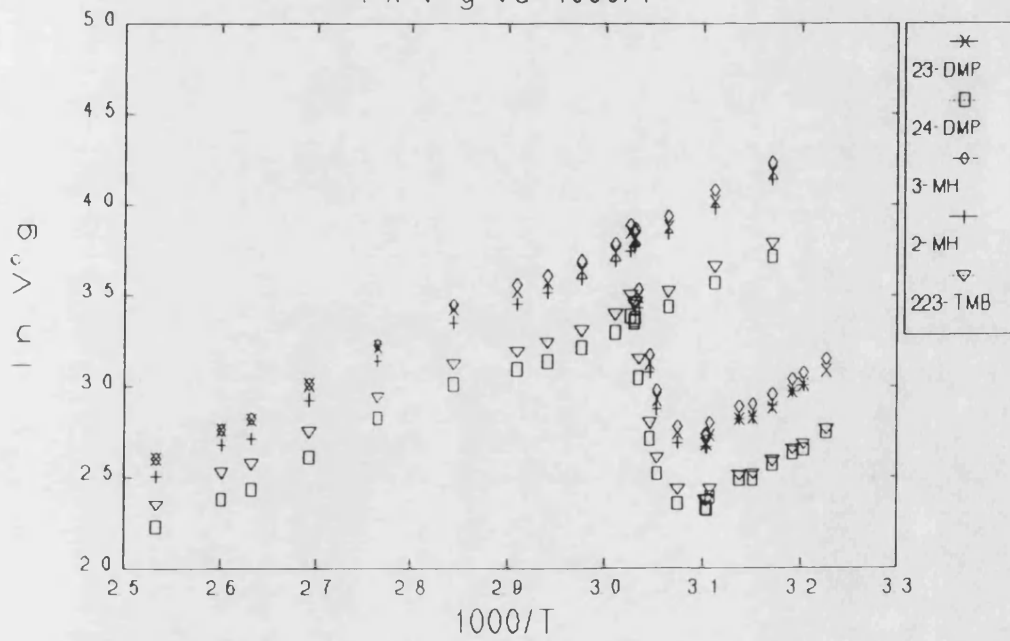
OBIB: Aromatic probes
l n V°g vs 1000/T
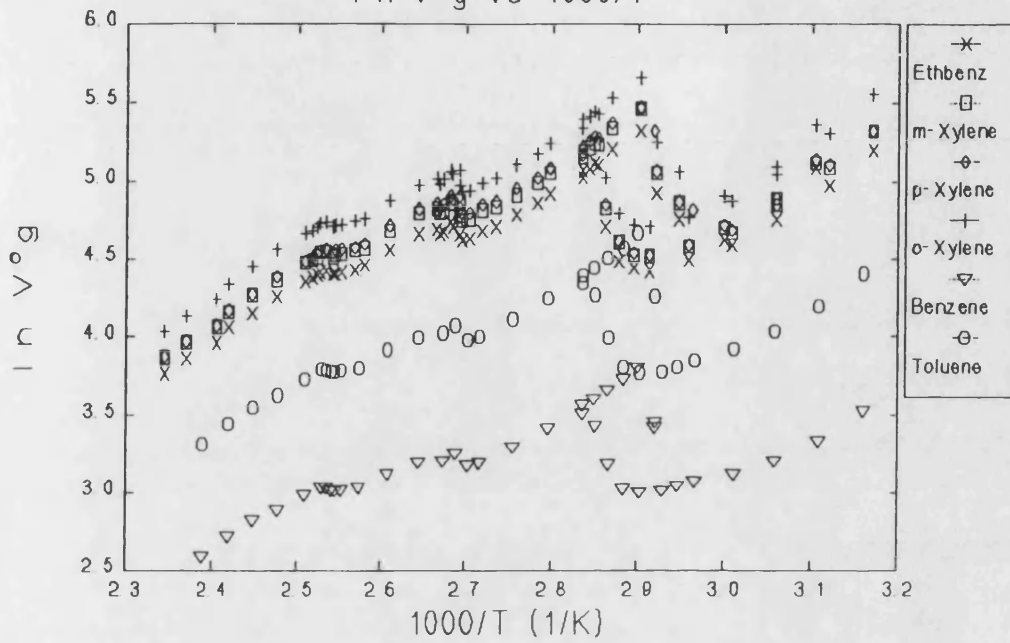
OBIB: n-Alkanes
l n V°g vs 1000/T
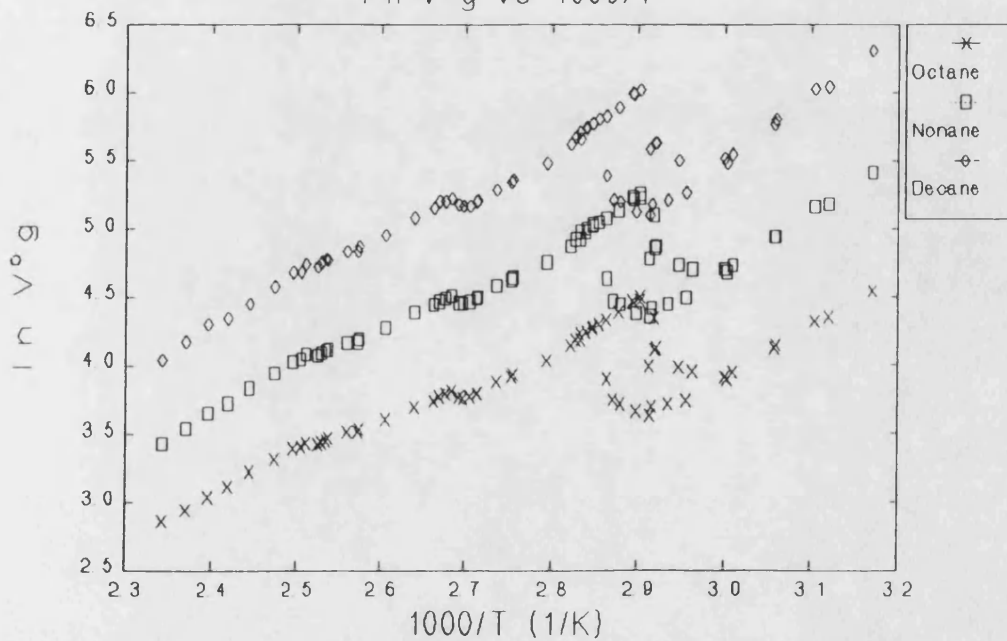
OCB: "C6" probes
In V°g vs 1000/T
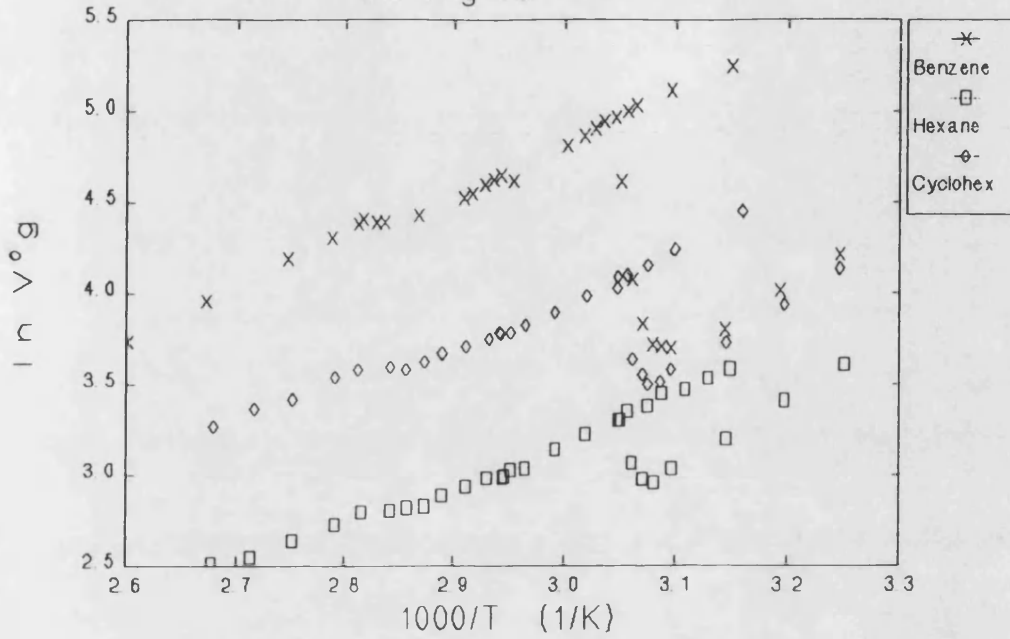
OCB: Heptane isomers
In V°g vs 1000/T
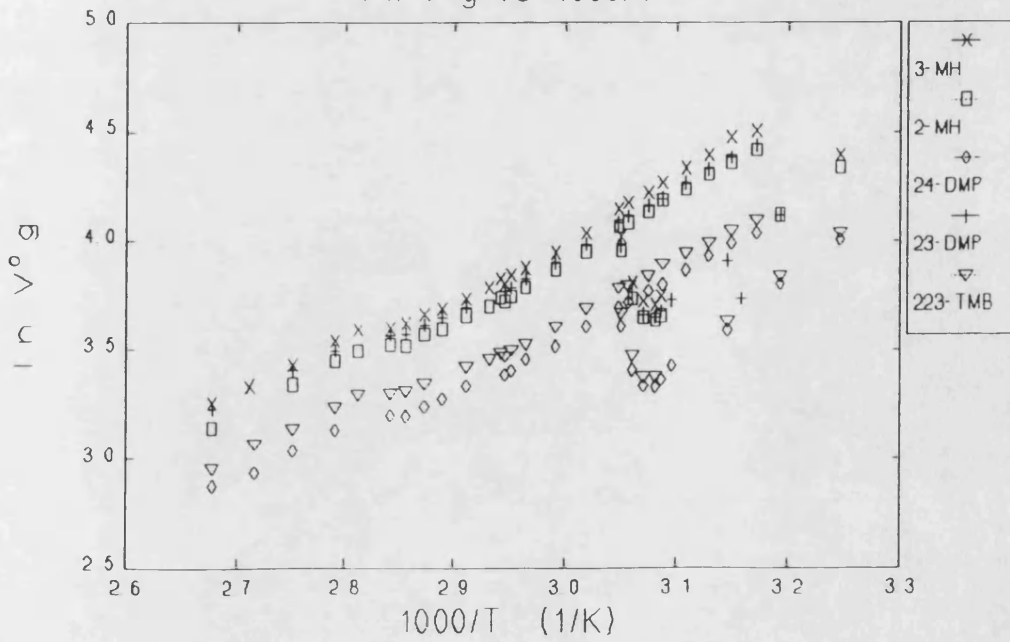
OCB: Aromatic probes
l n V°g vs 1000/T
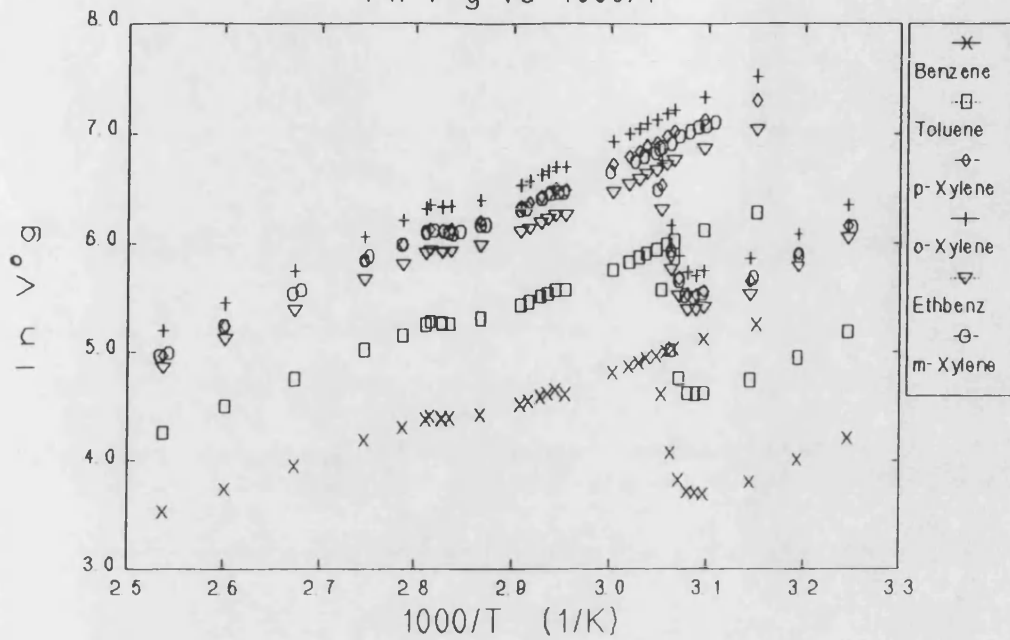
OCB: n-Alkanes
l n V°g vs 1000/T

LCP: n-Alkanes
l n V°g vs 1000/T

Pentane
Hexane
Heptane
Octane
Nonane

LCP: Aromatic probes
l n V°g vs 1000/T

Benzene
Toluene
p-Xylene
m-Xylene
o-Xylene
Ethbenz
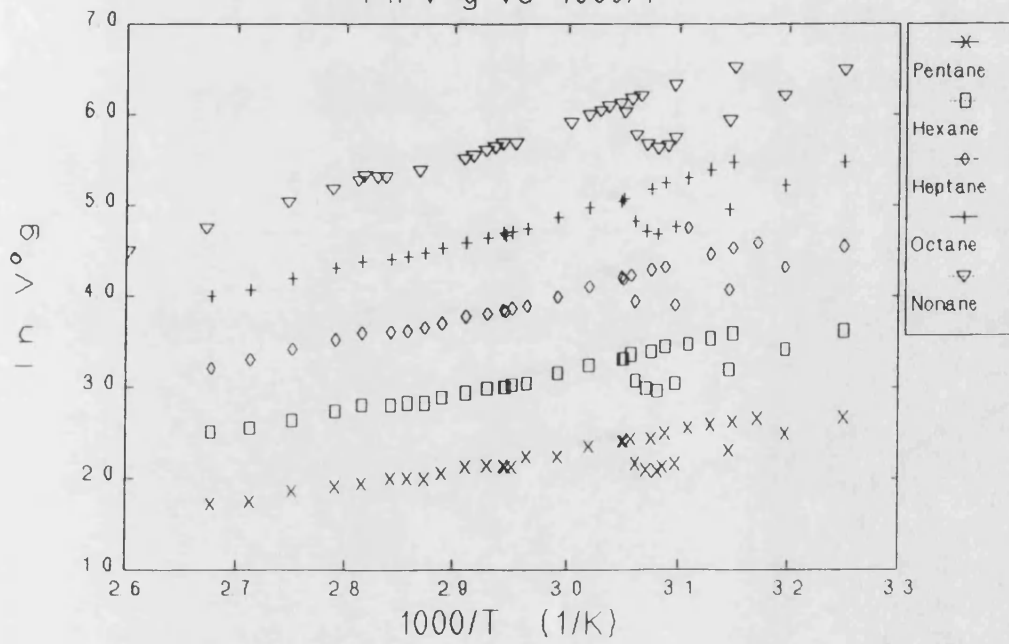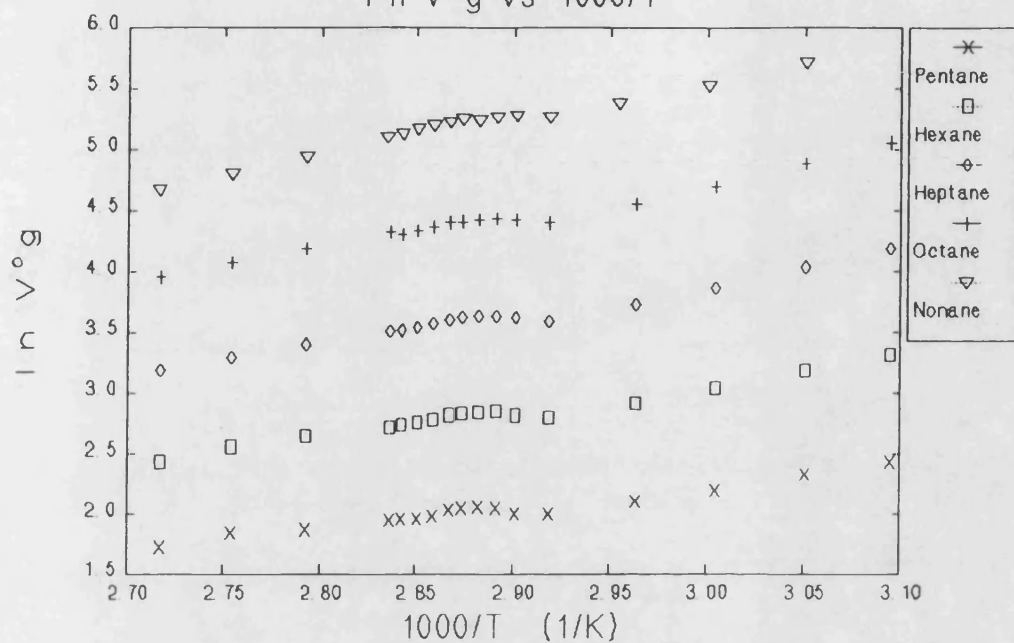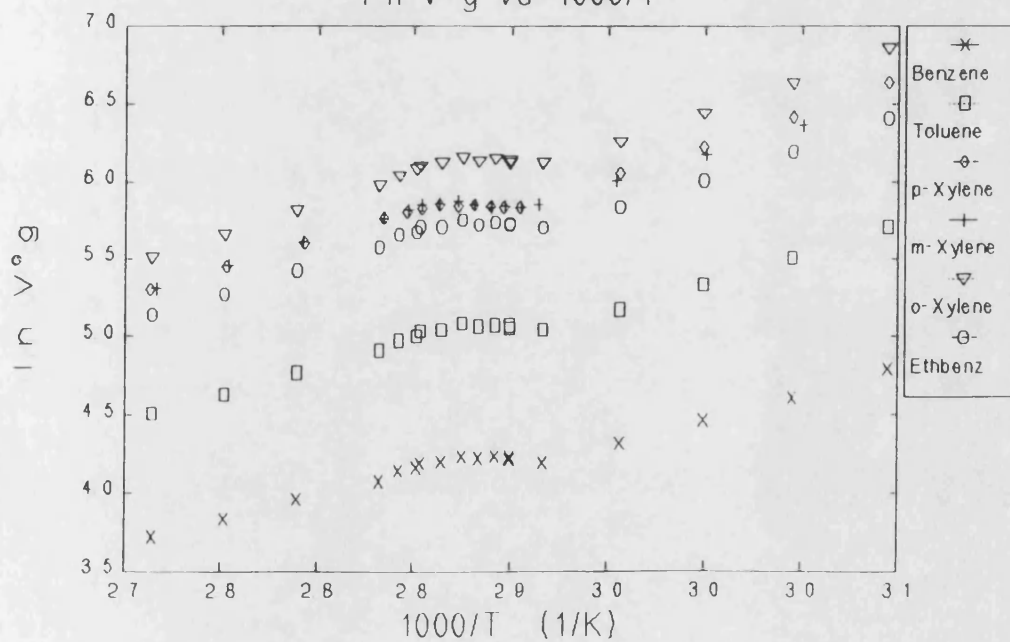
LCP: Heptane isomers
ln V°g vs 1000/T
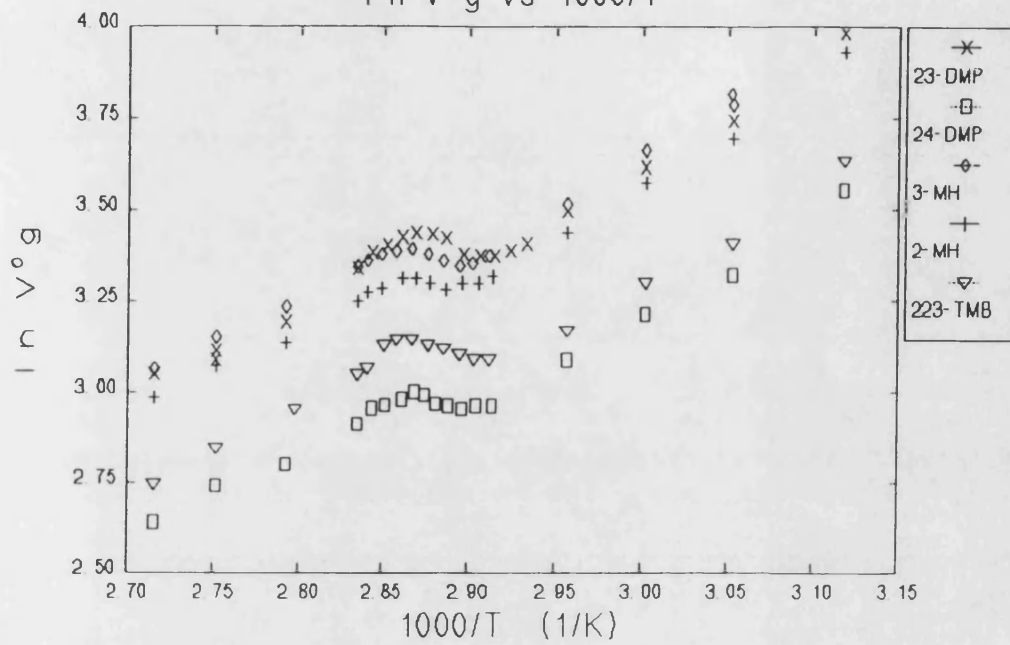
LCP: "C6" probes
ln V°g vs 1000/T
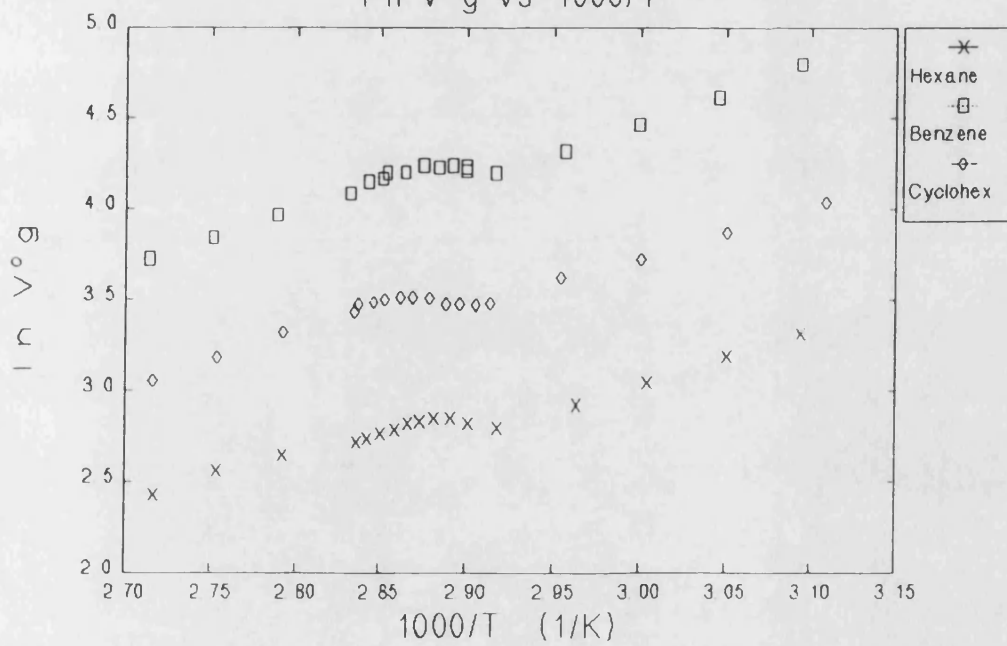
PDMS: n-Alkanes
l n V°g vs 1000/T
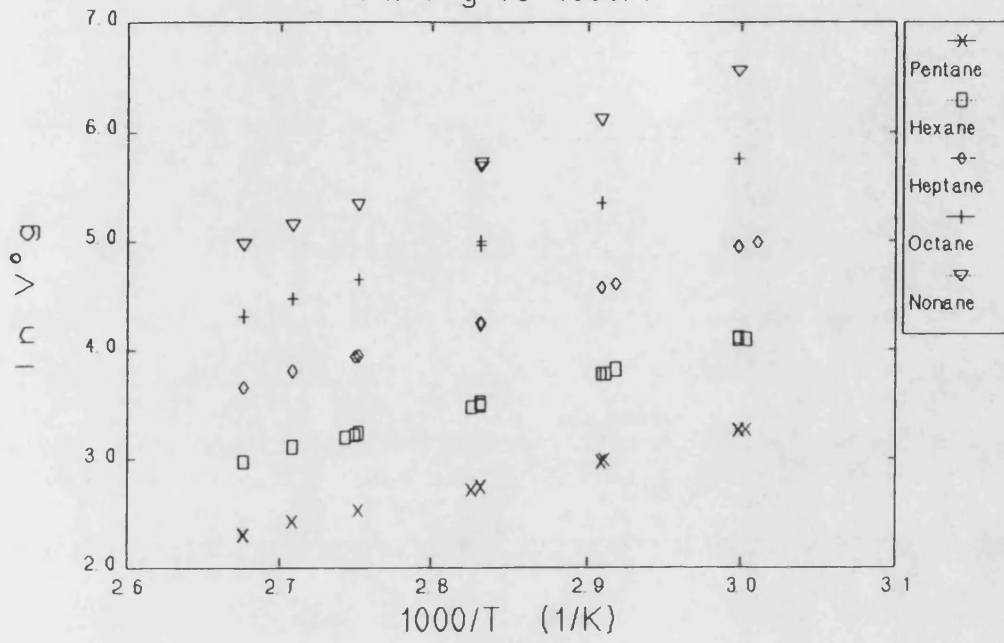
PDMS: Aromatic probes
l n V°g vs 1000/T
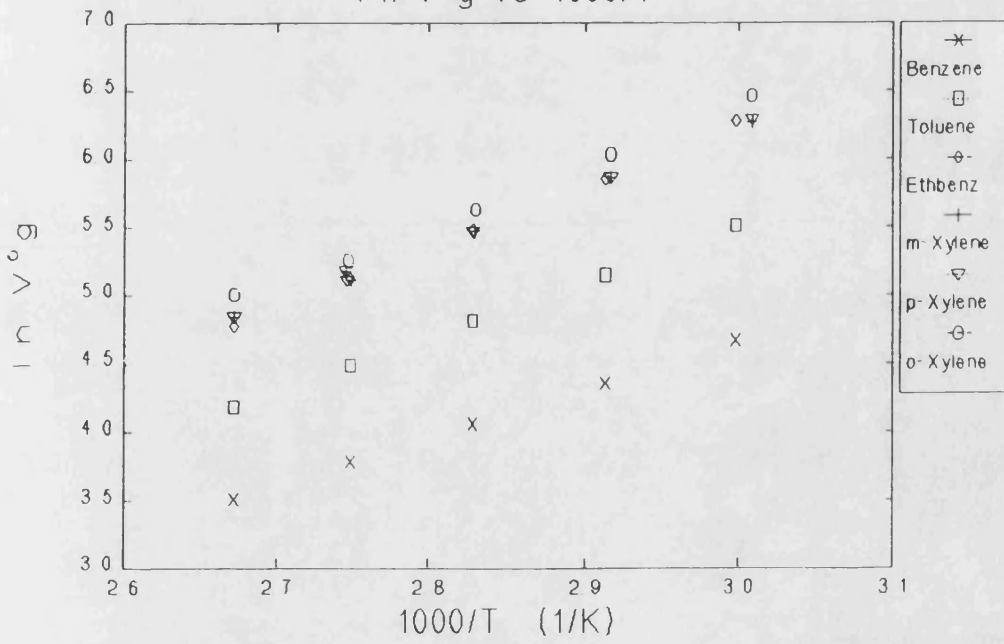
PDMS: Heptane isomers
In V°g vs 1000/T

PDMS: "C6" probes
In V°g vs 1000/T

80:20 w:w HCB:PDMS
l n V°g vs 1000/T: n-Alkanes

80:20 w:w HCB:PDMS
l n V°g vs 1000/T: Aromatic probes

80:20 w:w HCB:PDMS
l n V$_g^o$ vs 1000/T: Heptane isomers
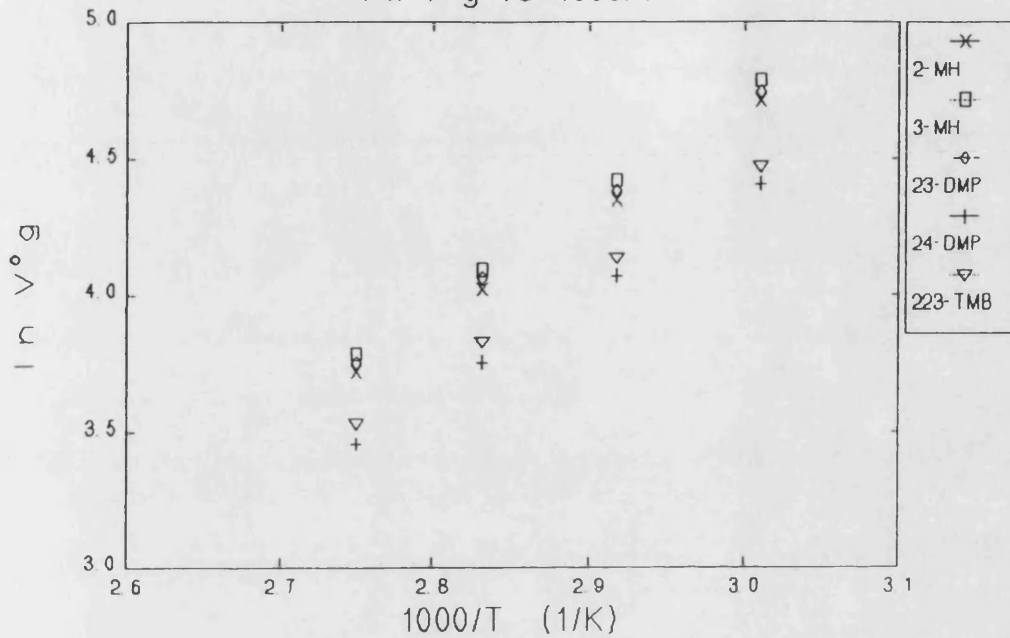
60:40 w:w HCB:PDMS
l n V^{o}g vs 1000/T: n-Alkanes
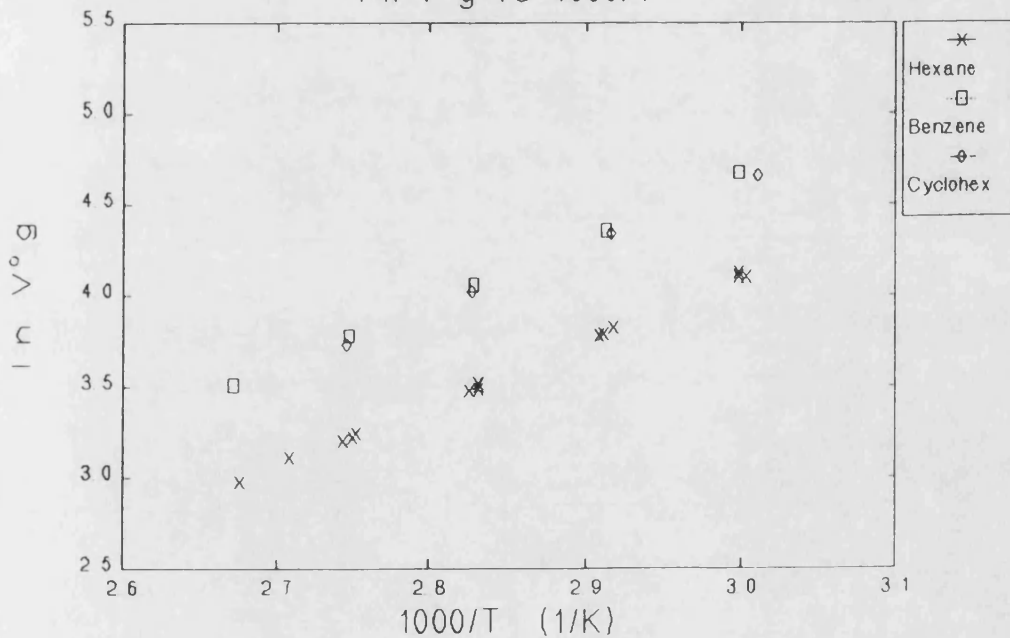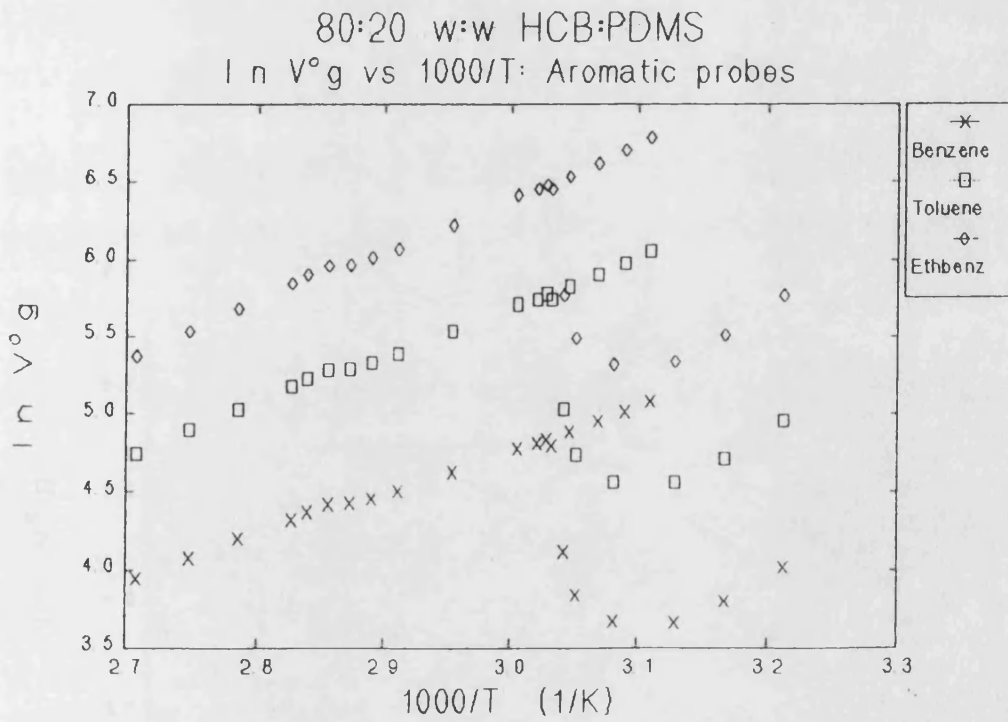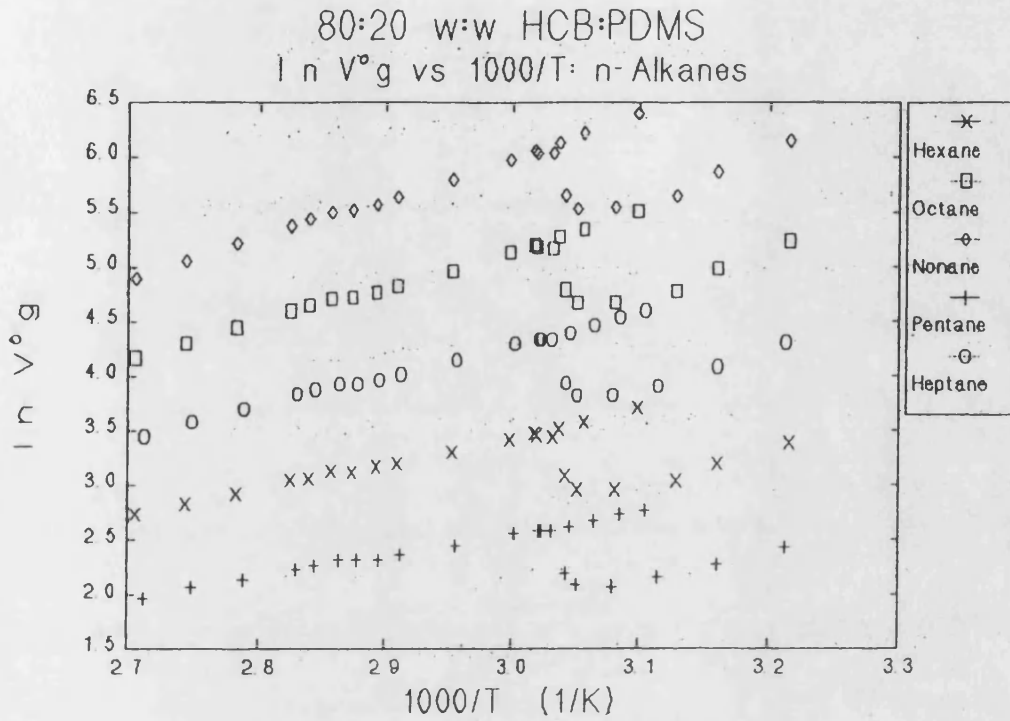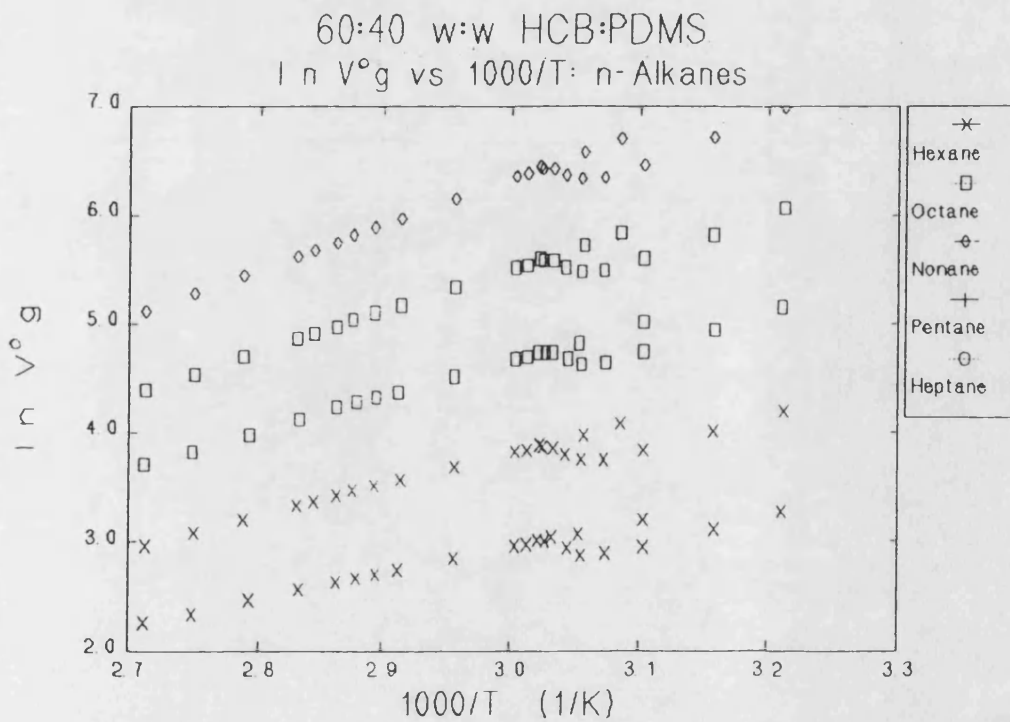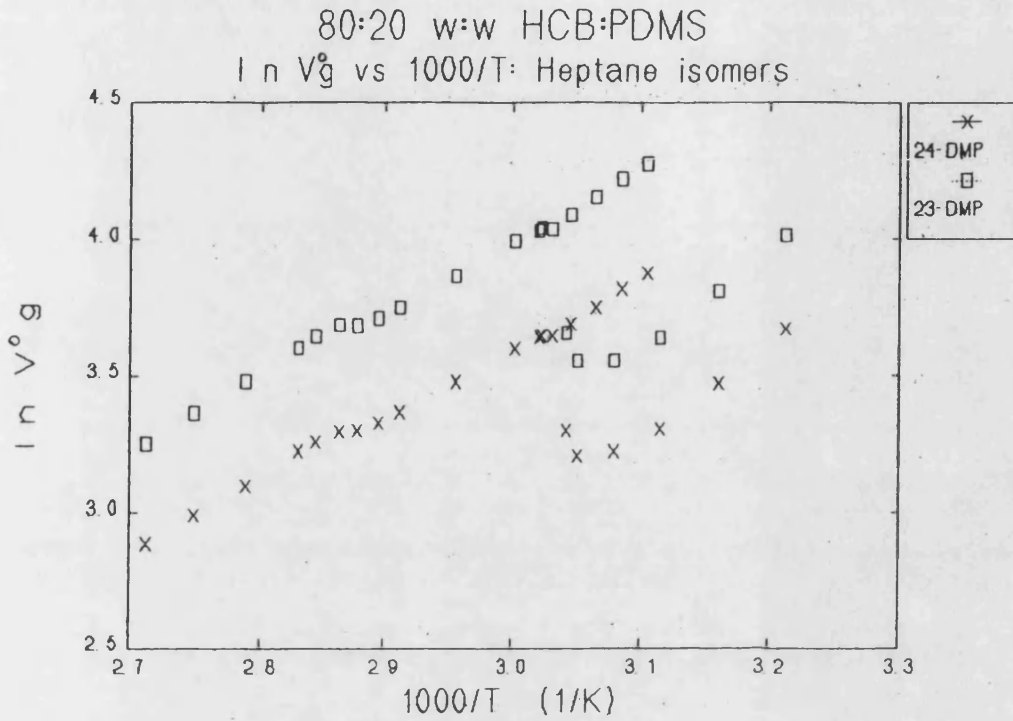
60:40 w:w HCB:PDMS
In V°g vs 1000/T: Aromatic probes
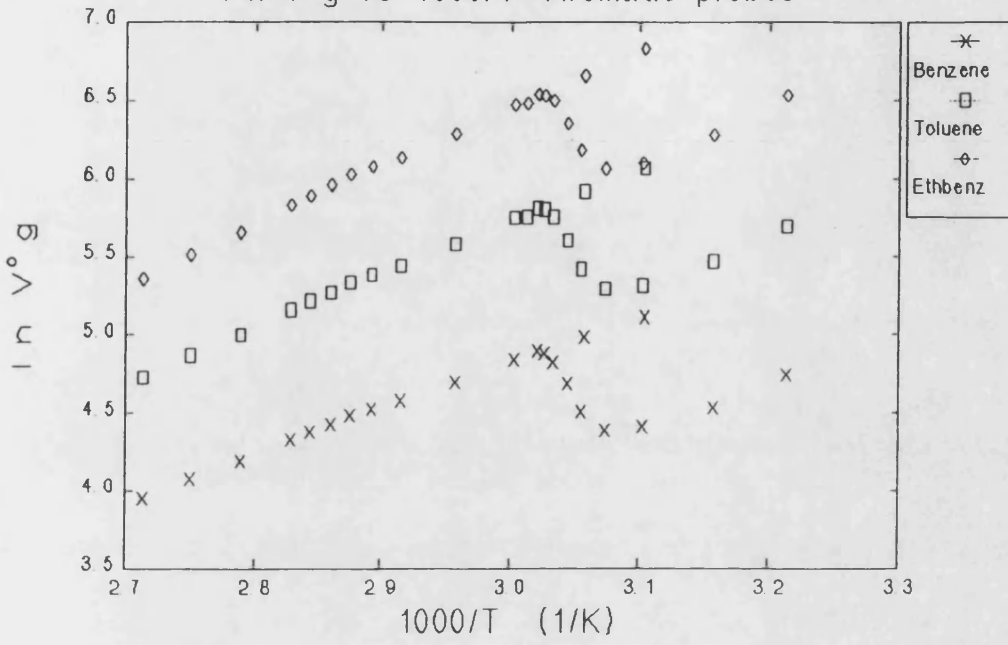
60:40 w:w HCB:PDMS
In V°g vs 1000/T: Heptane isomers
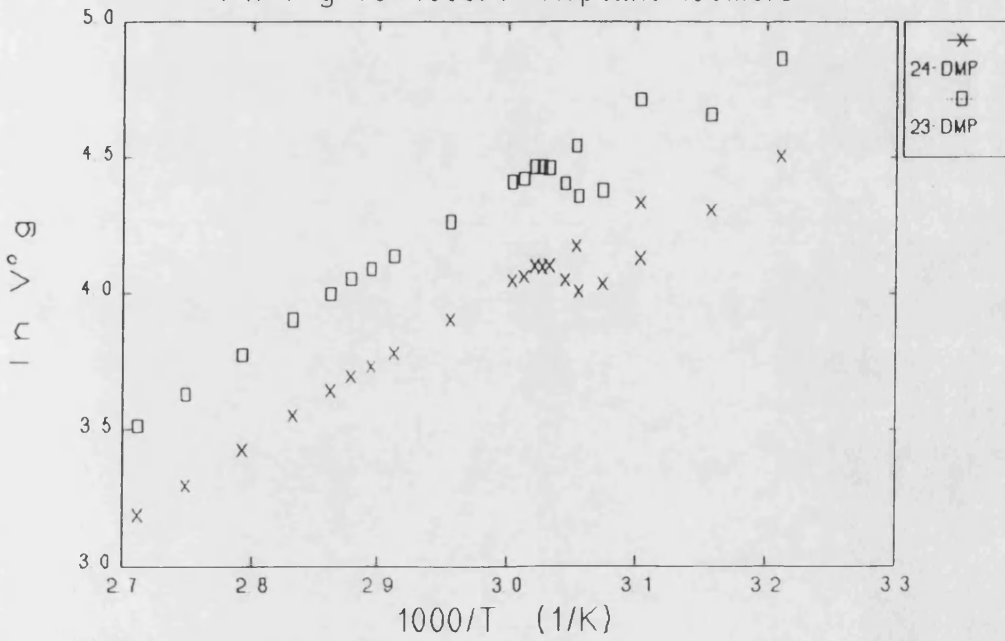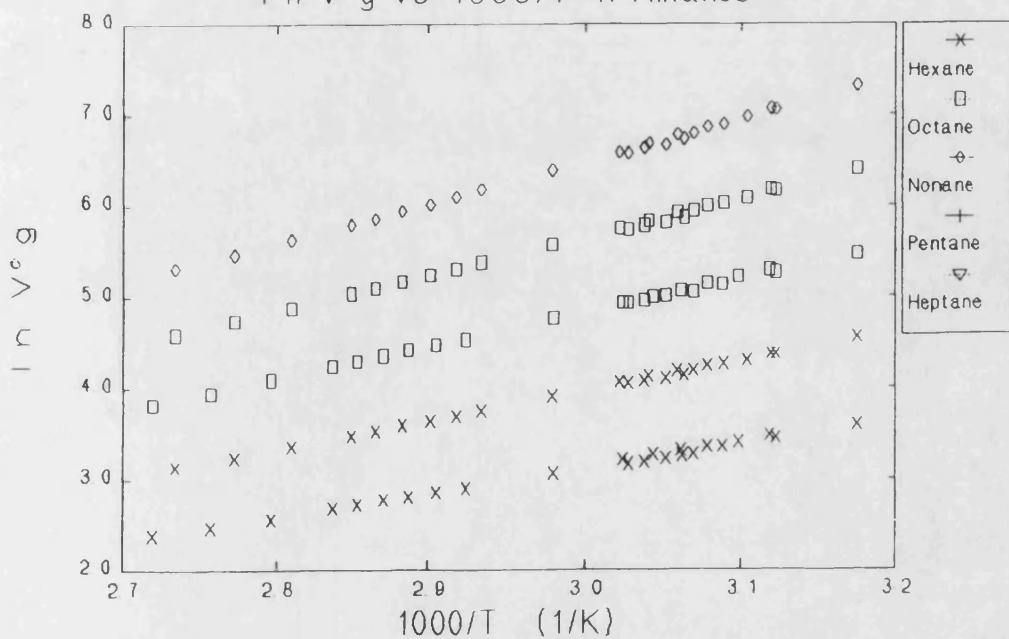
40:60 w:w HCB:PDMS
l n V°g vs 1000/T: n-Alkanes
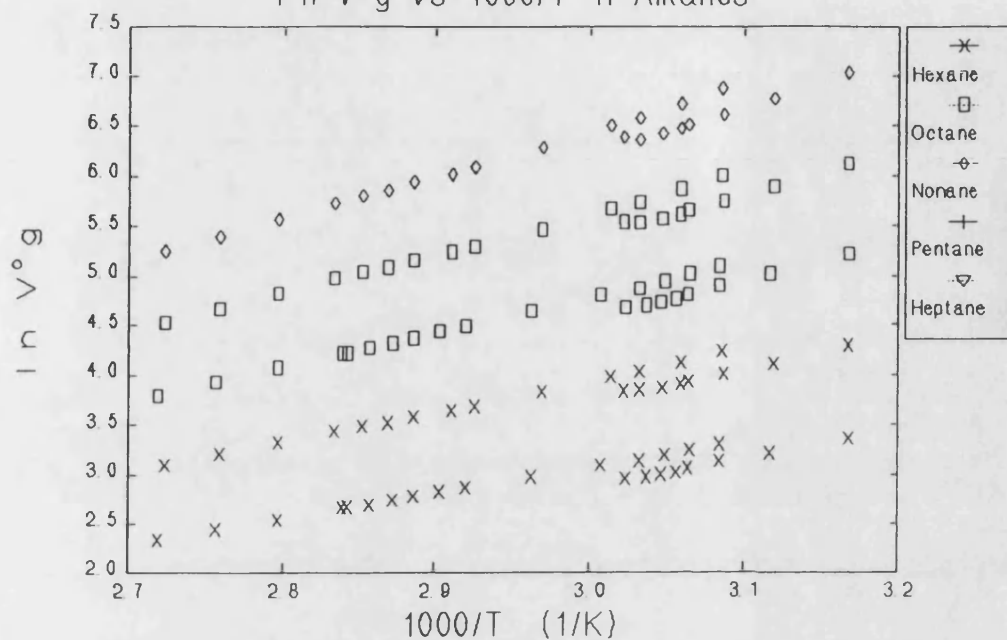
40:60 w:w HCB:PDMS
l n V°g vs 1000/T
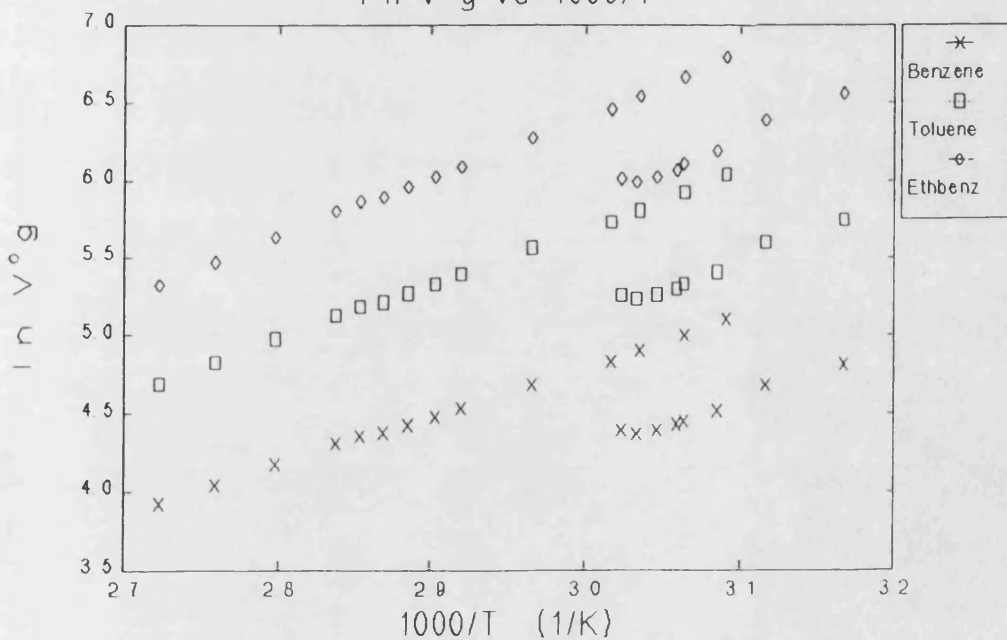
40:60 w:w HCB:PDMS
In V°g vs 1000/T: Heptane isomers

20:80 w:w HCB:PDMS
In V°g vs 1000/T: n-Alkanes

20:80 w:w HCB:PDMS
ln V°g vs 1000/T: Aromatic probes
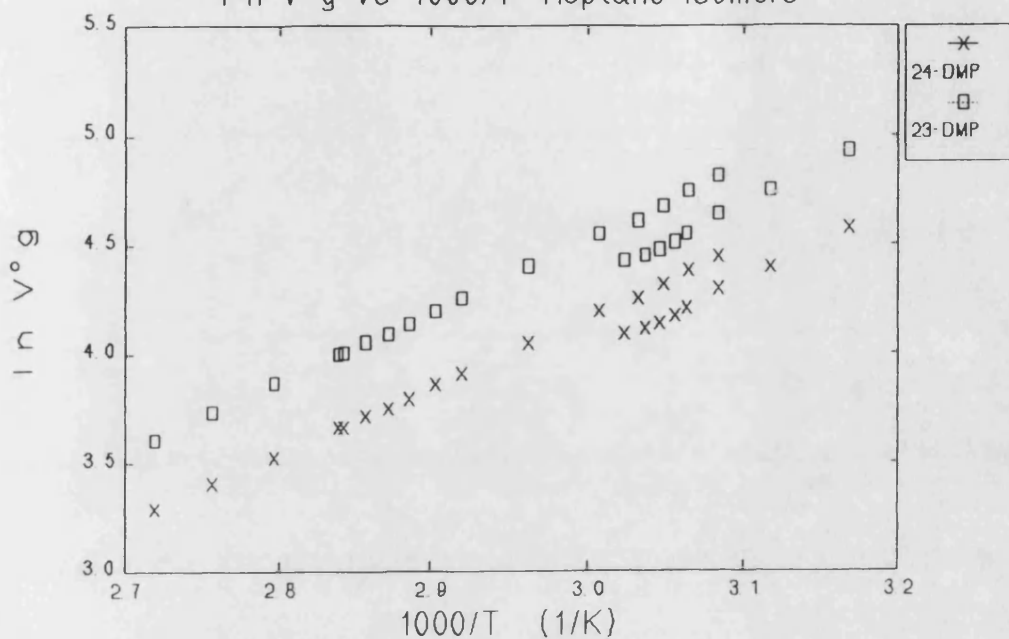
20:80 w:w HCB:PDMS
ln V°g vs 1000/T: Heptane isomers
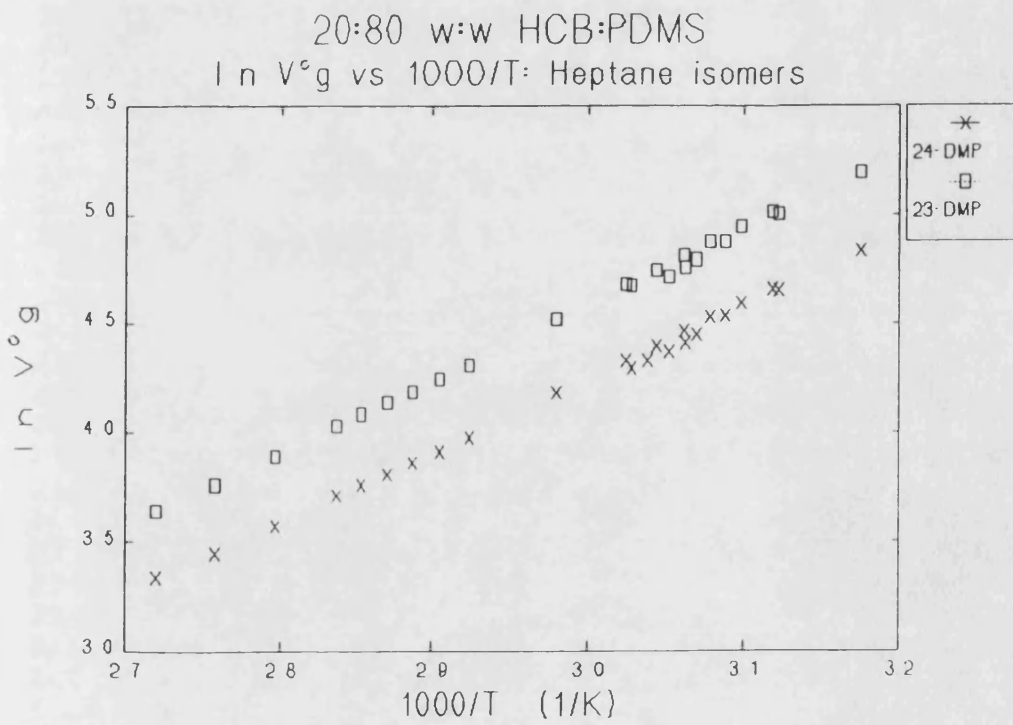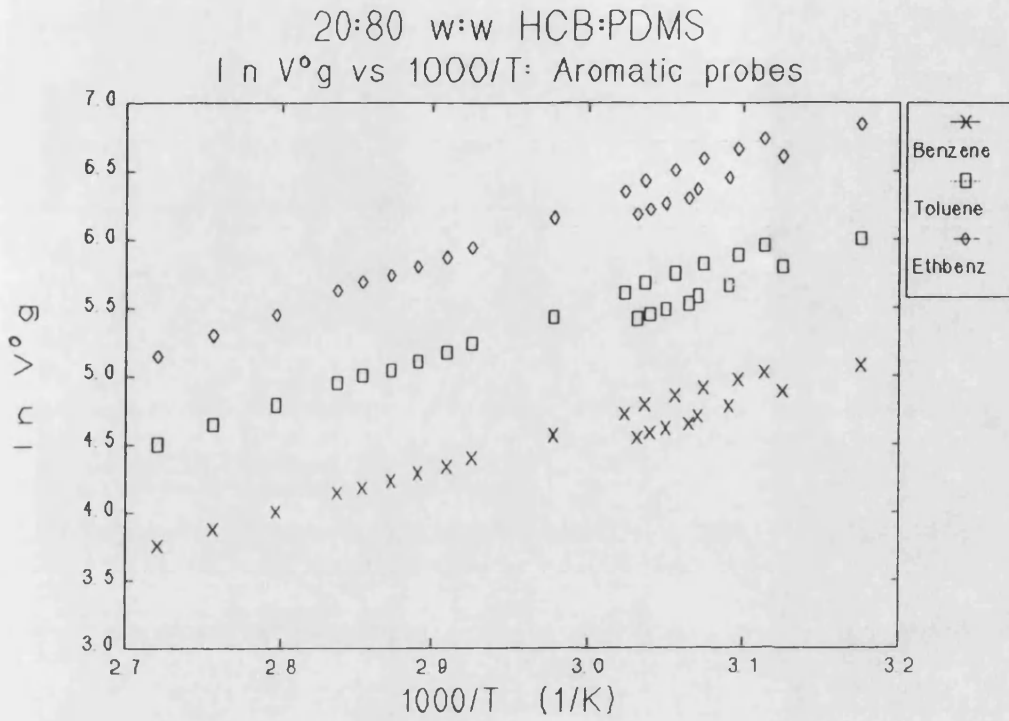
APPENDIX II

BASIC program "CHROM" used to calculate retention volumes and activity

coefficients.

```
10 CLS
20 PRINT
30 PRINT
40 PRINT TAB(18)"SPECIFIC RETENTION VOLUME AND ACTIVITY
"
50 PRINT
60 PRINT TAB(18)"COEFFICIENT CALCULATOR FOR"
70 PRINT
80 PRINT
90 PRINT TAB(20)"IIIIIIIIII"; TAB(32)"GGGGGGGGGG";  TAB
(45)"CCCCCCCCCC"
100 PRINT TAB(20)"IIIIIIIIII"; TAB(32)"GGGGGGGGGG";  TA
B(45)"CCCCCCCCCC"
110 PRINT TAB(20)"IIIIIIIIII"; TAB(32)"GGGGGGGGGG";  TA
B(45)"CCCCCCCCCC"
120 PRINT TAB(23)"IIII"; TAB(32)"GGGG"; TAB(45)"CCCC";
TAB(51)"CCCC"
130 PRINT TAB(23)"IIII"; TAB(32)"GGGG"; TAB(45)"CCCC"
140 PRINT TAB(23)"IIII"; TAB(32)"GGGG"; TAB(38)"GGGGG"
; TAB(45)"CCCC"; TAB(51)"CCCC"
150 PRINT TAB(20)"IIIIIIIIII"; TAB(32)"GGGGGGGGGGGGG";
TAB(45)"CCCCCCCCCC"
160 PRINT TAB(20)"IIIIIIIIII"; TAB(32)"GGGGGGGGGG";  T
AB(45)"CCCCCCCCCC"
170 PRINT TAB(20)"IIIIIIIIII"; TAB(32)"GGGGGGGGGG";  T
AB(45)"CCCCCCCCCC"
180 PRINT TAB(39)"GGGG"
190 PRINT
200 PRINT TAB(20)"-DEVISED BY AN OPTIMIST"
210 PRINT TAB(20)"-WRITTEN BY A PESSIMIST"
220 PRINT TAB(20)"-FOR USE BY A  CHEMIST"
230 PRINT
240 INPUT"PRESS RETURN TO CONTINUE";PAG$
250 CLS
260 REM COLUMN INPUTS
270 INPUT"ENTER 1 TO CALCULATE ACTIVITY COEFFICIENTS ON
LY, ELSE PRESS ANY OTHER NUMBER";CH
280 DIM PRO$(12),T(12,50),IT(12,50),V(12,50),LV(12,50),
AC(12,50),LAC(12,50),WAC(12,50),LWAC(12,50),AP(50),TC(5
0),TIM(50),VME(50)
290 INPUT"COLUMN STATIONARY PHASE";COL$
300 INPUT"MOLECULAR WEIGHT OF STATIONARY PHASE, (0 IF U
NKNOWN)";M
310 INPUT"MASS OF STATIONARY PHASE INCLUDING CHROMOSORB
";SM
320 INPUT"% LOADING";L
330 IF (L<0) OR (L>100) THEN PRINT"PERCENT!":GOTO 320
340 LET W=L*SM/100
350 LET Y=0
```

```
360 REM PROBE INPUTS
370 IF Y>12 THEN PRINT"OUT OF SPACE ON LIST":GOTO 1140
380 INPUT"PROBE [LETTERS ONLY IF IMPORTING TO ASEASY],
(S TO STOP)";PRO$(Y)
390 IF PRO$(Y)="S" THEN GOTO 1140
400 INPUT"MOLECULAR WEIGHT OF PROBE";MP
410 PRINT"ENTER ANTOINE CONSTANTS FOR PROBE,"
420 PRINT"LOG(PARTIAL PRESSURE)=A-B/(C+TEMP): TEMPERATU
RE IN 'C"
430 INPUT"A,B,C";A,B,C
440 IF (A<3) OR (A>10) THEN PRINT"A IS OUT OF RANGE!":G
OTO 430
450 IF B<C THEN PRINT"B/C NEEDS CHECKING!":GOTO 430
460 IF (B>2000) OR (C<100) THEN LET B=0:GOTO 450
470 PRINT"ENTER 2nd VIRIAL COEFFICIENT CONSTANTS FOR PR
OBE,"
480 INPUT"CRITICAL VOLUME, (cm3)";CV
490 IF CV<0 THEN PRINT"INPUT ERROR!":GOTO 480
500 INPUT"IS U/K OF THE FORM -A[1+B/T] (Y/N)";QUE$
510 IF QUE$<>"Y" THEN GOTO 540
520 INPUT" ENTER A,B";CA,CB
530 GOTO 560
540 INPUT"U/K, (KELVIN)";U
550 IF U>0 THEN PRINT"SHOULD BE NEGATIVE!":GOTO 540
560 INPUT"CONSTANTS R1,R2, AND R3";RA,RB,RC
570 IF ((RA<=0) OR (RB<=0)) OR (RC<=0) THEN PRINT"INPUT
 ERROR!":GOTO 560
580 IF((RA>1) OR (RB>2)) OR (RC>6) THEN LET RC=0:GOTO 5
70
590 LET Z=0
600 REM DATA FOR EACH RUN
610 FOR X=0 TO 50
620 IF CH=1 GOTO 790
630 PRINT"FOR FIRST 4 VARIABLES PRESS RETURN TO ENTER P
REVIOUS VALUE"
640 LET Z=Z+1
650 INPUT"ATMOSPHERIC PRESSURE, (mmHg)-1 TO STOP";AP(Z)
660 IF AP(Z)=1 GOTO 1120
670 IF AP(Z)=0 THEN LET AP(Z)=AP(Z-1)
680 INPUT"FLOWMETER TEMPERATURE, ('C)";TC(Z)
690 IF TC(Z)=0 THEN LET TC(Z)=TC(Z-1)
700 IF (TC(Z)<10) OR (TC(Z)>30) THEN PRINT"ROOM TEMPERA
TURE!":GOTO 680
710 LET TK=273.15+TC(Z)
720 INPUT"FLOWRATE: TIME (s)";TIM(Z)
730 INPUT"FOR VOLUME (cm3)";VME(Z)
740 IF TIM(Z)=0 THEN LET TIM(Z)=TIM(Z-1)
750 IF VME(Z)=0 THEN LET VME(Z)=VME(Z-1)
760 LET FM=VME(Z)*60/TIM(Z)
770 INPUT"MANOMETER READING, (mmHg)";MAN
780 LET IP=MAN+AP(Z)
790 INPUT"COLUMN TEMPERATURE, ('C)-(0 TO STOP)";T(Y,X)
800 IF T(Y,X)=0 THEN GOTO 1120 ELSE GOTO 810
810 LET K=T(Y,X)+273.15
820 LET IT(Y,X)=1000/K
```

```
830 IF CH=1 GOTO 960
840 INPUT"RETENTION TIME, (min)";RT
850 INPUT"MARKER RETENTION TIME, (min)";MT
860 IF MT>RT THEN PRINT"REFERENCE LARGER THAN PROBE!":G
OTO 840
870 REM WATER VAP PRESSURE IN FLOWMETER
880 LET WP=EXP(20.9792-5310.57/TK)
890 REM CORRECTION FOR GAS COMPRESSION
900 LET J=1.5*((IP/AP(Z))^2-1)/((IP/AP(Z))^3-1)
910 REM FLOWRATE CORRECTION
920 LET FC=FM*(273.15/TK)*(AP(Z)/760)*(1-WP/AP(Z))*J
930 REM SPEC. RET. VOL.
940 LET V(Y,X)=FC*(RT-MT)/W
950 GOTO 970
960 INPUT"SPECIFIC RETENTION VOLUME";V(Y,X)
970 LET LV(Y,X)=LOG(V(Y,X))
980 REM CALC. OF SECOND VIRIAL COEFF.
990 IF QUE$<>"Y" THEN GOTO 1010
1000 LET U=-CA*(1+(CB/T(Y,X)))
1010 LET SVC=2*CV*(RA-(RA-1)*(EXP(U/K)-1)-(RB-1)*(EXP(-
U/K)-1)-(RC-RB)*(EXP(-.21*U/K)-1))
1020 REM CALC OF PARTIAL PRESSURE
1030 LET PP=10^(A-(B/(C+T(Y,X))))
1040 REM CALC. OF MOLAR ACTIVITY COEFF.
1050 IF M=0 THEN GOTO 1080 ELSE GOTO 1060
1060 LET LAC(Y,X)=LOG(17044560#/(PP*M*V(Y,X)))-PP*SVC/(
62400!*K)
1070 LET AC(Y,X)=EXP(LAC(Y,X))
1080 REM WEIGHT ACTIVITY COEFF.
1090 LET LWAC(Y,X)=LOG(17044560#/(PP*MP*V(Y,X)))-PP*SVC
/(62400!*K)
1100 LET WAC(Y,X)=EXP(LWAC(Y,X))
1110 NEXT
1120 LET Y=Y+1
1130 GOTO 360
1140 REM PRINTOUTS
1150 LET I=0
1160 CLS
1170 PRINT TAB(15)"COLUMN:";COL$
1180 GOSUB 1760
1190 PRINT TAB(15)"% LOADING:";L
1200 GOSUB 1760
1210 LET Y=0
1220 IF PRO$(Y)="S" THEN GOTO 1360
1230 PRINT TAB(2)"PROBE:";PRO$(Y)
1240 GOSUB 1760
1250 PRINT TAB(4)"TEMP."TAB(12)"1/TEMP."TAB(21)"Vg"TAB(
28)"LnVg"TAB(36)"M.ACT"TAB(44)"W.ACT"TAB(52)"Ln(M.AC)"T
AB(60)"Ln(W.AC)"
1260 GOSUB 1760
1270 PRINT TAB(5)" 'C"TAB(12)"1000/K"TAB(21)"cm3"
1280 GOSUB 1760
1290 FOR X=0 TO 30
1300 IF V(Y,X)=0 THEN GOTO 1340
1310 PRINT USING"#####.##";T(Y,X);IT(Y,X);V(Y,X);LV(Y,X
);AC(Y,X);WAC(Y,X);LAC(Y,X);LWAC(Y,X)
```

```
1320 GOSUB 1760
1330 NEXT
1340 Y=Y+1
1350 GOTO 1220
1360 INPUT"DO YOU WANT TO STORE DATA (Y/N)";Z$
1370 IF Z$="N" THEN GOTO 1580
1380 IF Z$<>"Y" THEN PRINT "Y/N!":GOTO 1360
1390 INPUT"FILENAME (name.PPP CREATES ASCII FILE FOR AS
EASY)";NAM$
1400 INPUT"FILENUMBER (USUALLY 1)";N
1410 INPUT"DO YOU WISH TO AMMEND EXISTING FILES OR CREA
TE A NEW ONE (C/A)";ANS$
1420 IF ANS$="C" GOTO 1460
1430 IF ANS$<>"A" THEN PRINT"INPUT ERROR!":GOTO 1410
1440 OPEN"A",#N,NAM$
1450 GOTO 1470
1460 OPEN"O",#N,NAM$
1470 WRITE#N,COL$,L
1480 LET Y=0
1490 IF PRO$(Y)="S" THEN GOTO 1570
1500 WRITE #N,PRO$(Y)
1510 FOR X=0 TO 30
1520 IF V(Y,X)=0 THEN GOTO 1550
1530 WRITE #N,T(Y,X),IT(Y,X),V(Y,X),LV(Y,X),AC(Y,X),WAC
(Y,X),LAC(Y,X),LWAC(Y,X)
1540 NEXT
1550 LET Y=Y+1
1560 GOTO 1490
1570 CLOSE#N
1580 INPUT"DO YOU WANT A PRINTOUT (Y/N)";G$
1590 IF G$="Y" THEN GOTO 1620
1600 IF G$<>"N" THEN PRINT"INPUT ERROR":GOTO 1580
1610 END
1620 REM HARDCOPY
1630 LPRINT TAB(15)"COLUMN:";COL$
1640 LPRINT TAB(15)"% LOADING:";L
1650 LET Y=0
1660 IF PRO$(Y)="S" THEN GOTO 1610
1670 LPRINT TAB(2)"PROBE:";PRO$(Y)
1680 LPRINT TAB(4)"TEMP."TAB(12)"1/TEMP."TAB(21)"Vg"TAB
(28)"LnVg"TAB(36)"M.ACT"TAB(44)"W.ACT"TAB(52)"Ln(M.AC)"
TAB(60)"Ln(W.AC)"
1690 LPRINT TAB(5)" 'C"TAB(12)"1000/K"TAB(21)"cm3"
1700 FOR X=0 TO 30
1710 IF V(Y,X)=0 THEN GOTO 1740
1720 LPRINT USING"#####.##";T(Y,X);IT(Y,X);V(Y,X);LV(Y,
X);AC(Y,X);WAC(Y,X);LAC(Y,X);LWAC(Y,X)
1730 NEXT
1740 Y=Y+1
1750 GOTO 1660
1760 REM SUBROUTINE
1770 LET I=I+1
1780 IF I=23 THEN GOTO 1790 ELSE GOTO 1810
1790 LET I=0
1800 INPUT "PRESS RETURN TO CONTINUE";PAG$
1810 RETURN
```